

Technical Report

TR-14-24

Task Force on Engineered Barrier System (EBS)

Task 1 Laboratory tests

Antonio Gens, UPC-CIMNE

January 2019

Svensk Kärnbränslehantering AB

Swedish Nuclear Fuel
and Waste Management Co

Box 3091, SE-169 03 Solna
Phone +46 8 459 84 00



ISSN 1404-0344

SKB TR-14-24

ID 1451871

January 2019

Task Force on Engineered Barrier System (EBS)

Task 1 Laboratory tests

Antonio Gens, UPC-CIMNE

This report concerns a study which was conducted for Svensk Kärnbränslehantering AB (SKB). The conclusions and viewpoints presented in the report are those of the author. SKB may draw modified conclusions, based on additional literature sources and/or expert opinions.

A pdf version of this document can be downloaded from www.skb.se.

© 2019 Svensk Kärnbränslehantering AB

Executive summary

In May 2004, the Äspö HRL International Joint Committee (IJC) set up a Task Force on Engineered Barrier System (EBS) with the long term objective of developing general and effective tools for the advanced coupled THMC analysis of buffer and backfill behaviour. It was envisaged that the Task Force would focus on THM modelling of processes during water transfer in buffer, backfill and near-field rock. The activities of the Task Force are structured in a number of Tasks. This report concerns Task 1 devoted to the coupled THM modelling of small-scale laboratory tests.

The purpose of this report is to present the cases analysed, review the work performed by a number of modelling teams and to draw some conclusions based on the formulations used and the results obtained. It is not the goal of the report, however, to establish a ranked classification of codes and/or teams but to use the information gathered in the Task to advance in the understanding of the relationships between modelling choices and the outcomes of the numerical analyses.

Nine modelling groups (AECL, BGR, CIMNE, Clay Technology-1, Clay Technology-2, CRIEPI, GRS, MARINTEL and TUL) have participated in this Task using seven different codes (ABAQUS, CODE_BRIGHT, FreeFEM++, GEOSYS/ROCKFLOW, ISERIT, LOSTUF, VAPMOD/VIPER). This number provides a sufficient variety of approaches so that the Task does not simply become a validation exercise of a single code.

The basic equations solved by most codes (CODE_BRIGHT, GEOSYS, ABAQUS, LOSTUF, FreeFEM++) are the same: water mass balance, energy and equilibrium and the calculation is performed in a coupled manner. In addition CODE_BRIGHT also incorporates the air mass balance equation. Two of the formulations (VAPMOD/VIPER and ISERIT) are however different. They solve the problem of vapour flow for isothermal and non-isothermal conditions only. They also consider the transfer of water between vapour in the pores and absorbed water in the solid phase, a feature absent in the more general formulations.

There is a general agreement in using Fourier's law for heat conduction and the generalized Darcy's law for liquid flow (when included in the formulation). There is more variety concerning vapour diffusion. Some groups use Fick's law whereas others adopt a double diffusion coefficient approach. The largest variety of constitutive laws refers, not unexpectedly, to the mechanical behaviour (for the formulations that incorporate the mechanical component). All mechanical models, however, incorporate a specific ingredient devoted to the simulation of the key swelling properties of the bentonite.

The Task is organized in three subtasks corresponding to three different sets of experiments:

- Subtask 1.1. Mockup tests performed by CEA.
- Subtask 1.2. Thermal and isothermal infiltration tests performed by CIEMAT.
- Subtask 1.3. Heating test performed by UPC.

The full set of experiments provides a wide range of conditions for testing the performance of codes and formulations under THM conditions. Specifically, the effect of the following conditions and variables can, in principle, be observed:

- Type of bentonite: MX-80 vs. Febex.
- Maximum temperature: 150 °C in the CEA tests, lower temperatures in the CIEMAT and UPC tests.
- Isothermal vs. Thermal gradient tests in the CIEMAT experiments.
- Water content. Two values of water content are used in the CEA tests.
- Infiltration (CEA, CIEMAT rests) vs. no infiltration (UPC) conditions.

The tests meet two basic selection criteria: i) the experiments should incorporate many of the phenomena relevant to the EBS, and ii) the required modelling should not be too demanding on computer resources and code capabilities.

Selected results of the analyses performed by all the teams are presented, including comparisons with experimental results. The entire set of results and the full detail of the calculations are contained in the reports of the individual groups that are collected in the accompanying "Reports Annex". Comments are provided concerning the computational performance of the individual groups. The teams were also encouraged to perform special or sensitivity analyses to check the effects of some key parameters or uncertain conditions. Especially relevant results of those additional analyses are also included and discussed.

As a result of this extensive simulation exercise, a number of conclusions concerning formulations, codes, THM phenomena and modelling can be drawn. Considering the overall pattern of analyses, results and comparisons, it can be generally concluded that the THM behaviour has been successfully modelled by most teams. This indicates that the formulations incorporate the most relevant THM phenomena and their mutual interactions and that the codes are capable of solving the relevant equations in a satisfactory manner. The only exception concerns the failure to model adequately the observed slow hydration of non-isothermal tests. It is likely, however, that at least a substantial part of this failure may be due to vapour leakage from the cell.

Although the analyses performed have not been predictive, from the examination of the various computational processes it can be stated that it is likely that predictive capability of the thermal problem is quite high. However, it is unlikely that the same conclusion holds concerning the hydraulic problem. These cases have proved to be very sensitive to a large number of parameters making it doubtful that a stage of true reliable predictions in this area has been reached. The same remark is even more valid concerning the general mechanical problem although reasonable reliable predications can perhaps be achieved regarding partial aspects of mechanical behaviour such as swelling pressures in confined situations.

The first version of the report was sent to the participating modelling teams for comments. Although every effort has been made to incorporate in this final document the comments received, *the views expressed in the report should be attributed to the author alone and do not necessarily represent the opinions of other teams or participants.*

Contents

1	Introduction	7
2	Modelling teams, codes and formulations	9
2.1	General	9
2.2	AECL	11
2.3	BGR	11
2.4	CIMNE	12
2.5	Clay technology-1	12
2.6	Clay technology-2	13
2.7	CRIEPI	14
2.8	GRS	14
2.9	MARINTEL	15
2.10	TUL	15
2.11	Comments	16
3	Description of the laboratory experiments	19
3.1	Subtask 1.1 – Tests performed by CEA	19
3.2	Subtask 1.2 – Tests performed by CIEMAT	20
3.3	Subtask 1.3 – Test performed by UPC	22
3.4	Remarks	23
4	Modelling results	25
4.1	General	25
4.2	AECL	25
4.2.1	CEA mock-up tests – Subtask 1.1 [1]	25
4.2.2	CIEMAT infiltration tests – Subtask 1.2 [2]	36
4.2.3	UPC heating test – Subtask 1.3 [3]	38
4.2.4	Remarks	40
4.3	BGR	40
4.3.1	CEA mock-up tests – Subtask 1.1 [4]	40
4.3.2	CIEMAT infiltration tests – Subtask 1.2 [4]	46
4.3.3	UPC heating test – Subtask 1.3 [4]	48
4.3.4	Remarks	51
4.4	CIMNE	51
4.4.1	CEA mock-up tests – Subtask 1.1 [6]	51
4.4.2	CIEMAT infiltration tests – Subtask 1.2 [6]	58
4.4.3	UPC heating test – Subtask 1.3 [6]	61
4.4.4	Remarks	65
4.5	Clay Technology-1	65
4.5.1	CEA mock-up tests – Subtask 1.1 [7]	65
4.5.2	CIEMAT infiltration tests – Subtask 1.2 [8]	71
4.5.3	UPC heating test – Subtask 1.3 [9]	73
4.5.4	Remarks	73
4.6	Clay Technology-2	75
4.6.1	CEA mock-up tests – Subtask 1.1 [10]	75
4.6.2	CIEMAT infiltration tests – Subtask 1.2 [10]	78
4.6.3	UPC heating test – Subtask 1.3 [10]	80
4.6.4	Remarks	82
4.7	CRIEPI	82
4.7.1	CEA mock-up tests – Subtask 1.1 [11]	82
4.7.2	CIEMAT infiltration tests – Subtask 1.2 [11]	86
4.7.3	UPC heating test – Subtask 1.3 [11]	88
4.7.4	Remarks	90
4.8	GRS	90
4.8.1	CIEMAT infiltration tests – Subtask 1.2 [12]	90
4.8.2	Remarks	91

4.9	MARINTEL	92
4.9.1	CEA mock-up tests – Subtask 1.1 [13]	92
4.9.2	CIEMAT infiltration tests – Subtask 1.2 [13]	96
4.9.3	UPC heating test – Subtask 1.3 [14]	99
4.9.4	Remarks	101
4.10	TUL	101
4.10.1	CEA mock-up tests – Subtask 1.1 [15]	101
4.10.2	UPC heating test – Subtask 1.3 [16]	104
4.10.3	Remarks	106
5	Concluding remarks	107
	References	111
Appendix A	Specifications of Subtask 1.1	115
Appendix AA1	Location of the sensors	121
Appendix AA2	Properties of mx-80 bentonite	123
Appendix B	Specifications of Subtask 1.2	129
Appendix BA1	Properties of febex bentonite	135
Appendix C	Specifications of Subtask 1.3	139

1 Introduction

In May 2004, the Äspö HRL International Joint Committee (IJC) set up a Task Force on Engineered Barrier System (EBS) with the long term objective of developing general and effective tools for the advanced coupled THMC analysis of buffer and backfill behaviour. Ideally, the numerical tools developed should

- account for all relevant phenomena and their interactions (including interaction with host rock),
- deal with both short term and long term phenomena and behaviour,
- be computationally efficient in order to be applied to real engineering problems.

It was envisaged that the Task Force would focus on THM modelling of processes during water transfer in buffer, backfill and near-field rock.¹ The activities of the Task Force are structured in a number of Tasks. The tasks were initially called Benchmarks but the term Task is adopted for better compatibility with the work of the parallel Task Force on Modelling of Groundwater Flow and Transport of Solutes. It also reflects better the methodology adopted focusing on code development and application rather than on a conventional benchmark exercises. It was also recognized that codes used by different teams were at different stages of development. Teams also differed in the level of user experience and therefore a flexible approach was adopted instead of prescribing a uniform set of activities for all teams.

Therefore, the Task Force was not set up as a competition between codes to determine, from a blind prediction, the best fit to a particular set of experimental results. The basic idea was to allow freedom to the participants to use and develop formulations and codes to try to reproduce in the best possible way the tests results provided in the Tasks. The comparison with the experimental results should provide the bases to assess the capabilities of the different codes and to identify areas of required improvement. These considerations should be borne in mind when assessing the results obtained by different teams.

This report concerns Task 1 devoted to the coupled THM modelling of small-scale laboratory tests. The Task is organized in three subtasks corresponding to three different sets of experiments:

- Subtask 1.1. Mockup tests performed by CEA.
- Subtask 1.2. Thermal and isothermal infiltration tests performed by CIEMAT.
- Subtask 1.3. Heating test performed by UPC.

The two basic criteria for selecting the different subtasks were:

- The experiments should incorporate many of the phenomena relevant to the EBS.
- The Subtasks should not be too demanding on computer resources and code capabilities.

The main aim of this report is to present the cases analysed, review the work performed by a number of modelling teams and to draw some conclusions based on the formulations used and the results obtained. As indicated earlier, it is not the goal of the Task, however, to establish a ranked classification of codes and/or teams but to use the information gathered in the Task to advance in the understanding of the relationships between modelling choices and the outcomes of the numerical analyses.

This report is organized as follows: the codes used by the different participants together with their formulations and basic capabilities are presented in Chapter 2. Chapter 3 contains a summary description of the main features of the proposed Subtasks; a more detailed description is left to the appendices. The results provided by the various teams together with an individual evaluation are provided in Chapter 4. The Section draws on the Reports of the individual teams. The concluding Chapter 5 contains the main conclusions and some recommendations.

¹ Subsequently, in November 2006, another group was set up in the Task Force to deal with chemical issues but their activities are not covered in this report.

2 Modelling teams, codes and formulations

2.1 General

The teams and codes involved in this Task are listed in Table 2-1 together with the funding organisation. The table also contains the names of the files in which the individual groups reported their work. They are collected in an Annex.

Table 2-1. Modelling groups, funding organisations, codes used and report files.

Modelling group	Funding organisation	Code	Report files
AECL	OPG	CODE BRIGHT	[1] AECL Task 1.1.pdf [2] AECL Task 1.2.pdf [3] AECL Task 1.3.pdf
BGR	BMW	GEOSYS ROCKFLOW	[4] BGR Task 1.1.-1.2.pdf [5] BGR Task 1.3.pdf
CIMNE	ANDRA	CODE BRIGHT	[6] CIMNE Task 1.pdf
Clay Technology-1	SKB	CODE BRIGHT	[7] Clay Technology-1 Task 1.1.pdf [8] Clay Technology-1 Task 1.2.pdf [9] Clay Technology-1 Task 1.3.pdf
Clay Technology-2	SKB	ABAQUS	[10] Clay Technology-2 Task 1.pdf
CRIEPI	CRIEPI	LOSTUF	[11] CRIEPI Task 1.pdf
GRS	BMW	VAPMOD VIPER	[12] GRS Task 1.pdf
MARINTEL	POSIVA	FreeFEM++	[13] MARINTEL Task 1.1.-1.2.pdf [14] MARINTEL BGR Task 1.3.pdf
TUL	RAWRA	ISERIT	[15] TUL Task 1.1.pdf [16] TUL Task 1.3.pdf

There is a significant amount of common ground between many of the approaches and formulations of the different teams. For instance, the following phenomena are often incorporated in the computations:

- Thermal problem: conduction, liquid flow advection, vapour flow advection and phase changes (including latent heat).
- Hydraulic problem: liquid and vapour flow.
- Mechanical problem: thermal expansion of the material, swelling/suction effects.

For easier presentation, a reference formulation is now briefly presented. It is very much based on (but not identical to) the CODE_BRIGHT formulation (Olivella et al. 1994, 1996) that has been used by three of the modelling teams. In this way, in the description of the codes and formulations of the different teams it will only be necessary to highlight their specific features

It is useful in the context to distinguish between phases and species. In the notation the subscript is used to identify the phase (*s* for solid, *l* for liquid and *g* for gas) and the superscript indicates the species: *w* for water and *a* for air. No symbol is attributed to the mineral species, because it has been assumed that it coincides with the solid phase.

The balance equation for water mass can be written as:

$$\frac{\partial}{\partial t} (\theta_l^w S_l \phi + \theta_g^w S_g \phi) + \nabla \cdot (\mathbf{j}_l^w + \mathbf{j}_g^w) = f^w \quad (2-1)$$

where θ_l^w and θ_g^w are the masses of water per unit volume of liquid and gas phase respectively. ϕ is the porosity and S_α is the volumetric fraction of pore volume occupied by the alpha phase ($\alpha=l,g$). \mathbf{j}_l^w and \mathbf{j}_g^w denote the total mass fluxes of water in the liquid and gas phases with respect to a fixed reference system. f^w is the external mass supply of water per unit volume of medium.

The balance equation for energy is:

$$\frac{\partial}{\partial t} [E_s \rho_s (1-\phi)] + \frac{\partial}{\partial t} (E_l \rho_l S_l \phi + E_g \rho_g S_g \phi) + \nabla \cdot (\mathbf{i}_c + \mathbf{j}_{E_s} + \mathbf{j}_{E_l} + \mathbf{j}_{E_g}) = f^E \quad (2-2)$$

where E_s is the solid specific internal energy, E_l and E_g are specific internal energies corresponding to the liquid and gas phases respectively. ρ_l and ρ_g are the liquid and gas phase densities of the medium. f^E is the energy supply per unit volume of medium \mathbf{i}_c is the conductive heat flux. \mathbf{j}_s , \mathbf{j}_{E_l} and \mathbf{j}_{E_g} are the energy fluxes due to the motion of phase. Thus conduction, advection and phase change are considered.

Finally, the momentum balance equation is expressed as:

$$\nabla \cdot \boldsymbol{\sigma} + \mathbf{b} = 0 \quad (2-3)$$

where $\boldsymbol{\sigma}$ is the total stress tensor and \mathbf{b} the vector of body forces. Inertial terms have been neglected.

Constitutive laws define the thermo-hydro-mechanical behaviour of the materials involved in the calculations. They also contain, in most cases, the definition of the various THM couplings. Quite a number of the formulations adopt the following constitutive laws:

- Heat conduction: Fourier's law.

$$\mathbf{i}_c = -\lambda \nabla T \quad (2-4)$$

where λ is the global thermal conductivity of the porous medium, generally dependent on degree of saturation and porosity (and occasionally on temperature itself).

- Internal energy. As indicated in Equation (2-2), internal energy is additive, it is computed from the sum of the internal energies of the three phases:

$$E = E_s \rho_s (1-\phi) + E_l \rho_l S_l \phi + E_g \rho_g S_g \phi \quad (2-5)$$

Accordingly, the internal energy of each phase is also the sum of the internal energies of their components:

$$E_l = E_l^w \omega_l^w + E_l^a \omega_l^a \quad E_g = E_g^w \omega_g^w + E_g^a \omega_g^a \quad (2-6)$$

Note that the internal energy of vapour (E_g^w) incorporates the latent heat of vaporisation/condensation so that the thermal effects of phase change are taken into account.

- Liquid flow: generalized Darcy's law.

$$\mathbf{q}_l = -\mathbf{K}(\nabla P_l - \rho_l \mathbf{g}) \quad (2-7)$$

where P_l is the liquid pressure, \mathbf{K} is the liquid permeability tensor \mathbf{g} is the gravity vector. The permeability tensor is not constant and depends on other variables, according to:

$$\mathbf{K} = \mathbf{k} k_r / \mu \quad (2-8)$$

The intrinsic permeability tensor (\mathbf{k}) depends on the pore structure of the porous medium. k_r is the value of relative permeability that controls the variation of permeability in the unsaturated regime and μ denotes the dynamic viscosity (temperature dependent).

- Retention curve: it provides a relationship between degree of saturation and suction. Different relationships are used.
- Vapour diffusion: Fick's law.

$$\mathbf{i}_g^w = -\mathbf{D}_g^w \nabla \omega_g^w = -(\phi \rho_g S_g \tau D_m^w \mathbf{I} + \rho_g \mathbf{D}_g^m) \nabla \omega_g^w \quad (2-9)$$

where \mathbf{i}_g^w is the diffusive vapour flux, \mathbf{D}_g^w is the dispersion tensor, ω_g^w is the mass fraction of water in gas, τ is the tortuosity and \mathbf{D}_g^m the mechanical dispersion tensor. Mechanical dispersion can usually be neglected in the type of problems proposed in this Task. Note that the mass fraction of water in gas is equivalent to vapour density and it is proportional to vapour pressure. Therefore, vapour diffusion can be equally driven by vapour pressure, the two formulations are identical.

An often used expression for the molecular diffusion of vapour in air is:

$$D_m^w (m^2/s) = 5.9 \times 10^{-12} \frac{(273.15 + T)^{2.3}}{P_g (MPa)} \quad (2-10)$$

- The densities of the liquid and solid components are dependent on pressure and temperature.
- Vapour concentration in the gas phase. In equilibrium vapour concentration is governed by Kelvin's law:

$$\theta_g^w = (\theta_g^w)^0 \exp\left(\frac{\Psi M_w}{R(273.15 + T)\rho_l}\right) \quad (2-11)$$

where θ_g^w is the vapour concentration in the gas phase; $(\theta_g^w)^0$ is the vapour concentration in the gas phase in equilibrium with a liquid at flat surface (at the sample temperature), Ψ is the total water potential of the water (excluding gravity terms), M_w is the molecular mass of the water (0.018 kg/mol) and R the gas constant (8.314 J/mol/°K).

- The mechanical models contemplate not only the conventional stress strain behaviour but the effects of suction variation as well. Temperature effects are generally limited to the consideration of thermal expansion. Generally, the volumetric thermal expansion of the material is computed as:

$$\varepsilon_v = 3\alpha_l \Delta T \quad (2-12)$$

where α_l is the linear thermal expansion coefficient.

In the next sections the formulations and codes used by the different teams are summarily reviewed. Only the main departures from the common reference formulation outlined above are commented. For consistency, it has been decided to keep the notations of each team in that review; consequently, the variables are defined in each section as required. More information on the formulations and codes are provided in the individual team reports collected in the Annex.

2.2 AECL

The AECL team [1] used the computer code CODE_BRIGHT (version 2.2), a finite element code designed to perform coupled thermo-hydro-mechanical (THM) numerical analyses. The analysis involves the simultaneous solution, using a monolithic scheme, of the balance equations for water mass, air mass, momentum (i.e. equilibrium) and energy. The fundamental unknowns associated with each of these balance equations are, respectively, liquid pressure, gas pressure, displacements and temperature.

The constitutive laws used are those indicated in Section 2.1. For the mechanical behaviour, the elasto-plastic Barcelona Basic Model (BBM) is adopted. The law for the behaviour inside the yield locus is modified to take into account the expansive nature of the buffer material. The following expression for the nonlinear elastic volumetric strain is used:

$$d\varepsilon_v^e = \left(\frac{k}{1+e}\right)\left(\frac{dp'}{p'}\right) + \left(\frac{k_s}{1+e}\right)\left(\frac{ds}{s+0.1}\right) \quad (2-13)$$

where e is the void ratio; $p' = \frac{1}{3}(\sigma_x + \sigma_y + \sigma_z) - \max(p_g, p_l)$; s is suction, k_s is a dimensionless compressibility coefficient under suction changes (ds) and k is a dimensionless compressibility coefficient under mean stress changes.

2.3 BGR

The BGR team [4] used the code GEOSYS except for the Task 1.2 when the code ROCKFLOW was employed. GEOSYS solves the balance equations for water mass, momentum (i.e. equilibrium) and energy. The air mass equation is not included, so gas pressure is implicitly assumed to be constant. The code is based on a full Galerkin approximation and the equations are solved using a staggered scheme. The issue of mass conservation associated with the use of a full Galerkin approximation is explicitly addressed.

Regarding the set of constitutive laws, the following points can be noted:

- Vapour flow: The Philips and de Vries (1957) formulation is adopted where temperature effects on vapour diffusion are explicitly considered via the corresponding thermal diffusion coefficient. The relevant expressions are:

$$\mathbf{q}_v = -D_{pv} \nabla p - f_{Tv} D_{Tv} \nabla T \quad (2-14)$$

where f_{Tv} is a thermal enhancement coefficient taken as 1.0 in the analyses reported. D_{pv} and D_{Tv} are the pressure and temperature diffusion coefficients:

$$D_{pv} = \frac{D_v \rho_v}{\rho_w RT}; D_{Tv} = D \left(h \frac{\partial \rho_{vs}}{\partial T} - \frac{\rho_v p}{\rho_w RT^2} \right) \quad (2-15)$$

where ρ_v is the vapour density, ρ_{vs} the saturated vapor density, ρ_w is the water density, h is the relative humidity, R the universal gas constant, p is the water pressure and T the absolute temperature.

The molecular diffusion coefficient takes into account the potential tortuosity of the migration path as well as the gas volume available for gas movement according to:

$$D_v = \tau S_g n 2.1610^{-5} (T / 273.15)^{1.8} \quad (2-16)$$

where τ is the tortuosity, S_g the gas degree of saturation and n the effective porosity.

- Mechanical behaviour is defined in terms of the following stress tensor:

$$\boldsymbol{\sigma} = \chi p \mathbf{I} - \mathbf{p}_{sw} - \alpha \mathbf{D} \Delta T \quad (2-17)$$

where $\boldsymbol{\sigma}$ are total stresses, χ is a coefficient that is zero if the soil is unsaturated and 1 if saturated, α is the thermal expansion coefficient and \mathbf{D} is the elastic constitutive matrix. Therefore, net stresses are being used in the unsaturated range whereas Terzaghi's effective stresses are employed when the material is saturated. Swelling behaviour is incorporated via the swelling pressure \mathbf{p}_{sw} that depends on degree of saturation, S , according to:

$$\mathbf{p}_{sw} = S^2 p_{sw}^{\max} \mathbf{I} \quad (2-18)$$

where p_{sw}^{\max} is a model parameter.

2.4 CIMNE

The computations by CIMNE [6] were performed with computer code CODE_BRIGHT (version 2.2). The main characteristics of this code have already been presented in Section 2.1. The same thermo-hydraulic constitutive models have also been used. For the mechanical behaviour, the BBM without modifications has been adopted as mechanical constitutive model with an additional term to account for thermal expansion.

2.5 Clay technology-1

Again, the version 2.2 of CODE_BRIGHT has been used by Clay Tecnology-1 [7] to perform the coupled THM analyses (see Section 2.2). The specific feature in this case refers to the behaviour postulated inside the main yield surface in the BBM model. The nonlinear elastic volumetric strain is defined as:

$$d\varepsilon_v^e = \frac{\kappa_i(s)}{1+e} \frac{dp}{p} + \frac{\kappa_s(p,s)}{1+e} \frac{ds}{s+0.1} + (\alpha_0 + 2\alpha_2 \Delta T) dT \quad (2-19)$$

and

$$\kappa_i(s) = \kappa_{i0} \left[1 + \alpha_i s + \alpha_{its} \ln \left(\frac{s+0.1}{0.1} \right) \right] \quad (2-20)$$

$$\kappa_s(p, s) = \kappa_{s0} \left[1 + \alpha_{sp} \ln \left(\frac{p}{p_{ref}} \right) \right] e^{\alpha_{ss} s} \quad (2-21)$$

where p is the mean net stress, s is suction and T is temperature. κ_{i0} , κ_{s0} , α_o , α_2 , α_i , α_{ils} , α_{sp} and α_{ss} are model parameters. Different parameters for swelling and shrinking were used. For swelling:

$$\begin{aligned} \kappa_i(s) &= 0.25 \cdot \left[1 + 0.0009 \cdot s - 0.15 \cdot \ln \left(\frac{s+0.1}{0.1} \right) \right] \\ \kappa_s(p) &= 0.28 \cdot \left[1 - 0.21 \cdot \ln \left(\frac{p}{0.1} \right) \right] \end{aligned} \quad (2-22)$$

and for shrinking:

$$\kappa_i(s) = 0.02 \quad \kappa_s(s) = 0.16 \cdot e^{-0.04s} \quad (2-23)$$

2.6 Clay technology-2

The ABAQUS computer code was used by Clay Technology-2 [10] to perform the THM numerical computations. The code solves the balance equations for water mass, momentum (equilibrium) and energy using a staggered (T-HM) but coupled scheme (Figure 2-1).

With respect to the adopted constitutive laws, the following points can be made:

- Vapour flow is modelled as a diffusion process driven by a temperature gradient and a vapour pressure gradient:

$$q_v = -D_{Tv} \nabla T - D_{pv} \nabla p_v \quad (2-24)$$

where q_v is the vapour flux, D_{Tv} and D_{pv} are the thermal and pressure diffusion coefficients, T is temperature and p_v is the vapour pressure. Because thermal effects are generally dominant in non-isothermal problems, it was assumed that D_{pv} was zero. The variation of D_{Tv} with degree of saturation, S_r , was set empirically to:

$$D_{Tv} = D_{Tvb} \quad (0.3 \leq S_r \leq 0.7) \quad (2-25)$$

$$D_{Tv} = D_{Tvb} \cdot \cos^a \left(\frac{S_r - 0.7}{0.3} \cdot \frac{\pi}{2} \right) \quad (S_r \geq 0.7) \quad (2-26)$$

$$D_{Tv} = D_{Tvb} \cdot \sin^b \left(\frac{S_r}{0.3} \cdot \frac{\pi}{2} \right) \quad (S_r \leq 0.3) \quad (2-27)$$

- The mechanical model is established in terms of Bishop's (or average) stress:

$$\bar{\sigma}^* = \sigma + \chi u_w \mathbf{I} \quad (2-28)$$

where σ is the total stress, u_w is the pore water pressure, χ is a function of the degree of saturation ($\chi = S_r$ is assumed in this case), and \mathbf{I} the unit matrix. The constitutive models used are ABAQUS' *Porous Elastic Model* that assumes a logarithmic relationship between void ratio and mean effective stress and the well-known Drucker-Prager model together. Thermal expansion is accounted only by the thermal expansion of the phases (although the solid phase expansion is neglected), no thermal deformation of the soil structure is considered.

- The swelling properties of the bentonite are explicitly taken into account via a moisture swelling model that computes an additional volumetric strain increment as:

$$\Delta \varepsilon_v = f(S_r) = \ln(p_0/p) \cdot \kappa / (1 + e_0) \quad (2-29)$$

where p is the current effective mean stress, p_0 is the initial mean effective stress, κ is the bulk modulus and e_0 is the initial void ratio.

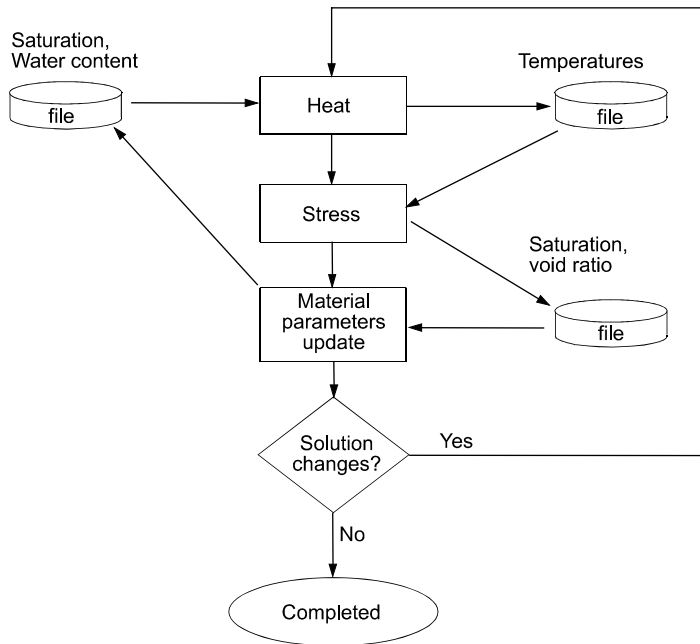


Figure 2-1. Staggered scheme used in the ABAQUS code.

2.7 CRIEPI

The CRIEPI team [11] used the code LOSTUF that solves in a coupled manner the balance equations for water mass, momentum (equilibrium) and energy. In contrast to other formulations, mechanical work is included in the energy balance equation although it is bound to be negligible in the type of problems include in this Task. Indeed, it was not included in the computations performed. Air mass balance is not considered, gas pressure is implicitly assumed constant.

Concerning the constitutive laws:

- Vapour flow: Fick's law as defined in Section 2.1.
- Mechanical behaviour: Using Bishop's effective stresses, the following expression is used:

$$d\sigma' = \mathbf{D} : (d\epsilon - d\epsilon_T - d\epsilon_{sw}) = \mathbf{D} : (d\epsilon - \mathbf{I}\beta_{TD}dT - \mathbf{I}d\omega_{sw}) \quad (2-31)$$

where \mathbf{D} is the elastic matrix, β_{TD} is drained linear thermal expansion coefficient of the medium, and ω_{sw} is the swelling expansion.

- The swelling expansion is modelled using the Komine and Ogata (1996, 2003) theoretical model that is based on the Gouy-Chapman diffuse double layer theory. In this case, the model is not empirically-based; specifying the physical and chemical properties of the buffer material, such as the density of montmorillonite, exchangeable ion capacity, the swelling pressure or swelling strain of the saturated buffer material can be calculated. The basic model has been modified by Tamaka and Nakamura (2004) to accommodate the swelling characteristics of calcium bentonite and the effect of saline water infiltration. A detailed description of this interesting model is presented in Appendix I of [11].

2.8 GRS

The computers codes VAPMOD (isothermal conditions) and VIPER (non-isothermal conditions) were used by GRS [12]. The formulation underlying them is drastically different from those outlined in the previous sections. It is assumed that vapour flow is the only relevant water transport mechanism (together with hydration of vapour in the clay minerals). It is assumed that the strain within the bentonite can be neglected under constant volume conditions; thereby mechanical effects are not considered. Also water transport is additionally considered to be decoupled from heat transport. The only equation solved is the water mass balance (considering vapour only):

$$\frac{\rho_d}{\rho_{v\text{ sat}}} \frac{\partial w}{\partial r_h} \frac{\partial \rho_v}{\partial t} + \rho_d \frac{\partial w}{\partial T} \frac{\partial T}{\partial t} - D_a \Delta \rho_v - \frac{\partial D_a}{\partial T} \nabla T \cdot \nabla \rho_v = 0 \quad (2-32)$$

where r_d is the bentonite dry density, w water content, r_h relative humidity, r_v the vapour pressure, T temperature and D_a the macroscopic diffusion coefficient.

The equation above is solved with the finite element method in one dimension. The energy balance equation was not included in the formulation. For the non-isothermal test the measured data was used to generate transient temperature fields by means of non-linear interpolation and extrapolation.

In this formulation, the basic constitutive law is that of vapour diffusion; Fick's law is assumed:

$$I_w = -\tau \Phi D \nabla \rho_v = D_a \nabla \rho_v \quad (2-33)$$

where I_w is the diffusive vapour mass flux, τ is tortuosity, Φ is porosity and D the coefficient of binary gas diffusion. The value of D is given by:

$$D = D^0 \frac{p^0}{p} \left(\frac{T}{T^0} \right)^\theta \quad (2-34)$$

where D^0 , p^0 and T^0 are the diffusion coefficient, pressure and temperature, respectively, under reference conditions.

2.9 MARINTEL

A specially developed finite element code (FreeFEM++) has been used by MARINTEL [13, 14]. It solves the balance equations for water mass, momentum (equilibrium) and energy in a staggered uncoupled manner. A feature of the formulation is to base the constitutive equations on continuum thermodynamics by deriving the equations of the state as partial derivatives of the Helmholtz free energy. As a result some extra terms appear that are generally not significant in the computations performed. For instance, the moisture mass flow is given by:

$$w^w = D_\varepsilon \nabla \varepsilon - D \nabla m^w - D_T \nabla T \quad (2-35)$$

where w^w is the water mass flux, ε are strains, m^w is the water mass per unit volume, T is temperature and D_ε, D, D_T the relevant diffusion coefficients. In this equation, only the second term is dominant.

It is a departure from other models the fact that water flow is a diffusion process driven by moisture gradients instead of potential gradients. The two can be closely related but difficulties may arise if different materials are considered in the same problem. The effect of liquid pressure (without the gravity term) is in fact reintroduced by the expression:

$$w^w / \rho^w = -k_{sat}^* (S_r)^\delta \frac{\nabla p_L^w}{\rho^w g} \quad (2-36)$$

where ρ^w is the water density, k_{sat} the saturated intrinsic permeability, S_r the degree of saturation, p_L^w is the liquid pressure and g is the gravity constant.

Finally, a poroelastic model is used for the mechanical constitutive law. Terzaghi's effective stress is used for saturated materials and Biot's stress for the unsaturated ones with rather low values of Biot's coefficient (0.3 for MX-80 bentonite and 0.12 for Febex bentonite).

2.10 TUL

The TUL team [15,16] used the computer code ISERIT, a finite element code that solves the set of balance equations in a fully coupled (monolithic) manner (Hokr and Frydrych 2012). The water mass balance (including water vapour and absorbed water only) and energy balance equations are considered. In addition the transfer of water between vapour in the pores and absorbed water in the solid phase is also taken into account. There is no flow of the adsorbed water; all water movement is by vapour migration. In this respect, the formulation is similar to that outlined in Section 2.8.

The relevant balance equations are:

$$c_{v(T,C_a,C_b)} \frac{\partial T}{\partial t} = \nabla \cdot (\lambda_{(T,C_a,C_b)} \nabla T) + \chi_{(T,C_a,C_b)} \frac{\partial C_b}{\partial t} \quad (2-37)$$

$$\varepsilon \frac{\partial C_a}{\partial t} + (1-\varepsilon) \frac{\partial C_b}{\partial t} = \nabla \cdot (D_{a(T,C_a,C_b)} \frac{\varepsilon}{\tau} \nabla C_a) \quad (2-38)$$

$$\frac{1}{\varepsilon} \frac{\partial C_b}{\partial t} = \left(\frac{C_a}{C_a^{100}} - \varphi(C_b) \right) \gamma_{(T,C_a,C_b)} \quad (2-39)$$

where T is the temperature, C_a concentration of air humidity, C_b concentration of bentonite humidity (adsorbed), t time, c_v volumetric specific heat capacity, χ latent heat of adsorption, λ coefficient of heat conductivity, ε porosity, D_a diffusion coefficient of water vapor, τ tortuosity, C_a^{100} concentration of humidity for 100 % relative humidity (RH) of air (absolute humidity of saturated vapor), $\varphi(C_b)$ inverse sorption curve, φ meaning the relative humidity and γ is the coefficient of water transfer rate between bentonite and air. The water content [%] can be evaluated as $w = C_b/C_b(100 \%)$. All the required coefficients and relationships are a function of relative humidity and temperature.

2.11 Comments

A large variety of codes have been used. Although it is true that three teams (AECL, CIMNE and Clay Technology-1) employ the same code (CODE_BRIGHT), in total 7 different codes have been used. This number provides a sufficient variety of approaches so that the Task is not simply a validation exercise of a single code. Table 2-2 lists the balance equations solved by the different codes as well as the type of formulation (i.e. whether it is coupled or uncoupled).

Table 2-2. Codes used, balance equations solved and type of formulation. Y/N: balance equation included/not included in the formulation. Y(V): only water vapour considered.

Group	Code	Balance equations				Type of formulation
		Water	Air	Energy	Equil.	
AECL	CODE BRIGHT	Y	Y	Y	Y	Coupled
BGR	GEOSYS	Y	N	Y	Y	Staggered coupled
	ROCKFLOW					
CIMNE	CODE BRIGHT	Y	Y	Y	Y	Coupled
Clay Technology1	CODE BRIGHT	Y	Y	Y	Y	Coupled
Clay Technology2	ABAQUS	Y	N	Y	Y	Staggered coupled
CRIEPI	LOSTUF	Y	N	Y	Y	Coupled
GRS	VAPMOD VIPER	Y(V)	N	N	N	Single equation
MARINTEL	FreeFEM++	Y	N	Y	Y	Staggered not fully coupled
TUL	ISERIT	Y(V)	N	Y	N	Coupled

It can be noted that the equations solved by most codes (CODE_BRIGHT, GEOSYS, ABAQUS, LOSTUF, FreeFEM++) are the same: water mass balance, energy and equilibrium and that the calculation is performed in a coupled manner. The computational scheme of some of these codes is staggered but coupled (GEOSYS and ABAQUS); this is a choice that should not affect the final result. Only FreeFEM++ performs the staggered scheme in an uncoupled manner thus not ensuring full convergence at the end of each step. FreeFEM++ bases the formulation, at the cost of some generality, in a consistent thermodynamic approach but the resulting equations differ little from those of the other codes obtained adopting a phenomenological approach. Only the CODE_BRIGHT formulation includes the balance equation for dry air.

Two of the formulations (VAPMOD/VIPER and ISERIT) are however quite different. They only solve the problem of vapour flow in non-isothermal conditions. In both cases, equivalent storage terms arise from the transfer of water between vapour in the pores and absorbed water in the solid phase. In this way they lack the flexibility to address other problems in which this phenomenon is not the dominant one. This is the reason why they have not performed computations in some of the cases proposed. ISERIT solves the non-isothermal problem coupling the energy balance equation with the vapour transport one. In contrast, VIPER does not consider the energy balance equation, experimentally observed temperature variation are introduced directly into the calculation.

Table 2-3 indicates the different phenomena that are taken into account by the different formulations. They mostly reflect the difference in the formulation. Thus mechanical behaviour and liquid flow are not part of the formulation of VAPMOD/VIPER and ISERIT. Some of the general formulations do not consider advective transport of heat but, in this case, it has no practical consequences since heat conduction is dominant due to the low permeability of the material. It is noteworthy that all formulations include vapour flow and, except VAPMOD/VIPER, heat conduction.

Finally, Table 2-4 summarises some information on the constitutive laws adopted by different teams. Not included in the Table is heat conduction since all teams use Fourier's law as constitutive relationship. It should also be noted that in all models where liquid flow is considered, the phenomenon is assumed governed by the generalized Darcy's law (in the case of MARINTEL via a diffusion equation). There is more variety concerning vapour diffusion. Some groups use Fick's law whereas others adopt a double diffusion coefficient approach, related to Philip and de Vries (1957) formulation. The use of Fick's law probably complies better with the basic physical principle but the double coefficient approach provides some additional flexibility. In turn, the double coefficient approach requires more information to determine the required parameters. It is also interesting to observe that tortuosity is included in the vapour diffusion laws to take into account that vapour migration takes place in the voids of a porous material.

Table 2-3. Phenomena incorporated in the formulation. Y/N: Yes/No. Notation: Cond: Conduction, Adv: advection, Lat. heat: latent heat, Liq.: Liquid, Vap: Vapour, Therm exp.: Thermal expansion.

Group	Heat transport				Water flow		Air flow	Mechanical behaviour	
	Cond	Adv. (l)	Adv. (v)	Lat. heat	Liq.	Vap.	Gas	Therm. exp.	Suction effect
AECL	Y	Y	Y	Y	Y	Y	Y	Y	Y
BGR	Y	Y	Y	Y	Y	Y	N	Y	Y
CIMNE	Y	Y	Y	Y	Y	Y	Y	Y	Y
Clay Technology 1	Y	Y	Y	Y	Y	Y	Y	Y	Y
Clay Technology 2	Y	Y	N	N	Y	Y	N	Y	Y
CRIEPI	Y	Y	Y	Y	Y	Y	N	Y	Y
GRS	N	N	N	N	N	Y	N	N	N
MARINTEL	Y	N	N	N	Y	Y	N	N	Y
TUL	Y	N	N	Y (a)	N	Y	N	N	N

The largest variety of constitutive laws concerns, not unexpectedly, the mechanical behaviour (for the formulations that incorporate the mechanical component). There is general agreement in using Terzaghi's effective stress as the relevant stress variable in saturated conditions. In the unsaturated range, some (CODE_BRIGHT, GEOSYS) adopt net stress as the constitutive variables while others (ABAQUS, LOSTUF) use the Bishop stress. In FreeFEM++, a Biot stress definition is used with fixed values (depending on the type of bentonite) of the Biot coefficient. This is equivalent to the use of Bishop stress with a fixed χ parameter, independently of the degree of saturation.

There is also variety in the mechanical constitutive laws employed. CODE_BRIGHT uses the elastoplastic Barcelona Basic Model (BBM), ABAQUS the elastoplastic Drucker-Prager model whereas elastic and poroelastic laws are used by GEOSYS, CRIEPI and FreeFEM++. More relevant in the context of this Task is the fact that all mechanical models incorporate a specific ingredient devoted to the simulation of the key swelling properties of the bentonite. In CODE_BRIGHT a number of modifications of the nonlinear elastic behaviour inside the main yield locus are used whereas in other

codes (GEOSYS, ABAQUS, LOSTUF) an additional swelling component is incorporated for this purpose. It should be noted that the swelling model of LOSTUF is derived from basic physical principles at the cost, inevitably, of some degree of flexibility. In Abaqus a special procedure (moisture swelling) is used for unsaturated soil in order to cope with the fact that the effective stress theory only handles one variable while two are required in partly saturated soil. With this procedure the degree of saturation affects the mechanical response.

Table 2-4. Main constitutive equations and stress variables adopted by the different modelling teams.

Group	Code	Liquid flow	Vapour diffusion	Mechanical	Stress variables
AECL	CODE BRIGHT	Generalized Darcy	Fick	BBM (modified elastic part)	Net stress (unsaturated) Effect. stress (saturated)
BGR	GEOSYS ROCKFLOW	Generalized Darcy	Double diffusion coefficient	Elastic + swelling model	Net stress (unsaturated) Effect. stress (saturated)
CIMNE	CODE BRIGHT	Generalized Darcy	Fick	BBM	Net stress (unsaturated) Effect. stress (saturated)
Clay Technology1	CODE BRIGHT	Generalized Darcy	Fick	BBM (modified elastic part)	Net stress (unsaturated) Effect. stress (saturated)
Clay Technology2	ABAQUS	Generalized Darcy	Double diffusion coefficient	Drucker Prager + porous elastic + swelling model for unsaturated conditions	Bishop stress
CRIEPI	LOSTUF	Generalized Darcy	Fick	Elastic + swelling model	Bishop stress
GRS	VAPMOD VIPER	–	Fick	–	–
MARINTEL	FreeFEM++	Diffusion law (Generalized Darcy)	Temperature gradient driven	Poroelastic model	Biot coeff. (unsaturated) Effect. stress (saturated)
TUL	ISERIT	–	Double diffusion coefficient	–	–

3 Description of the laboratory experiments

The Task is structured in three different SubTasks corresponding to three different sets of experiments that are briefly described in this Section. The full description of the tests as given to the modelling teams is presented in Appendices A to C.

3.1 Subtask 1.1 – Tests performed by CEA

CEA performed two THM mock up tests in the laboratory on compacted MX-80 bentonite using two different initial water contents (Gatabin and Billaud 2005). Each test is composed of two phases. In Phase 1 heat is applied to one end of the column while the temperature at the other end is kept constant and equal to 20 °C. A maximum temperature of 150 °C is applied. Phase 2 starts after thermal equilibrium has been achieved and involves the gradual hydration of the sample. A constant water pressure is applied to the end opposite to the one where the temperature variation was prescribed. Constant volume conditions are ensured in the two phases of the test.

The following parameters were measured during the tests:

- Temperatures
- Relative humidity
- Pore pressure
- Total axial stress
- Total radial stress

The samples have both a diameter and a height of 203 mm. The specimens are tested in an apparatus the diagram of which is shown in Figure 3-1. The samples are tightly enclosed in a PTFE sleeve. To minimize heat losses, the cells were insulated with a heatproof envelope. Experiments are not gas tight. Heat is applied at the bottom plate whereas hydration proceeds from the top of the sample. Figure 3-2 shows a picture of one of experiments under way.

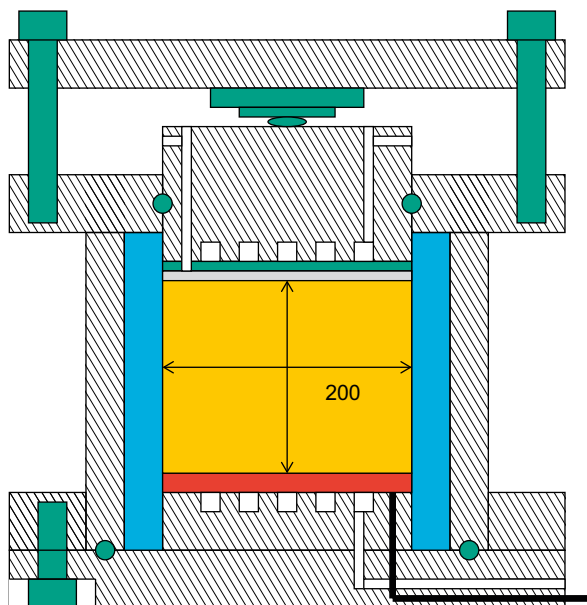


Figure 3-1. Layout of the experimental cell.

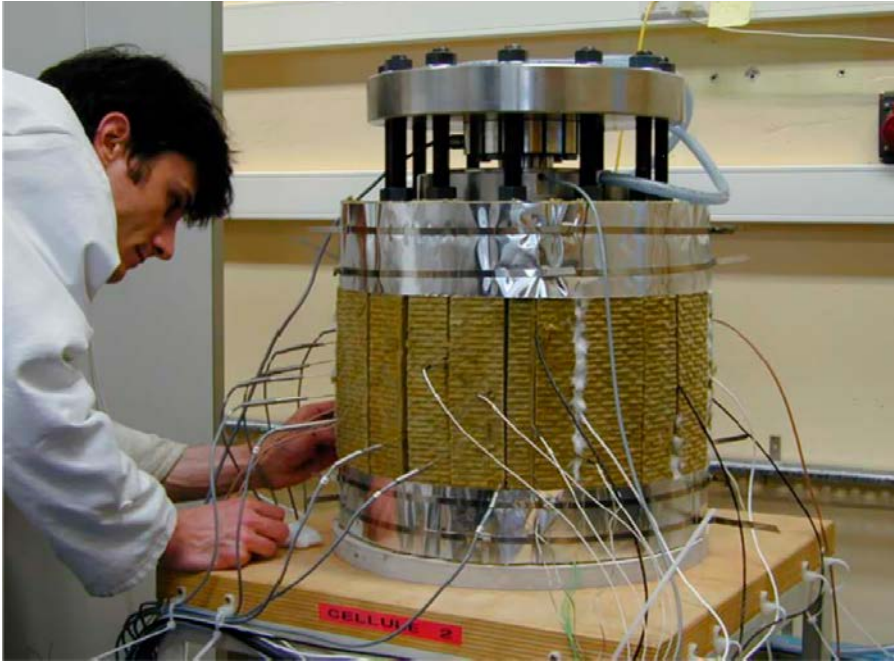


Figure 3-2. Mock up experiment by CEA.

Compacted MX-80 bentonite has been used to manufacture the specimens tested. For the specimen of Cell 1, the bentonite was stabilised in an atmosphere with a relative humidity of 60 % whereas for the specimen of Cell 2, the bentonite was stabilised in an atmosphere with a relative humidity of 90 %. A target dry density of 1.7 g/cm³ was adopted for compaction. A more comprehensive description of the SubTask, the characteristics of the material at the time of emplacement and the properties of MX-80 bentonite are collected in Appendix A.

3.2 Subtask 1.2 – Tests performed by CIEMAT

Two infiltration experiments were performed in CIEMAT's large cells (Figure 3-3); the first one is an isothermal test whereas the second one is a test with a thermal gradient applied (Villar et al. 2005).

The following parameters are measured during the tests:

- Temperatures
- Relative humidity

Water intake was also measured but the observations were not considered reliable. No mechanical parameters are measured during the test.

The infiltration tests were performed in cylindrical cells enclosing a specimen 7 cm diameter and 40 cm long (Figure 3-4). The 15 mm thick cell wall is made of Teflon PTFE. A 4 mm thick stainless steel shell provides mechanical reinforcement to resist the swelling pressures developed during the tests. The cell containing the thermal gradient test is additionally surrounded by a 15-mm thick foam layer for insulation purposes. Heat was applied to the bottom of the specimen and hydration was performed from the top end of the specimen where a cooling system maintained the temperature constant.

The material tested is FEBEX bentonite. The clay was statically compacted (average compaction pressure of 30 MPa) at hygroscopic water content (around 13 %–14 % gravimetric water content) to a nominal dry density of 1.65 g/cm³. Information on the properties of this bentonite is collected in Appendix B.



Figure 3-3. Infiltration tests performed by CIEMAT.

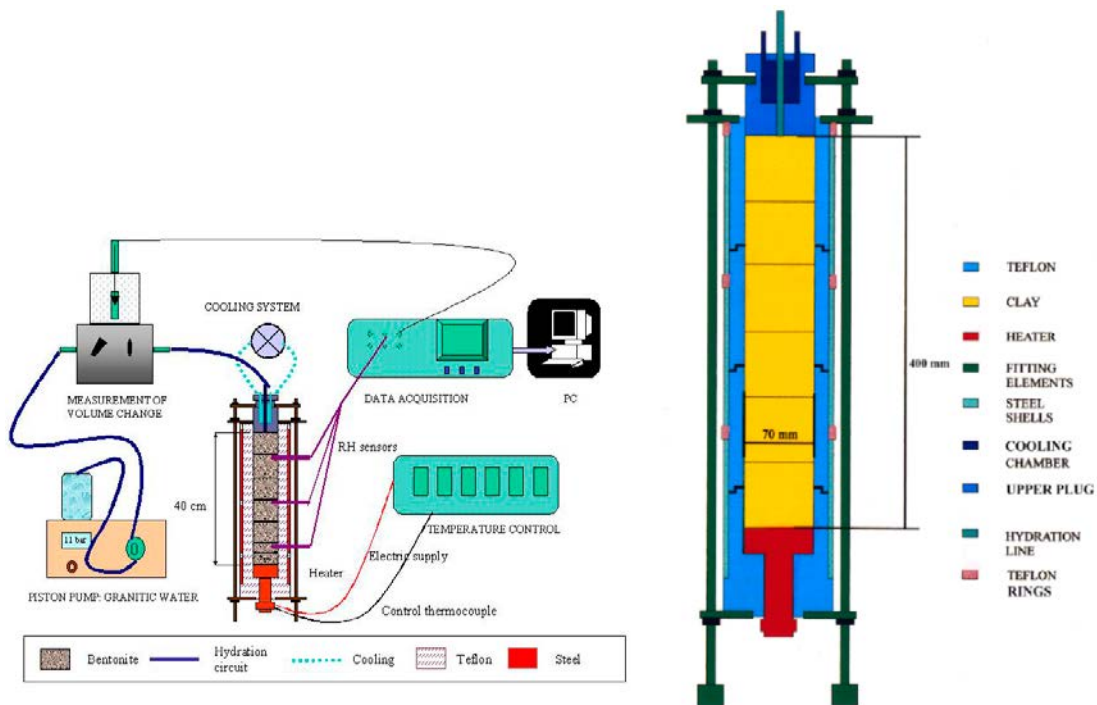


Figure 3-4. Layout of the infiltration test.

In the *isothermal test (test I40)*, the hydration system was connected 18 hours after data acquisition started. In the *thermal gradient test (test GT40)*, the cooling system and the heater were started simultaneously after cell assembly and instrument installation (initial phase). A temperature of 100 °C was applied at the bottom of the sample. After 65 hours of heating, hydration was started (second phase).

In both cases hydration was performed using low salinity water at a pressure of 1.2 MPa. The temperature applied by the cooling system corresponds to the ambient temperature of the laboratory and it underwent some moderate variations that were recorded.

3.3 Subtask 1.3 – Test performed by UPC

This Subtask was incorporated to the Task 1 specifications at a later stage to cover ranges of behaviour not adequately covered by SubTask 1 and 2. It involves a heating test performed at UPC with no infiltration. This test allows a more direct observation of vapour transfer phenomena since, in the absence of water infiltration, it is the main mechanism of water transfer.

Conceptually, the test is depicted in Figure 3-5. Two cylindrical samples of compacted Febex bentonite are subjected to a prescribed heat flow from one end. The temperature is kept constant at the other end. The two specimens are symmetrically placed with respect to the heater.

The following parameters are measured:

- Temperatures at various points throughout the test.
- Water content at the end of the test.
- Specimen diameter at the end of the test.

The layout of the apparatus used for performing the test is depicted in Figure 3-6. The two cylindrical specimens (38 mm diameter, 76 mm height) were placed vertically in the apparatus, with the heater located between them. A latex membrane that allowed deformation and keeps constant the overall water content and a layer of heat insulating material (composed of deformable foam, expanded polystyrene and glass fibre) surrounded the specimens. The ensemble was contained in a perspex tube. Pictures of the experiment and of the sample preparation are shown in Figure 3-7.

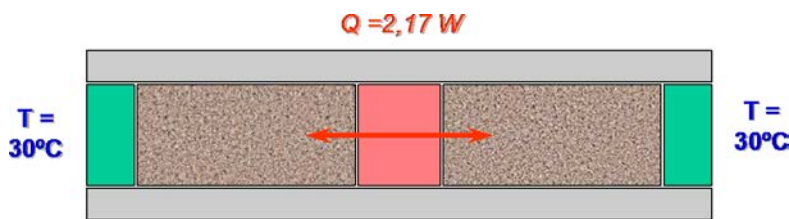


Figure 3-5. Conceptual scheme of the UPC heating test.

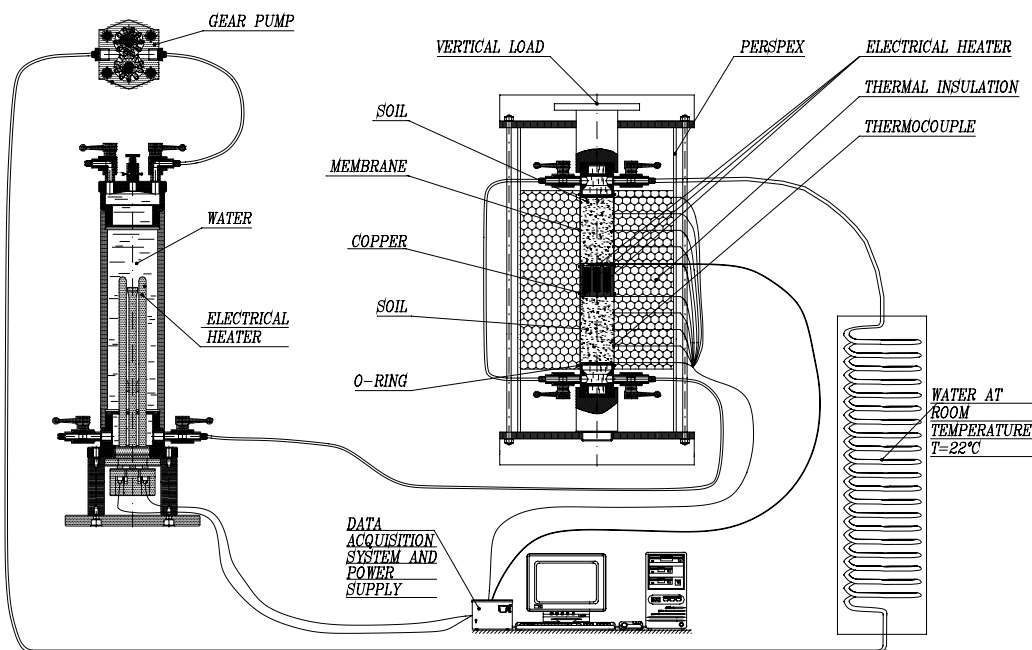


Figure 3-6. Layout of the UPC heating test.

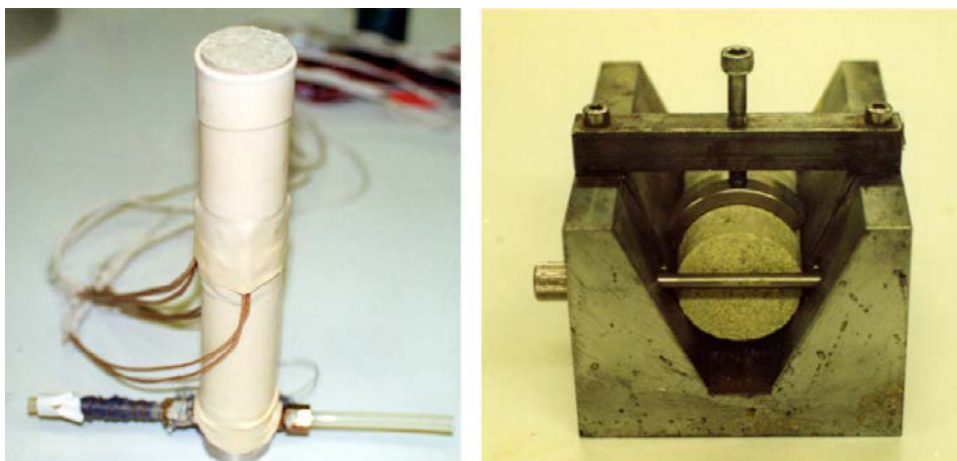


Figure 3-7. Experiment and sample preparation.

The heater was a copper cylinder (38 mm diameter, 50 mm height) with five small electrical resistances inside. The resistances were connected to an adjustable source of direct current that allows the control of input power from 0 to 5 W. At the cool ends, a constant temperature was maintained by flowing water through a stainless steel cap in contact with the soil. A temperature regulation system maintained the temperature of the contact between the cap and the soil practically constant, with variations smaller than 0.5 °C. In order to ensure a good contact between the caps and the samples, a light stress (about 0.05 MPa) was applied to the top of the test ensemble.

Only temperatures were measured during the test. Temperatures measurements were concentrated in one of the specimens; three measurements were made in the inside of the sample and two more on the hot and cool ends of the specimen. In the second sample, only one inside temperature measurement was made in the centre of the specimen that confirmed the symmetry of the temperature distribution.

A constant power of 2.17 W has been supplied by the heater during 7 days whereas at the opposite ends of the specimens a temperature of 30 °C was maintained. At the end of the 7 days, the heaters were switched off, the apparatus dismantled and the diameter and water content at different points of the specimens were determined. The diameter of the specimen was measured at 7 sections in each specimen with an accuracy of 0.01mm. To obtain the distribution of water content, each specimen was cut into six small cylinders, and the water content of each cylinder was determined.

Again Febex bentonite was used in this SubTask. The bentonite was compacted at a dry density of 1.63 g/cm³ and with a water content of 15.33 % (degree of saturation of 0.63).

3.4 Remarks

Table 3-1 contains the main features of the laboratory tests selected for Task 1. It can be noted that the full set of experiments provides a wide range of conditions for testing the performance of codes and formulations under THM conditions. Specifically, the effect of the following conditions and variables can, in principle, be observed:

- Type of bentonite: MX-80 vs. Febex.
- Maximum temperature: 150 °C in the CEA tests, lower temperatures in the CIEMAT and UPC tests.
- Isothermal vs. Thermal gradient tests in the CIEMAT experiments.
- Water content. Two values of water content in the CEA tests.
- Infiltration (CEA, CIEMAT rests) vs. no infiltration (UPC) conditions.

It is also apparent that the tests used in the Task meet the basic criteria set out above, i.e.: i) the experiments should incorporate many of the phenomena relevant to the EBS, and ii) the required modelling should not be too demanding on computer resources and code capabilities.

Table 3-1. Features of the laboratory tests of Task 1.

	Type of test	Bentonite	Dry density (g/cm ³)	w/c (%)	Maximum temperature	Laboratory
Subtask 1	Infiltration under thermal gradient	MX-80	1.791	13.66	150 °C	CEA
	Infiltration under thermal gradient	MX-80	1.735	17.86	150 °C	CEA
Subtask 2	Isothermal infiltration	Febex	1.65	12.7–13.5	Laboratory	CIEMAT
	Infiltration under thermal gradient	Febex	1.65	12.7–13.5	100 °C	CIEMAT
Subtask 3	Heating without infiltration	Febex	1.63	15.33	75 °C	UPC

4 Modelling results

4.1 General

In this section, the computations performed by the different teams are presented and discussed. Only selected results, those deemed most relevant, are shown here and are compared with the experimental results. The full set of results, parameters used and boundary and initial conditions adopted can be seen in the individual reports collected in the Report's Annex. As there is generally little difficulties in obtaining good results of the thermal problem, attention will be focused on the hydraulic output and, when available, mechanical variables. Thus, the following plots will be presented for all groups that have carried out the corresponding analyses:

Subtask 1.1:

- Temperature vs. time (Cell 1 and Cell 2)
- Distribution of temperatures at different times (Cell 1 and Cell 2)
- Relative humidity vs. time (Cell 1 and Cell 2)
- Distributions of relative humidity at different times (Cell 1 and Cell 2)
- Axial stress vs. time (Cell 1 and Cell 2)

Subtask 1.2:

- Relative humidity vs. time (Isothermal test)
- Temperature vs. time (Cell 1 and Cell 2)
- Relative humidity vs. time (Thermal gradient test)

Subtask 1.3:

- Temperature vs. time
- Distributions of temperatures at different times
- Distribution of water content at the end of the test
- Sample diameter change vs. distance

The teams were also encouraged to perform special computations or sensitivity analyses to check the effects of some key parameters or uncertain conditions. Again especially relevant results of those analyses are included in this section. Teams were also asked to check the mass conservation implicit in their codes using the Subtask 1.3 case where no water inflow or outflow is allowed.

It should be noted that those analyses were by no means a prediction exercise. The experimental results were known to the modellers and the teams had freedom to vary parameters (within certain bounds), numerical formulation and boundary conditions in order to achieve a good reproduction of the observations. In this way, the capabilities of the different codes and formulations could be determined, shortcomings recognized and areas of improvement and development identified.

4.2 AECL

4.2.1 CEA mock-up tests – Subtask 1.1 [1]

AECL performed THMg analyses, i.e. analyses in which the air balance equation was considered and gas pressures computed. This is commendable as the maximum temperatures achieved are above 100 °C and therefore a gas pressure constant and equal to atmospheric pressure is not a realistic assumption. For comparison THg (i.e. without the mechanical component) analyses have also been performed. Indeed, some severe convergence problems have been reported when the mechanical problem has been incorporated in the computations. This is why the computations of Phase 2 only reach 1 300 hours for Cell 1 and 400 hours for Cell 2 although 6 000 hours observations were available. The axisymmetric geometry and mesh used are shown in Figure 4-1a. They comprise 240 4-noded elements and 279 nodes.

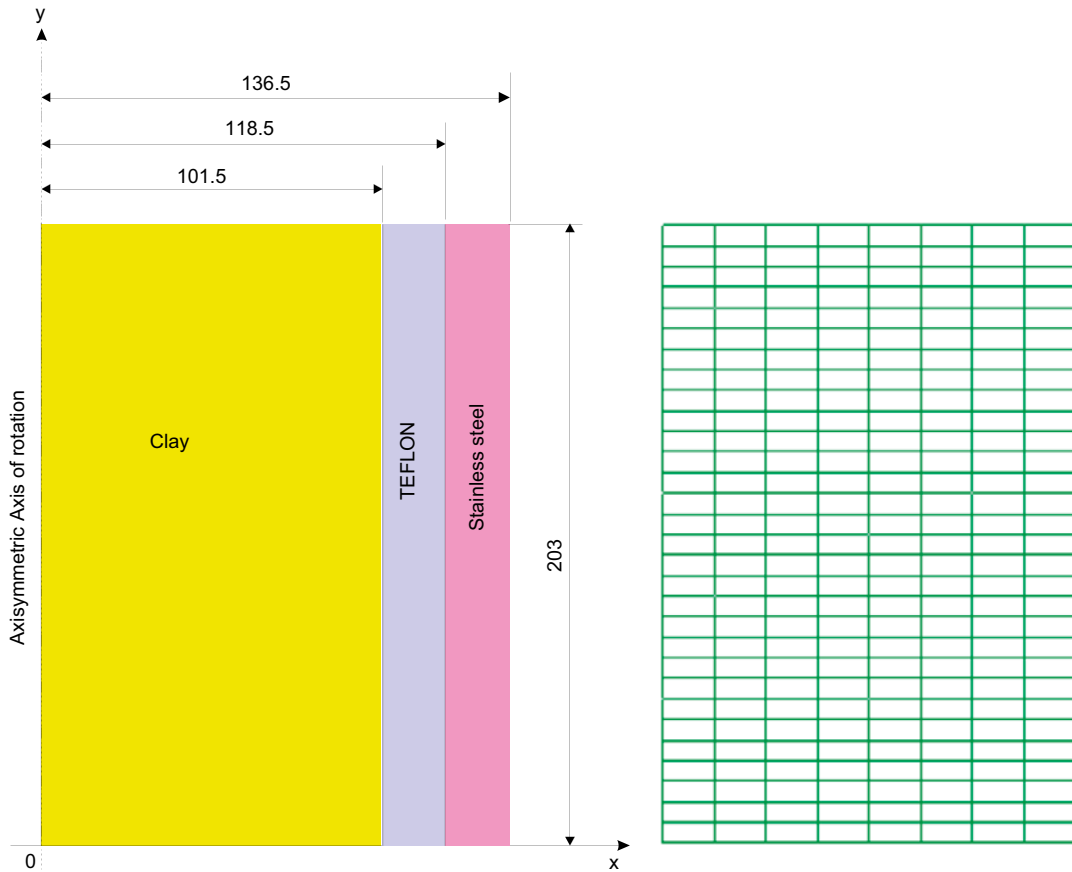


Figure 4-1a. Model geometry and mesh. AECL

Selected results for the THMg analyses for Cell 1 (water content: 13.66 %) are offered in Figures 4-1b to 4-1i. Note that this team presented the results of Phase 1 and 2 in separate plots. As this team performed THMg and THg analyses, their comparison provides an opportunity to check the effects of mechanical coupling. No differences were obtained in the computed temperatures but some mechanical effects were apparent in the evolution of relative humidifies. Results of the THg computations for Cell 1 are presented in Figures 4-1j to 4-1m. The effect is not large and, paradoxically, the results of the THg appear somewhat closer to observations. It should be noted that the THg analysis reached longer times as no significant convergence problems arose.

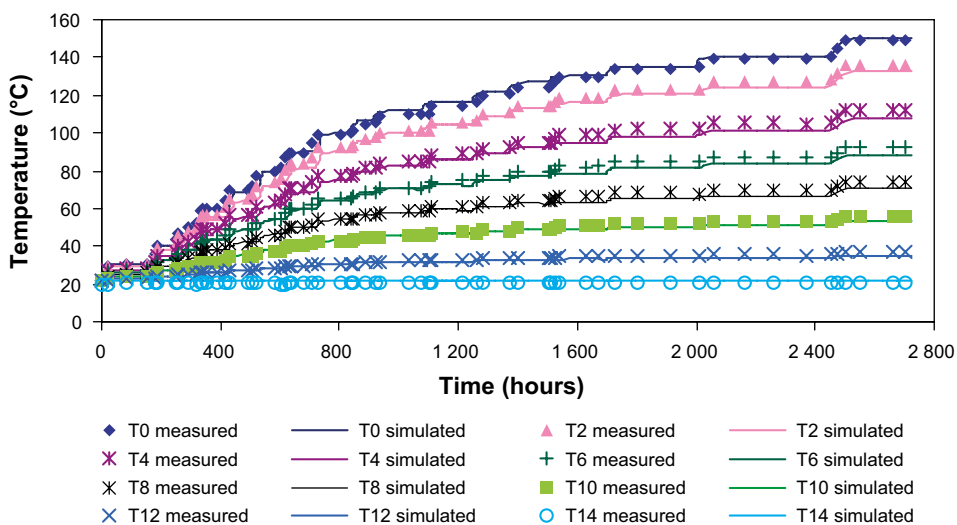


Figure 4-1b. Evolution of temperature with time, Cell 1, Phase 1. Computed results and observations. AECL.

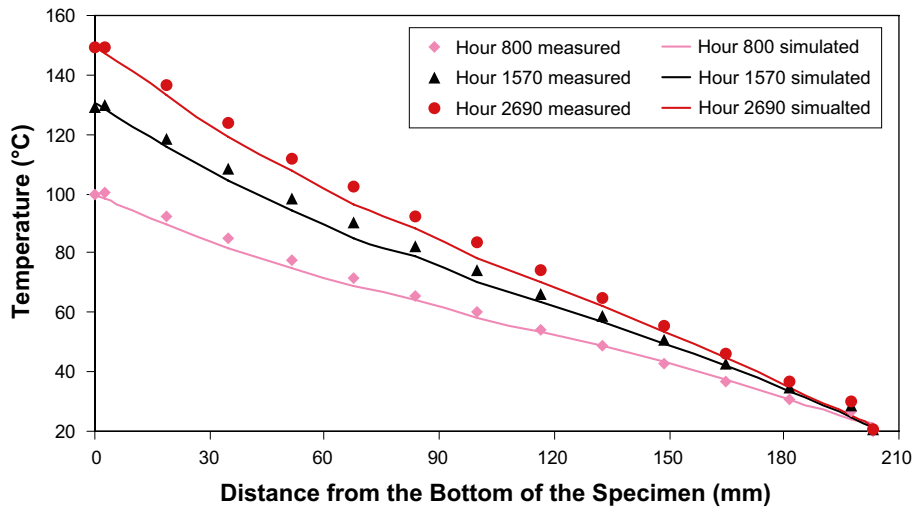


Figure 4-1c. Distributions of temperatures at different times. Cell 1, Phase 1. Computed results and observations. AECL.

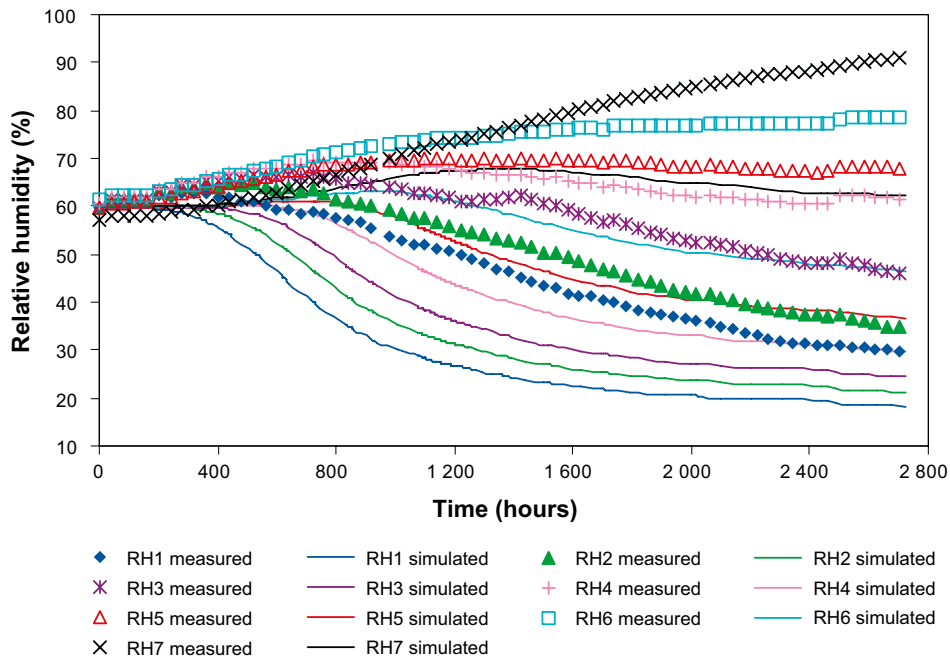


Figure 4-1d. Evolution of relative humidity with time, Cell 1, Phase 1. Computed results and observations. AECL.

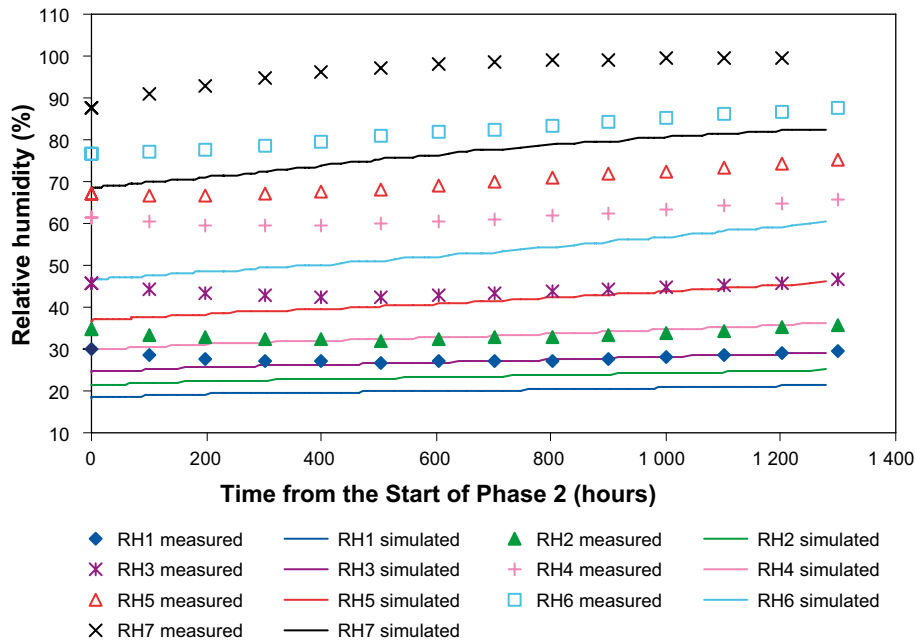


Figure 4-1e. Evolution of relative humidity with time, Cell 1, Phase 2. Computed results and observations. AECL.

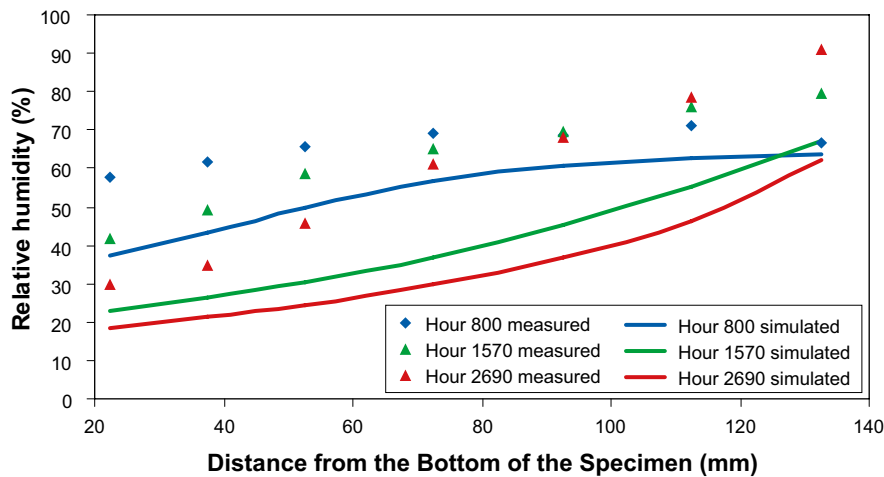


Figure 4-1f. Distributions of relative humidity at different times. Cell 1, Phase 1. Computed results and observations. AECL.

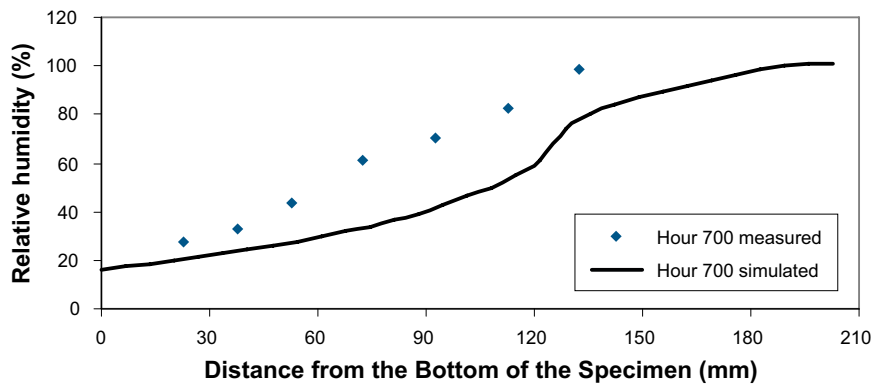


Figure 4-1g. Distributions of relative humidity at different times. Cell 1, Phase 2. Computed results and observations. AECL.

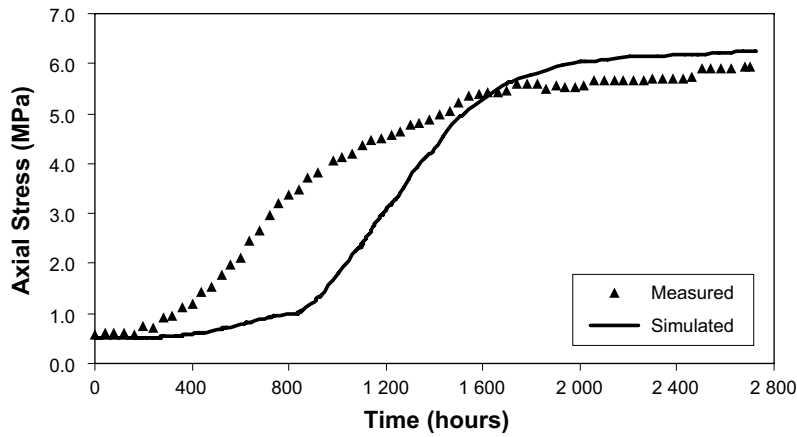


Figure 4-1h. Evolution of axial stress with time, Cell 1, Phase 1. Computed results and observations. AECL.

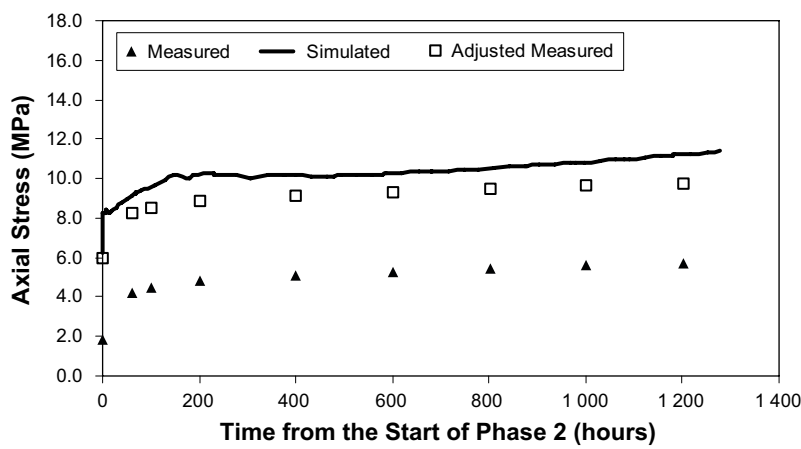


Figure 4-1i. Evolution of axial stress with time, Cell 1, Phase 2. Computed results and observations. The adjusted measured results are the observed results shifted upwards by 4 MPa for consistency with the end of Phase 1. AECL.

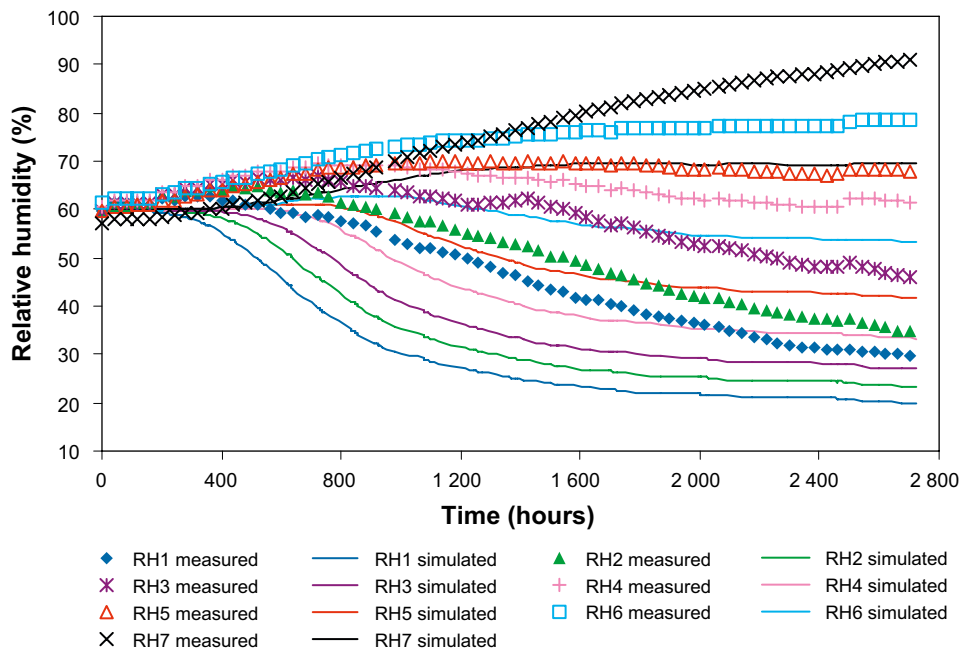


Figure 4-1j. Evolution of relative humidity with time, Cell 1, Phase 1. Computed results and observations. THg analysis. AECL.

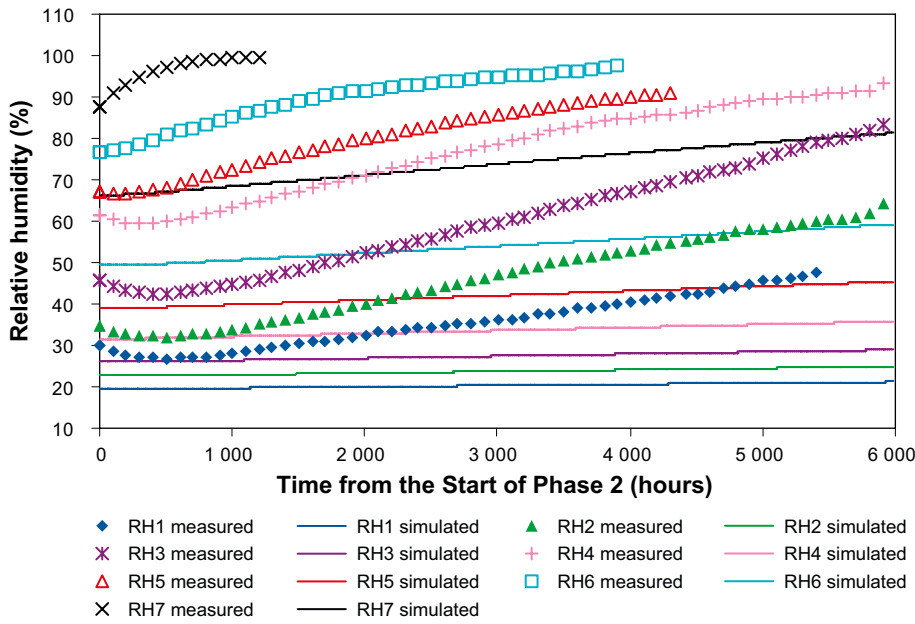


Figure 4-1k. Evolution of relative humidity with time, Cell 1, Phase 2. Computed results and observations. THg analysis. AECL.

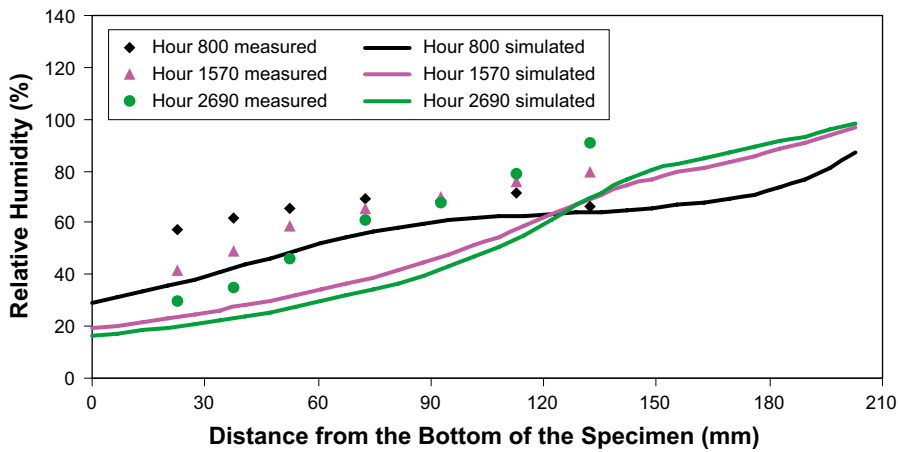


Figure 4-1l. Distributions of relative humidity at different times. Cell 1, Phase 1. Computed results and observations. THg analysis. AECL.

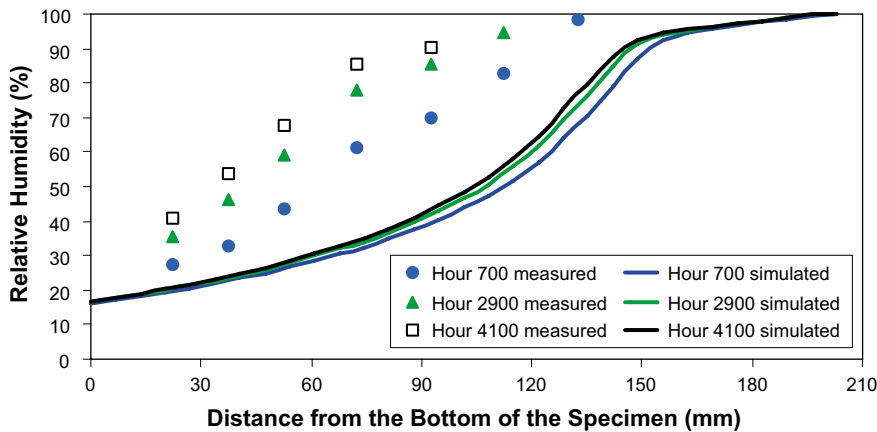


Figure 4-1m. Distributions of relative humidity at different times. Cell 1, Phase 2. Computed results and observations. THg analysis. AECL.

The selected results of the THMg analyses for Cell 2 (water content: 17.86 %) are collected in Figures 4-1n to 4-1t. Comparison with the results of the corresponding THg analysis (Figures 4-1u to 4-1x) is similar to that for Cell 1. Again, the THg analyses allow to examine the computed results for longer times.

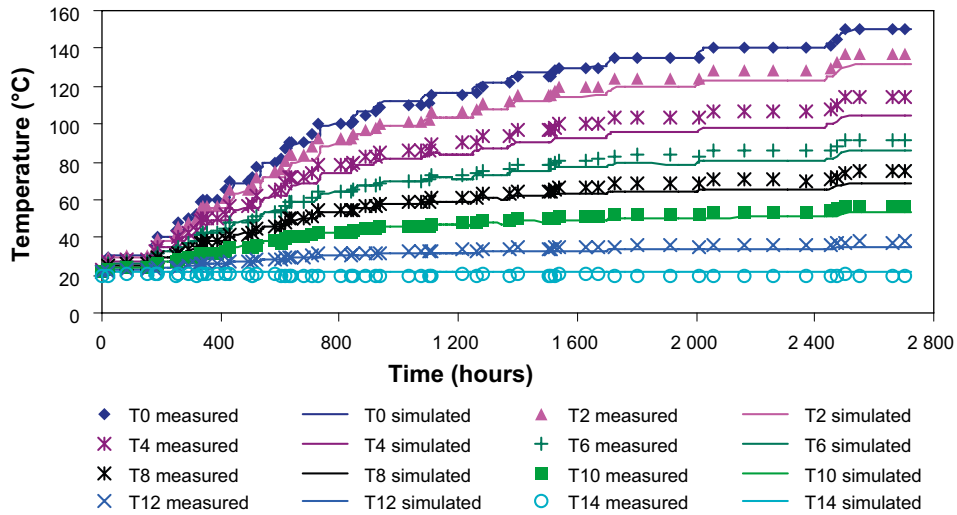


Figure 4-1n. Evolution of temperature with time, Cell 2, Phase 1. Computed results and observations. AECL.

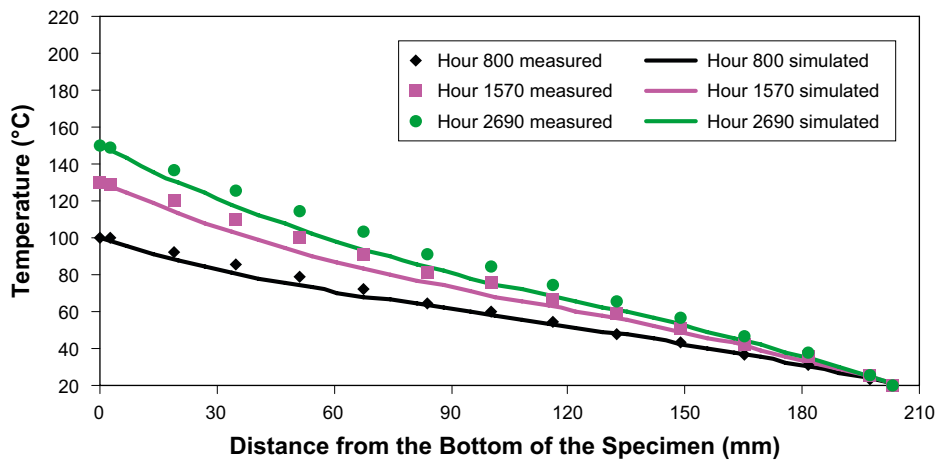


Figure 4-1o. Distributions of temperatures at different times. Cell 2, Phase 1. Computed results and observations. AECL.

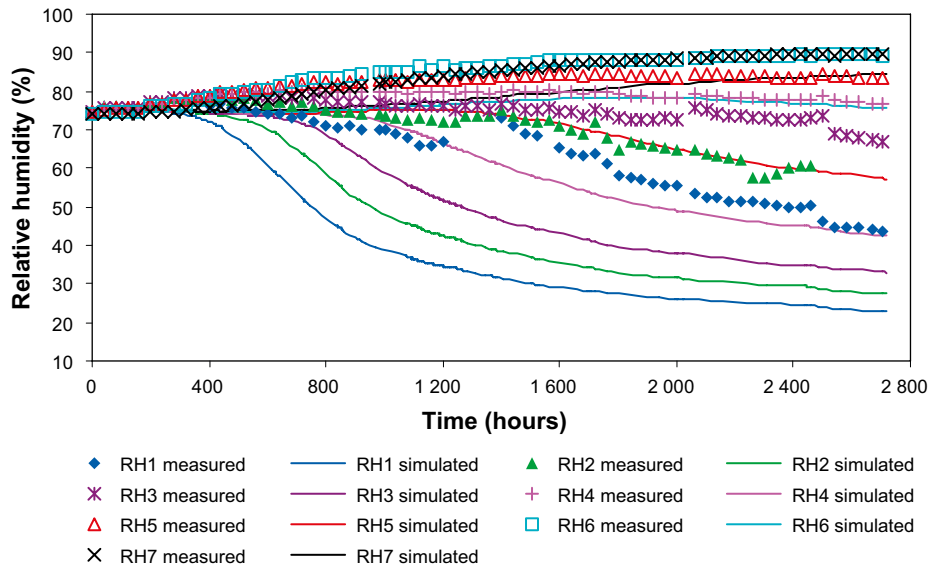


Figure 4-1p. Evolution of relative humidity with time, Cell 2, Phase 1. Computed results and observations. AECL.

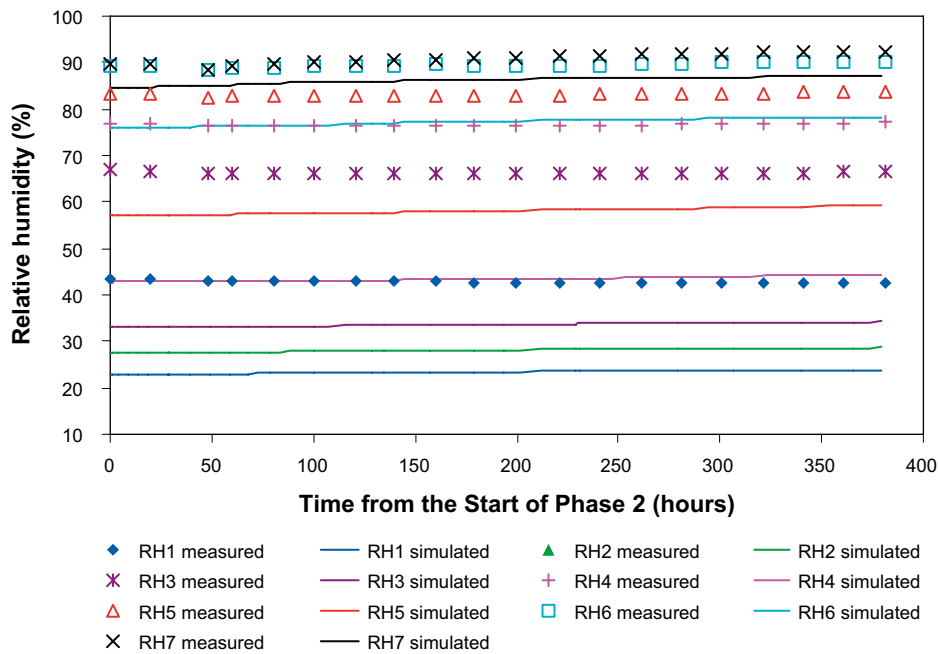


Figure 4-1q. Evolution of relative humidity with time, Cell 2, Phase 2. Computed results and observations. AECL.

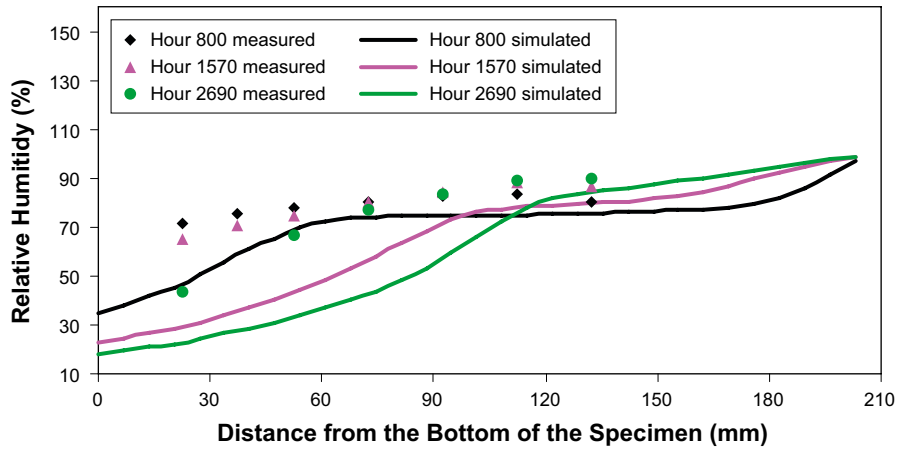


Figure 4-1r. Distributions of relative humidity as functions of distance from the Bottom of the Specimen (mm), at different times. Cell 2, Phase 1. Computed results and observations. AECL.

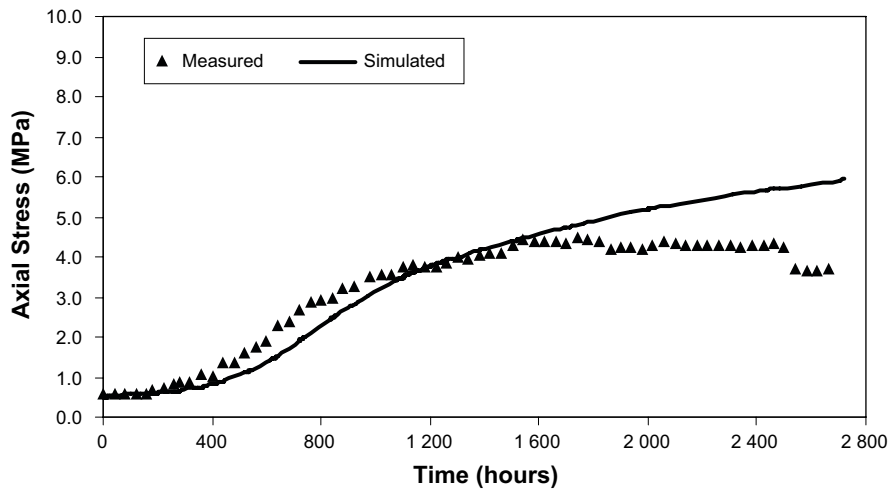


Figure 4-1s. Evolution of axial stress with time, Cell 2, Phase 1. Computed results and observations. AECL.

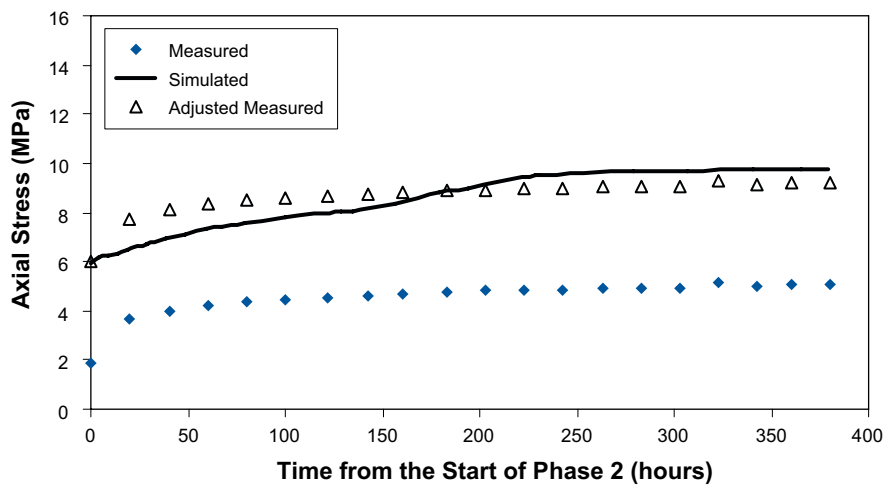


Figure 4-1t. Evolution of axial stress with time, Cell 2, Phase 2. Computed results and observations. The adjusted measured results are the observed results shifted upwards by 4 MPa for consistency with the end of Phase 1. AECL.

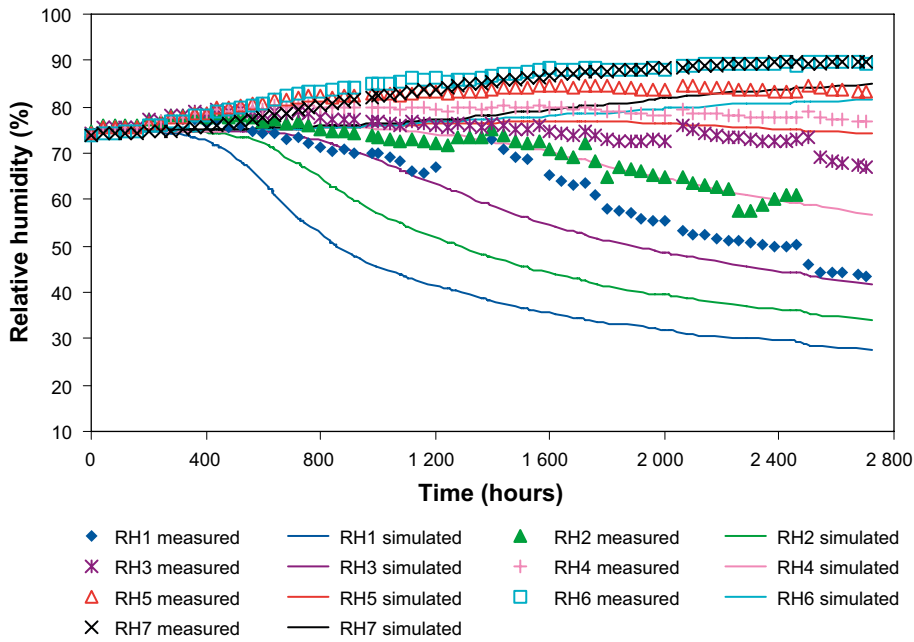


Figure 4-1u. Evolution of relative humidity with time, Cell 2, Phase 1. Computed results and observations. THg analysis. AECL.

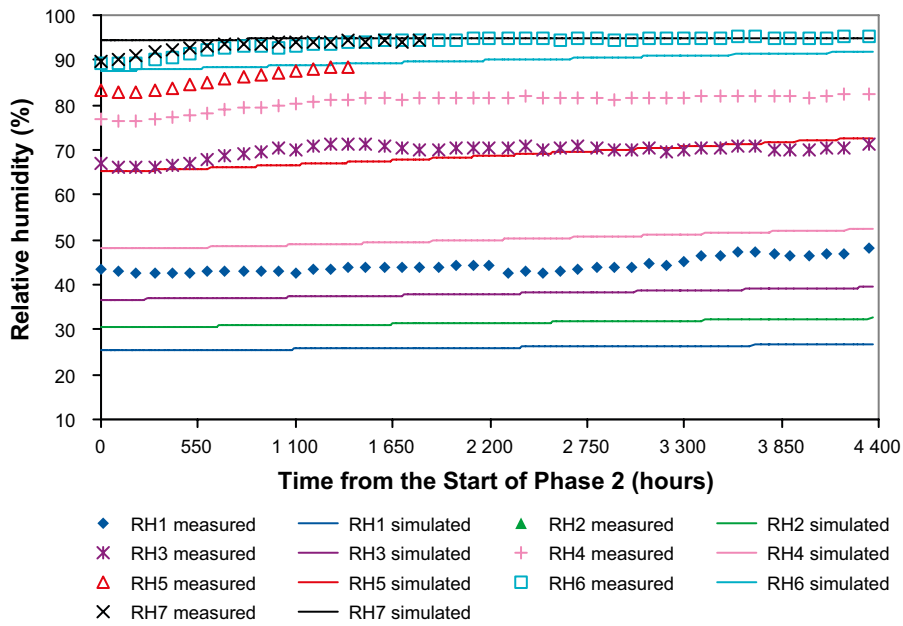


Figure 4-1v. Evolution of relative humidity with time, Cell 2, Phase 2. Computed results and observations. THg analysis. AECL.

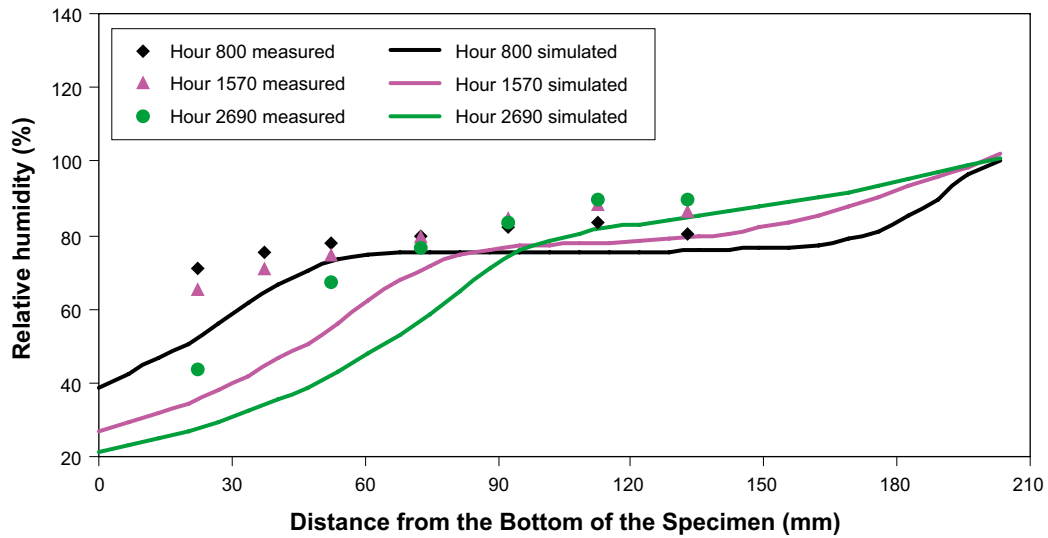


Figure 4-1w. Distributions of relative humidity at different times. Cell 2, Phase 1. Computed results and observations. THg analysis. AECL.

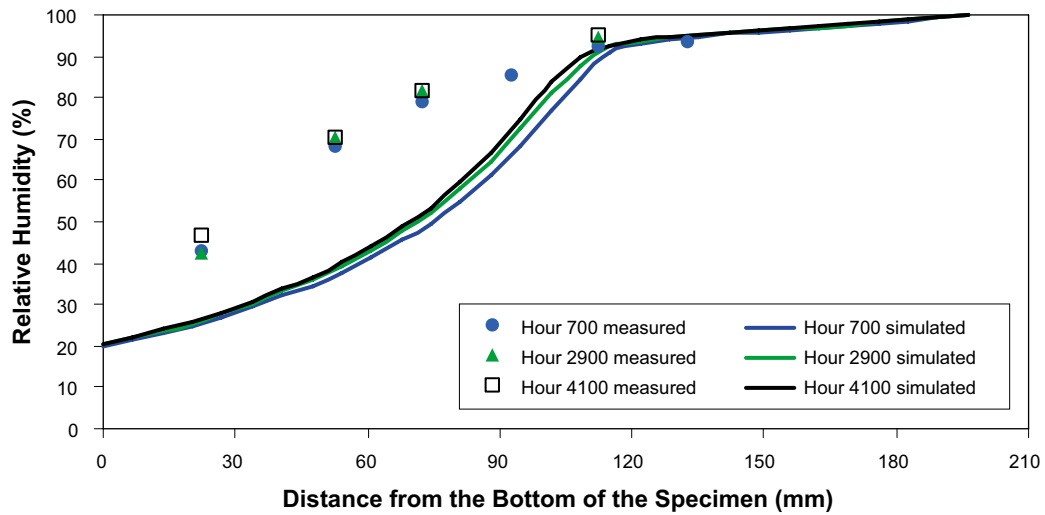


Figure 4-1x. Distributions of relative humidity at different times. Cell 2, Phase 2. Computed results and observations. THg analysis. AECL.

4.2.2 CIEMAT infiltration tests – Subtask 1.2 [2]

The axisymmetric geometry and mesh used are shown in Figure 4-2a. They comprise 120 4-noded elements with a total of 147 nodes. The mechanical problem was not modelled to avoid convergence problems. Therefore a H analysis was performed for the Isothermal Test and a TH analysis for the Thermal Gradient Test. The main results for the Isothermal Test are shown in Figure 4-2b and for the Thermal Gradient Test in Figures 4-2c and 4-2d.

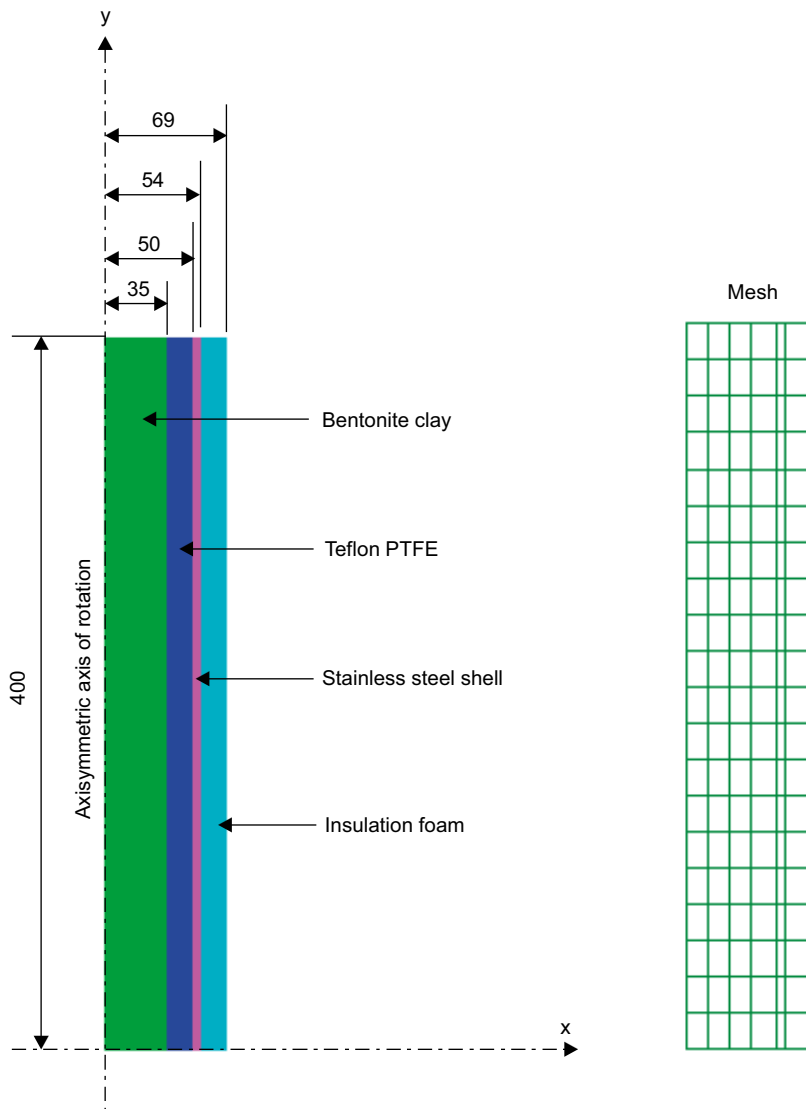


Figure 4-2a. Model geometry and mesh. AECL.

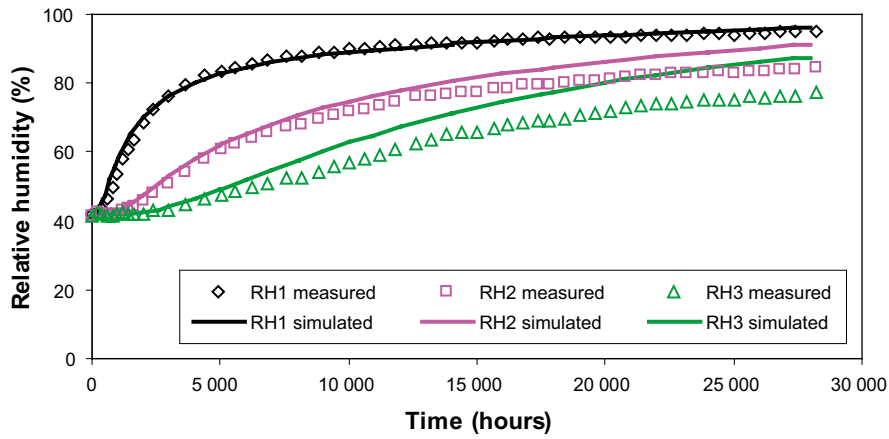


Figure 4-2b. Evolution of relative humidity with time. Isothermal test. Computed results and observations. AECL.

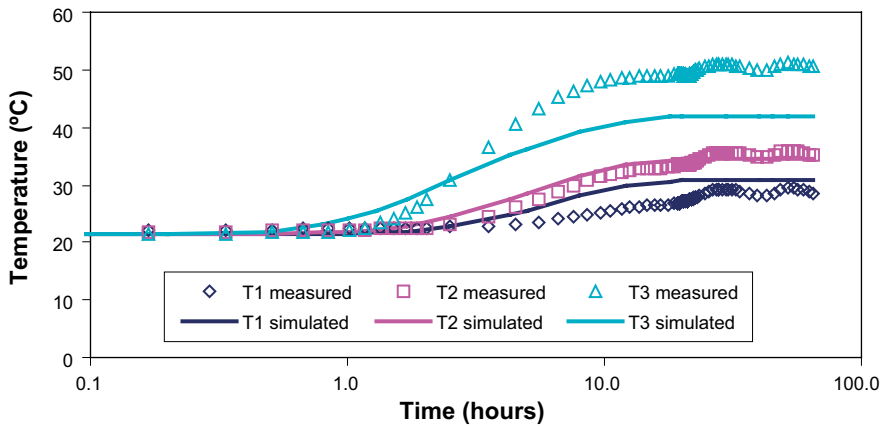


Figure 4-2c. Evolution of temperatures with time. Thermal Gradient Test. Phase I. Computed results and observations. AECL.

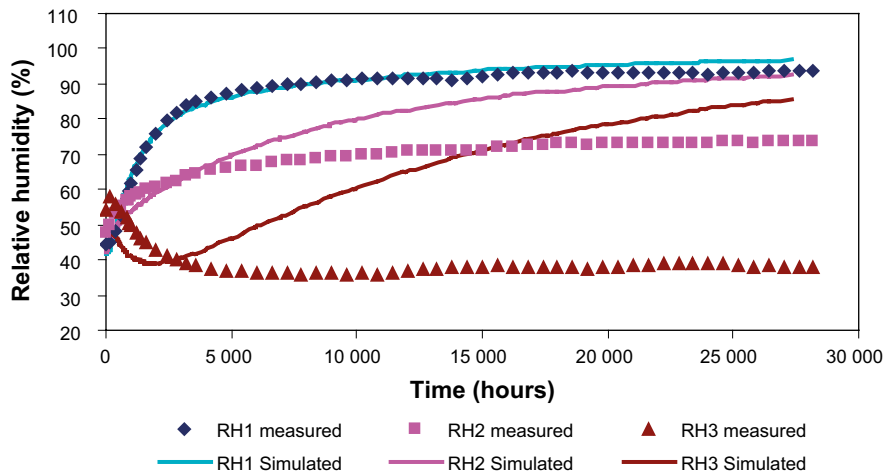


Figure 4-2d. Evolution of relative humidity with time. Thermal Gradient Test. Phase 2. Computed results and observations. AECL.

4.2.3 UPC heating test – Subtask 1.3 [3]

A two-dimensional axisymmetric model of the lower half of the heater test, takes advantage of symmetry has been used. The mesh contains are 861 four-noded elements with 924 nodes. Geometry and mesh are depicted in Figure 4-3a. A THM analysis has been performed selected results of which are presented in Figures 4-3b–e.

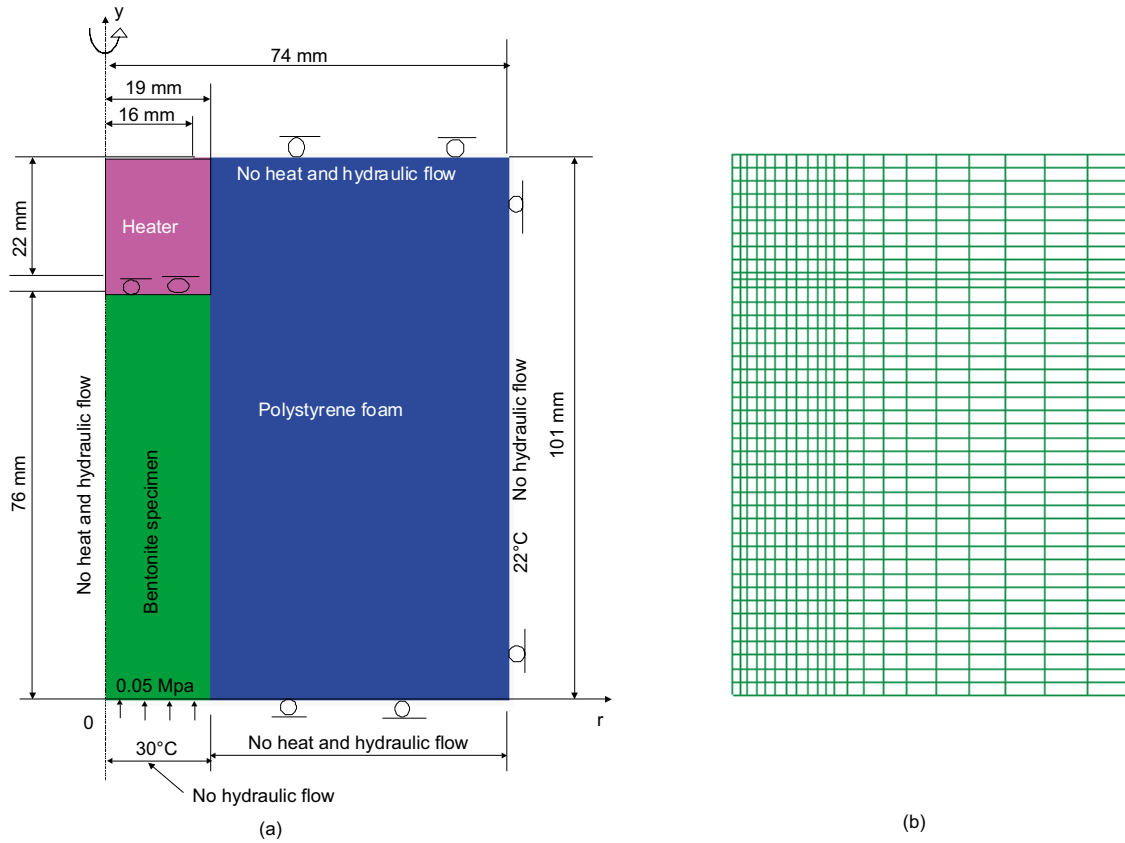


Figure 4-3a. Model geometry and mesh.

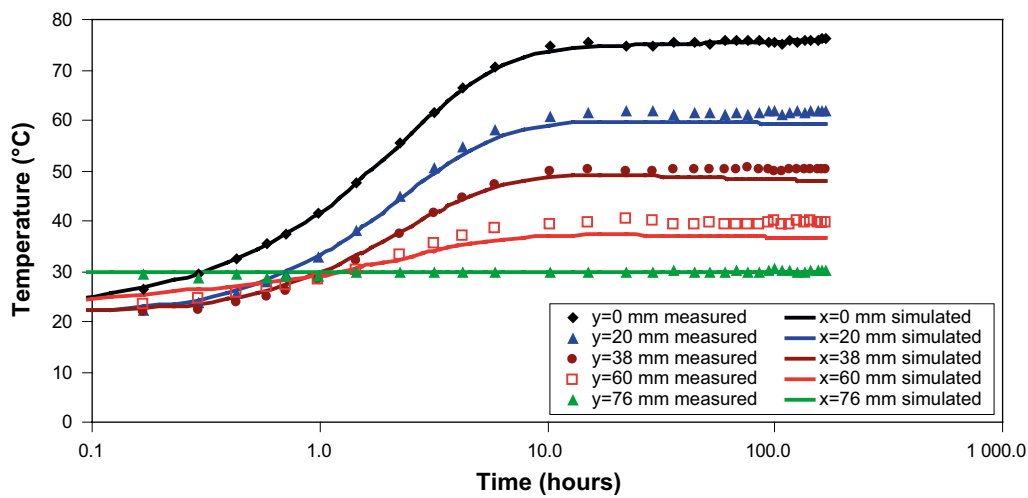


Figure 4-3b. Evolution of temperatures with time. Computed results and observations.

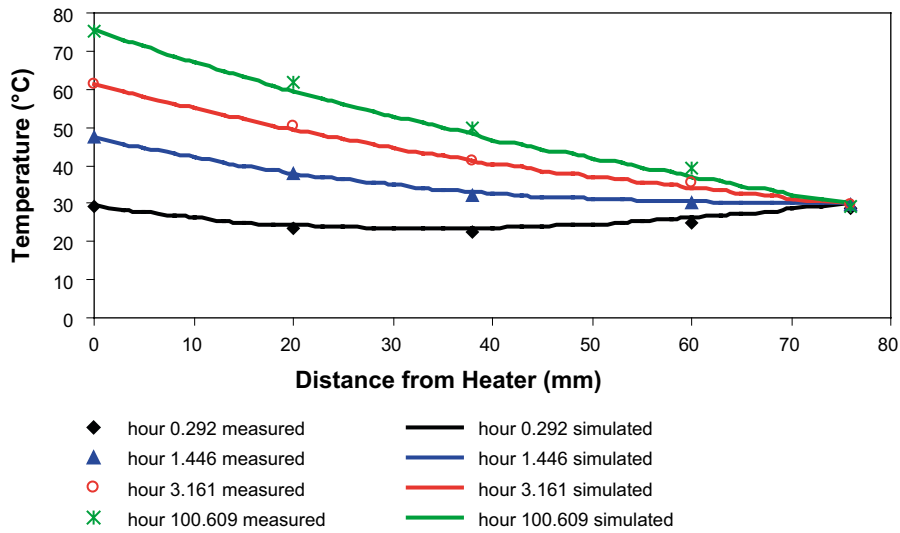


Figure 4-3c. Distribution of temperatures with time. Computed results and observations. AECL.

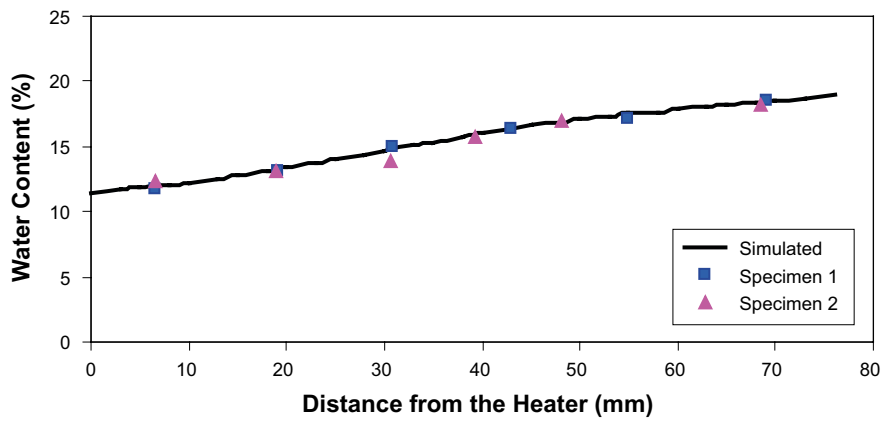


Figure 4-3d. Distribution of water content at the end of test. Computed results and observations. AECL.

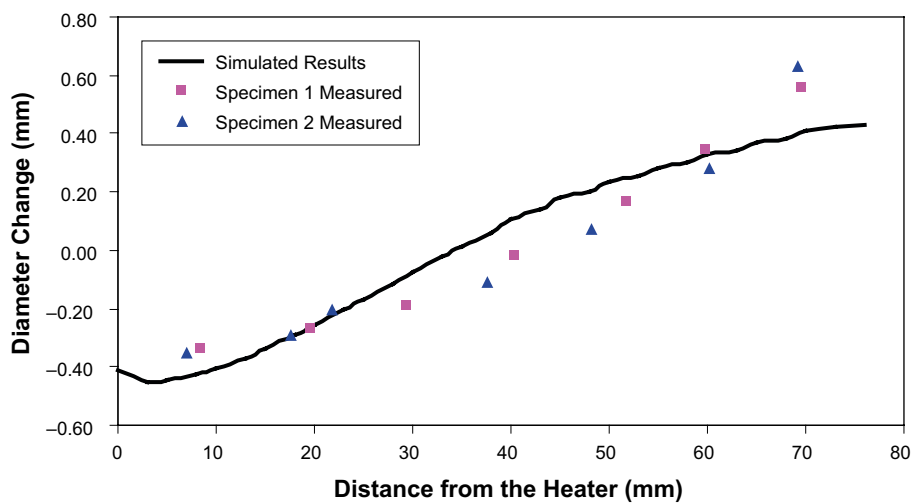


Figure 4-3e. Change of diameter along the specimens at the end of the test. Computed results and observations. A higher value of $k_s = 007$ has been used to obtain agreement. AECL.

4.2.4 Remarks

The analyses performed by the AECL team exhibited serious problem of convergence when the mechanical component of the formulation was activated. These problems could perhaps be associated with the use of a full elastoplastic model that imposes stricter requirements on the numerical procedures. This resulted in an incomplete THM modelling of the Subtask 1.1 (the calculations did not reach the full duration of the second phase of the mockup tests) and the not inclusion of mechanical analysis in Subtask 1.2. Comparison of TH and THM results showed, however, that the effects on temperatures were small and only moderate on hydraulic variables (relative humidity), not changing significantly the overall pattern of results.

Concerning Subtask 1.1, temperatures were correctly reproduced throughout. Of special interest is the comparison of relative humidity distributions, the good agreement indicate that the variation of thermal conductivity with hydration (degree of saturation) is correctly described. Computed vapour migration is faster than observed resulting in a larger short term reduction of relative humidity. The test duration is too short to check on the long term evolution of hydration. The development of axial stresses is correctly modelled, implying that the evolution of swelling pressure is correctly reproduced. In contrast, there are significant differences with observed radial stresses (not shown here) but this is not unexpected as this variable is very sensitive to the fine details of the mechanical model. The performance of the model is very similar for the two tests performed at different water contents.

With respect to Subtask 1.2, temperatures are basically well reproduced although a better agreement with observations can be achieved if the thermal conductivity of the Teflon cover is modified with respect to the nominal value provided in the specifications. The long term evolution of the relative humidity measurements in the thermal gradient test is not captured by the model.

Finally, observed temperatures and water content at the end of the test in Subtask 1.3 is satisfactorily modelled indicating that the vapour diffusion phenomenon, dominant in this case, is well formulated (Fick's law is used) and solved. To achieve a good reproduction of the diameter change, it was necessary to adopt a much higher value of stiffness with respect to suction changes than that used in Subtask 1.1.

4.3 BGR

4.3.1 CEA mock-up tests – Subtask 1.1 [4]

Fully coupled THM analyses have been performed by the BGR group. The mesh used is depicted in Figure 4-4a together with the thermal, hydraulic and displacement boundary conditions. The specimen has been modeled with 2D plane strain elements because the code lacks the axisymmetric option. This simplification leads to deviations with respect to the mechanical response of the specimen to the swelling process, but the effect of swelling can still be reproduced qualitatively. The results for Cell 1 (water content: 13.66 %) are presented in Figures 4-4b to 4-4f and for Cell 2 (water content: 17.86 %) in Figures 4-4g to 4-4k.

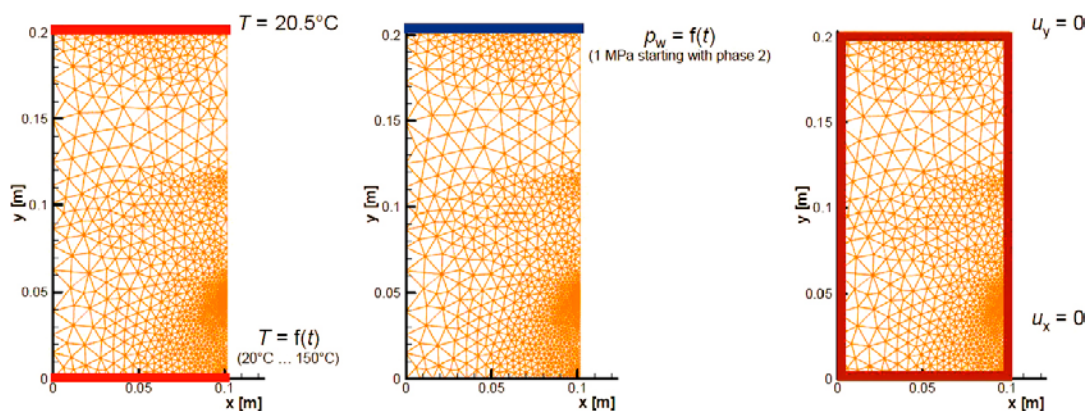


Figure 4-4a. Model geometry and mesh. Boundary conditions for temperature, water pressure, and displacements are indicated. BGR.

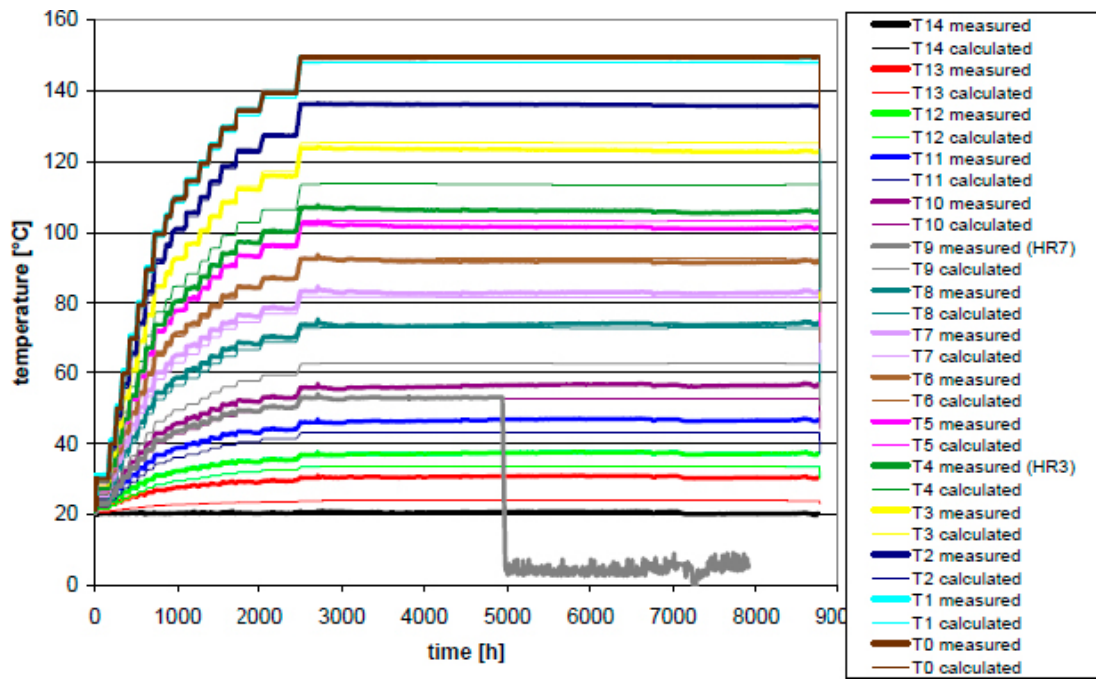


Figure 4-4b. Evolution of temperature with time, Cell 1, Computed results and observations. BGR.

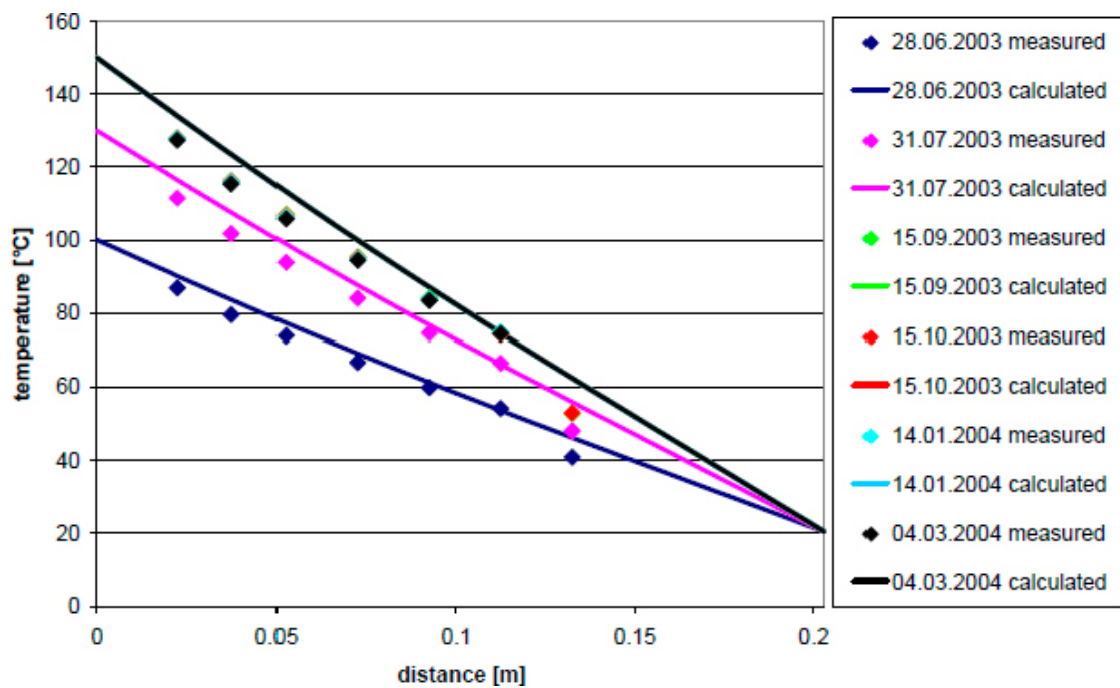


Figure 4-4c. Distributions of temperatures at different times. Cell 1. Computed results and observations. BGR.

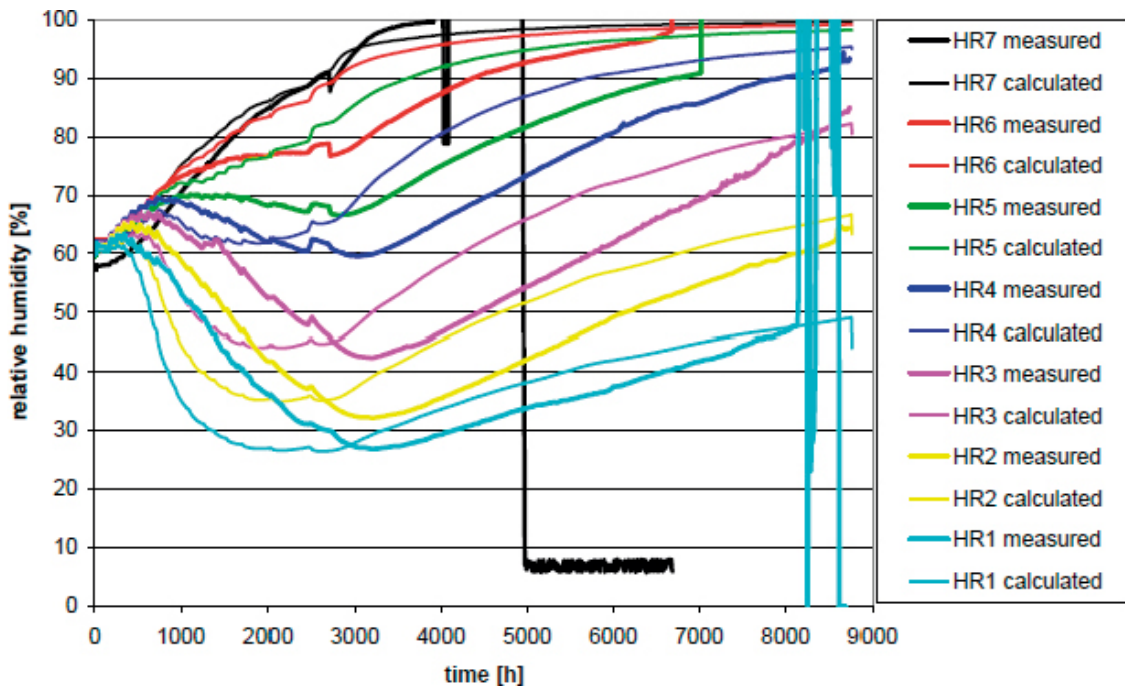


Figure 4-4d. Evolution of relative humidity with time, Cell 1. Computed results and observations. BGR.

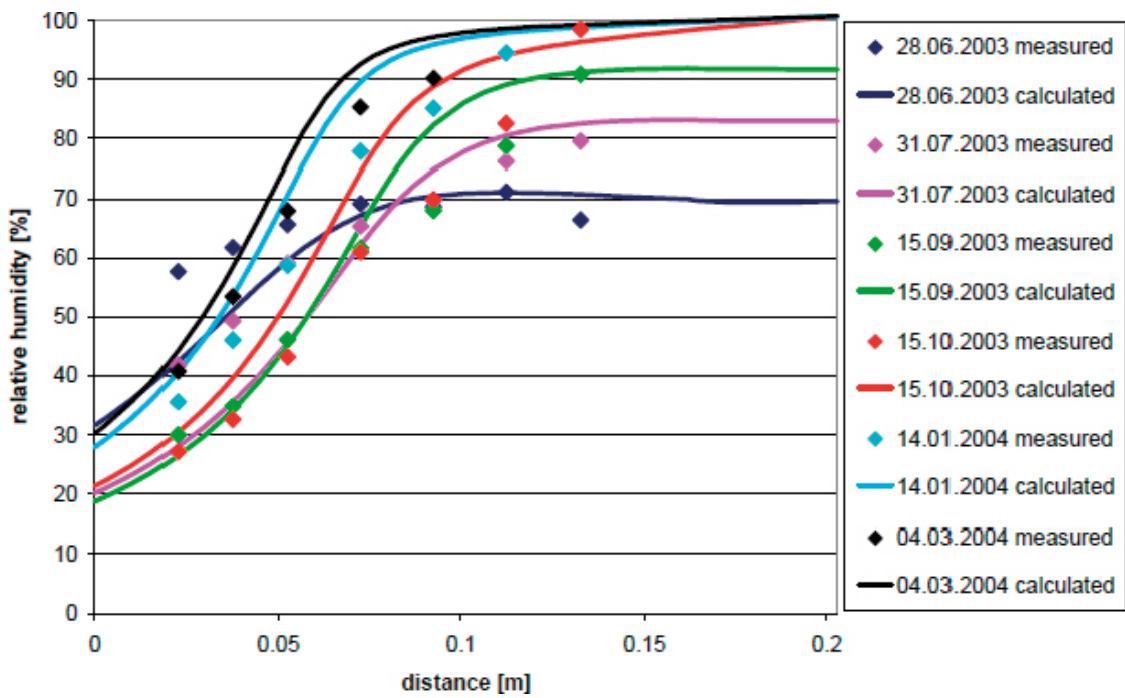


Figure 4-4e. Distributions of relative humidity at different times, Cell 1. Computed results and observations. BGR.

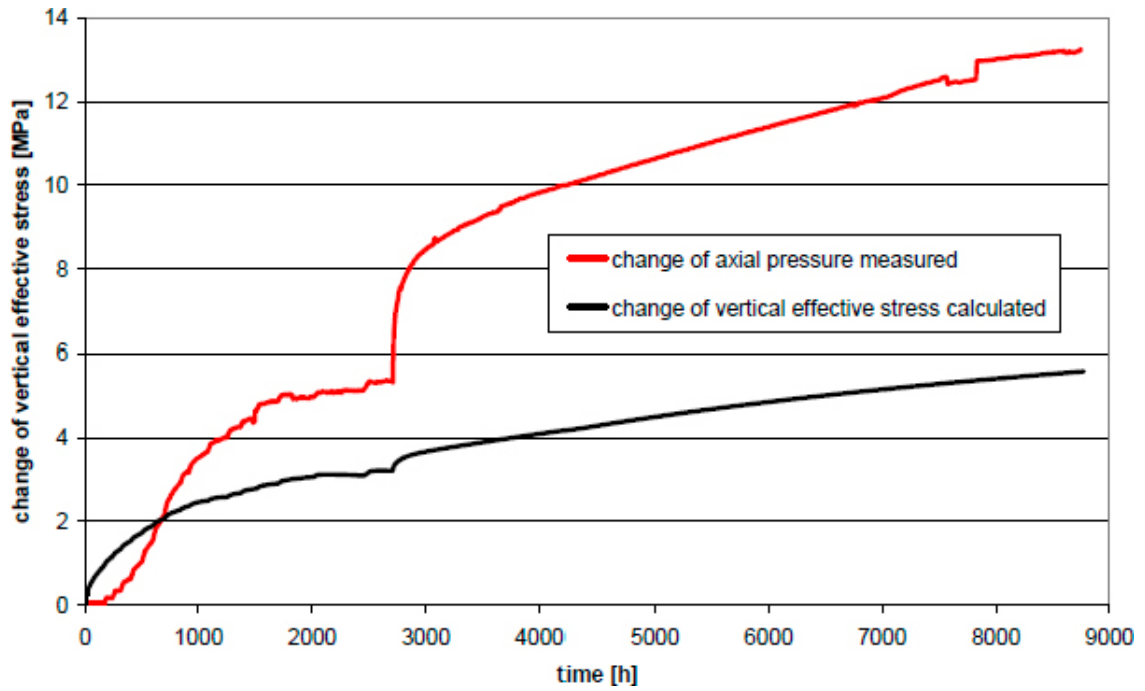


Figure 4-4f. Evolution of axial stress with time, Cell 1. Computed results and observations. BGR.

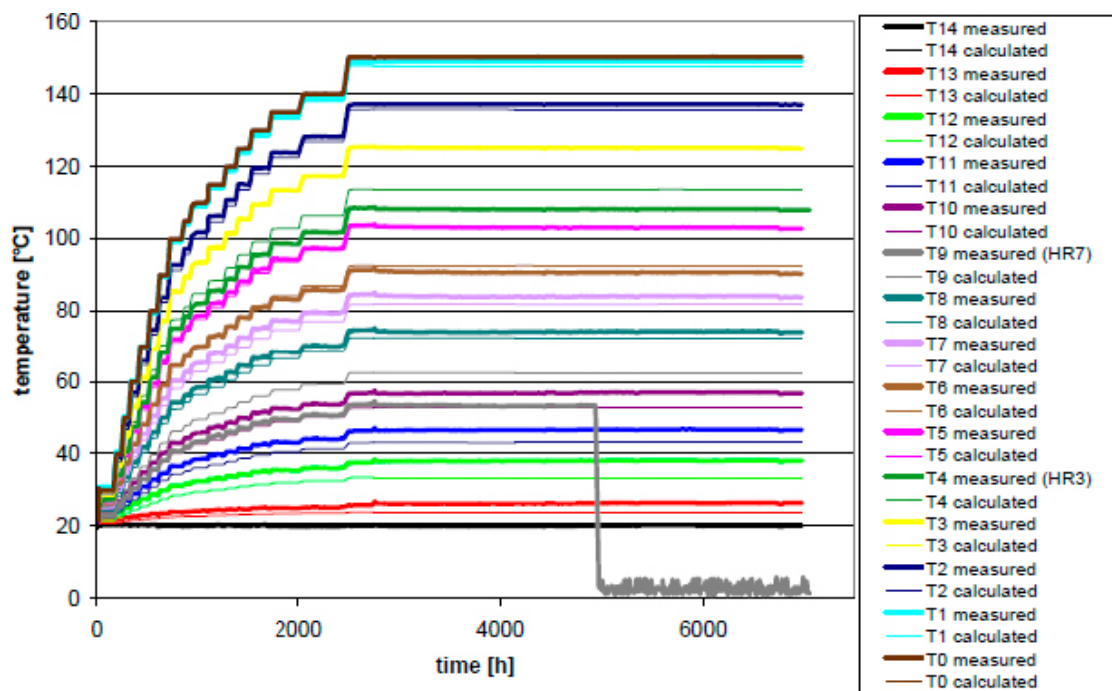


Figure 4-4g. Evolution of temperature with time, Cell 2, Computed results and observations. BGR.

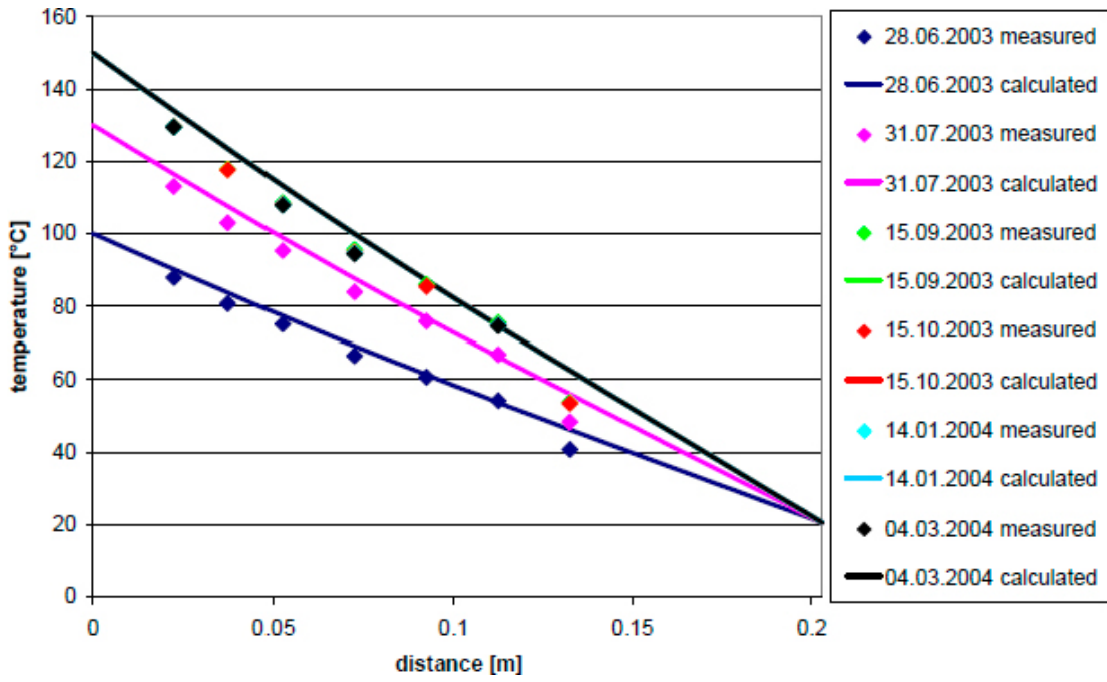


Figure 4-4h. Distributions of temperatures at different times. Cell 2. Computed results and observations. BGR.

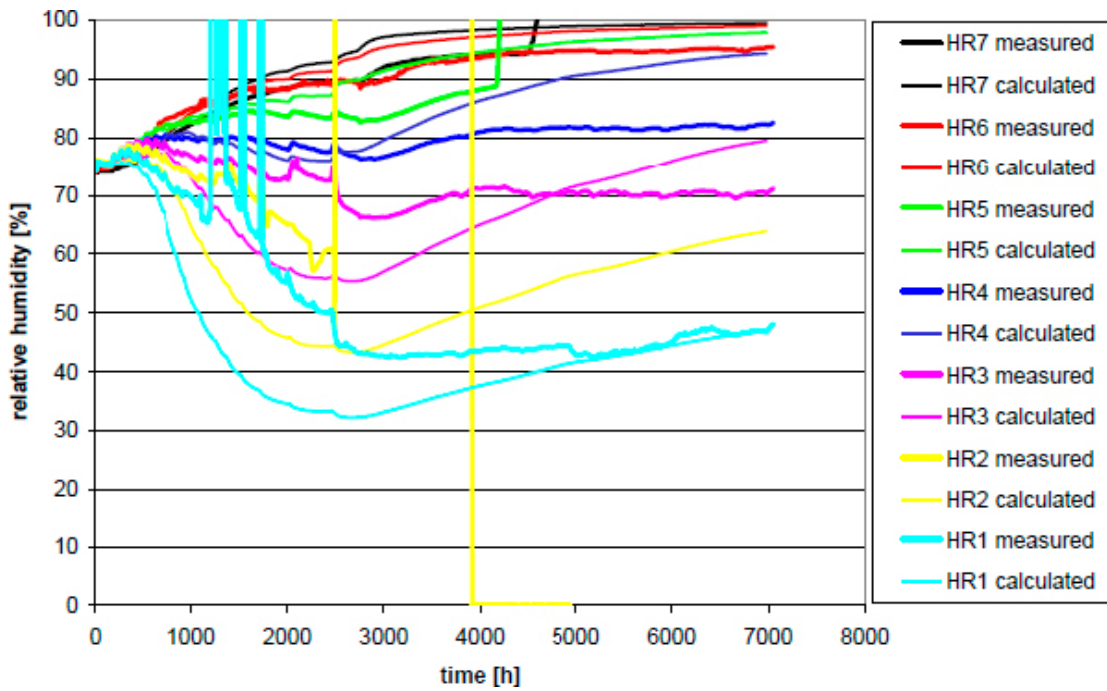


Figure 4-4i. Evolution of relative humidity with time, Cell 2. Computed results and observations. BGR.

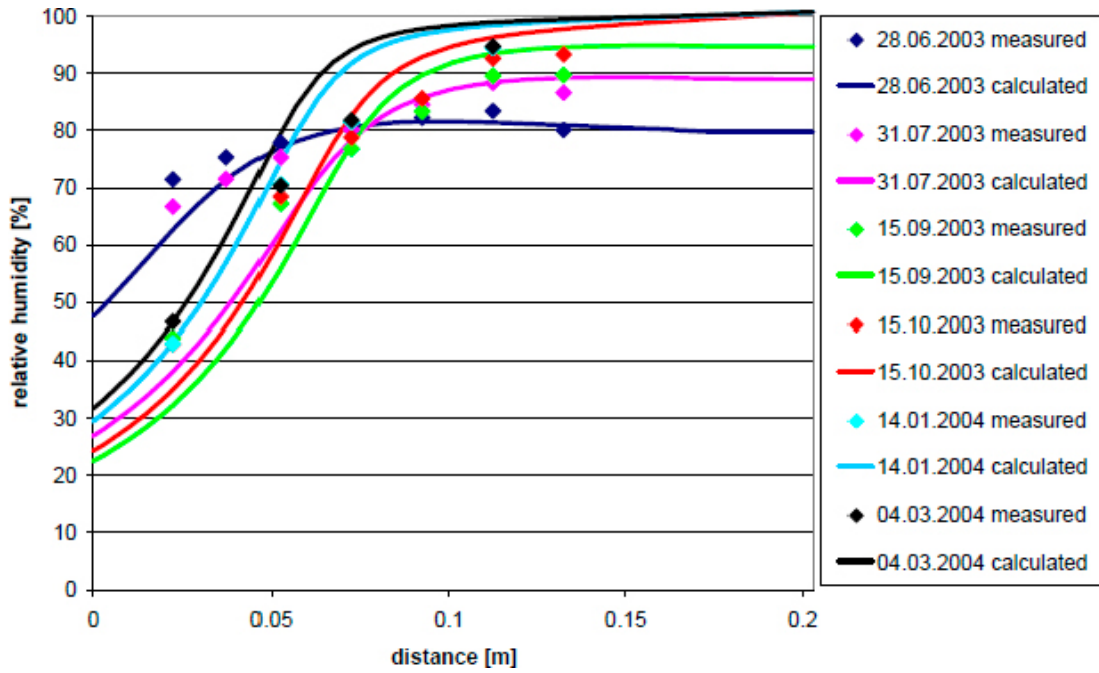


Figure 4-4j. Distributions of relative humidity at different times, Cell 2. Computed results and observations. BGR.

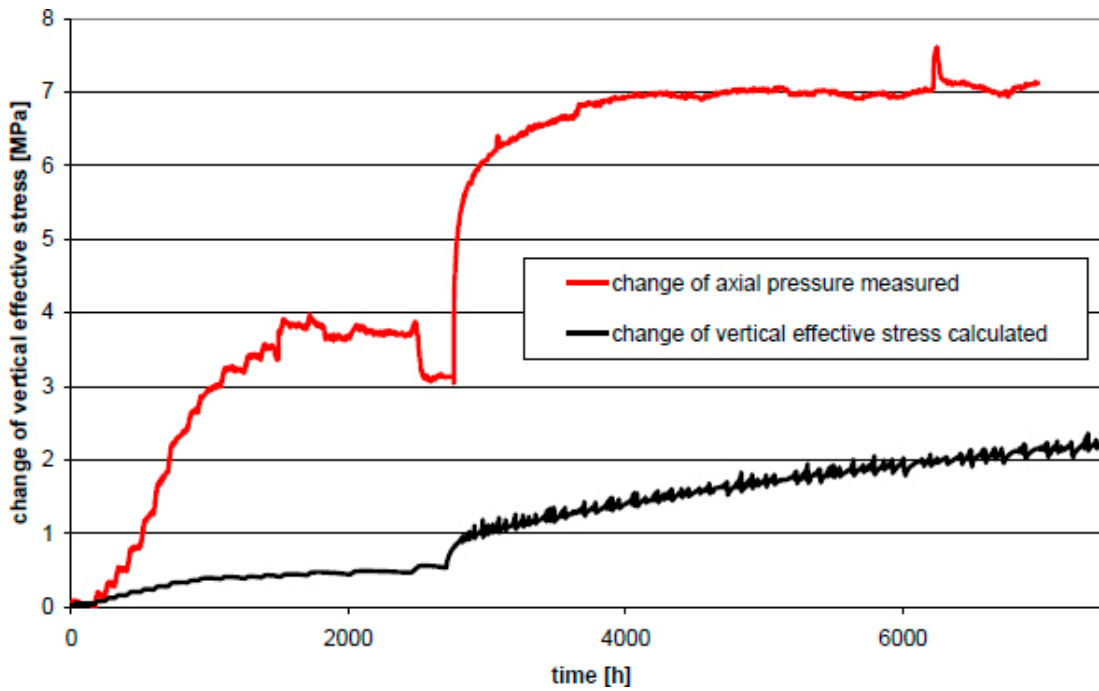


Figure 4-4k. Evolution of axial stress with time, Cell 1. Computed results and observations. BGR.

4.3.2 CIEMAT infiltration tests – Subtask 1.2 [4]

For this Subtask, two different models have been employed. For the isothermal test a H analysis using the two-phase formulation of ROCKFLOW has been performed. A THM analysis of the thermal gradient test has been carried out using the GEOSYS code. The mesh is made up of 2D plane strain elements. Geometry and mesh are shown in Figure 4-5a. Selected results are presented in Figures 4-5b to 4-5d.

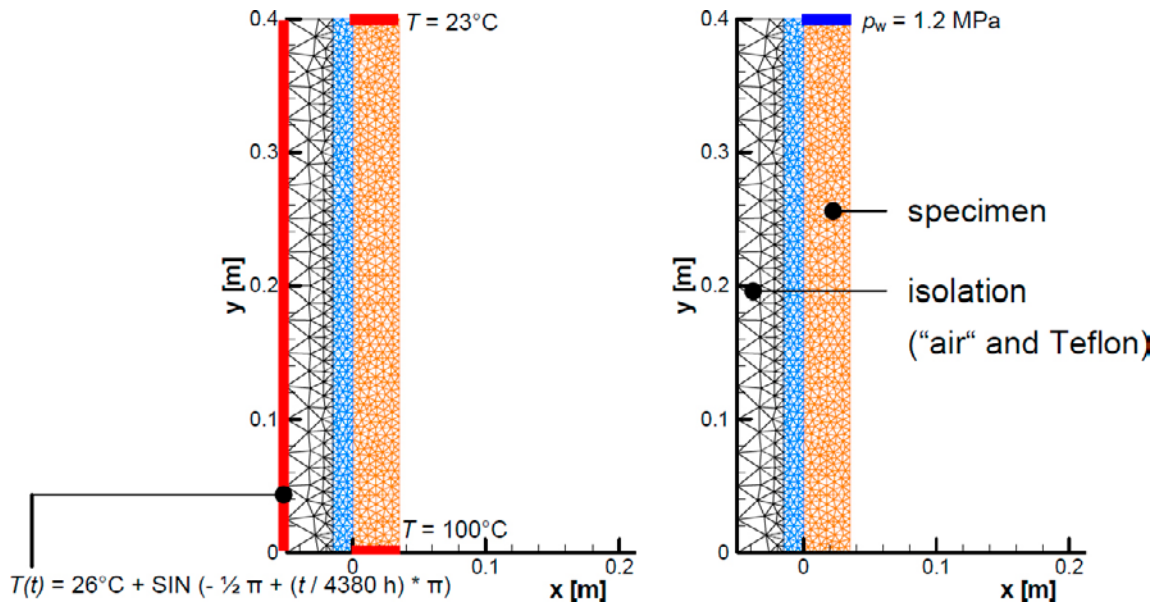


Figure 4-5a. Model geometry and mesh. Boundary conditions for temperature, water pressure are indicated. BGR.

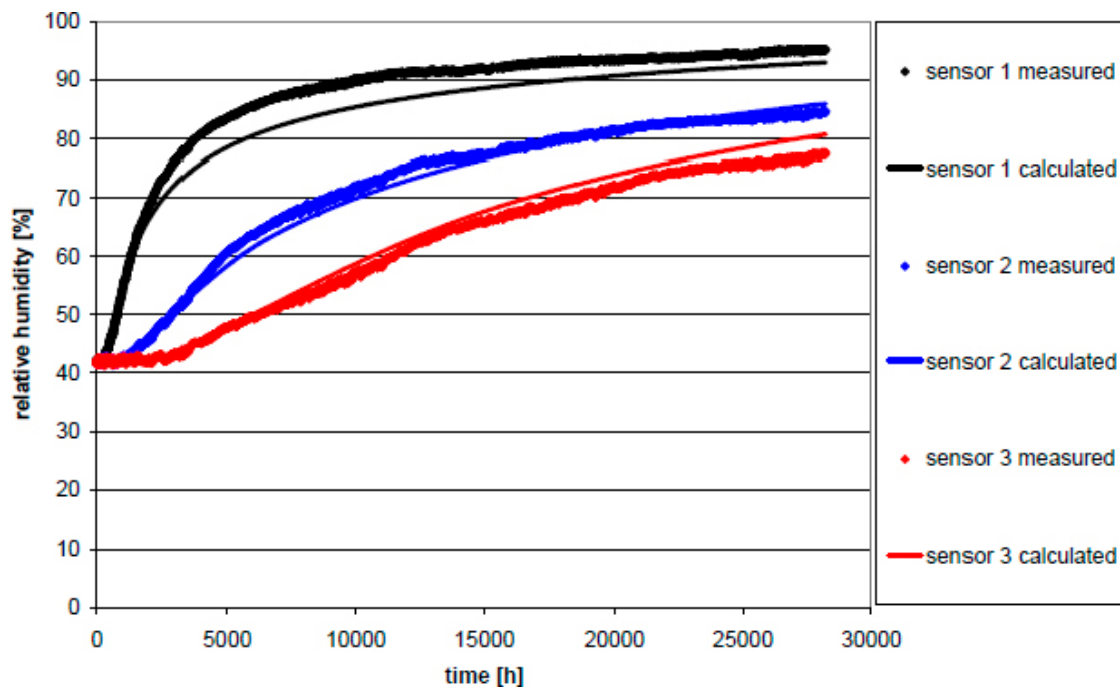


Figure 4-5b. Evolution of relative humidity with time. Isothermal test. Computed results and observations. BGR.

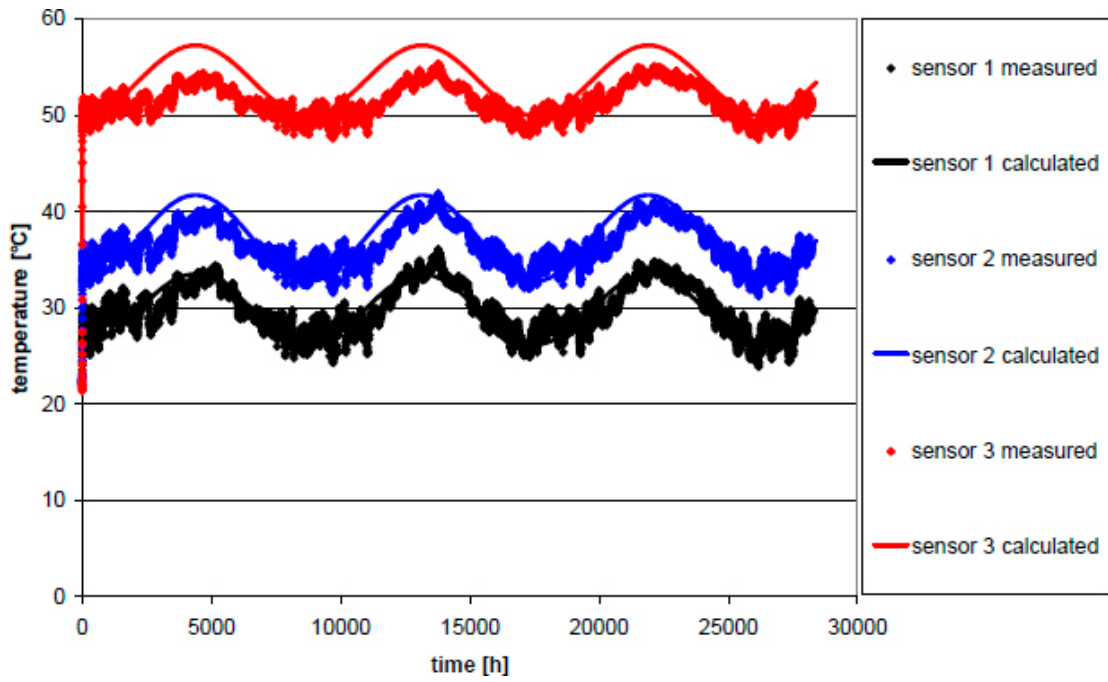


Figure 4-5c. Evolution of temperatures with time. Thermal Gradient Test. Computed results and observations. BGR.

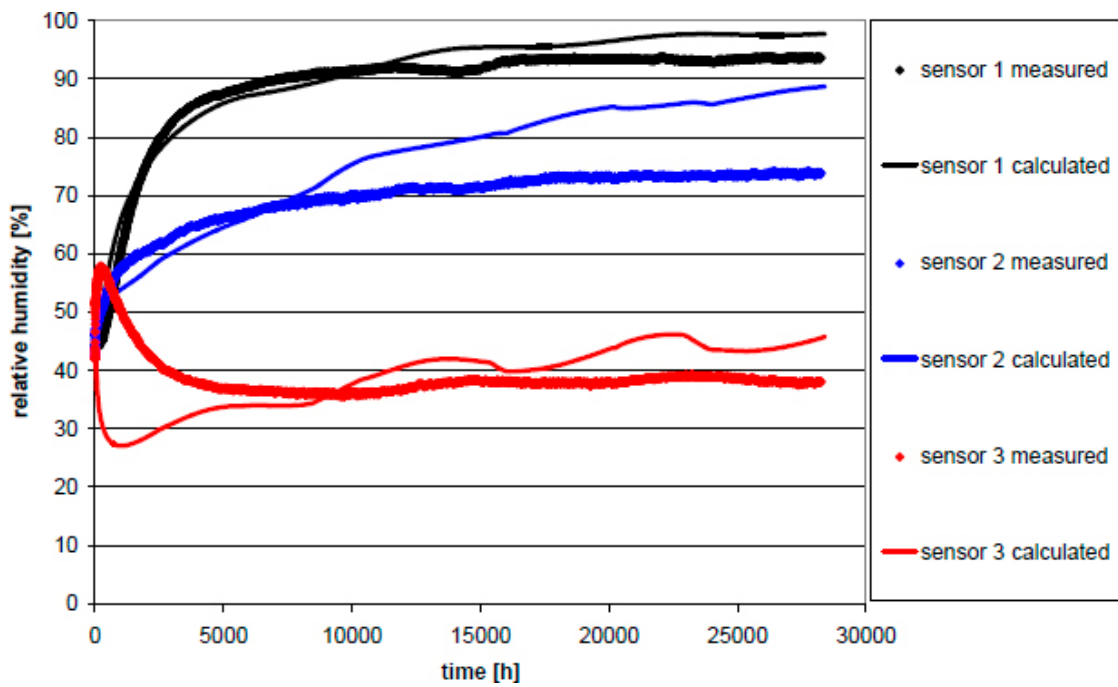


Figure 4-5d. Evolution of relative humidity with time. Thermal Gradient Test. Computed results and observations. BGR.

4.3.3 UPC heating test – Subtask 1.3 [4]

The test was simulated by means of a THM analysis using the geometry and mesh depicted in Figure 4-6b. Plane strain elements were used. Measured temperatures were used as boundary conditions for simplicity. The selected results are presented in Figures 4-6b to 4-6e. A variety of permeability and tortuosity values were tested as it can be observed in the results plotted in Figure 4-6d. Water mass conservation was checked and the results are shown in Figure 4-6f. It can be observed that the variation is less than 0.1 %, an excellent result. It is noteworthy the slight jump in mass when cooling starts.

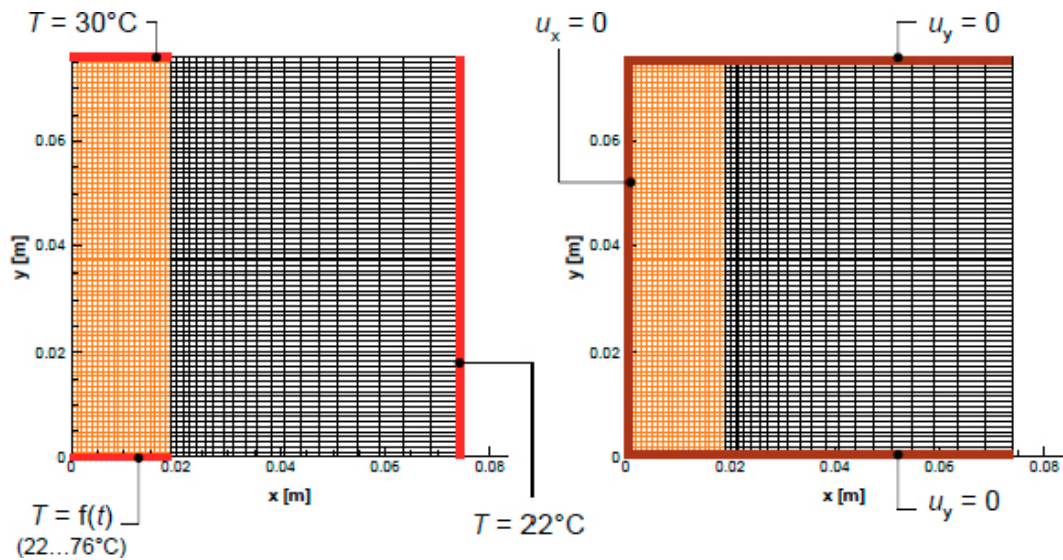


Figure 4-6a. Model geometry and mesh. Boundary conditions for temperature and water pressure are indicated. BGR.

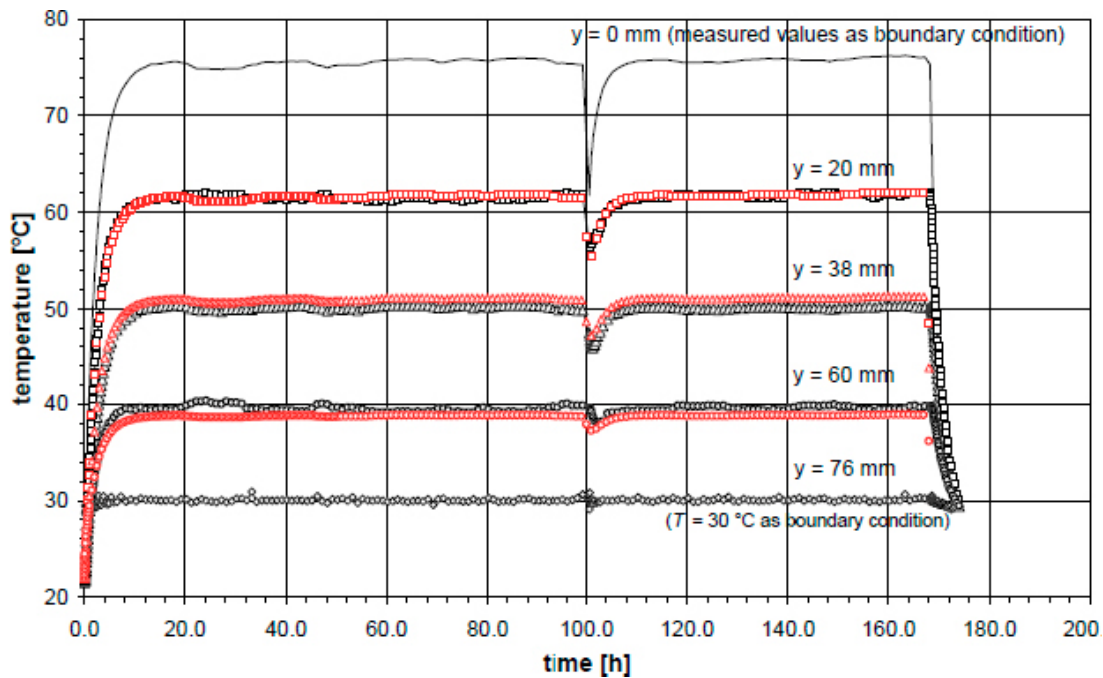


Figure 4-6b. Evolution of temperatures with time. Computed results and observations. BGR.

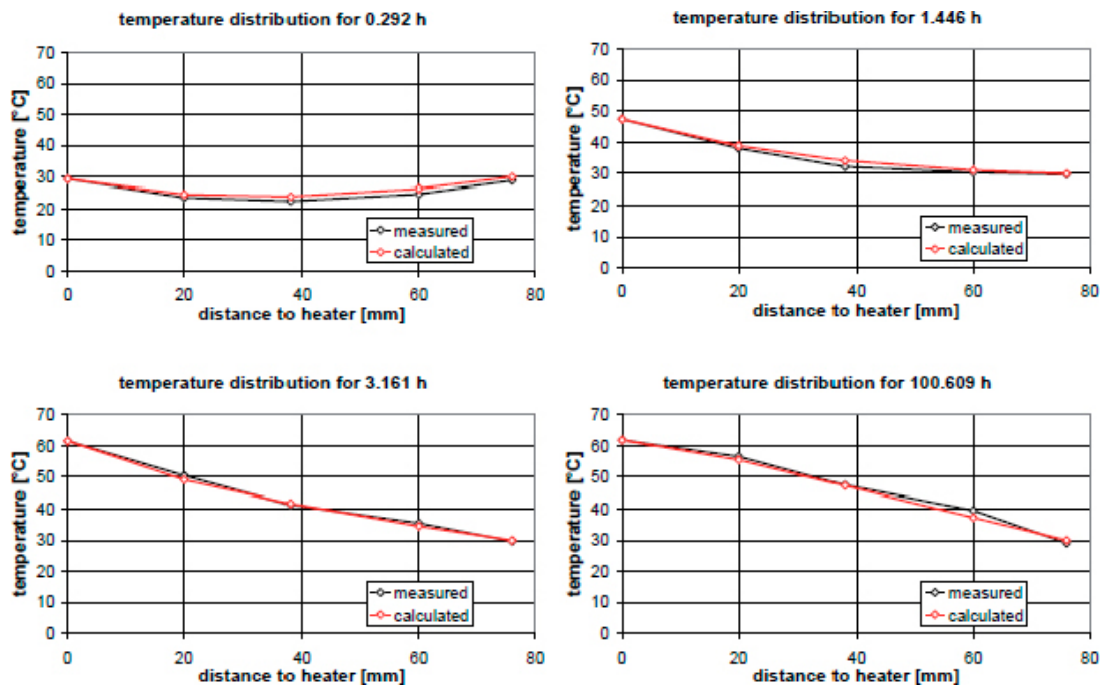


Figure 4-6c. Distribution of temperatures at different times. Computed results and observations. BGR.

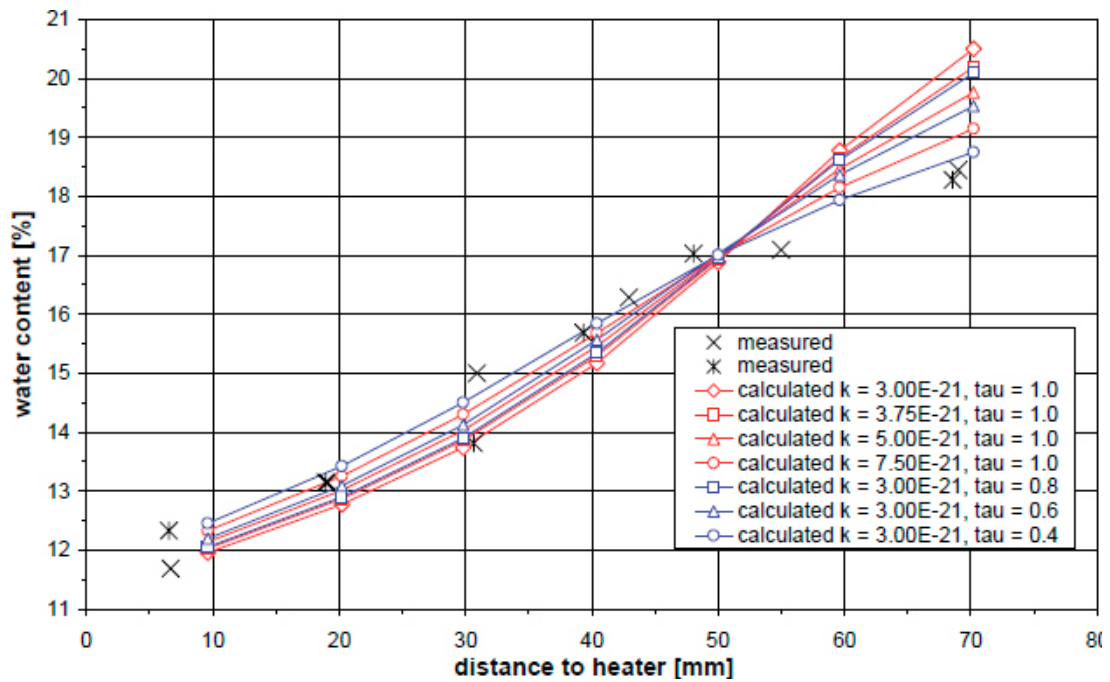


Figure 4-6d. Distribution of water content at the end of test. Computed results and observations. Different combinations of intrinsic permeability and tortuosity have been used. BGR.

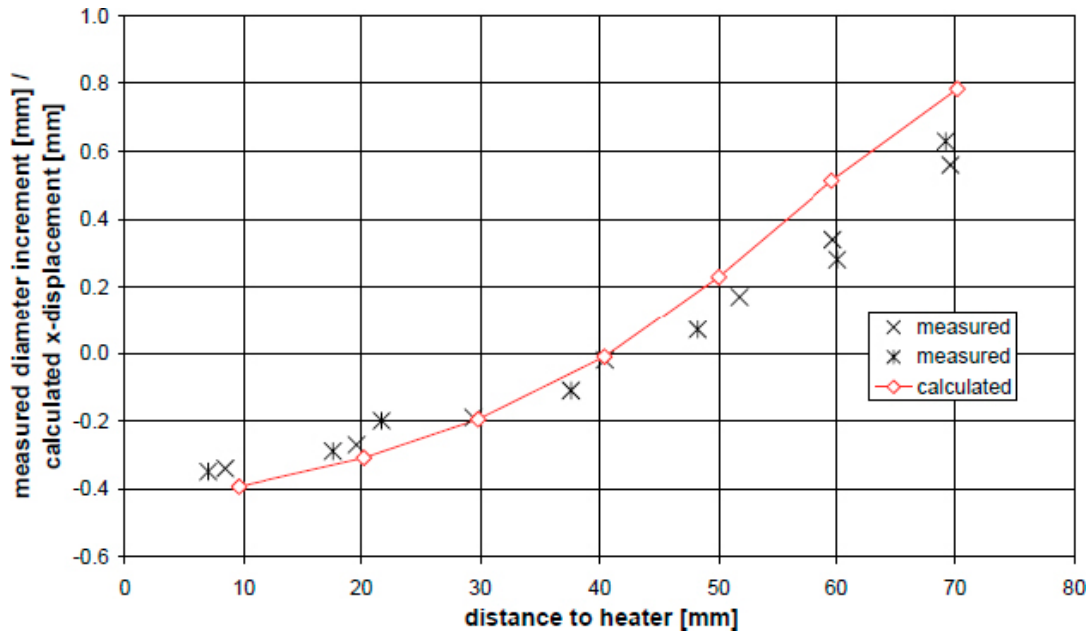


Figure 4-6e. Change of diameter along the specimens at the end of the test. Computed results and observations. A lower value of Young's modulus has been used to obtain agreement. BGR.

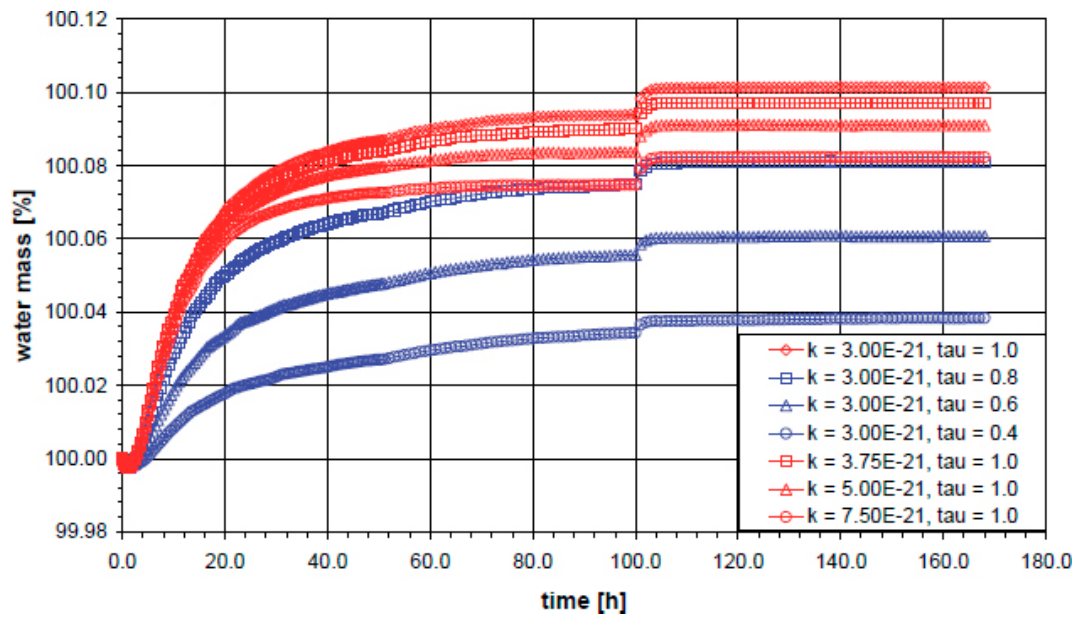


Figure 4-6f. Evolution of water mass with time. BGR.

4.3.4 Remarks

A shortcoming of the BGR results is the use of a 2-D plane strain domain instead of an axisymmetric one. This impacted the loss of heat through lateral surfaces and the mechanical results. However, the qualitative trends of THM behaviour can still be recovered from the analysis. Thus, it can be easily checked that the overall patterns of behaviour were adequately reproduced. Some oscillations are observed in the output that the modelling group suggests may be due to the choice of stress variables that imply a jump when going from unsaturated to saturated range.

Regarding Subtask 1.1, the computed vapour diffusion exhibits the correct trends but it is faster than observed. In this case, gas pressure was assumed constant but the results do not seem to be significantly affected by this option. The computed overall hydration of Cell 1 appears to be similar to observations but the slow hydration of Cell 2 is not captured. The computed axial stress is significantly lower than observed showing differences in the time evolution too. This can be attributed, at least partially, to the use of plane strain elements.

The isothermal test of Subtask 1.2 is well reproduced but the slow hydration of the thermal gradient is not captured. A number of sensitivity analyses were performed in relation to Subtask 1.3 achieving a satisfactory reproduction of the test results. It is interesting to note that the final redistribution of water content appears to be directly related to the tortuosity/permeability (τ/k) ratio; a parameter that combines the laws for liquid and vapour flow. To obtain a good correspondence with the observed sample diameter changes, a more deformable bentonite had to be postulated (i.e. using a lower Young's modulus). It is not clear how this issue is affected by the use of a plane strain analysis. This case was also used to check the mass conservation characteristics of the code with very good results.

4.4 CIMNE

4.4.1 CEA mock-up tests – Subtask 1.1 [6]

The geometry and mesh used in the simulations are shown in Figure 4-7a. It is an axisymmetric geometry and the mesh is made up of 732 4-noded quadrilateral elements and 792 nodes. Fully coupled THMg analyses have been performed; selected results of the Base Case are shown in Figures 4-7b to 4-7k.

Apart from the Base Case, three other analyses have been performed for Cell 1 to check i) the effect of tortuosity, b) the influence of a variation in the retention curve, and iii) the effect of not considering the gas flow equation. Comparing Figure 4-7l with 4-7d, it can be noted that an increase of the value of tortuosity leads to a worse agreement with the measured relative humidity; the vapour diffusion is too fast. Lower axial stresses also result. It is also found that a change of retention curve influences the evolution of relative humidity and axial stress prediction. Variation of the same parameters are also obtained if the computations are performed without the gas flow equation (compare Figure 4-7d and 4-7m), especially during the second phase of the experiment.

Water mass conservation has been checked in the calculations of Phase 1 where no water inflow or outflow is allowed. The computed variation is only 0.83 % for Cell 1 and 0.3 % for Cell 2, a quite satisfactory result.

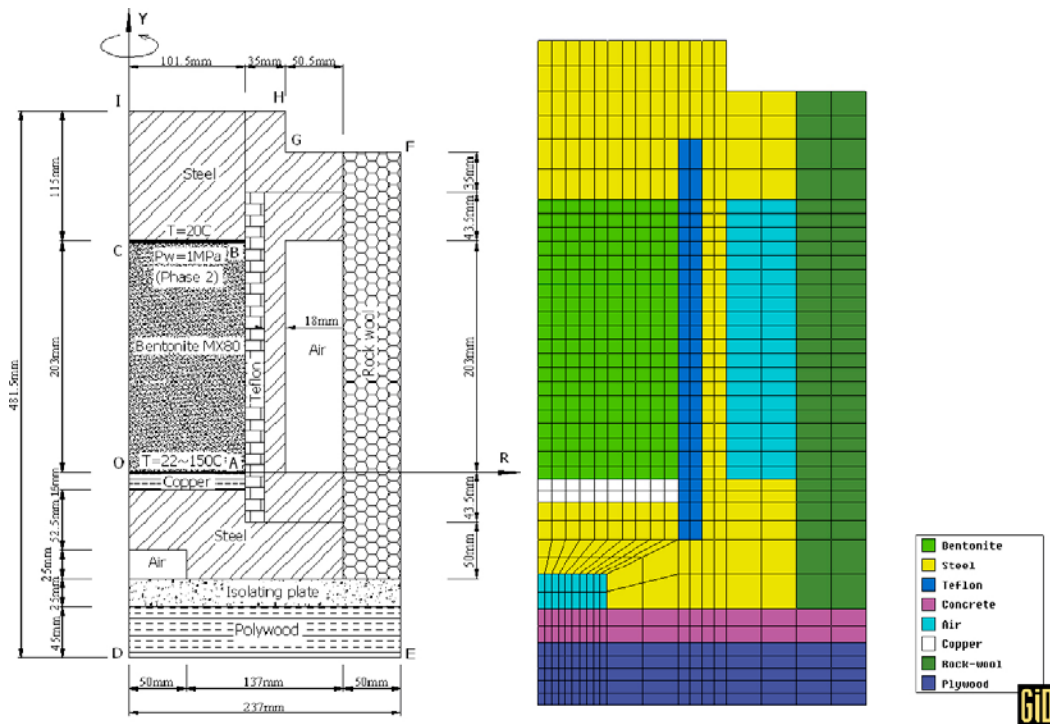


Figure 4-7a. Model geometry and mesh. CIMNE.

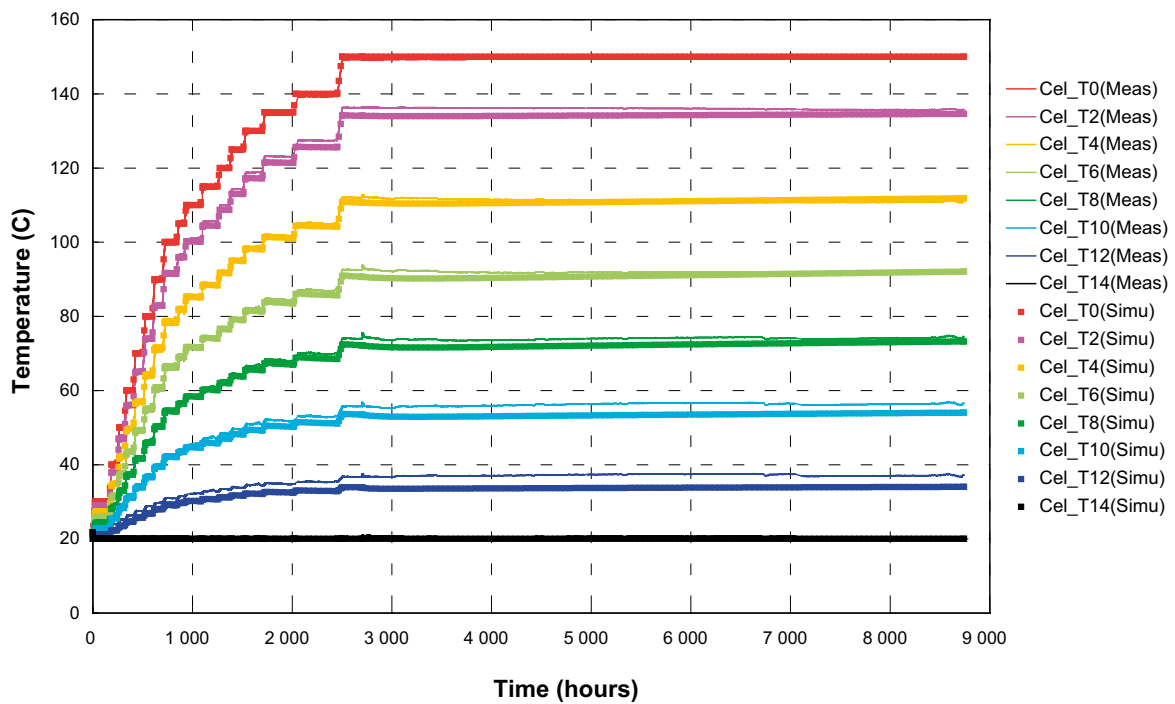


Figure 4-7b. Evolution of temperature with time, Cell 1, Computed results and observations. CIMNE.

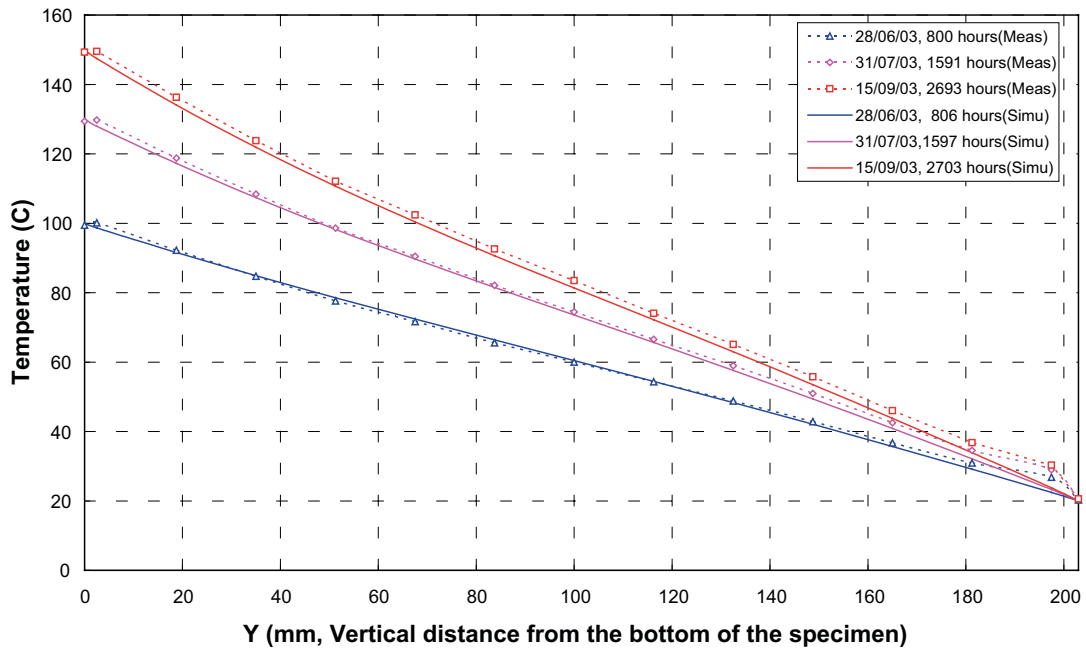


Figure 4-7c. Distributions of temperatures at different times. Cell 1. Computed results and observations. CIMNE.

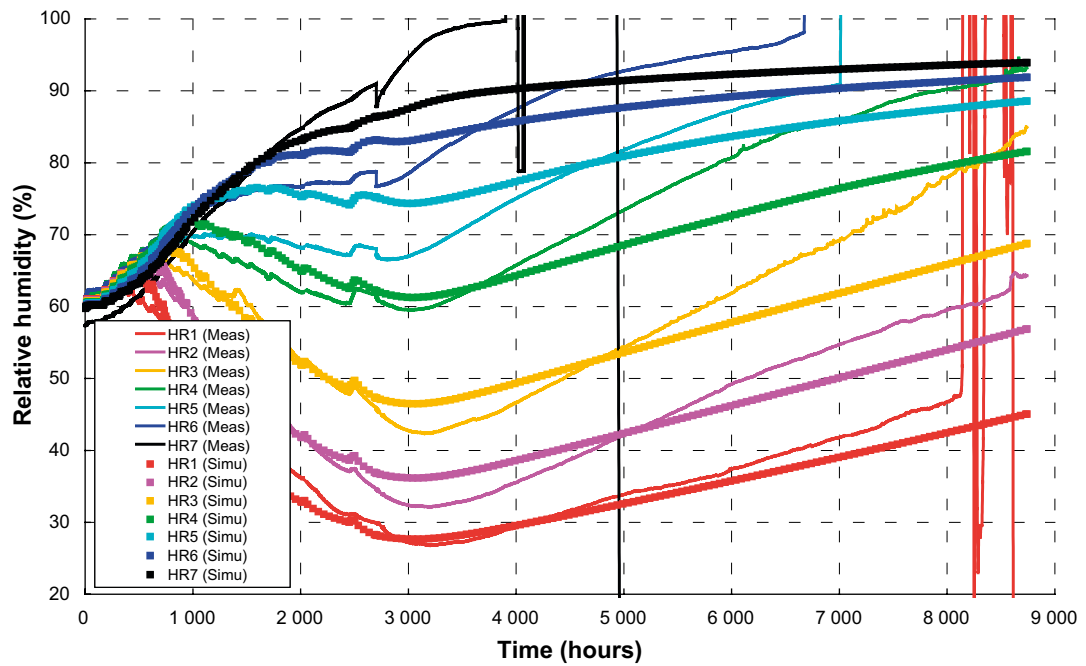


Figure 4-7d. Evolution of relative humidity with time, Cell 1. Computed results and observations. CIMNE.

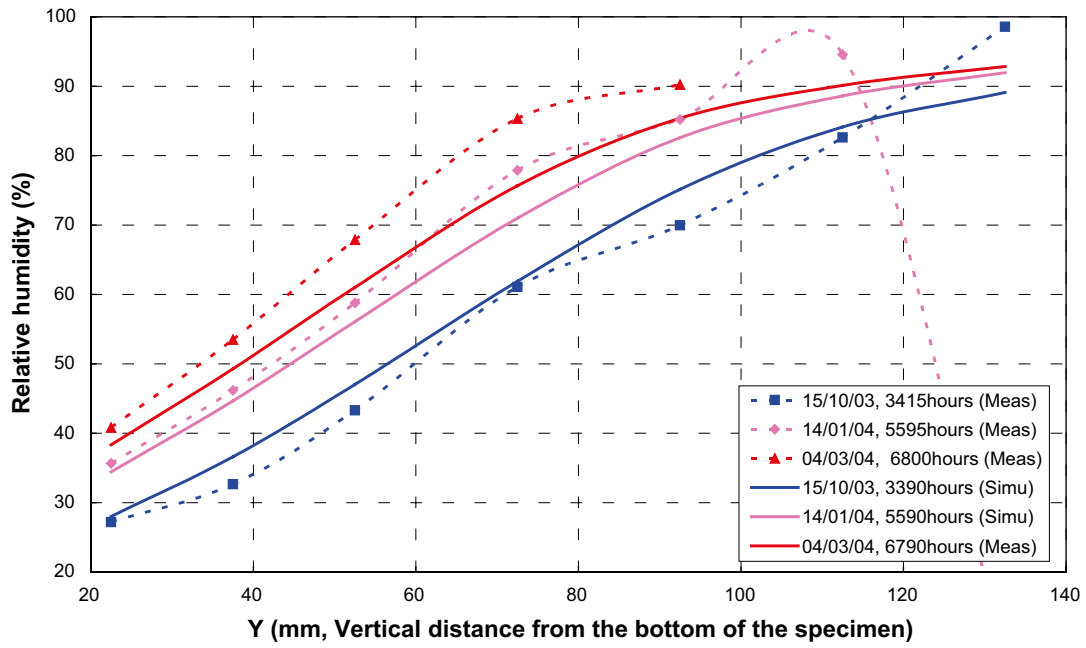


Figure 4-7e. Distributions of relative humidity at different times, Cell 1. Computed results and observations. CIMNE.

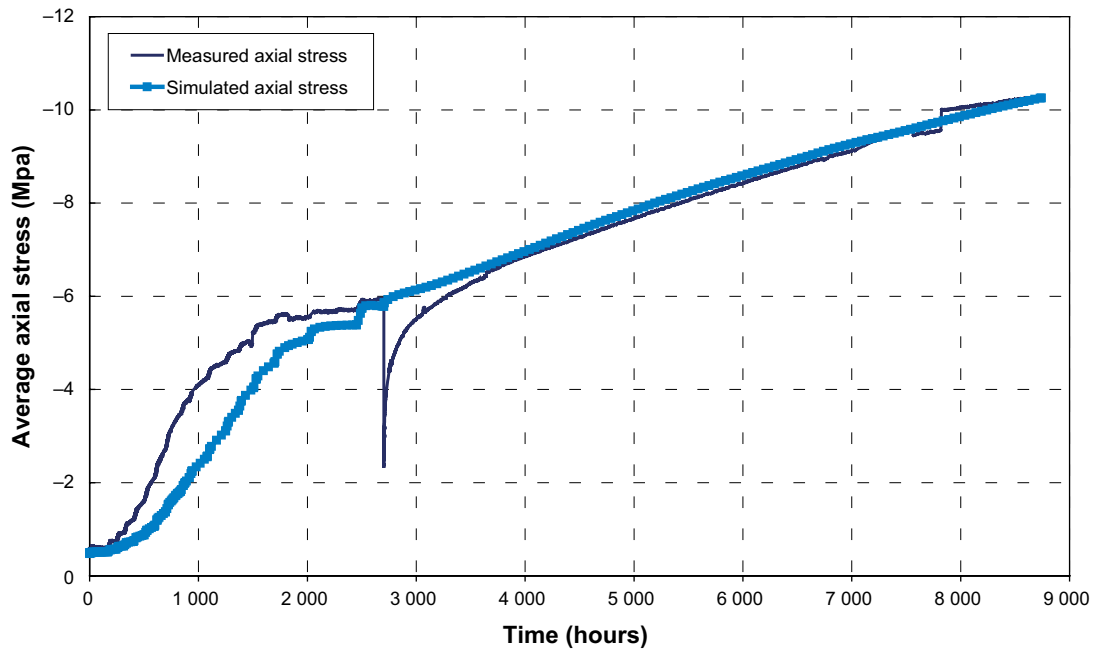


Figure 4-7f. Evolution of axial stress with time, Cell 1. Computed results and observations. CIMNE.

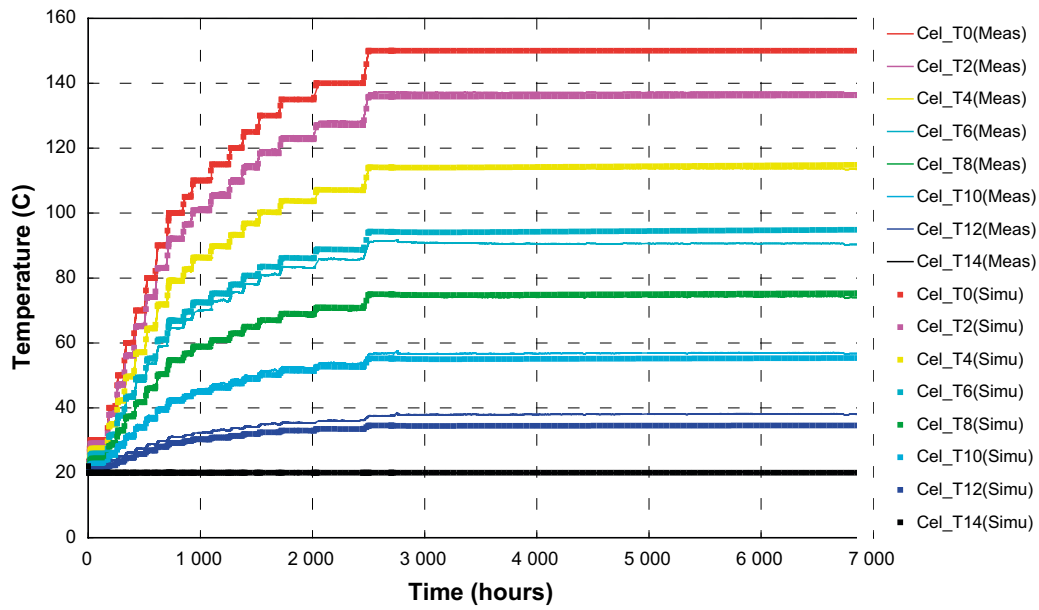


Figure 4-7g. Evolution of temperature with time, Cell 2, Computed results and observations. CIMNE.

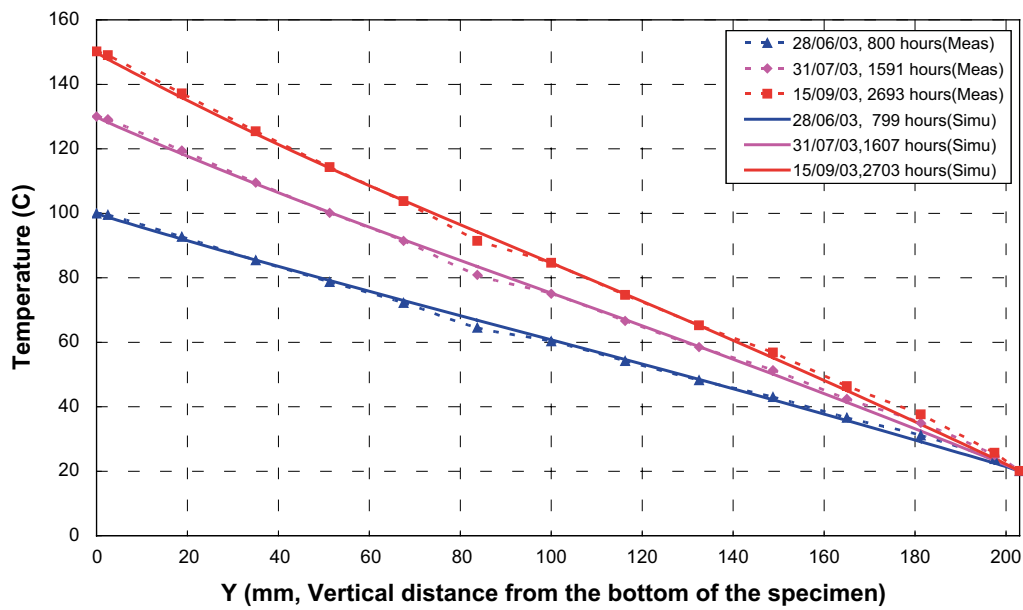


Figure 4-7h. Distributions of temperatures at different times. Cell 2. Computed results and observations. CIMNE.

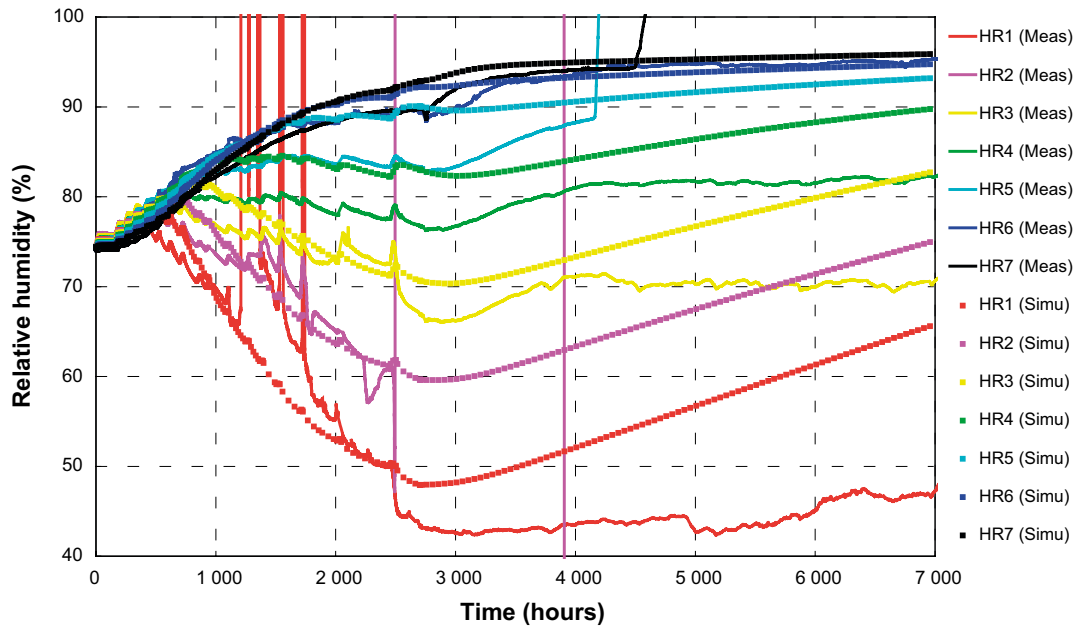


Figure 4-7i. Evolution of relative humidity with time, Cell 2. Computed results and observations. CIMNE.

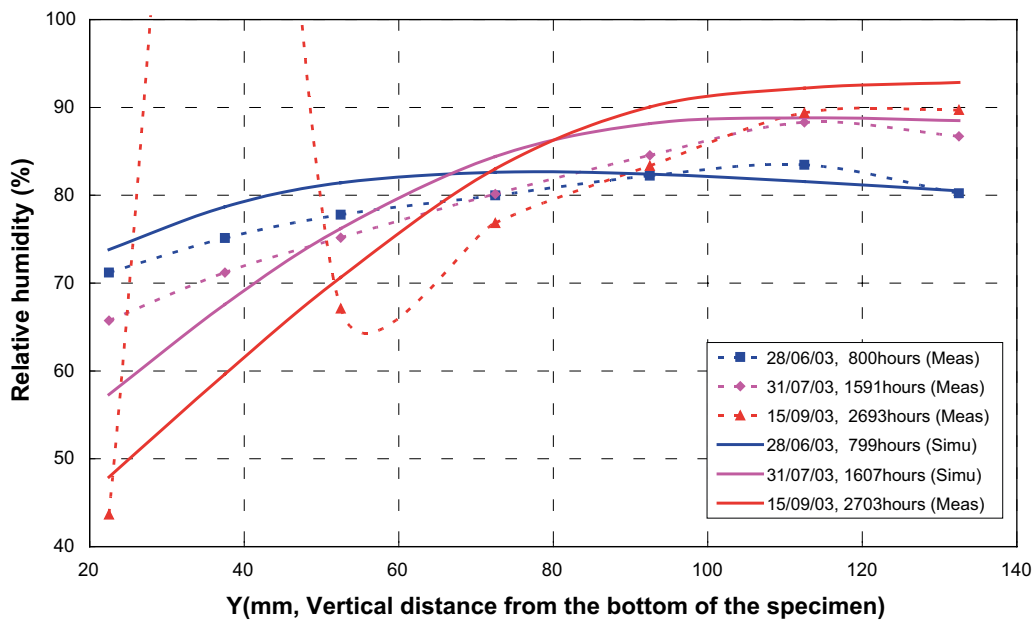


Figure 4-7j. Distributions of relative humidity at different times, Cell 2. Computed results and observations. CIMNE.

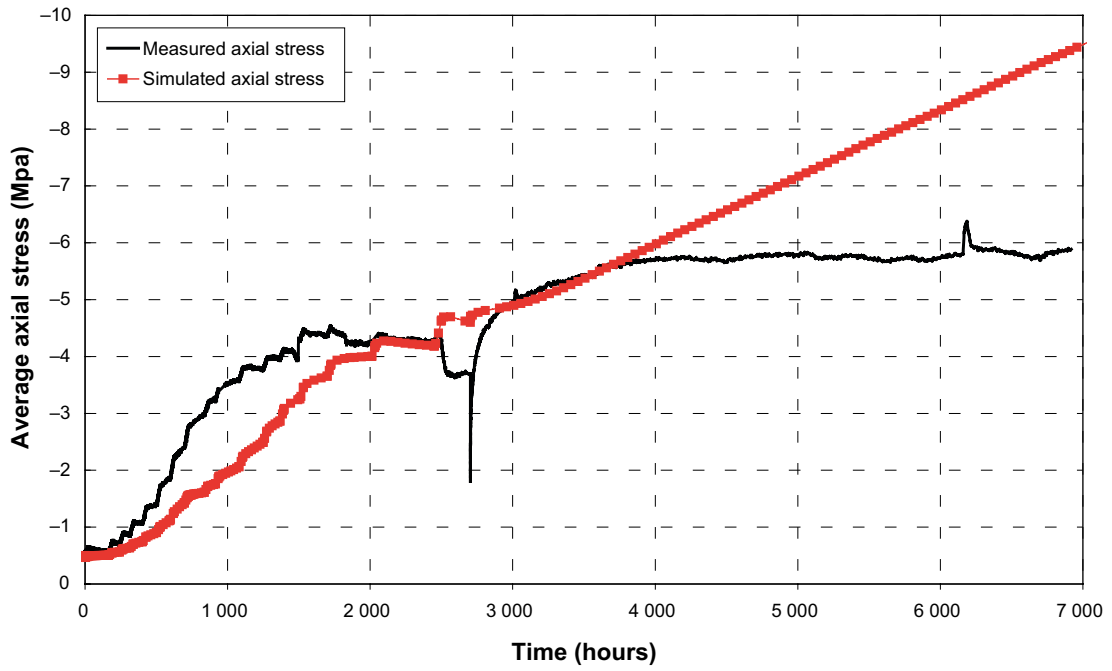


Figure 4-7k. Evolution of axial stress with time, Cell 1. Computed results and observations. CIMNE.

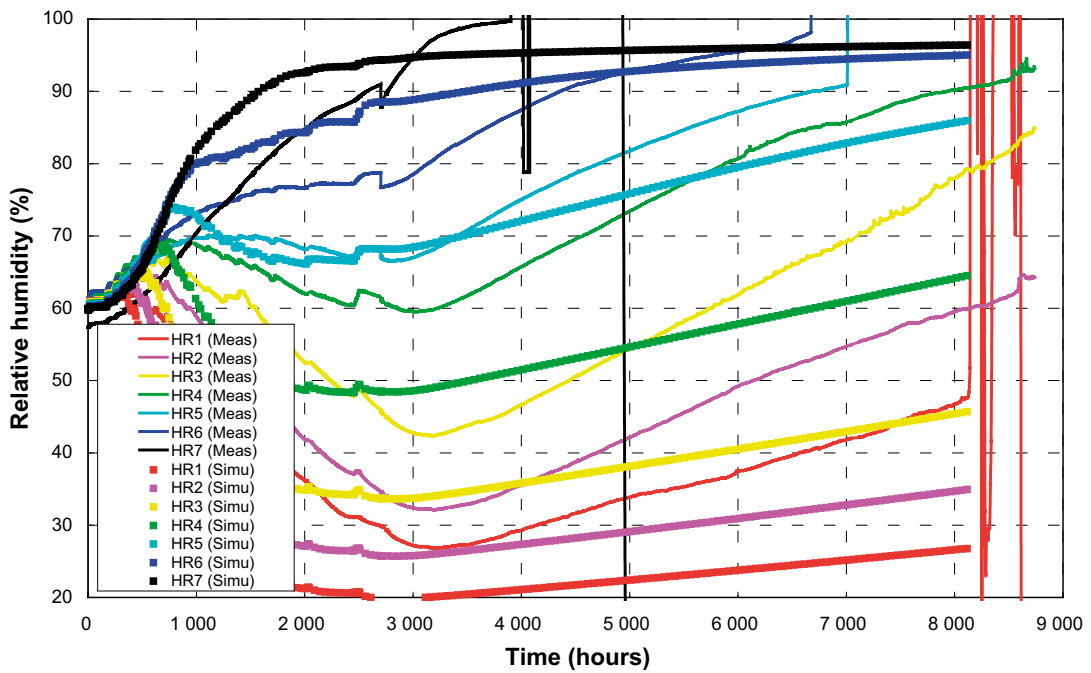


Figure 4-7l. Evolution of relative humidity with time, Cell 1. Computed results and observations. Tortuosity increased from 0.2 to 0.8. CIMNE.

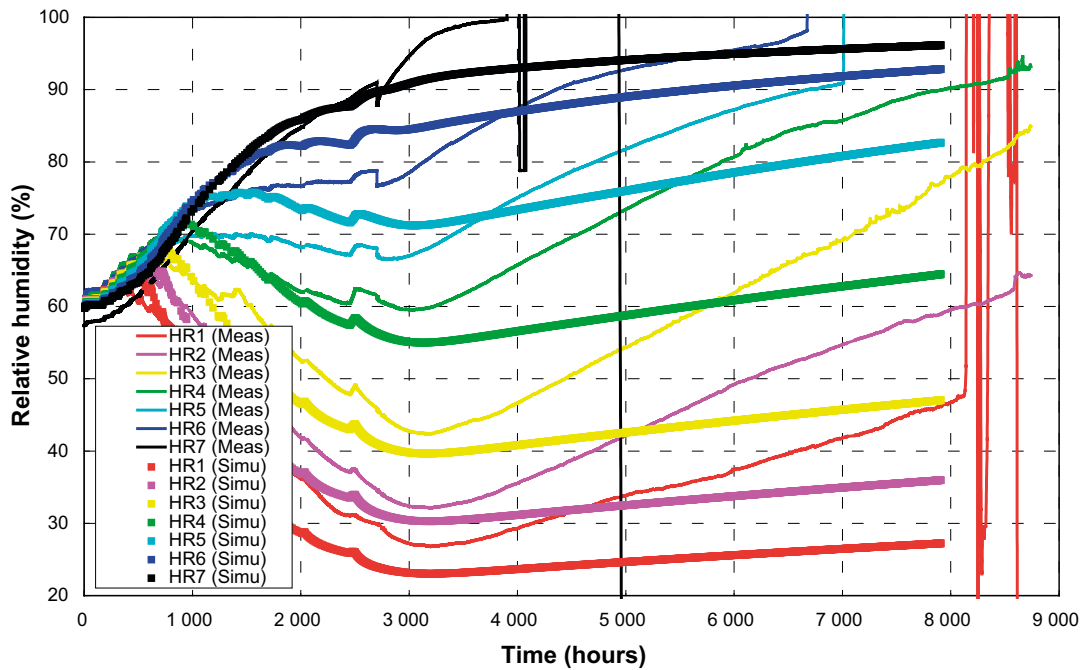


Figure 4-7m. Evolution of relative humidity with time, Cell 1. Computed results and observations. THM analysis without the gas flow equation. CIMNE.

4.4.2 CIEMAT infiltration tests – Subtask 1.2 [6]

The axisymmetric domain and finite element mesh employed in the coupled HM analysis of the Isothermal Test are presented in Figure 4-8a. It is an axisymmetric geometry and the mesh is made up of 400 4-noded quadrilateral elements and 451 nodes. The evolution of degree of saturation is plotted in Figure 4-8b. This team used a different mesh for the Thermal Gradient Test, as shown in Figure 4-8c, the mesh contains 750 4-noded quadrilateral elements and 816 nodes. In this case a THMg analysis has been performed, the results are presented in Figures 4-8d and 4-8e. The performance of a THM tests for this case revealed that the effect of ignoring the gas pressure is quite small in this case in which the temperature remains below 100 °C.

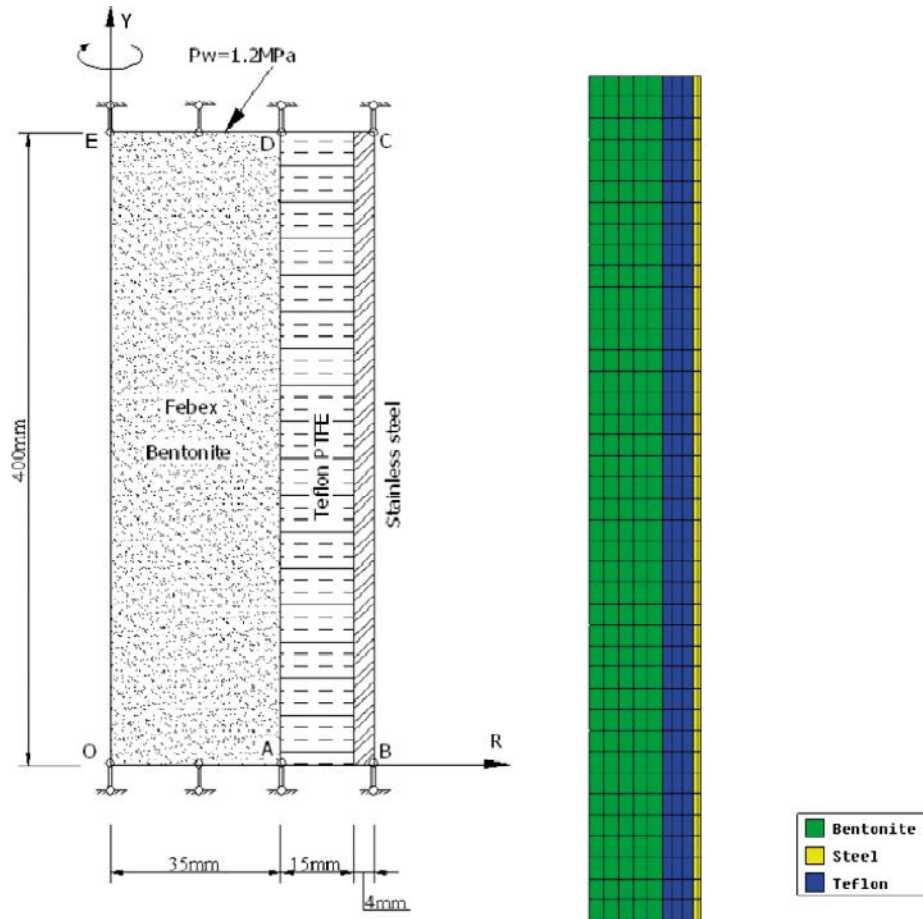


Figure 4-8a. Model geometry and mesh for Isothermal Test. CIMNE.

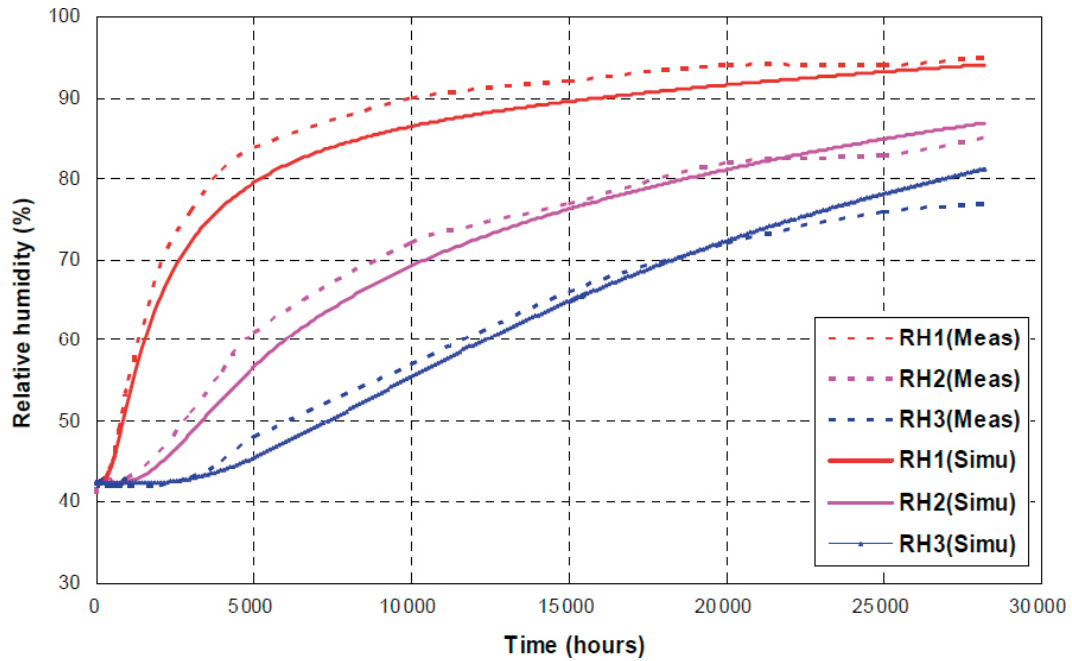


Figure 4-8b. Evolution of relative humidity with time. Isothermal test. Computed results and observations. CIMNE.

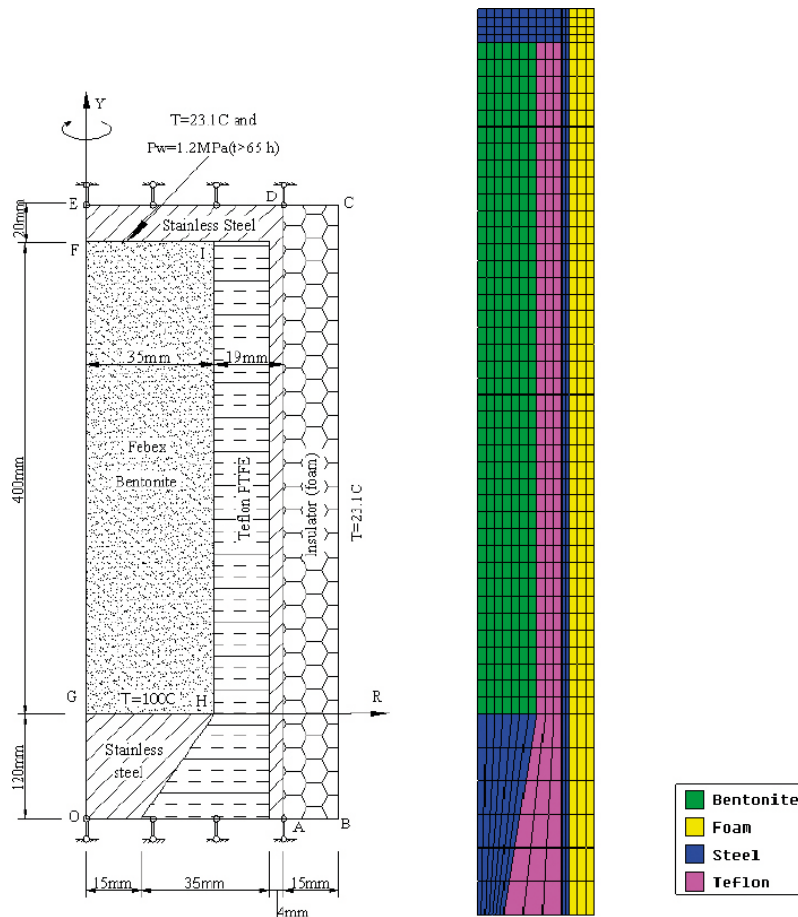


Figure 4-8c. Model geometry and mesh for Thermal Gradient Test. CIMNE.

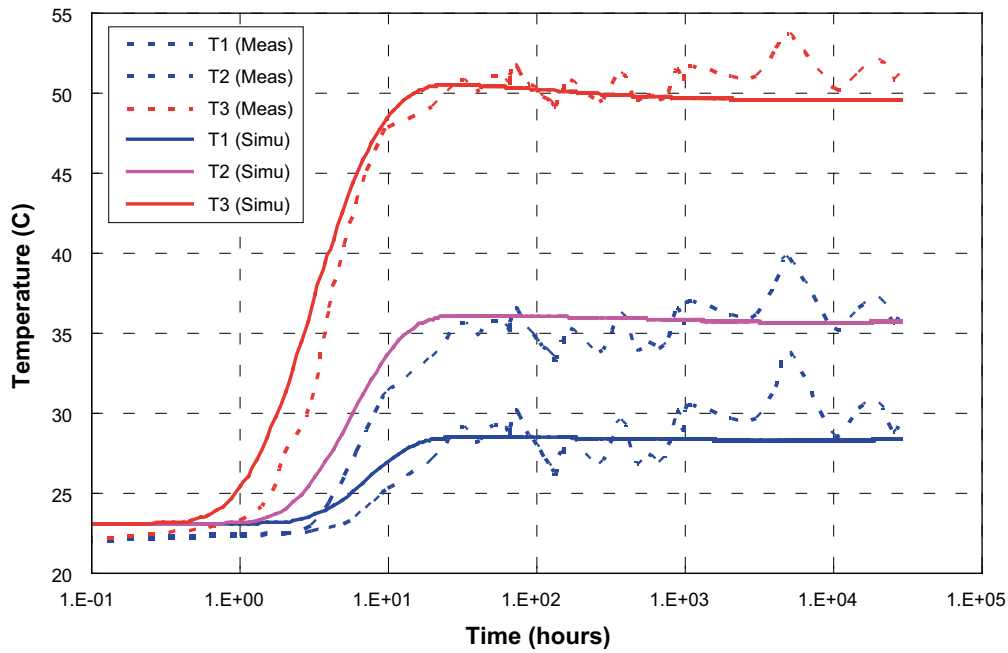


Figure 4-8d. Evolution of temperatures with time. Thermal Gradient Test. Computed results and observations. CIMNE.

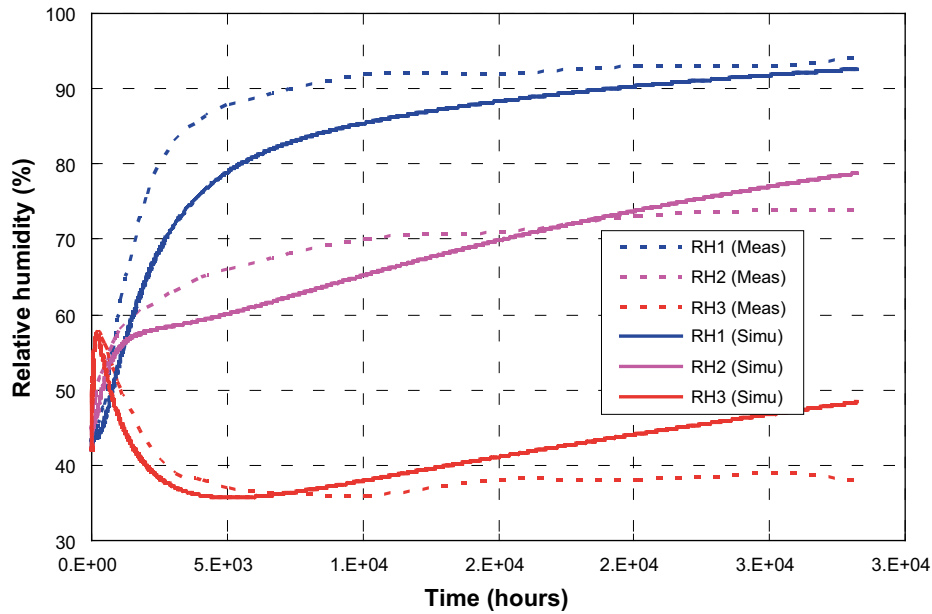


Figure 4-8e. Evolution of relative humidity with time. Thermal Gradient Test. Computed results and observations. CIMNE.

4.4.3 UPC heating test – Subtask 1.3 [6]

This test has been modelled using the axisymmetric geometry and mesh of Figure 4-9a. The mesh is composed of 264 4-noded quadrilateral elements and 300 nodes. The results of the coupled THM analysis are shown in Figures 4-9b to 4-9e. This group performed additional analyses using the parameters of Pintado et al. (2002) backcalculated from TH analyses. Interestingly, the addition of the mechanical component worsens the agreement of final water content. Figure 4-9f shows the evolution of water mass throughout the test. It can be observed that mass conservation is satisfactorily achieved. This team also checked the effect of including the gas balance equation by performing a THMg analysis. As Figure 4-9g shows, gas pressure practically remains constant, so the effects of considering the gas flow are minimal.

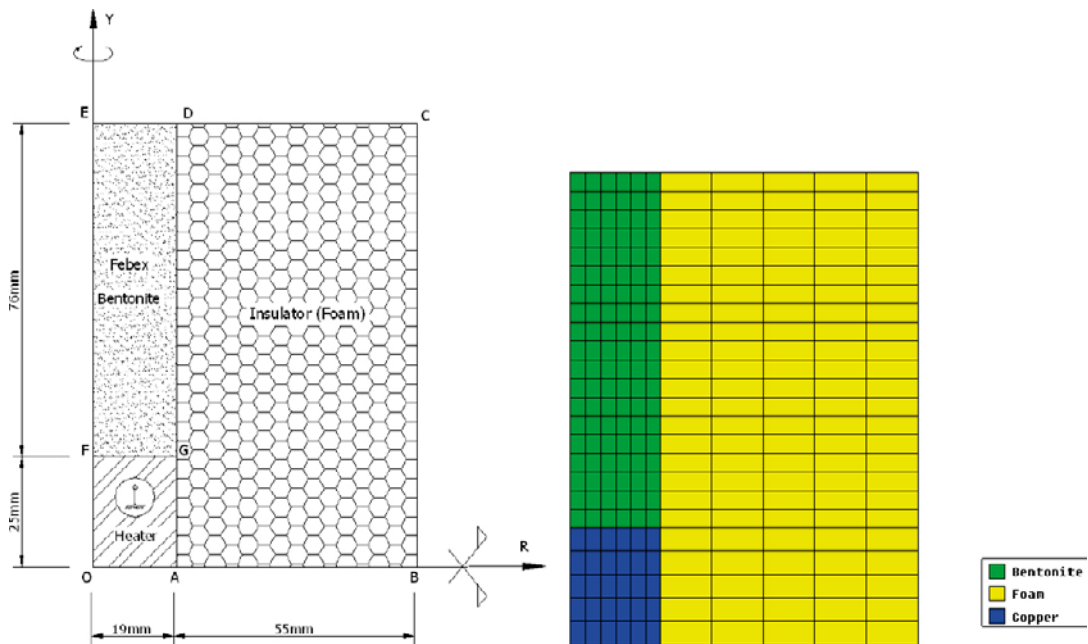


Figure 4-9a. Model geometry and mesh. CIMNE.

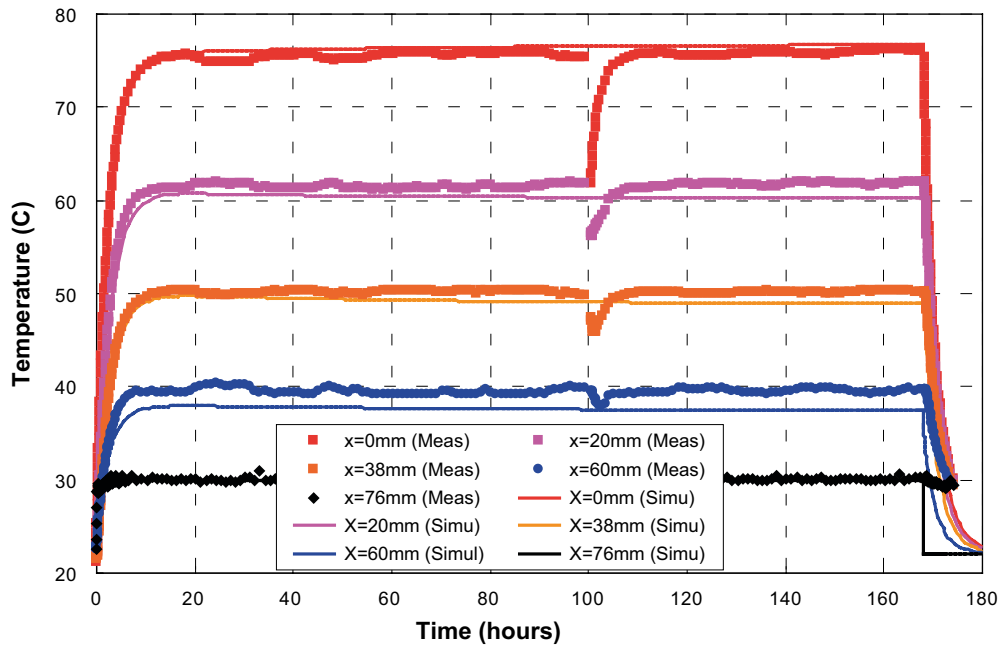


Figure 4-9b. Evolution of temperatures with time. Computed results and observations. CIMNE.

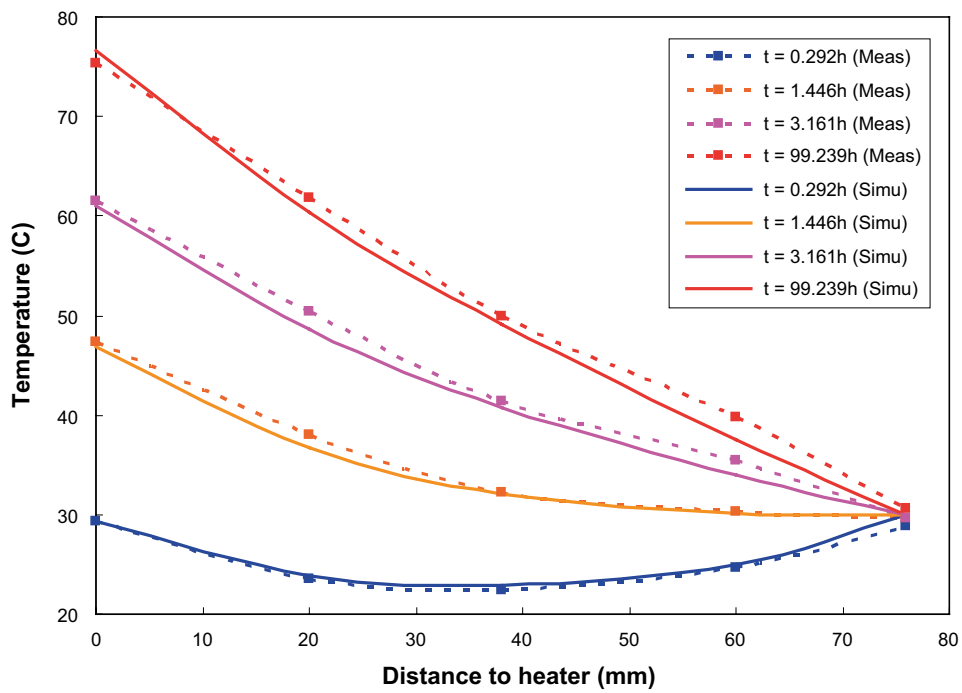


Figure 4-9c. Distribution of temperatures at different times. Computed results and observations. CIMNE.

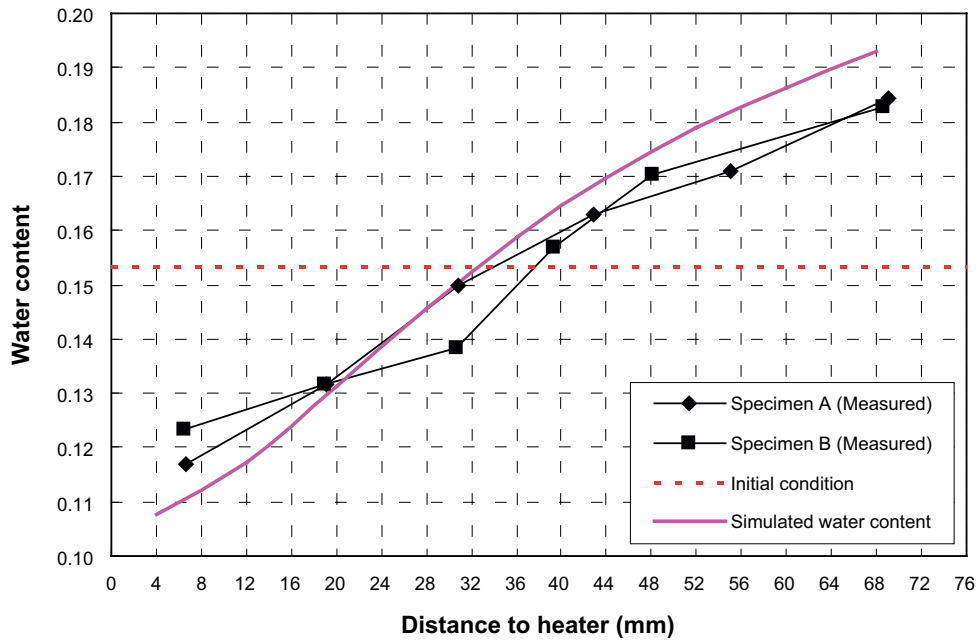


Figure 4-9d. Distribution of water content at the end of test. Computed results and observations. CIMNE.

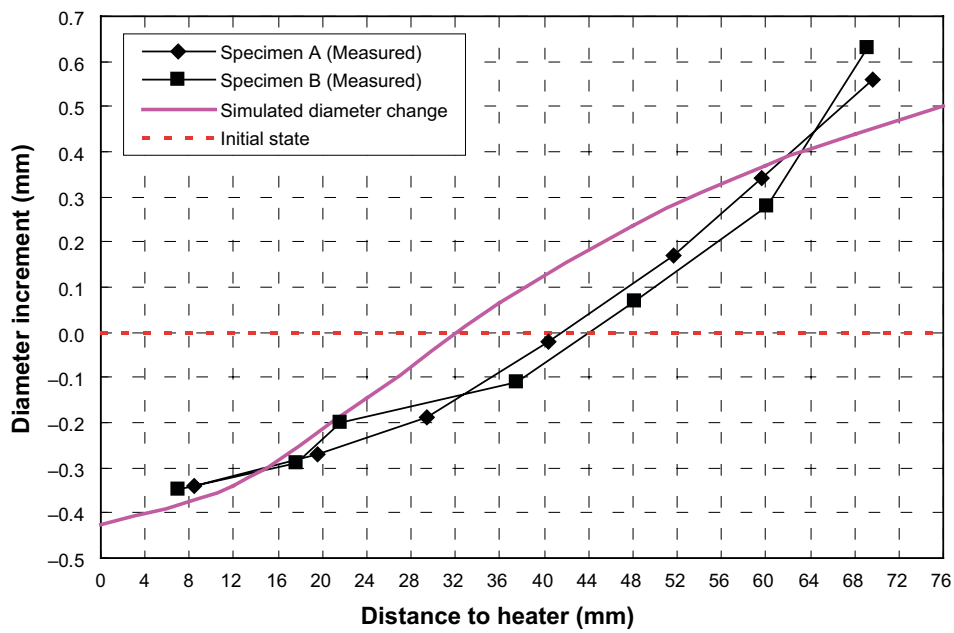


Figure 4-9e. Change of diameter along the specimens at the end of the test. Computed results and observations. CIMNE.

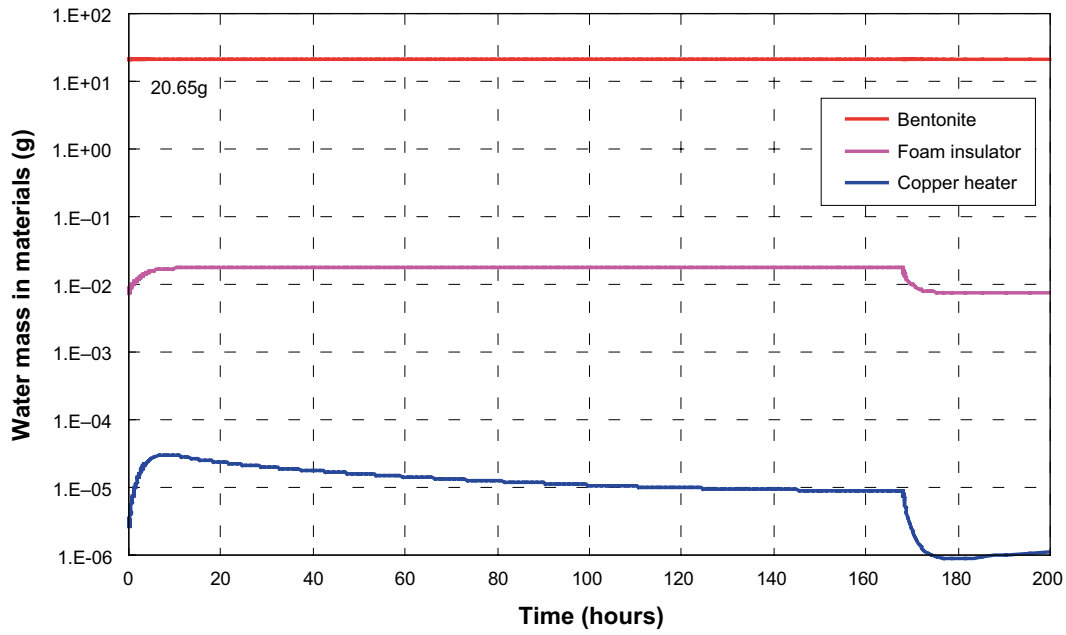


Figure 4-9f. Computed evolution of water mass with time. CIMNE.

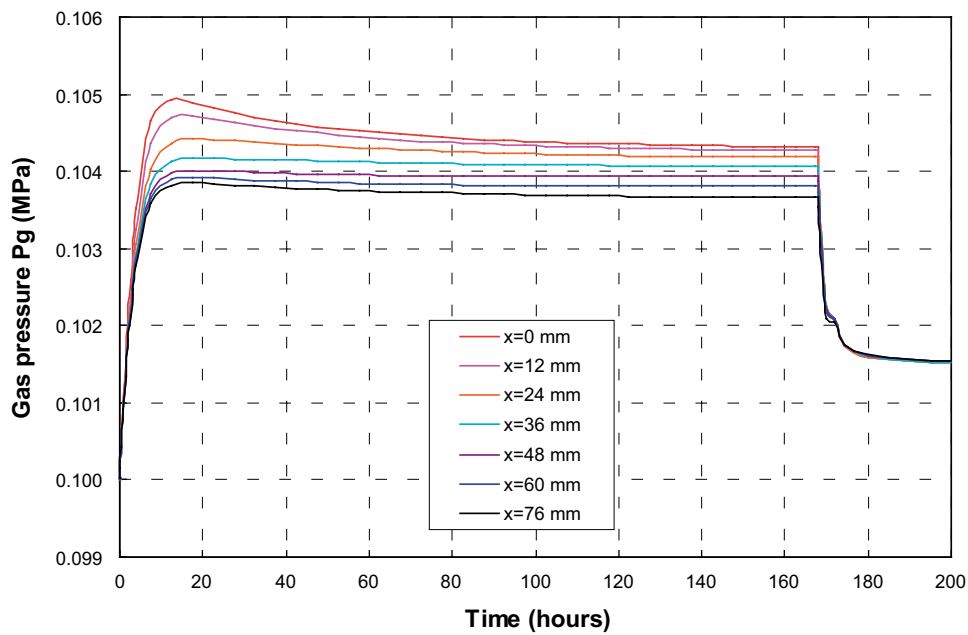


Figure 4-9g. Computed evolution of gas pressure with time. Analysis THMg. CIMNE.

4.4.4 Remarks

There are two distinctive features of the analyses performed by CIMNE: they performed THMg analysis throughout and they used an elastoplastic model for the mechanical constitutive law although it must be said that the plastic component was seldom engaged. An interesting conclusion is that the incorporation of the gas flow equation only has noticeable (but not drastic) effects in cases in which temperatures rise above 100 °C. Whenever water mass conservation has been checked it has been found to be satisfactory. The team used basically the same parameters in Subtasks 1.2 and 1.3; there were only modest variations in some hydraulic parameters (intrinsic permeability and tortuosity).

Overall, thermal and hydraulic effects appear satisfactorily modelled. In Subtask 1, the evolution of relative humidity is reasonably well captured but the slow hydration of Cell 2 is not reproduced. Consequently, the good agreement between computed and observed axial stresses in Cell 1 cannot be repeated for the Cell 2 case. Finally, the thermohydraulic results in Subtask 3 are satisfactorily modelled; reasonable agreement is also obtained with the measured sample deformation.

4.5 Clay Technology-1

4.5.1 CEA mock-up tests – Subtask 1.1 [7]

The team Clay Technology-1 performed analyses using the axisymmetric geometry and boundary conditions shown in Figure 4-10a. They adapted the gas flow parameters and boundary condition so that reasonable values of gas pressures were obtained in the computations. The experiment was not considered air-tight. The main results are plotted in Figures 4-10b to 4-10k. Figure 4-10l shows the variation with time of the computed vapour pressure for Cell 2. It is interesting to note that in the lower part of the cell (close to the heating boundary), vapour pressure is well above 1 atmosphere, consistent with the high temperatures in this zone.

Additional analyses were performed by this group to check the effects of a number of features and parameters: tortuosity, intrinsic permeability, retention curve and porosity. As expected, variations in the hydraulic results are obtained. Again, it is found that the resulting relative humidity results depend more directly in the ratio tortuosity/intrinsic permeability ratio (τ/k) rather than on the individual parameters.

Mass conservation has also been checked for a variety of boundary and analysis conditions for Phase 1 of Cell 1 (Figure 4-10m). Computed mass variation is always below 1 %.

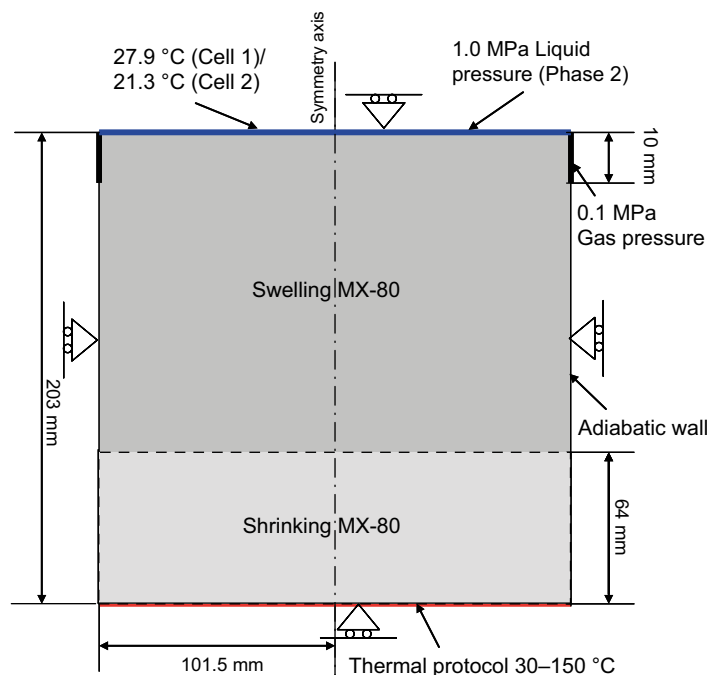


Figure 4-10a. Model geometry and boundary conditions. Clay Technology-1.

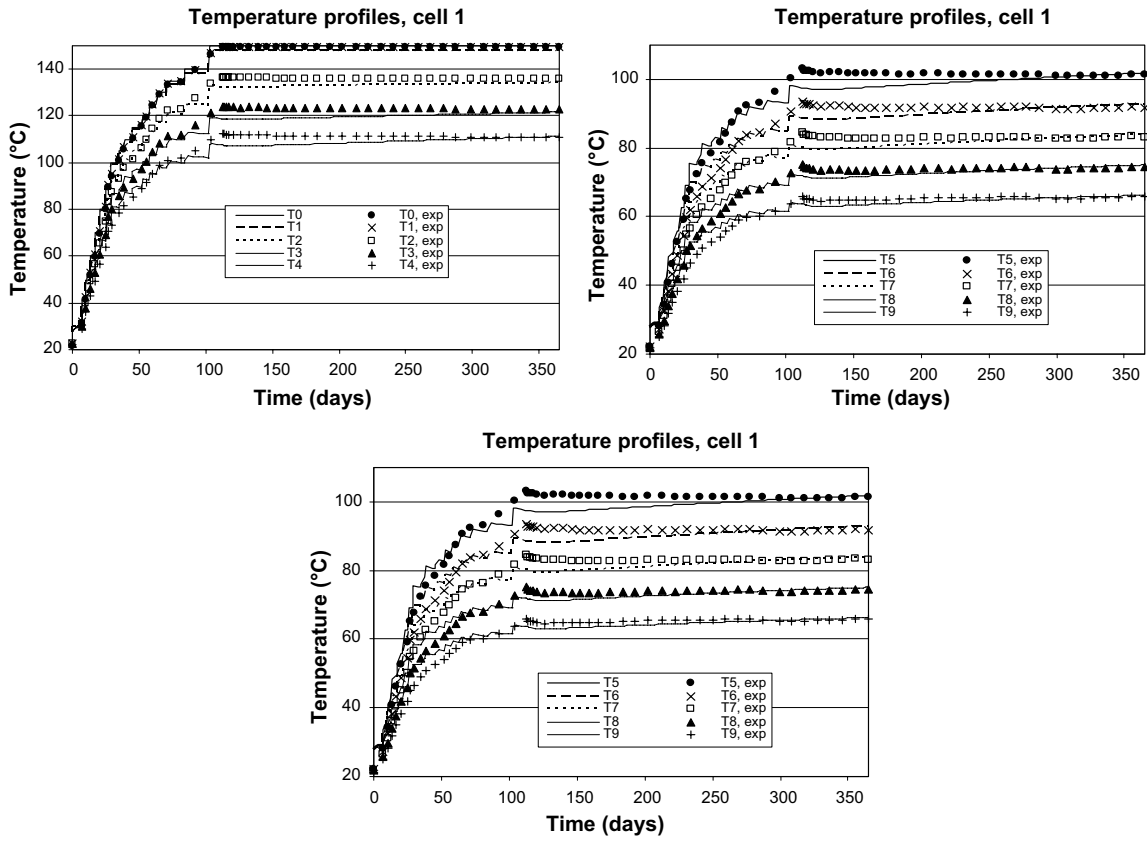


Figure 4-10b. Evolution of temperature with time, Cell 1, Computed results and observations. Clay Technology-1.

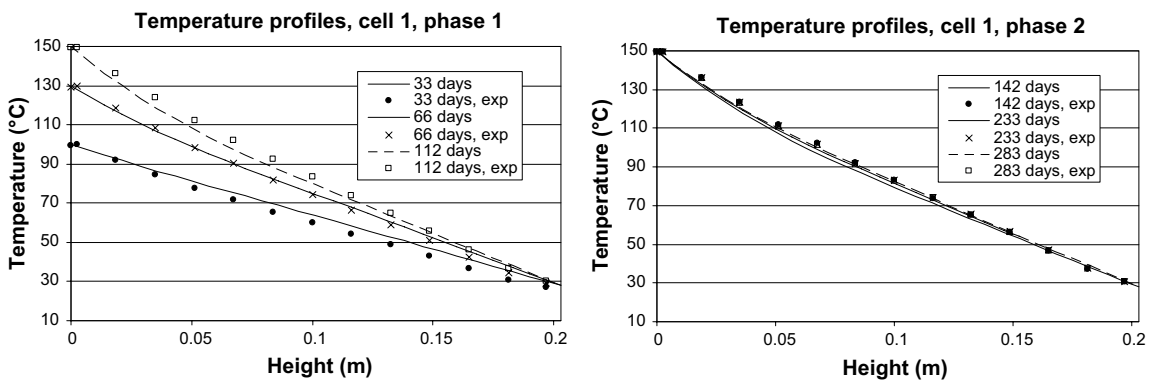


Figure 4-10c. Distributions of temperatures at different times. Cell 1. Computed results and observations. Clay Technology-1.

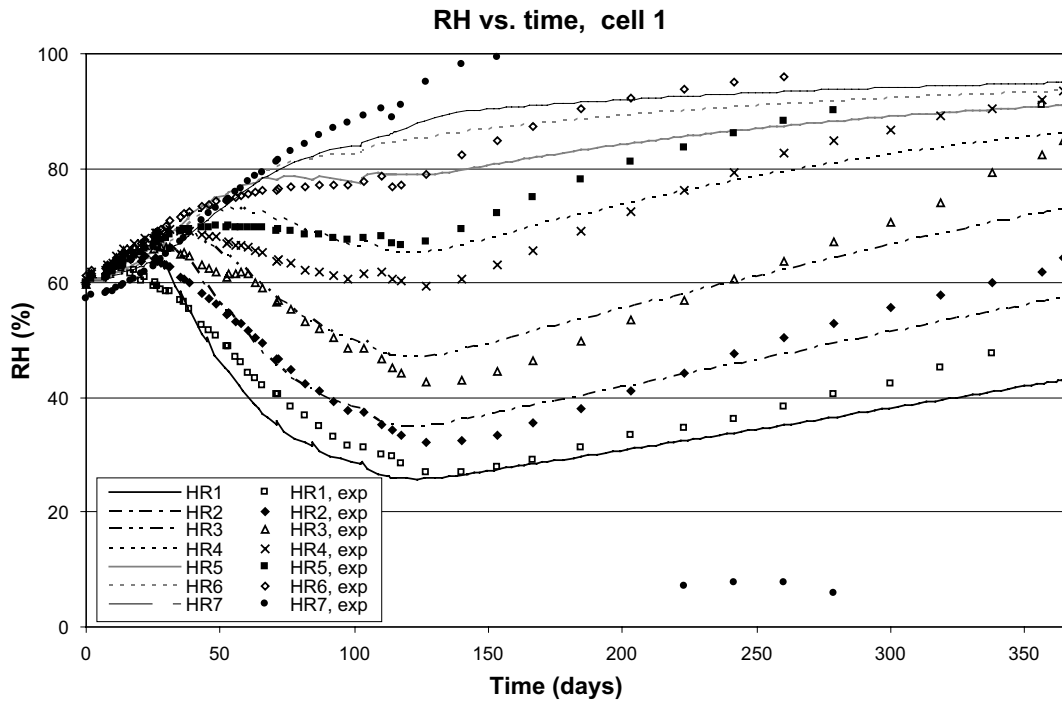


Figure 4-10d. Evolution of relative humidity with time, Cell 1. Computed results and observations. Clay Technology-1.

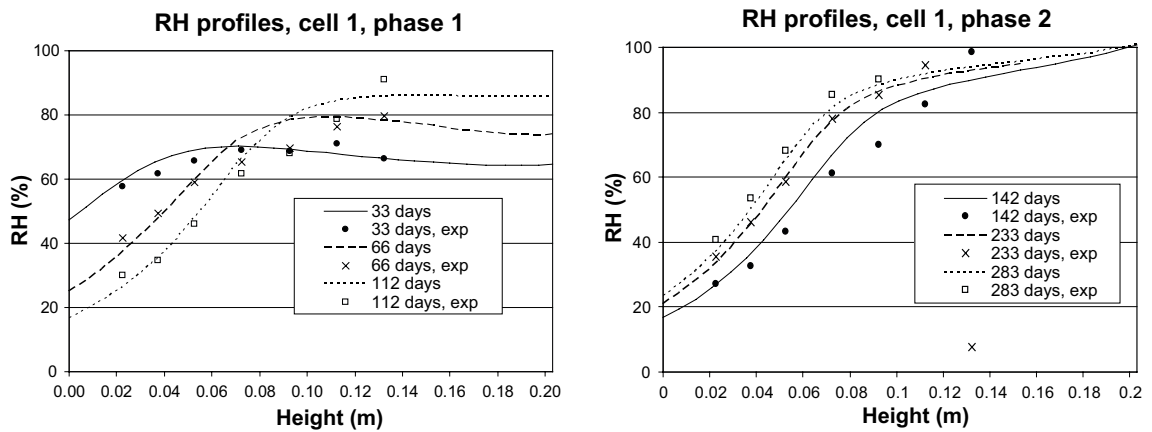


Figure 4-10e. Distributions of relative humidity at different times, Cell 1. Computed results and observations. Clay Technology-1.

Axial stress vs. time, Cell 1

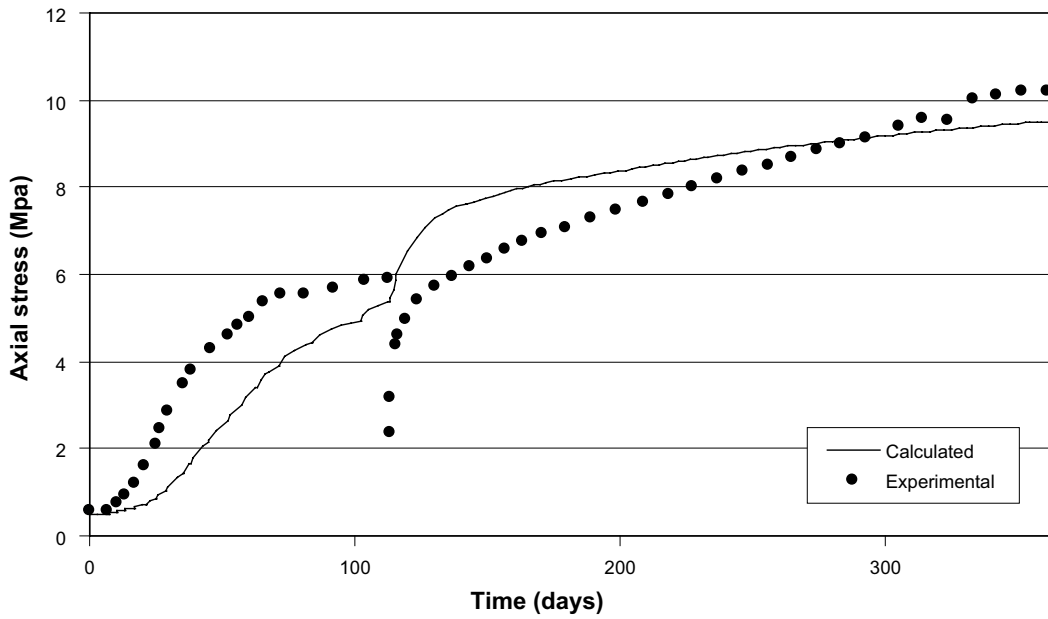
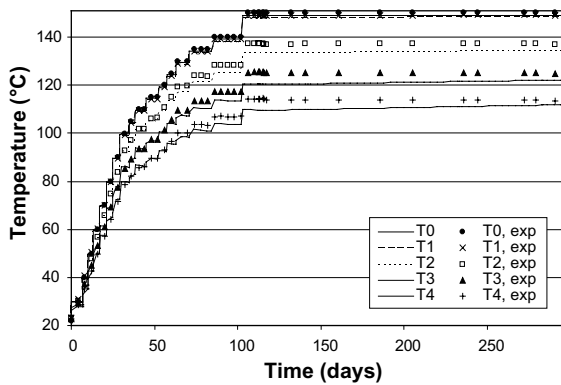
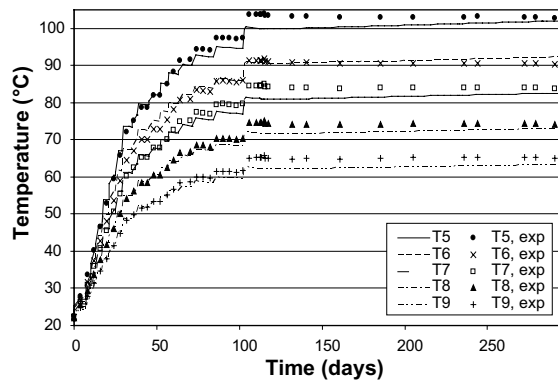


Figure 4-10f. Evolution of axial stress with time, Cell 1. Computed results and observations. Clay Technology-1.

Temperature vs. Time, cell 2



Temperature vs. Time, cell 2



Temperature vs. Time, cell 2

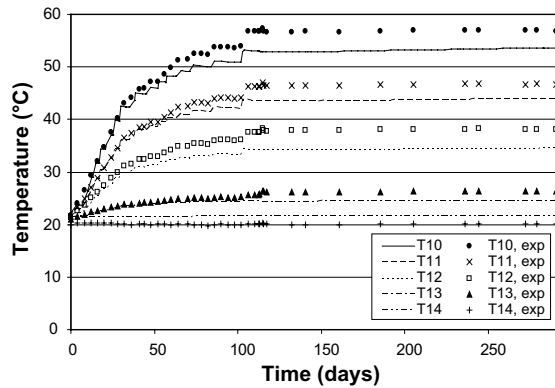


Figure 4-10g. Evolution of temperature with time, Cell 2, Computed results and observations. Clay Technology-1.

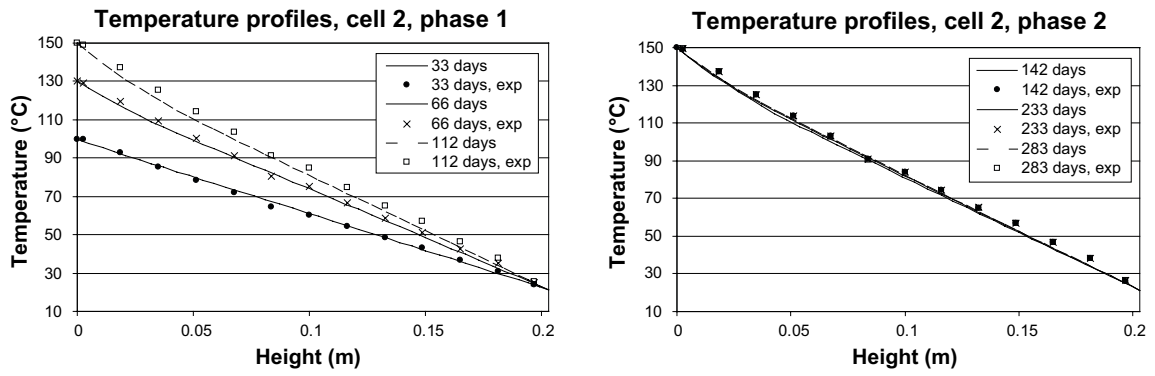


Figure 4-10h. Distributions of temperatures at different times. Cell 2. Computed results and observations. Clay Technology-1.

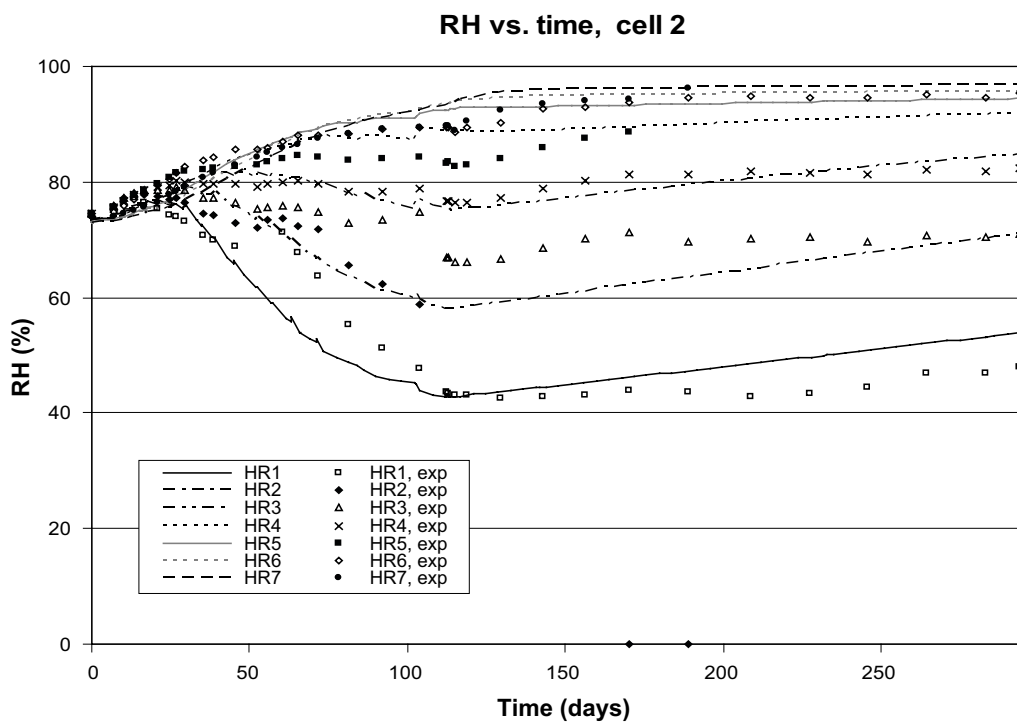


Figure 4-10i. Evolution of relative humidity with time, Cell 2. Computed results and observations. Clay Technology-1.

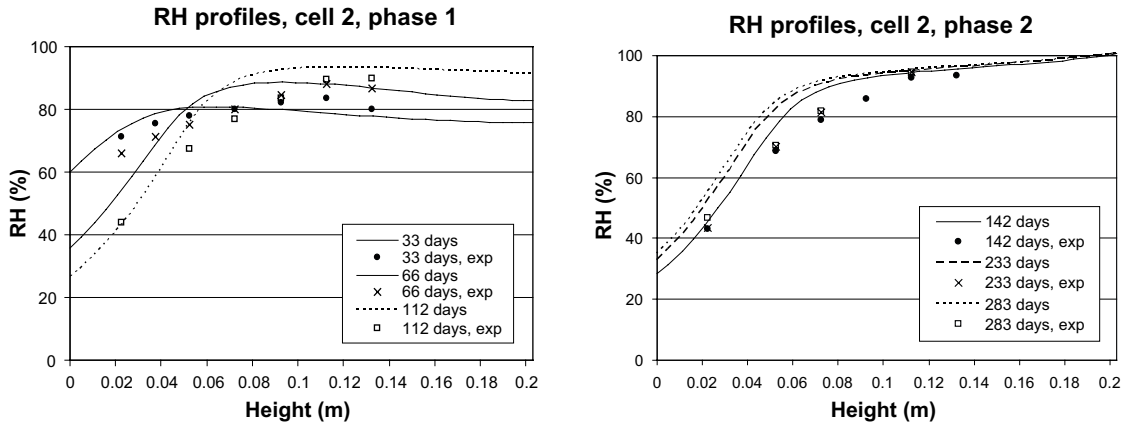


Figure 4-10j. Distributions of relative humidity at different times, Cell 2. Computed results and observations. Clay Technology-1.

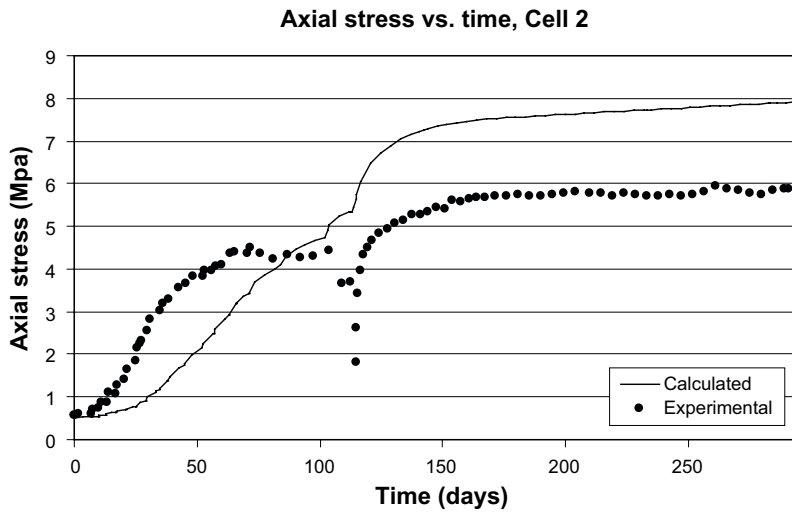


Figure 4-10k. Evolution of axial stress with time, Cell 2. Computed results and observations. Clay Technology-1.

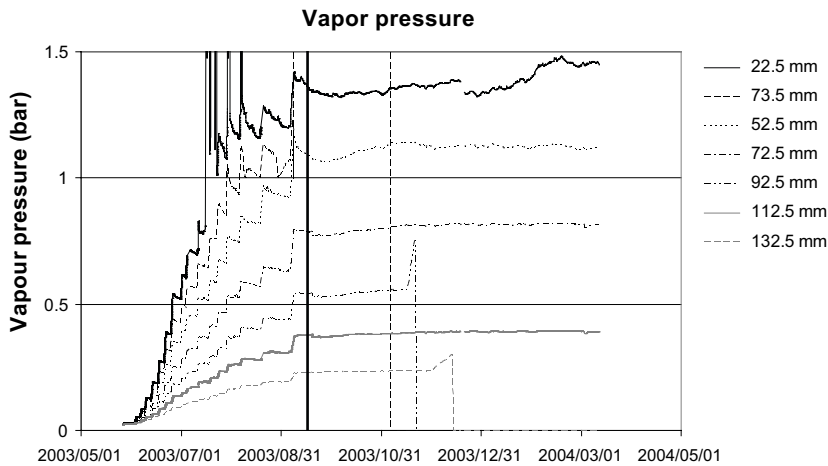


Figure 4-10l. Computed evolution of vapour pressure with time. Cell 2. Clay Technology-1.

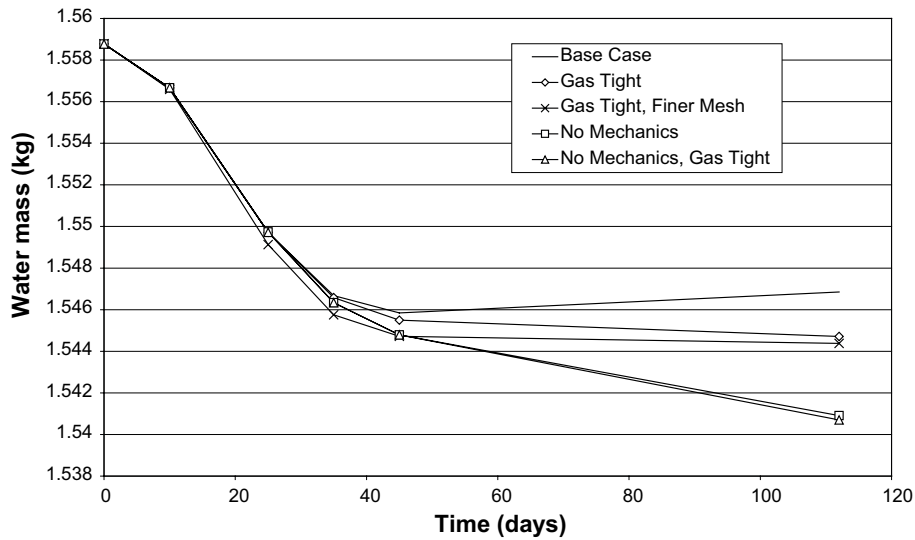


Figure 4-10m. Evolution of water mass with time for various boundary and analysis conditions. Cell 1, Phase 1. Clay Technology-1.

4.5.2 CIEMAT infiltration tests – Subtask 1.2 [8]

The same axisymmetric geometry is used for the Isothermal Test and for the Thermal Gradient Test, as shown in Figure 4-11a. The mesh contains 1 414 4-noded quadrilateral elements and TH (no mechanical problem) analyses were performed. Constant gas pressure equal to atmospheric is assumed. The results are presented in Figures 4-11b to 4-11d. The sensitivity analyses focused on the effects of changes in tortuosity and intrinsic permeability. The results are shown in Figure 4-11e in terms of the variation of relative humidity for the sensor closes to the heater.

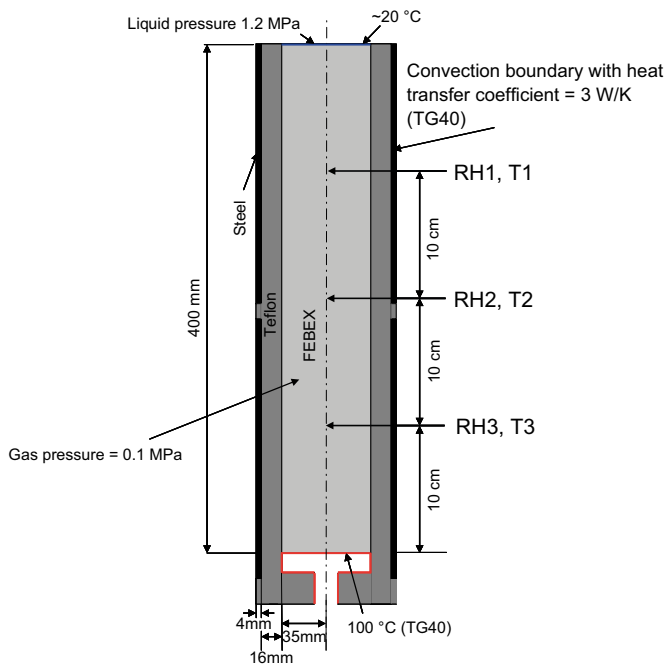


Figure 4-11a. Model geometry and boundary conditions. Clay Technology-1.

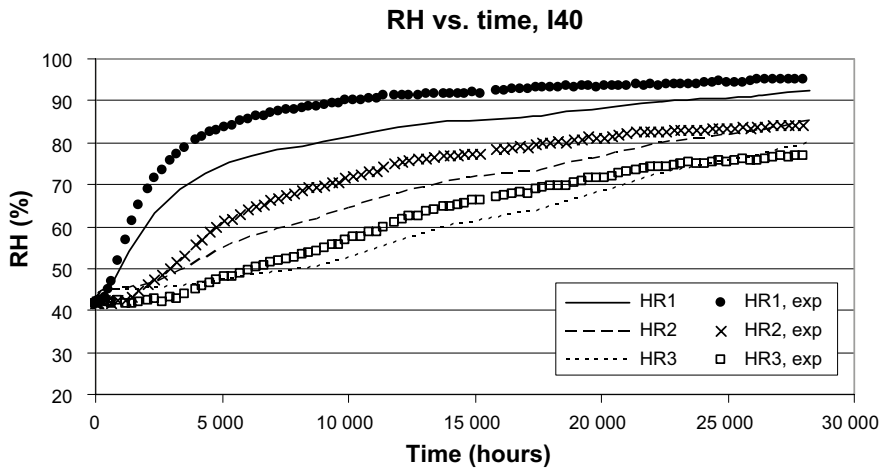


Figure 4-11b. Evolution of relative humidity with time. Isothermal test. Computed results and observations. Clay Technology-1.

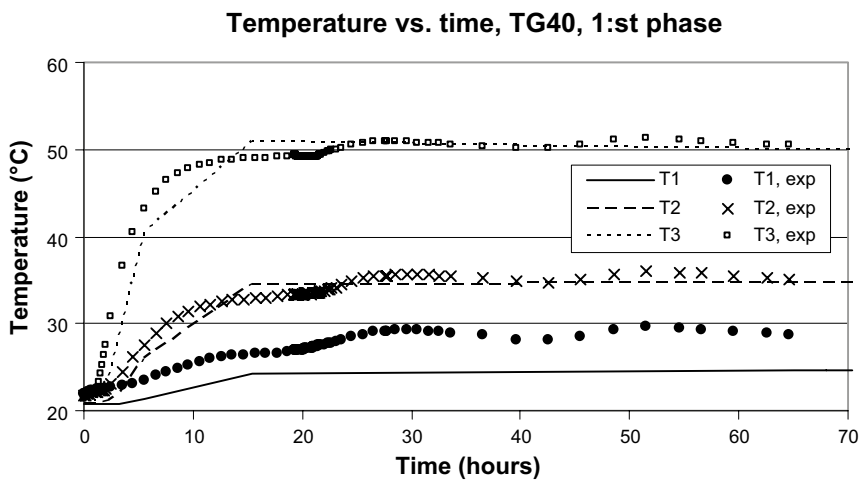


Figure 4-11c. Evolution of temperatures with time. Thermal Gradient Test. Computed results and observations. Clay Technology-1.

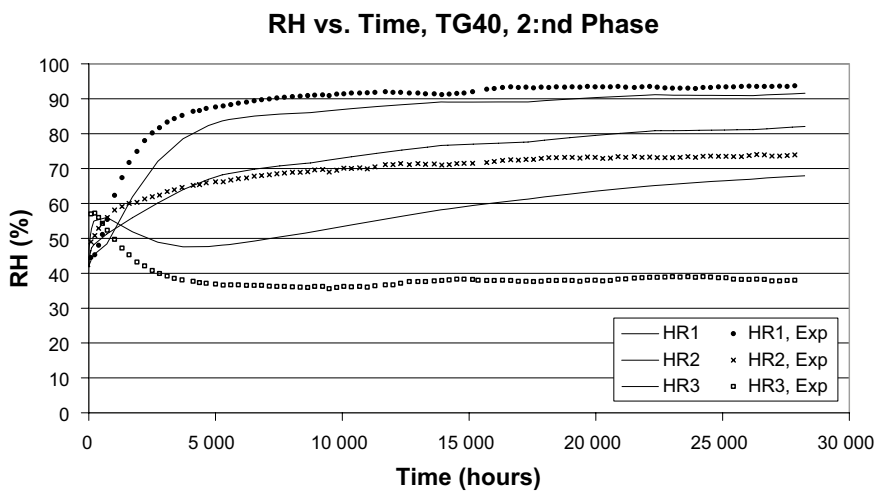


Figure 4-11d. Evolution of relative humidity with time. Thermal Gradient Test. Computed results and observations. Clay Technology-1.

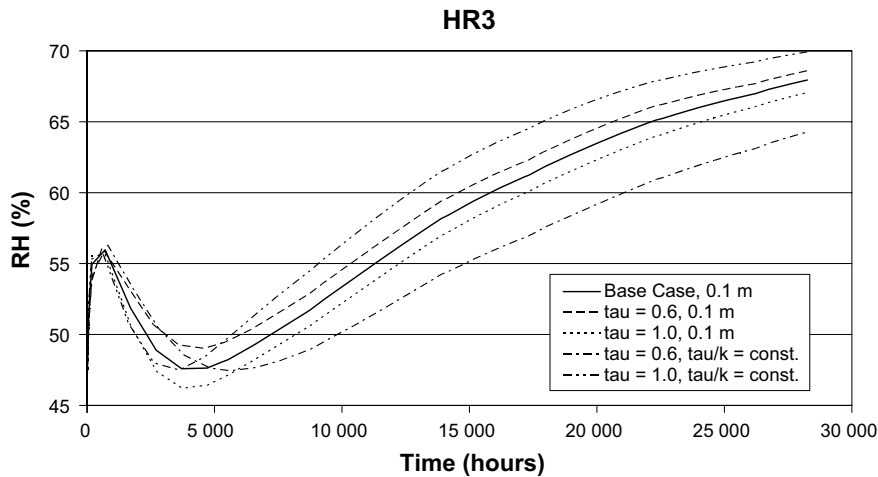


Figure 4-11e. Evolution of relative humidity with time of the sensor closest to the heater (HR3). Thermal Gradient Test. Computed results using various values of tortuosity and permeability. Clay Technology-1.

4.5.3 UPC heating test – Subtask 1.3 [9]

An axisymmetric THM analysis has been performed. The model geometry and boundary conditions are depicted in Figure 4-12a. The results of the analyses are presented in Figures 4-12b to 4-12e.

4.5.4 Remarks

The formulation incorporated the air balance equation but it has only been used in Subtask 1.1, where the occurrence of temperatures above 100 °C makes it very advisable. The analyses have confirmed that gas pressures higher than atmospheric occur in the high temperature zones. Sensitivity analyses carried out by this group have demonstrated the sensitivity of the hydraulic results to a variety of parameters such as tortuosity, permeability, retention curve and porosity. Whenever checked, water mass conservation has proved satisfactory. Temperatures and overall hydraulic behaviour are generally satisfactorily modelled.

In Subtask 1.1, the evolution of relative permeability appears well reproduced but the slow hydration of Cell 2 is not captured although the results of this group are closer to the observations when compared to most other teams. Axial swelling pressure is satisfactorily predicted. Concerning Subtask 1.2, the Isothermal Test is well reproduced but the slow hydration of the Thermal Gradient Test is not well described. Also the modelling in Subtask 1.3 is satisfactory achieving good agreement with observations. It should be noted, however, a TH analysis was performed in Subtask 1.2 whereas a full THM analysis was performed in Subtask 1.3. Also, the retention laws and hydraulic parameters are somewhat different in spite that the material was the same and the initial conditions quite similar.

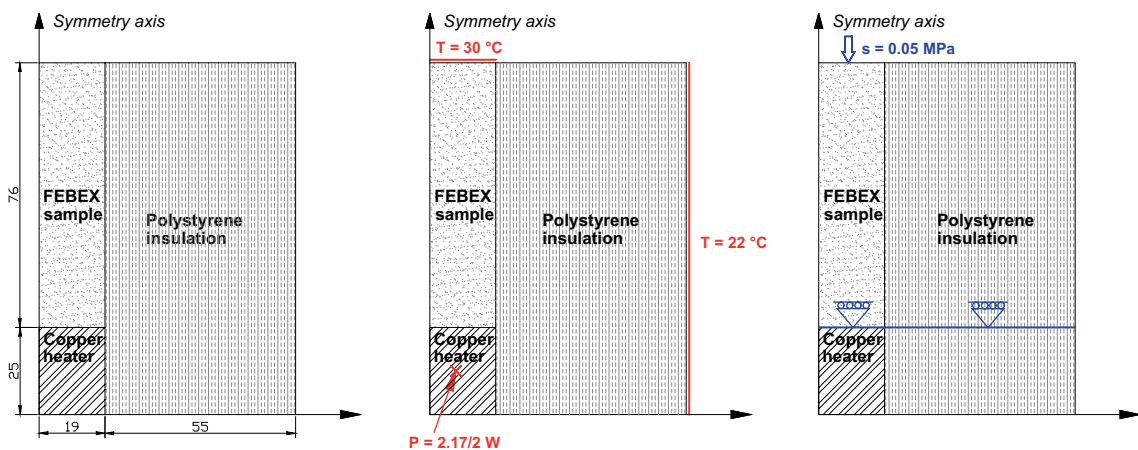


Figure 4.12a. Model geometry and boundary conditions. Clay Technology-1

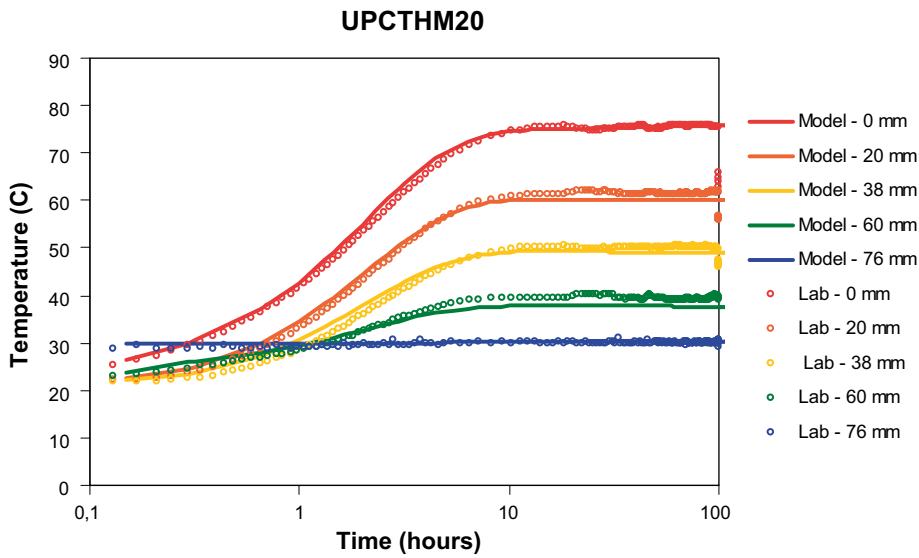


Figure 4-12b. Evolution of temperatures with time. Computed results and observations. Clay Technology-1.

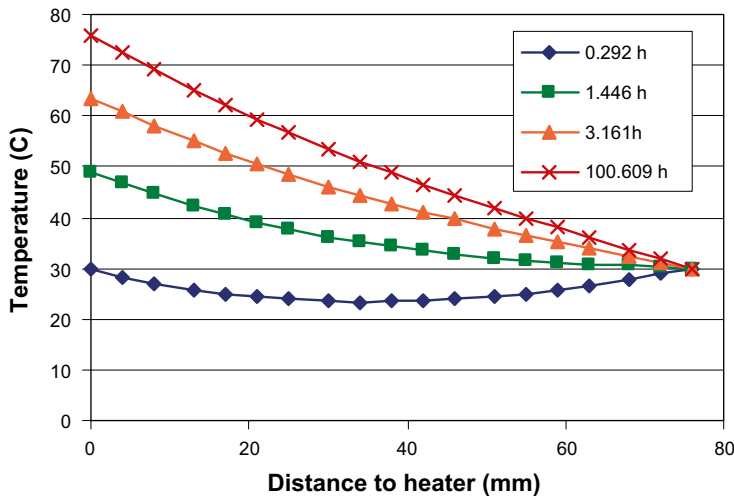


Figure 4-12c. Distribution of temperatures at different times. Computed results and observations. Clay Technology-1.

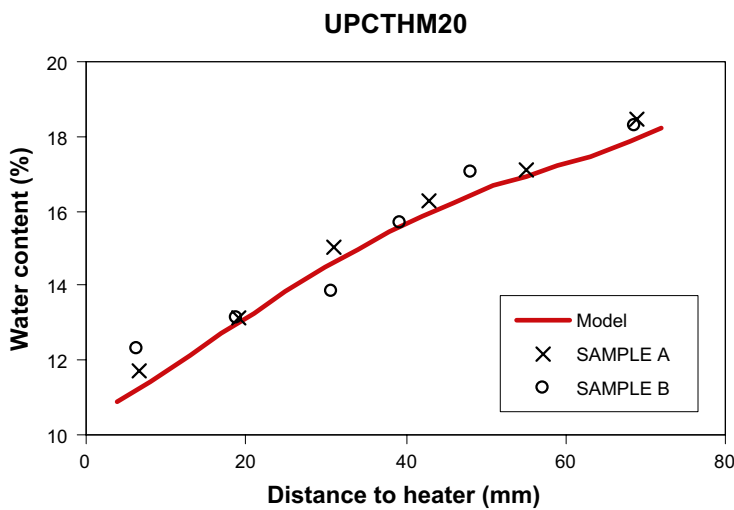


Figure 4-12d. Distribution of water content at the end of test. Computed results and observations. Clay Technology-1.

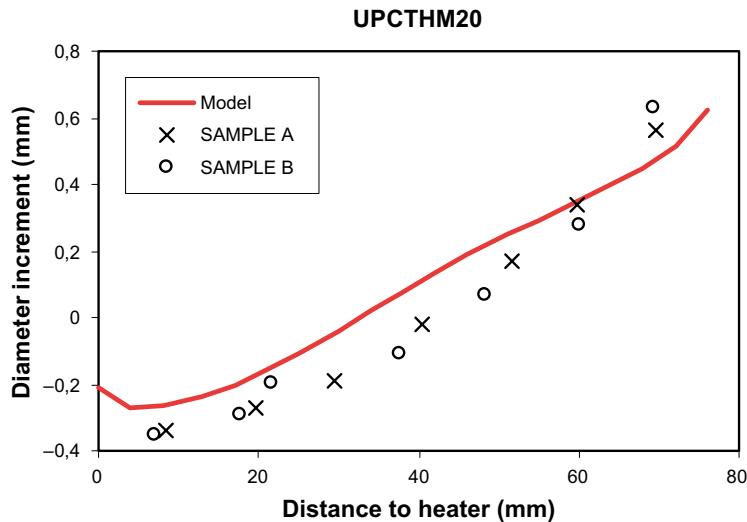


Figure 4-12e. Change of diameter along the specimens at the end of the test. Computed results and observations. Clay Technology-1.

4.6 Clay Technology-2

4.6.1 CEA mock-up tests – Subtask 1.1 [10]

For this Subtask no thermal modelling was carried out because of lack of data concerning the thermal properties of the insulation and applied power. Measured temperatures were applied assuming a linear distribution inside the specimen. The finite element mesh used in the HM analyses is depicted in Figure 4-13a. It consists of 3 200 axisymmetric elements.

The results selected for presentation are shown in Figures 4-13b to 4-13g. It should be noted that the distributions of temperatures (Figures 4-13b and 4-13e) refers to applied temperatures and not to computed ones. This team also checked the effects of assuming that the retention curve varied with temperature; the calculated results did not show a better agreement with observations. For Cell 2, the evolutions of void ratio for different points located in the axis of the sample were plotted (Figure 4-13h). It can be noticed that the distribution of void ratio is not uniform and that the computed heterogeneity remains at the end of the test.

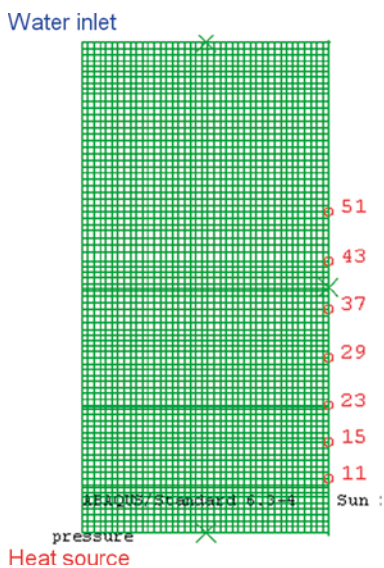


Figure 4-13a. Model mesh. Clay Technology-2.

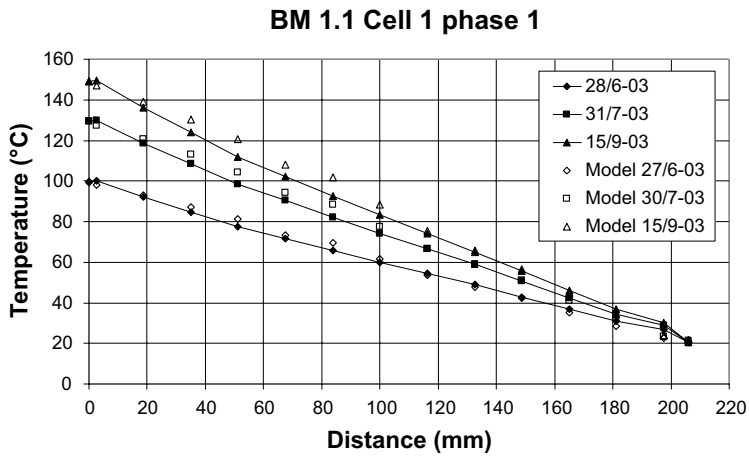


Figure 4-13b. Distributions of applied and observed temperatures at different times. Cell 1. Clay Technology-2.

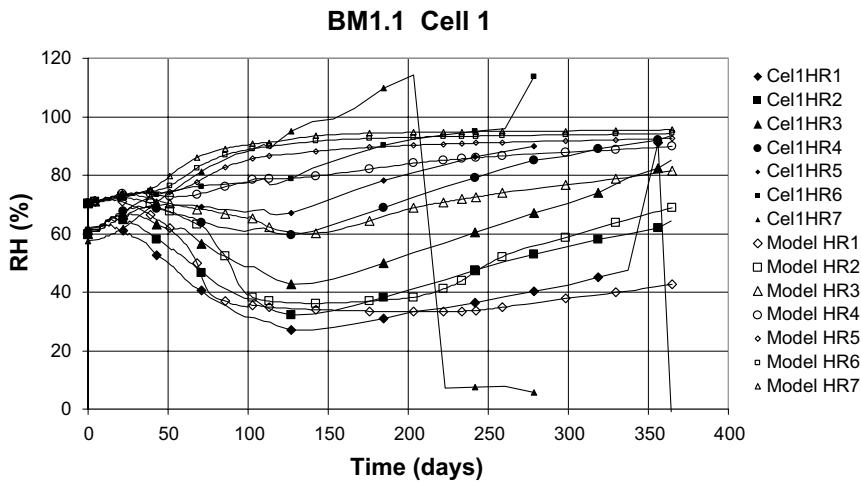


Figure 4-13c. Evolution of relative humidity with time, Cell 1. Computed results and observations. Clay Technology-2.

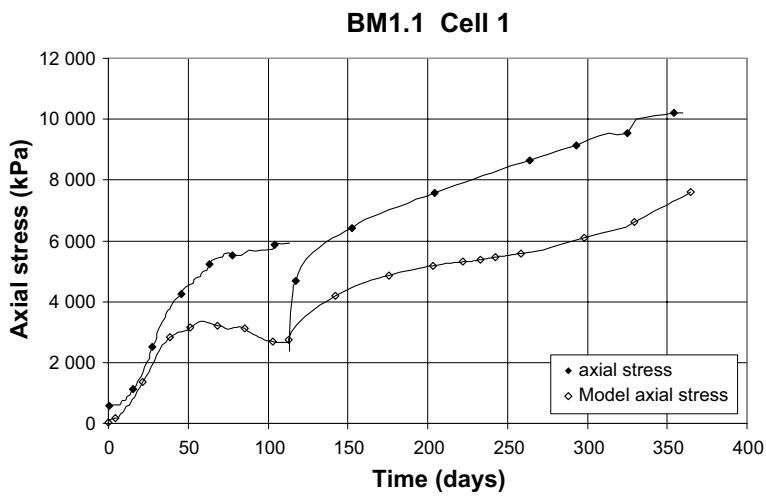


Figure 4-13d. Evolution of axial stress with time, Cell 1. Computed results and observations. Clay Technology-2.

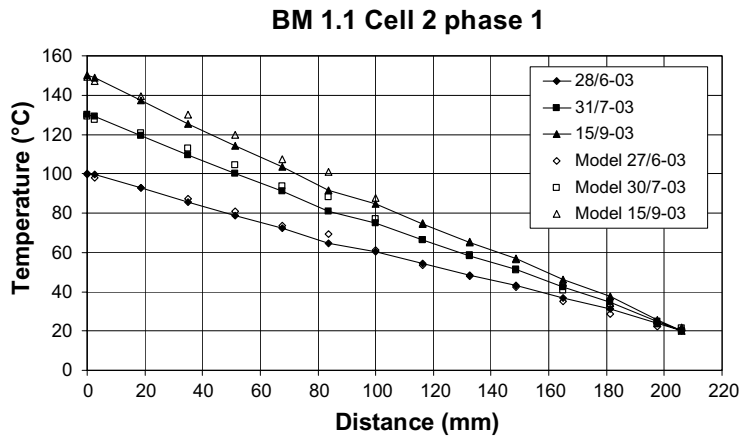


Figure 4-13e. Distributions of applied and observed temperatures at different times. Cell 2. Clay Technology-2.

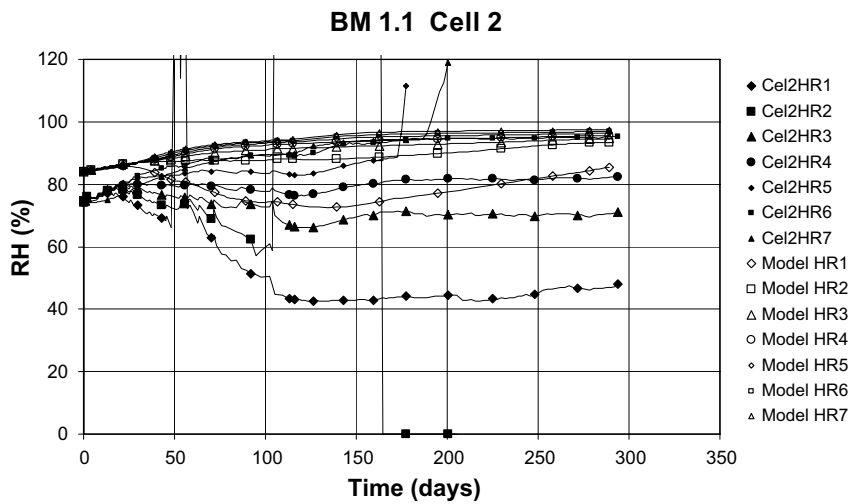


Figure 4-13f. Evolution of relative humidity with time, Cell 2. Computed results and observations. Clay Technology-2.

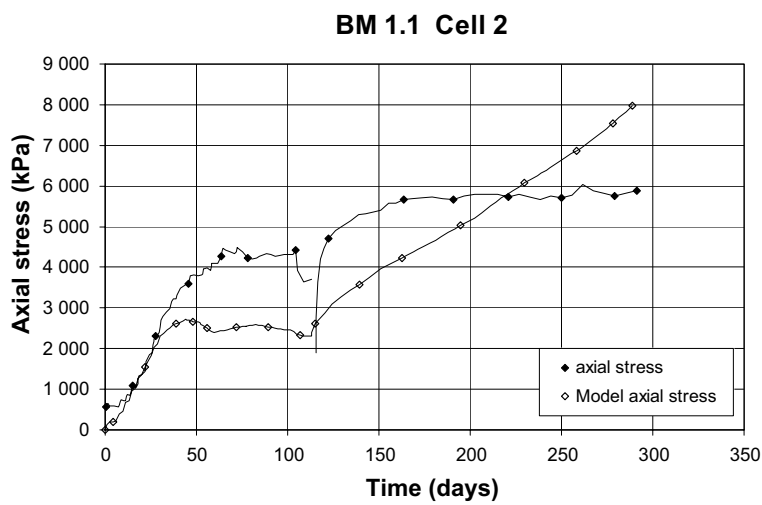


Figure 4-13g. Evolution of axial stress with time, Cell 2. Computed results and observations. Clay Technology-2.

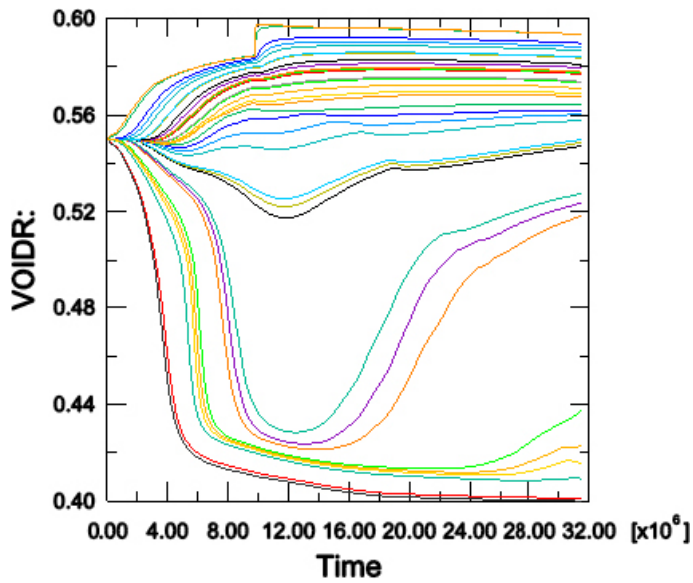


Figure 4-13h. Computed evolution of void ratio with time for points located in the axis of the specimen. Cell 1. Clay Technology-2.

4.6.2 CIEMAT infiltration tests – Subtask 1.2 [10]

Again, no thermal modelling was done for this Subtask for the same reasons as indicated in 4.6.1. The measured temperatures were used as thermal input. The mesh for the HM modelling was composed of 3 200 axisymmetric elements (Figure 4-14a). The main results are shown in Figures 4-14b to 4-14d. The effect of the coefficient for thermal vapour flow diffusivity, D_{Tvb} , was checked (Figure 4-14e)

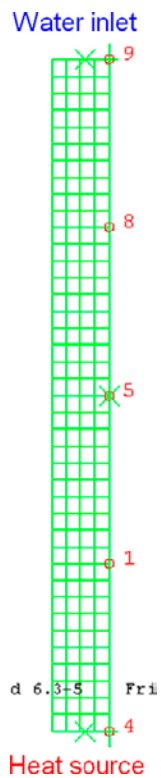


Figure 4-14a. Model mesh. Clay Technology-2.

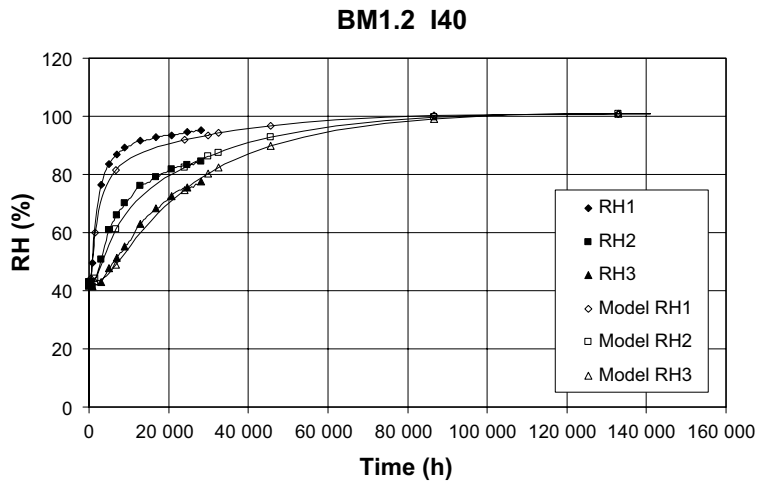


Figure 4-14b. Evolution of relative humidity with time. Isothermal test. Computed results and observations. Clay Technology-2.

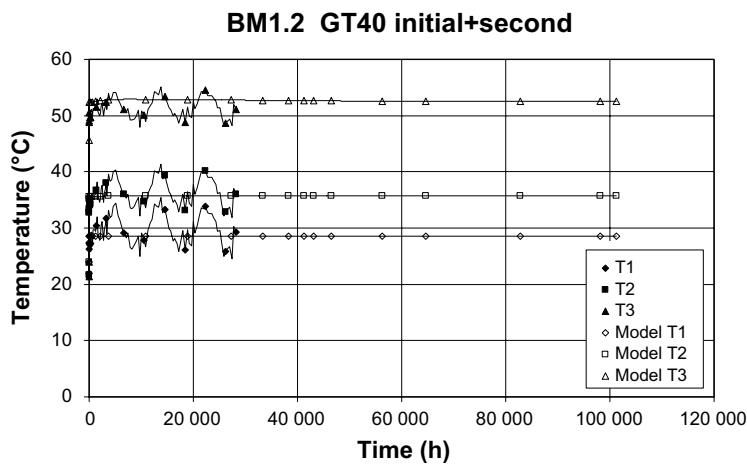


Figure 4-14c. Evolution of temperatures with time. Thermal Gradient Test. Computed results and observations. Clay Technology-2.

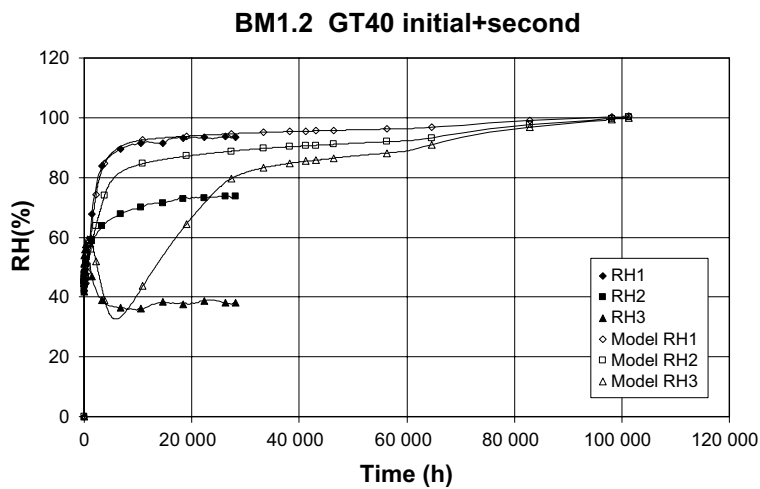


Figure 4-14d. Evolution of relative humidity with time. Thermal Gradient Test. Computed results and observations. Clay Technology-2.

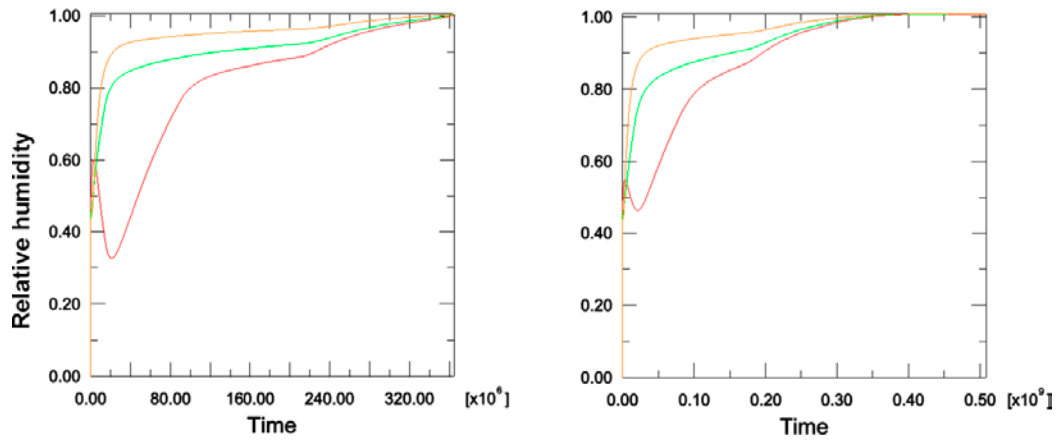


Figure 4-14e. Evolution of relative humidity with time. Thermal Gradient Test. Effect of the coefficient for thermal vapour flow diffusivity a) $D_{Tvb} = 0.7 \cdot 10^{-11} \text{ m}^2/\text{sK}$, b) $D_{Tvb} = 0.4 \cdot 10^{-11} \text{ m}^2/\text{sK}$. Clay Technology-2.

4.6.3 UPC heating test – Subtask 1.3 [10]

In this Subtask, coupled THM analyses were performed. A total of 2 200 axisymmetric elements were used in the mesh (Figure 4-15a). The results are shown in Figures 4-15b to 4-15e.

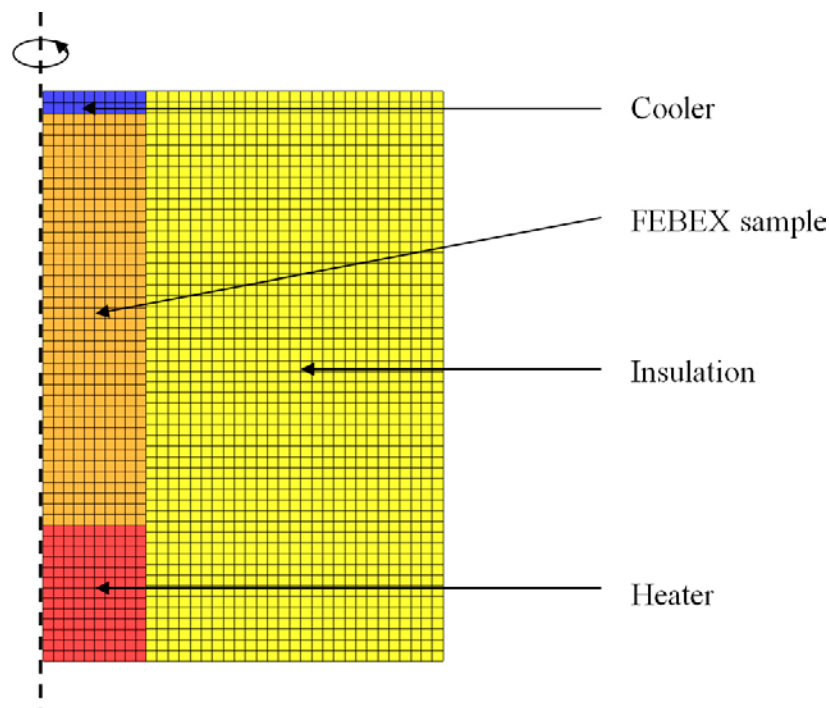


Figure 4-15a. Model mesh. Clay Technology-2.

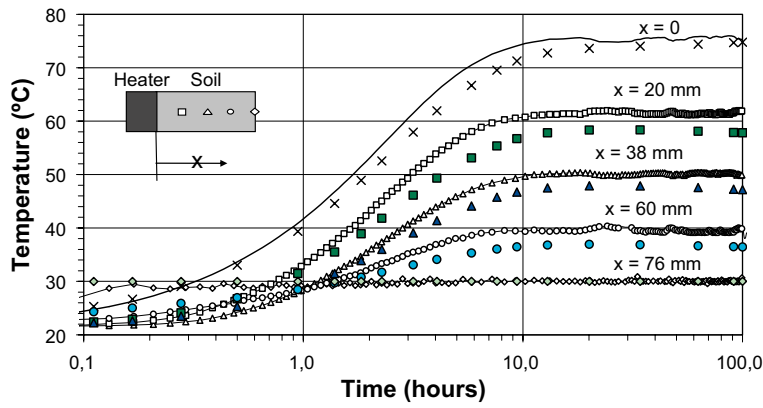


Figure 4-15b. Evolution of temperatures with time. Computed results and observations. Clay Technology-2.

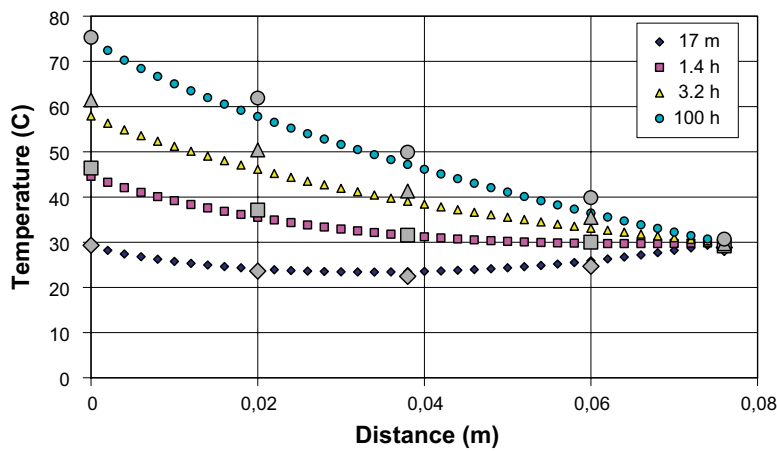


Figure 4-15c. Distributions of temperatures at different times. Computed results and observations. Clay Technology-2.

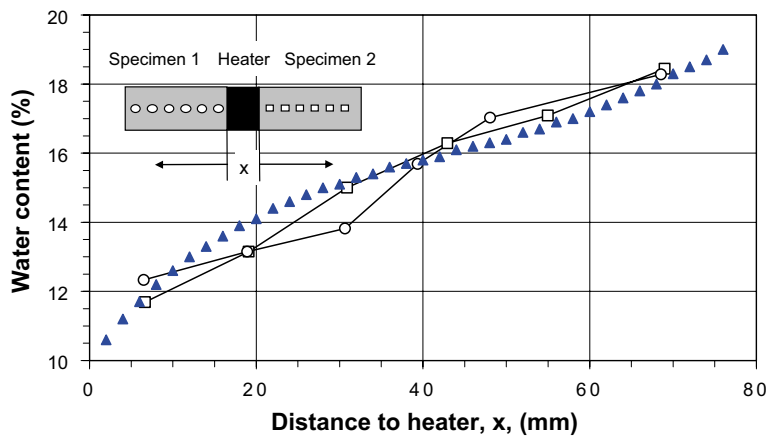


Figure 4-15d. Distribution of water content at the end of test. Computed results and observations. Clay Technology-2.

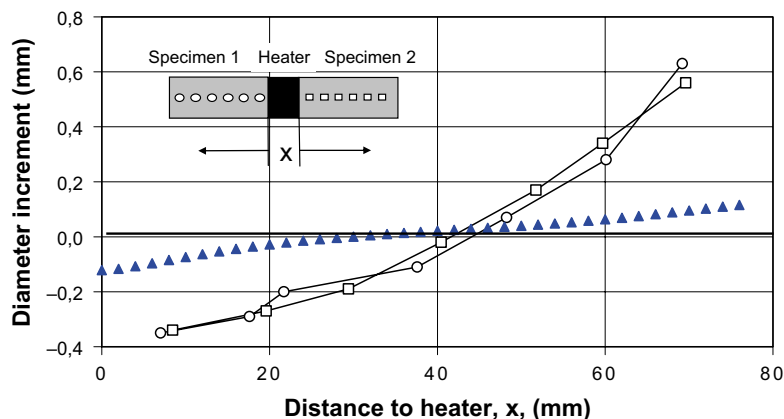


Figure 4-15e. Change of diameter along the specimens at the end of the test. Computed results and observations. Clay Technology-2.

4.6.4 Remarks

A differential feature of the analyses carried out by this team is that no thermal calculations were performed for Subtasks 1.1 and 1.2 although they were indeed incorporated in Subtask 1.3. However, as the temperatures are generally well predicted, there will be no significant differences in the hydraulic and mechanical results whether temperatures are derived from calculations or directly from observations. This group paid special attention to the issues of parameter determination and calibration and examined the effect of variation of retention curve and the non-uniformity of the bentonite void ratio/density. It should be stressed that this modelling team used the same model and parameters for Subtasks 1.2 and 1.3.

Regarding Subtask 1.1, Cell 1 was satisfactorily modelled but the slow hydration of Cell 2 is not captured. There are however differences between the computed and measured evolution of axial stresses but the trends are qualitatively similar for the most part. For Subtask 1.2, the Isothermal Test is well reproduced but the slow hydration of the Thermal Gradient Test is not well simulated. The agreement between computed and observed results in Subtask 1.3 is good except for the change of diameter of the sample. The group attributes those divergences to shortcomings of the moisture swelling model that has been added to general mechanical constitutive law. This model may be adequate for quasi-constant volume conditions but not so much for free swelling situations.

4.7 CRIEPI

4.7.1 CEA mock-up tests – Subtask 1.1 [11]

The dimensions of the axisymmetric geometry used in the THM analyses are shown in Figure 4-16a. The mesh uses 4-noded quadrilateral elements. Selected results are collected in Figures 4-16b to 4-16k.

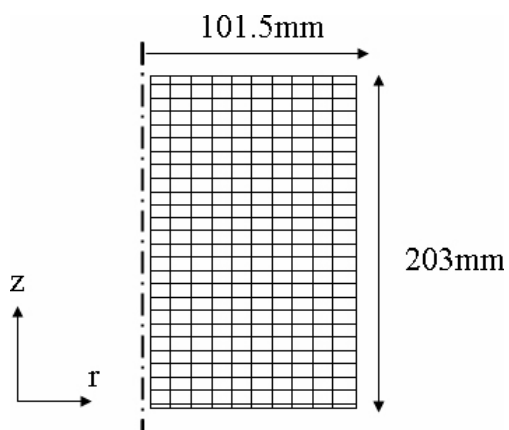


Figure 4-16a. Model mesh. CRIEPI.

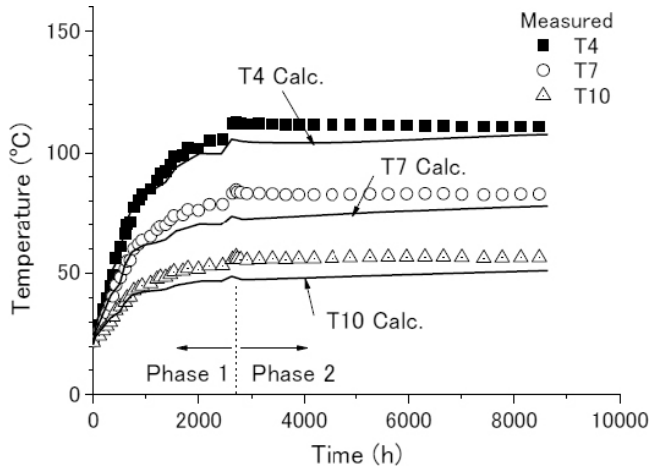


Figure 4-16b. Evolution of temperature with time, Cell 1, Computed results and observations. CRIEPI.

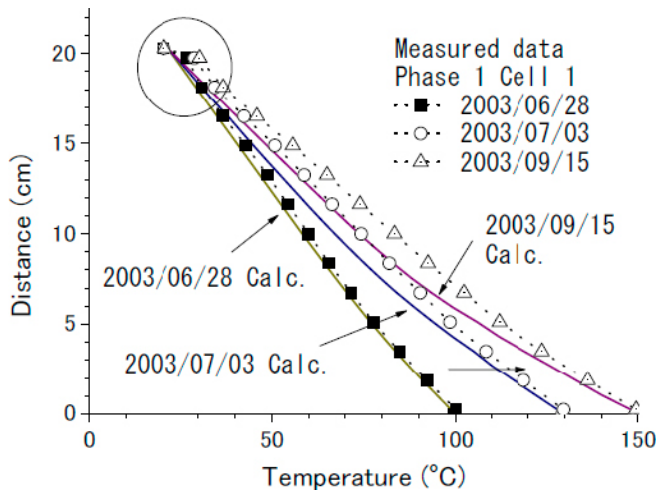


Figure 4-16c. Distributions of temperatures at different times. Cell 1. Computed results and observations. CRIEPI.

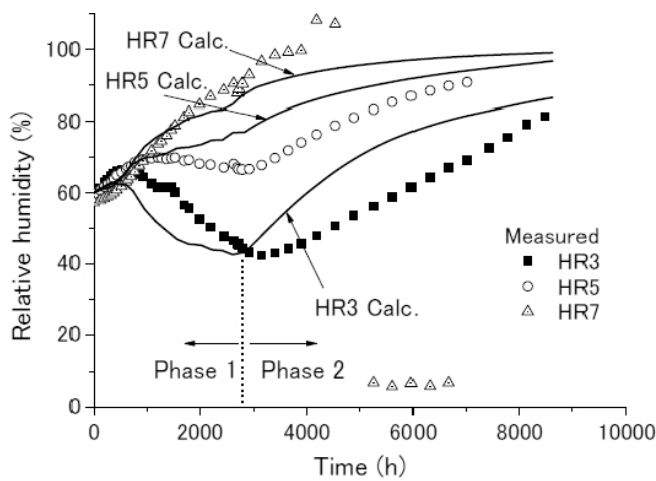


Figure 4-16d. Evolution of relative humidity with time, Cell 1. Computed results and observations. CRIEPI.

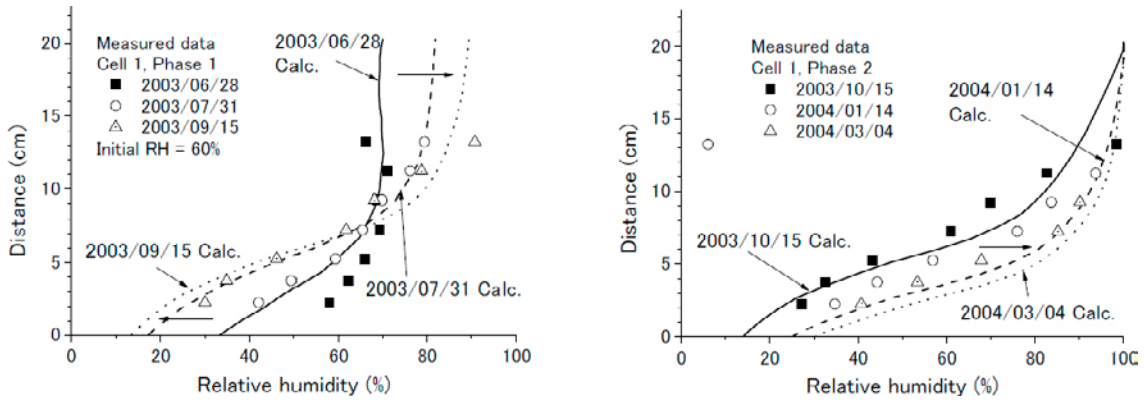


Figure 4-16e. Distributions of relative humidity with time, Cell 1. Computed results and observations. CRIEPI.

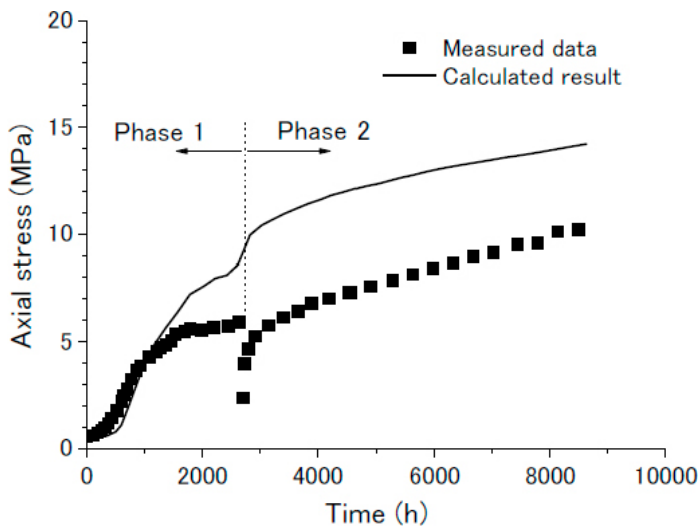


Figure 4-16f. Evolution of axial stress with time, Cell 1. Computed results and observations. CRIEPI.

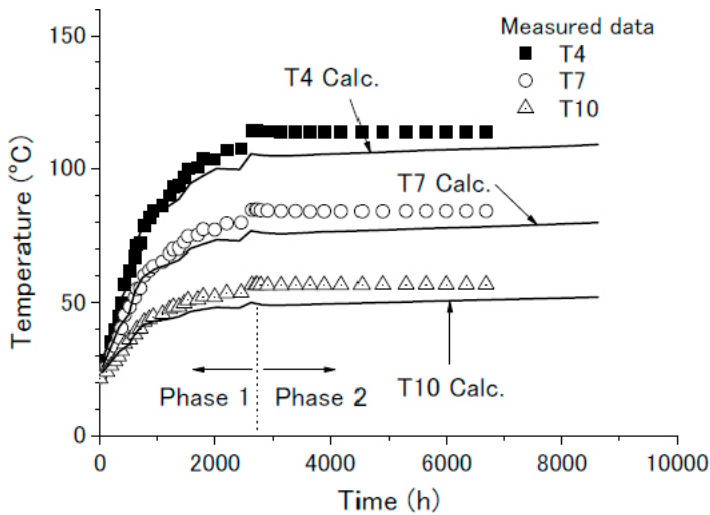


Figure 4-16g. Evolution of temperature with time, Cell 2. Computed results and observations. CRIEPI.

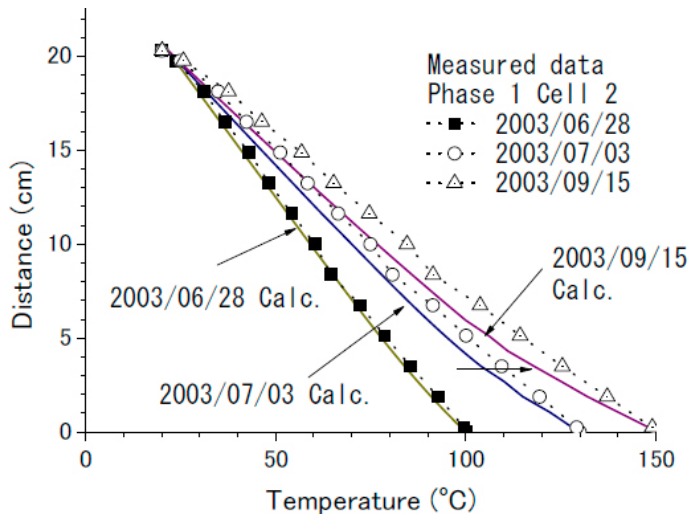


Figure 4-16h. Distributions of temperatures at different times. Cell 2. Computed results and observations. CRIEPI.

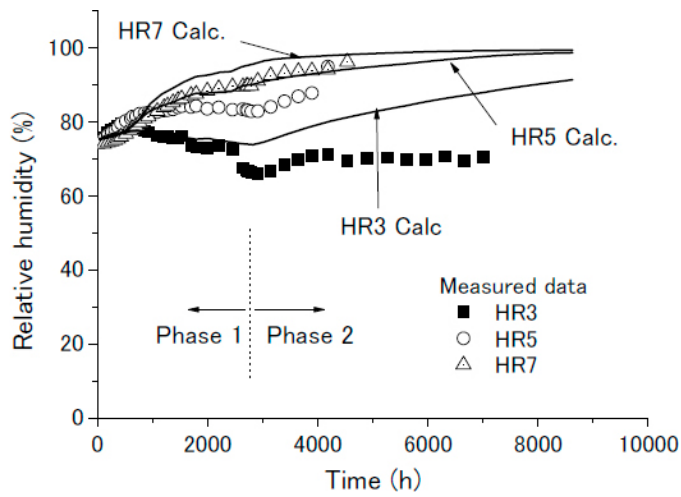


Figure 4-16i. Evolution of relative humidity with time, Cell 2. Computed results and observations. CRIEPI.

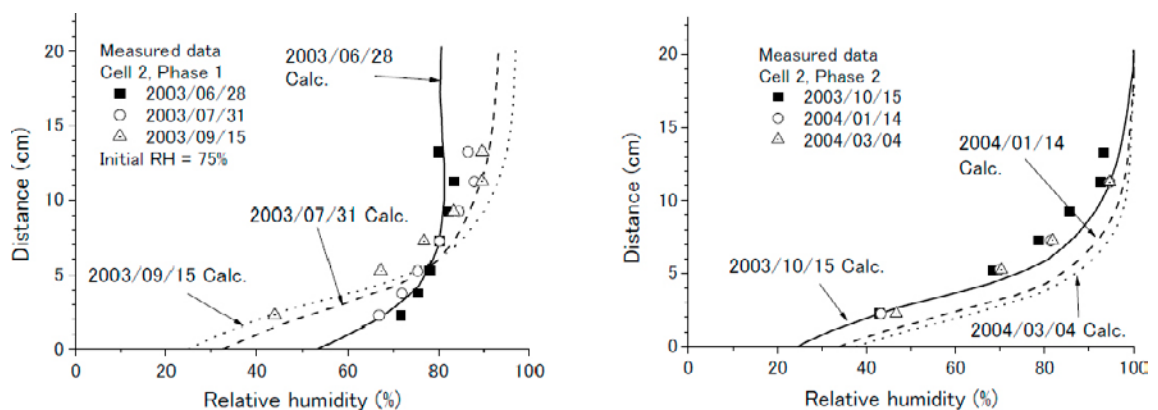


Figure 4-16j. Distributions of relative humidity at different times, Cell 2. Computed results and observations. CRIEPI.

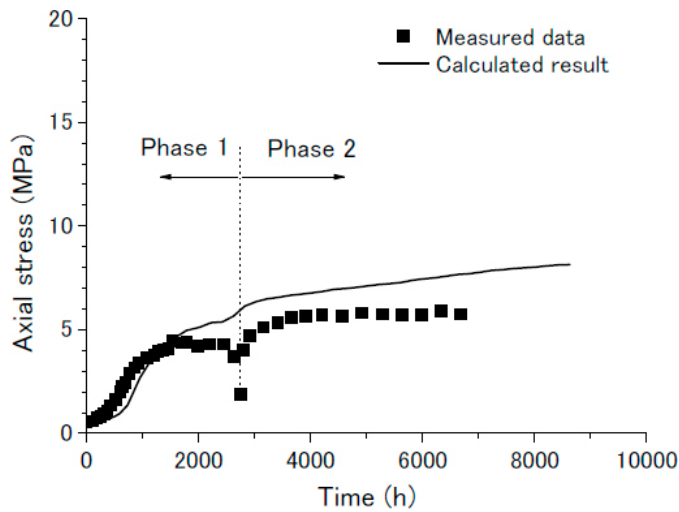


Figure 4-16k. Evolution of axial stress with time, Cell 1. Computed results and observations. CRIEPI.

4.7.2 CIEMAT infiltration tests – Subtask 1.2 [11]

The two geometries used for this Subtask (Figure 4-17a) are axisymmetric. In the Isothermal test, only the bentonite is modelled whereas in the Thermal Gradient Test the materials surrounding the cell are included. 4-noded quadrangular elements are used to form the mesh for the THM analyses. The results selected for presentation are in Figures 4-17b to 4-17d. Effects of varying intrinsic permeability and tortuosity have also been examined (Figure 4-17e).

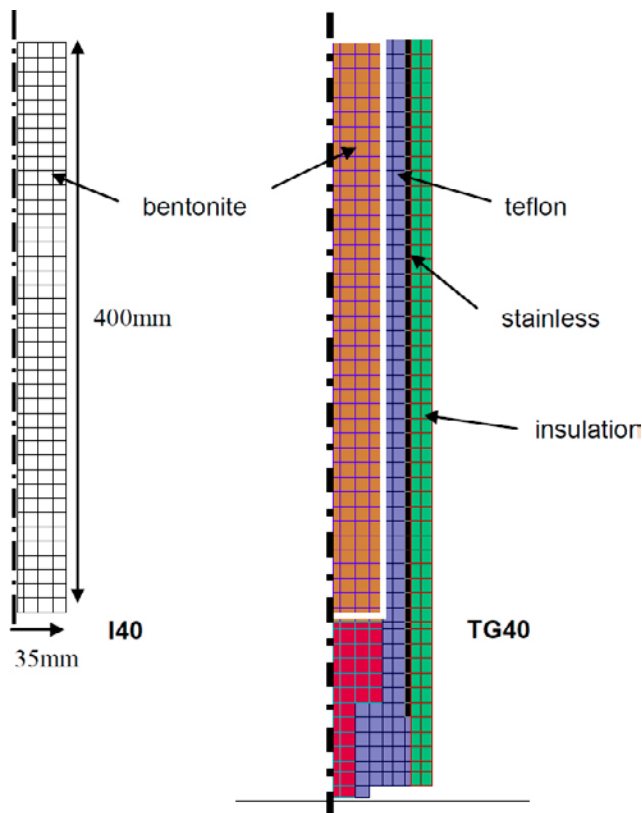


Figure 4-17a. Model geometries and meshes. I40: Isothermal test. TG40: Thermal Gradient Test. CRIEPI.

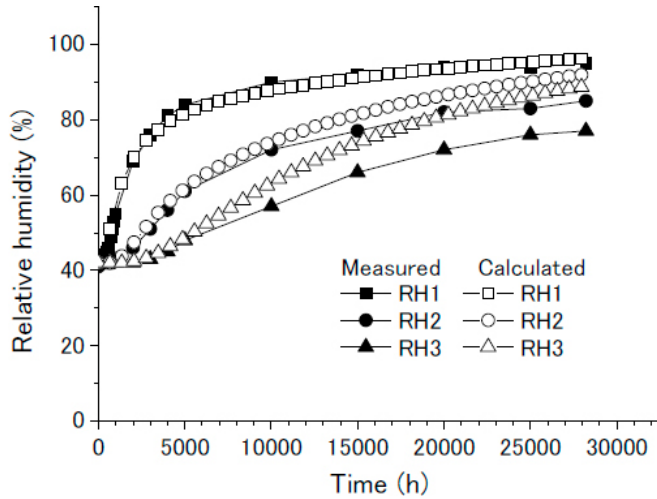


Figure 4-17b. Evolution of relative humidity with time. Isothermal test. Computed results and observations. CRIEPI.

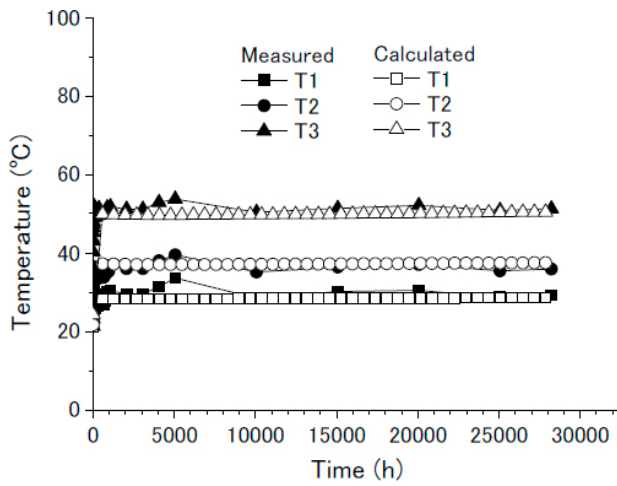


Figure 4-17c. Evolution of temperatures with time. Thermal Gradient Test. Computed results and observations. CRIEPI.

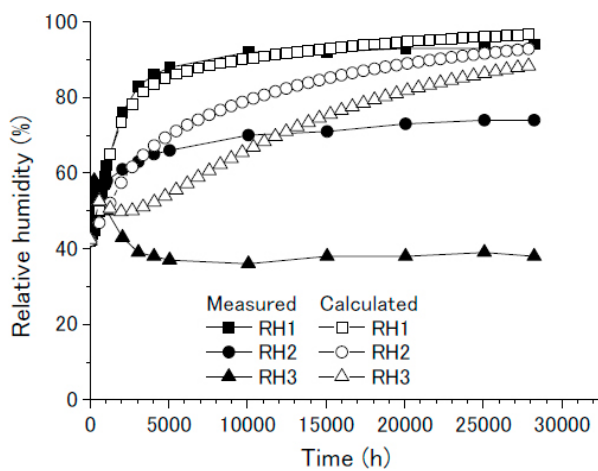


Figure 4-17d. Evolution of relative humidity with time. Thermal Gradient Test. Computed results and observations. CRIEPI.

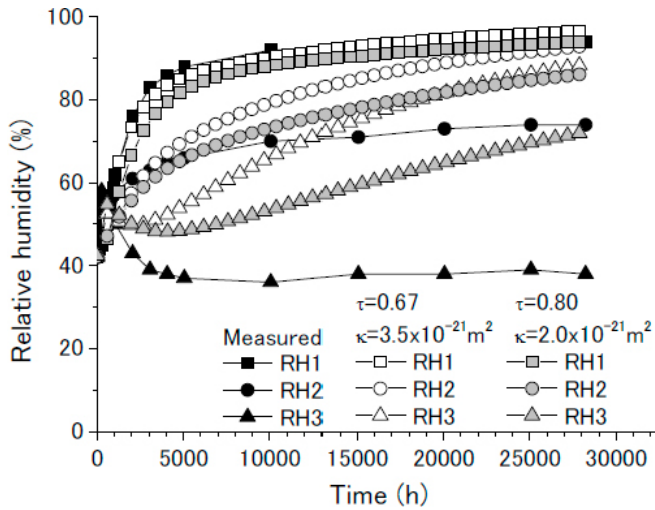


Figure 4-17e. Evolution of relative humidity with time. Thermal Gradient Test. Computed results, using different values of tortuosity (τ) and intrinsic permeability (k), and observations. CRIEPI.

4.7.3 UPC heating test – Subtask 1.3 [11]

The geometry used in the computations together with the boundary conditions are shown in Figure 4-18a. Again, insulation is included in the coupled THM analysis. Results are provided in Figures 4-18b to 4-18 e. Two sets of hydraulic parameters have been used:

- Case 1 (standard): Intrinsic permeability, $k = 4.34 \times 10^{-21} \text{ m}^2$, tortuosity, $\tau = 0.67$
- Case 2 (best fit): Intrinsic permeability, $k = 2.0 \times 10^{-21} \text{ m}^2$, tortuosity, $\tau = 0.80$

Results for the two cases are given in Figures 4-18b to 4-18e.

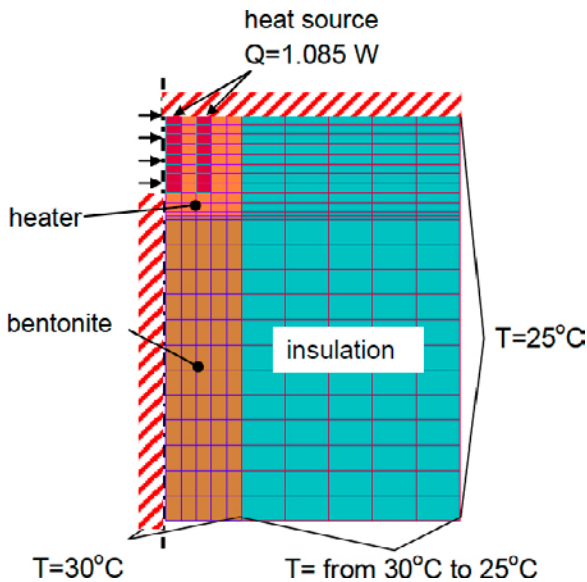


Figure 4-18a. Model mesh and boundary conditions. CRIEPI.

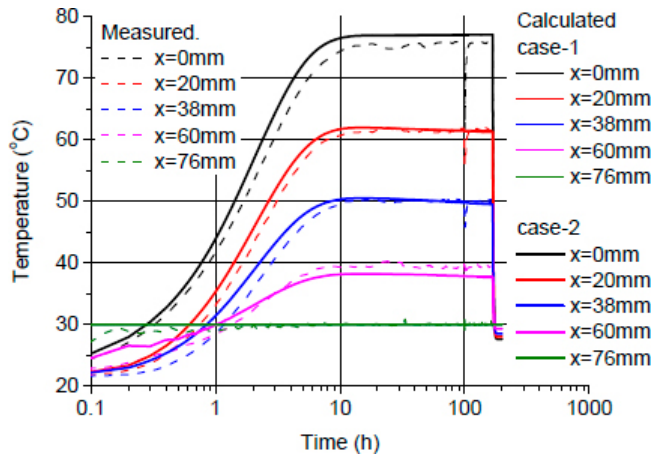


Figure 4-18b. Evolution of temperatures with time. Computed results and observations. CRIEPI.

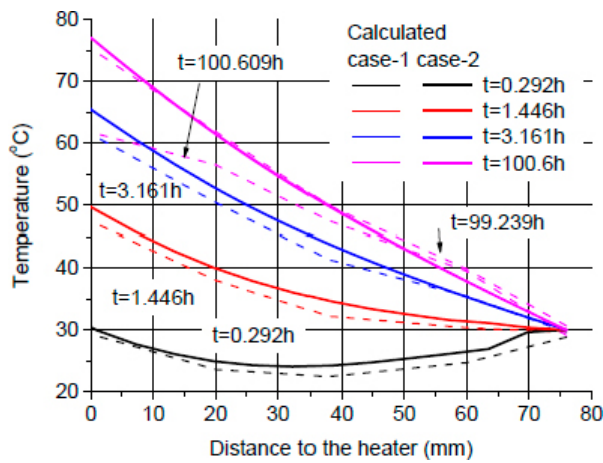


Figure 4-18c. Distributions of temperatures at different times. Computed results and observations. CRIEPI.

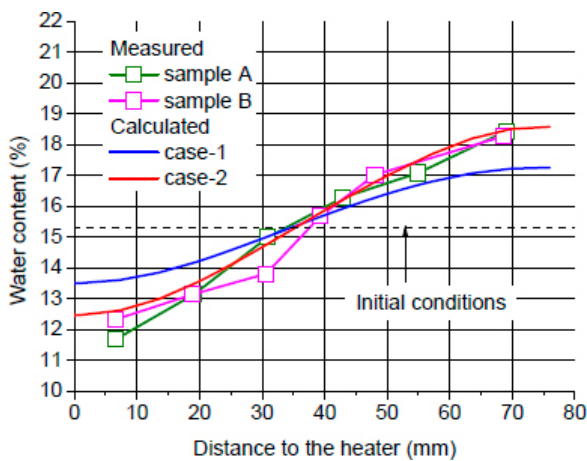


Figure 4-18d. Distribution of water content at the end of test. Computed results and observations. CRIEPI.

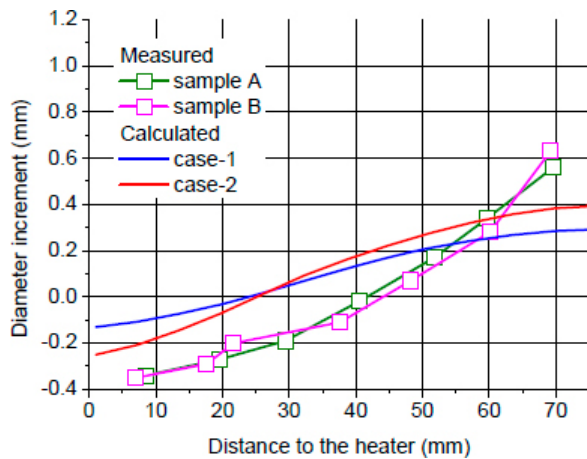


Figure 4-18e. Change of diameter along the specimens at the end of the test. Computed results and observations. CRIEPI.

4.7.4 Remarks

Temperature fields are satisfactorily modelled throughout. In Subtask 1.1, the hydration of Cell 1 is satisfactorily reproduced but the slow hydration of Cell 2 is not. Axial stresses are generally overestimated but the overall trend is adequate. It should be remembered that, for this group, the mechanical constitutive model is derived directly from diffuse double layer theory, with less opportunity to adapt the parameters to achieve better fit with observations.

In Subtask 1.2, the Isothermal Test is well modelled but the slow hydration of the Thermal Gradient Test is not captured. Alternative analyses with changed tortuosity and intrinsic permeability also fail to achieve a satisfactory reproduction of the test. With some quite limited modification of hydraulic parameters (intrinsic permeability and tortuosity), Subtask 1.3 is well modelled in terms of temperature and water content at the end of the test, but it underestimates the diameter change of the specimen. Again, the especial characteristics of the mechanical constitutive model used by this team should be recalled.

4.8 GRS

4.8.1 CIEMAT infiltration tests – Subtask 1.2 [12]

The Isothermal and Thermal Gradient Test have been modelled. Only the vapour transport equation is solved (hydraulic). In the Thermal Gradient Test, temperature input is based on the observed experimental values. The analysis is 1-D with 20 elements. A postulated pressure-dependent displacement of the water-air boundary shifted the inflow boundary for the models 5 cm inwards from the actual water-bentonite interface. Figures 4-19a and 4-19b show the evolution of relative humidity obtained in the calculations of this team.

4.8.2 Remarks

Only Subtask 2 was modelled by this team. The formulation used allows a more explicit consideration of the vapour transport phenomena but it does not include, by choice, the full set of THM phenomena, so that some cases may be beyond its range of applicability.

It can be observed that the evolutions of the relative humidity for both the Isothermal Test and the Thermal Gradient Test are well reproduced. Steady state conditions have been reached at the end of the calculation; so no further hydration will take place at future times.

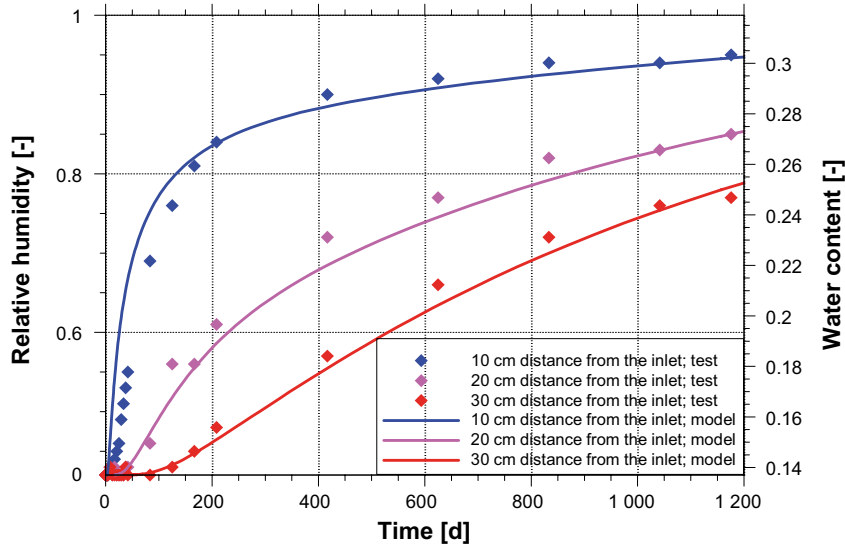


Figure 4-19a. Evolution of relative humidity with time. Isothermal test. Computed results and observations. GRS.

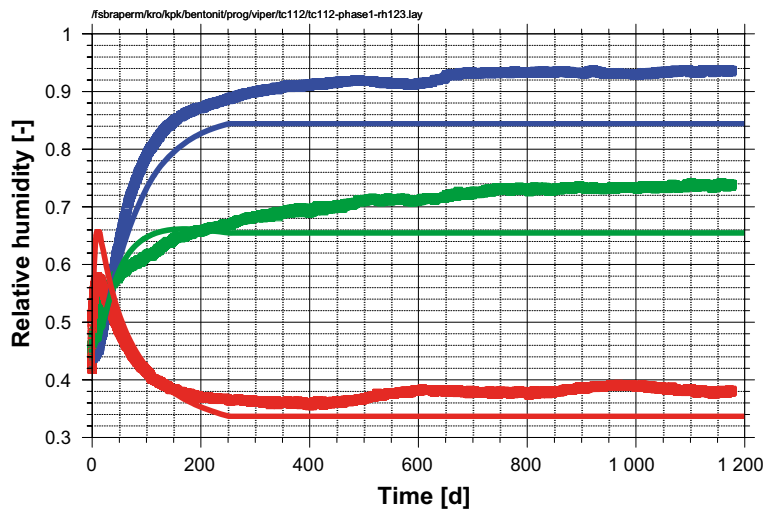


Figure 4-19b. Evolution of relative humidity with time. Thermal Gradient Test. Computed results using an alternative hypothesis and observations. GRS.

4.9 MARINTEL

4.9.1 CEA mock-up tests – Subtask 1.1 [13]

The mesh used in the calculations of Subtask 1.1 is shown in Figure 4-20a. It is composed of 444 axisymmetric triangular elements. T-HM (not fully coupled) analyses have been performed. Selected results are presented in Figures 4-20b to 4-20i.

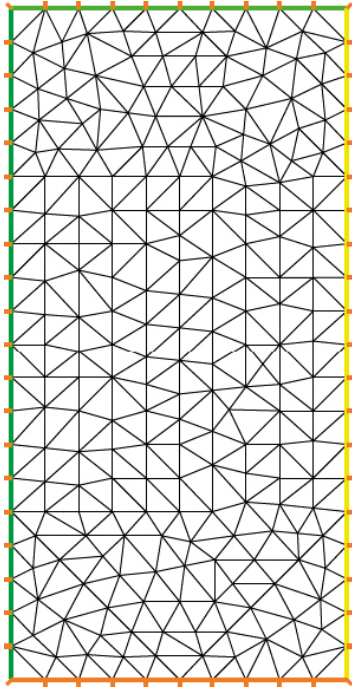


Figure 4-20a. Model mesh (203mm long and 202.7 mm diameter). MARINTEL.

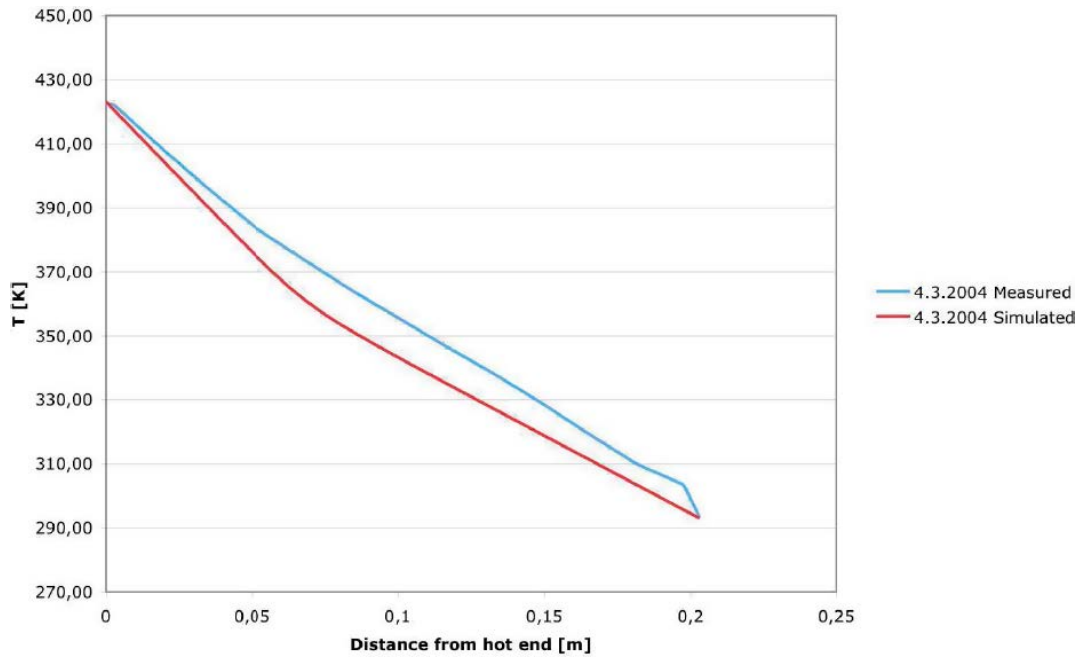


Figure 4-20b. Distributions of temperatures. Cell 1. Computed results and observations. MARINTEL.

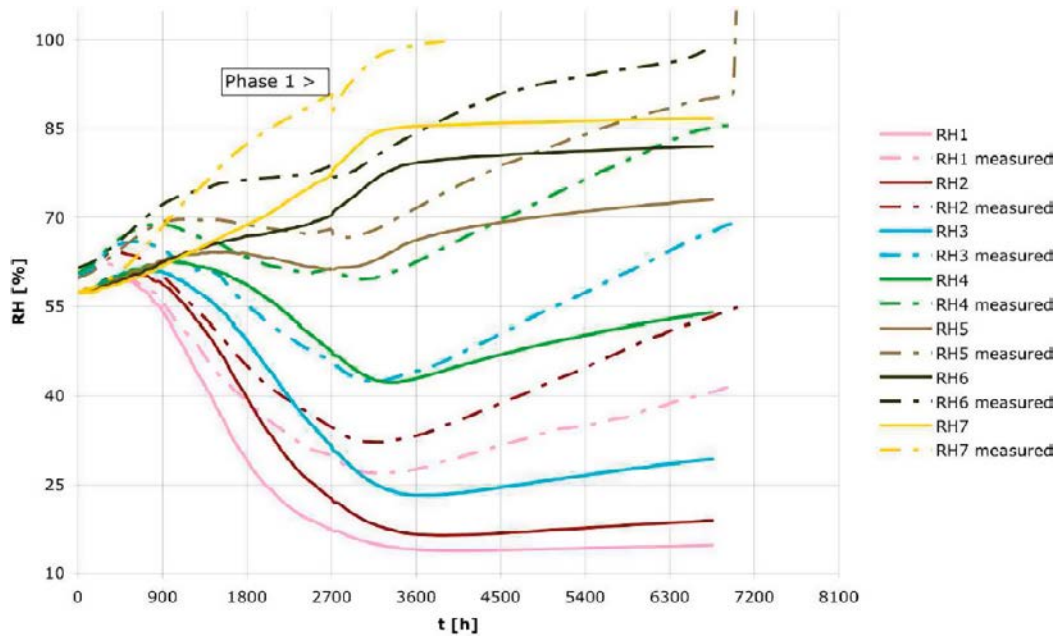


Figure 4-20c. Evolution of relative humidity with time, Cell 1. Computed results and observations. MARINTEL.

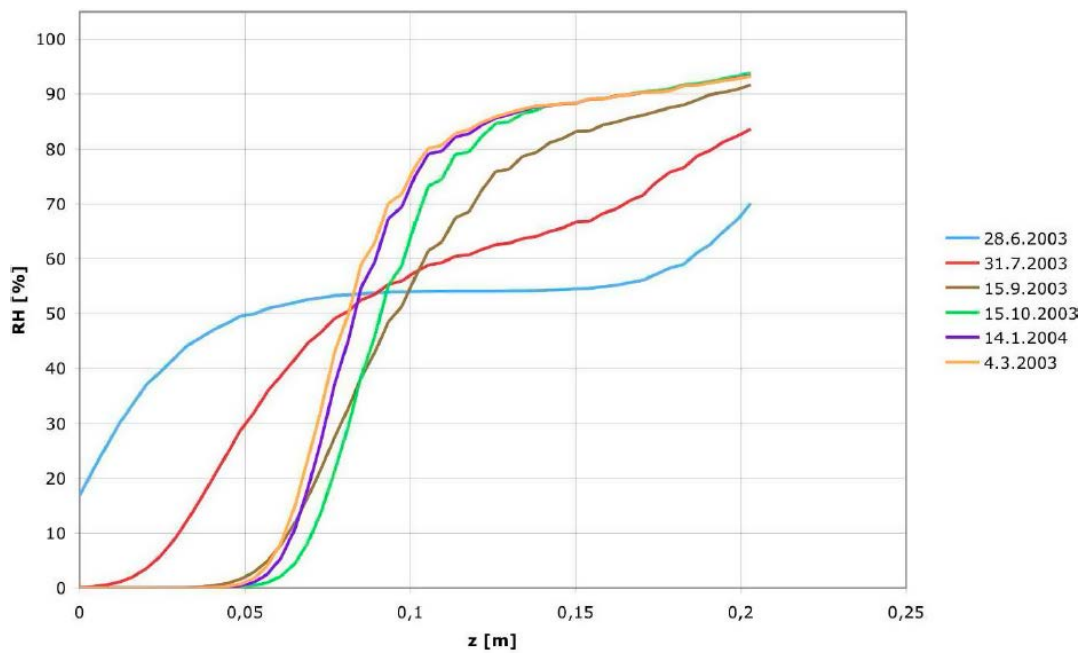


Figure 4-20d. Distributions of relative humidity with time, Cell 1. Computed results. MARINTEL. Note that 4.3.2003 in the legend should be 4.3.2004.

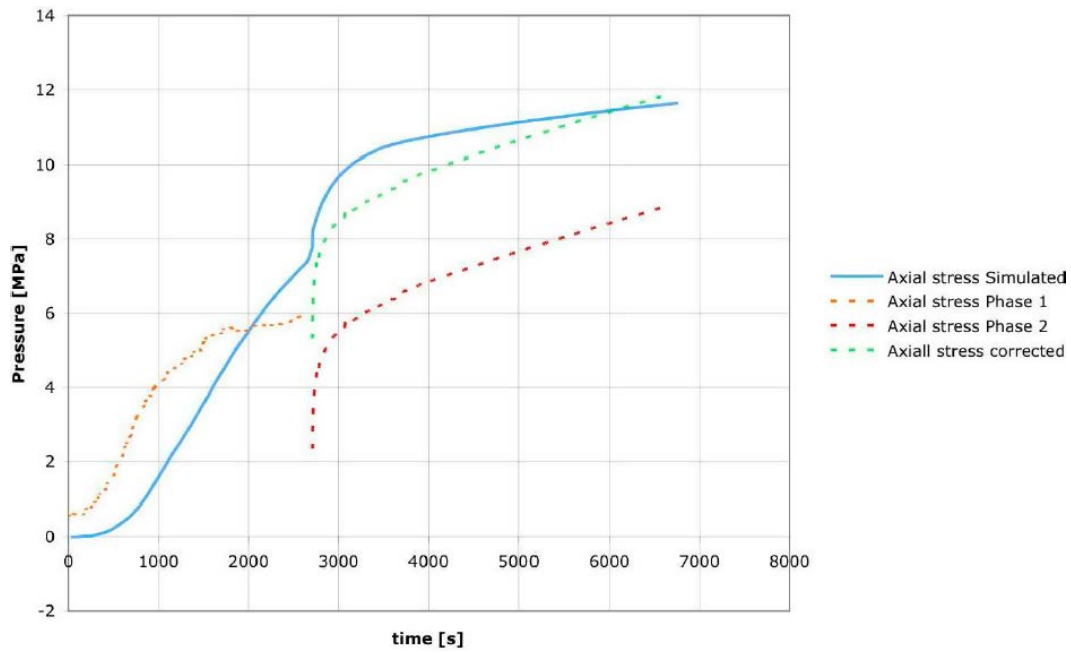


Figure 4-20e. Evolution of axial stress with time, Cell 1. Computed results and observations. MARINTEL.

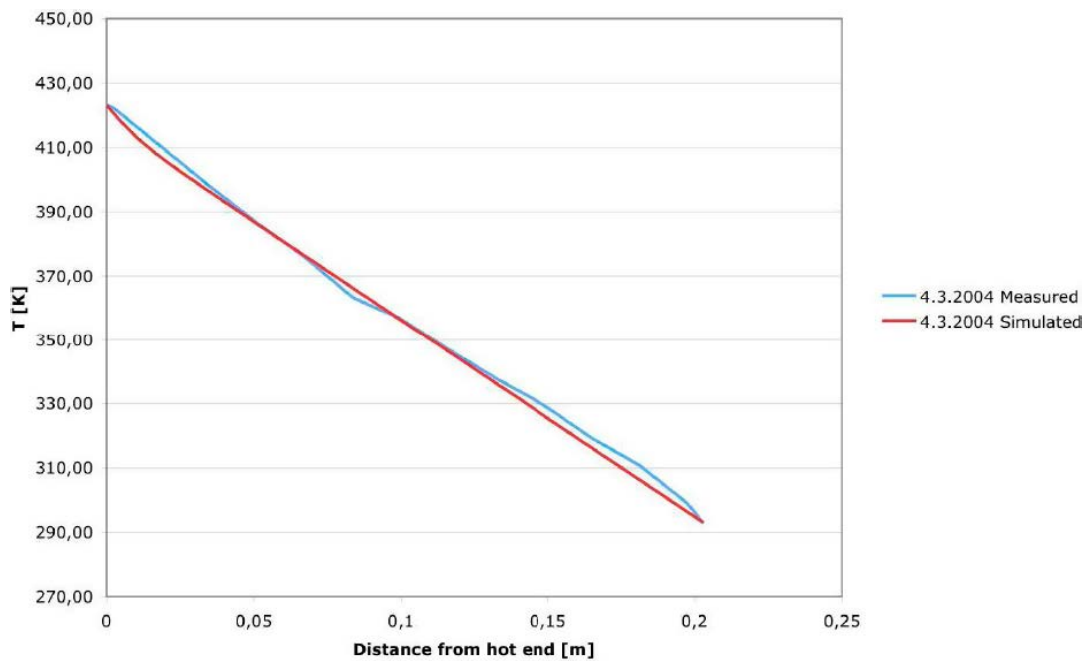


Figure 4-20f. Distributions of temperatures. Cell 2. Computed results and observations. MARINTEL.

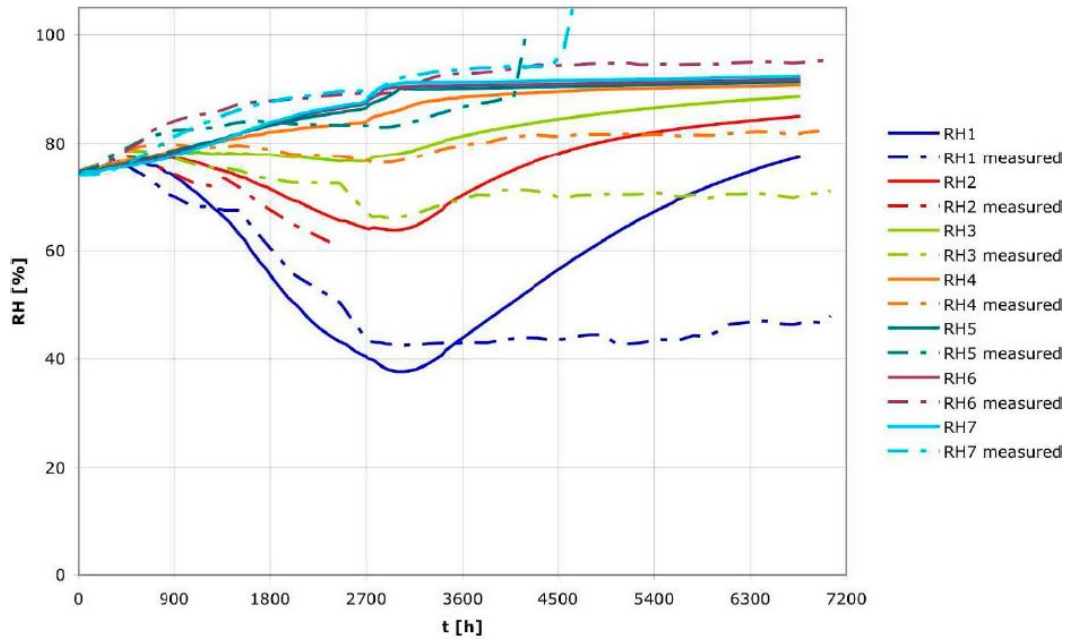


Figure 4-20g. Evolution of relative humidity with time, Cell 2. Computed results and observations. MARINTEL.

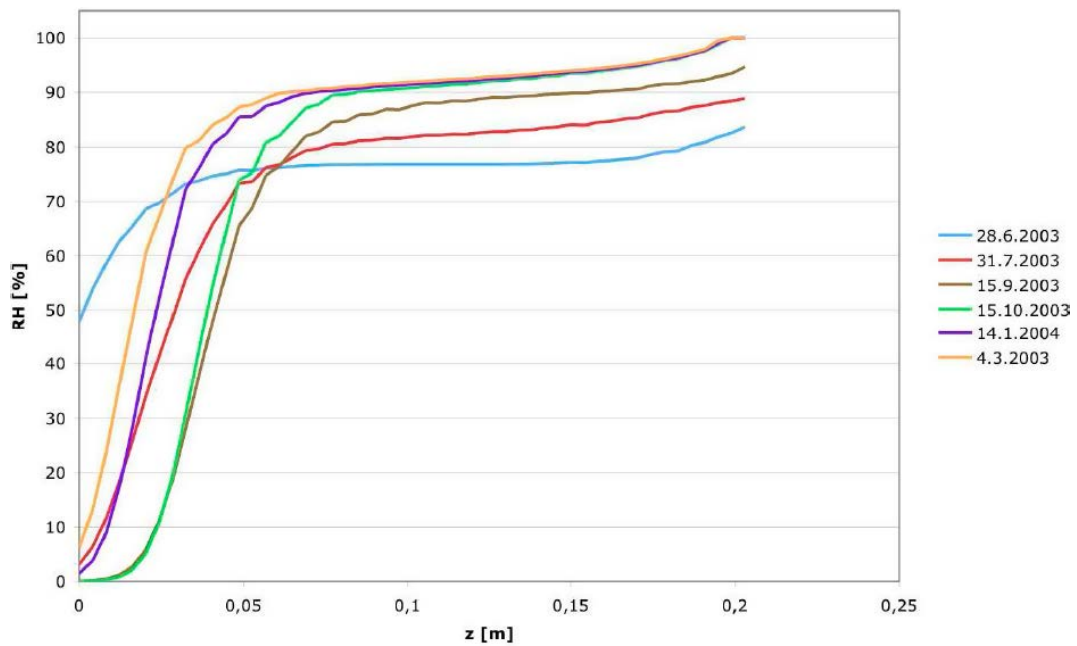


Figure 4-20h. Distributions of relative humidity at different times, Cell 2. Computed results. MARINTEL. Note that 4.3.2003 in the legend should be 4.3.2004.

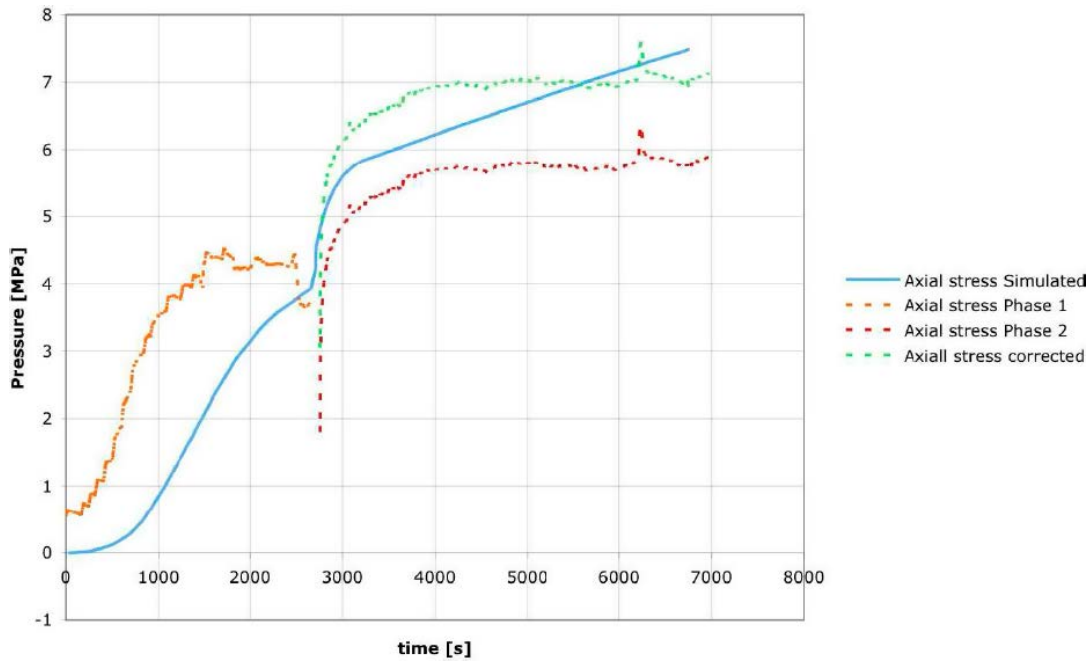


Figure 4-20i. Evolution of axial stress with time, Cell 1. Computed results and observations. MARINTEL.

4.9.2 CIEMAT infiltration tests – Subtask 1.2 [13]

For Subtask 1.1 the mesh is made up of 1 174 axisymmetric triangular elements (Figure 4-21a). The results of the coupled HM analysis (Isothermal Test) and T-HM (not fully coupled) analysis for the Thermal Gradient Test are plotted in Figures 4-21c to 4-21d.

The two tests have been analysed again using parameters derived from the analysis of the UPC heating test of Subtask 1.3. The results in terms of evolution of relative humidity are shown in Figures 4-21e and 4-21f.

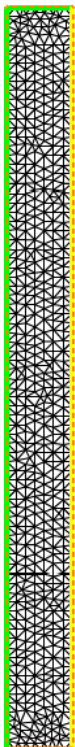


Figure 4-21a. Model mesh (400 mm long and 70 mm diameter). MARINTEL

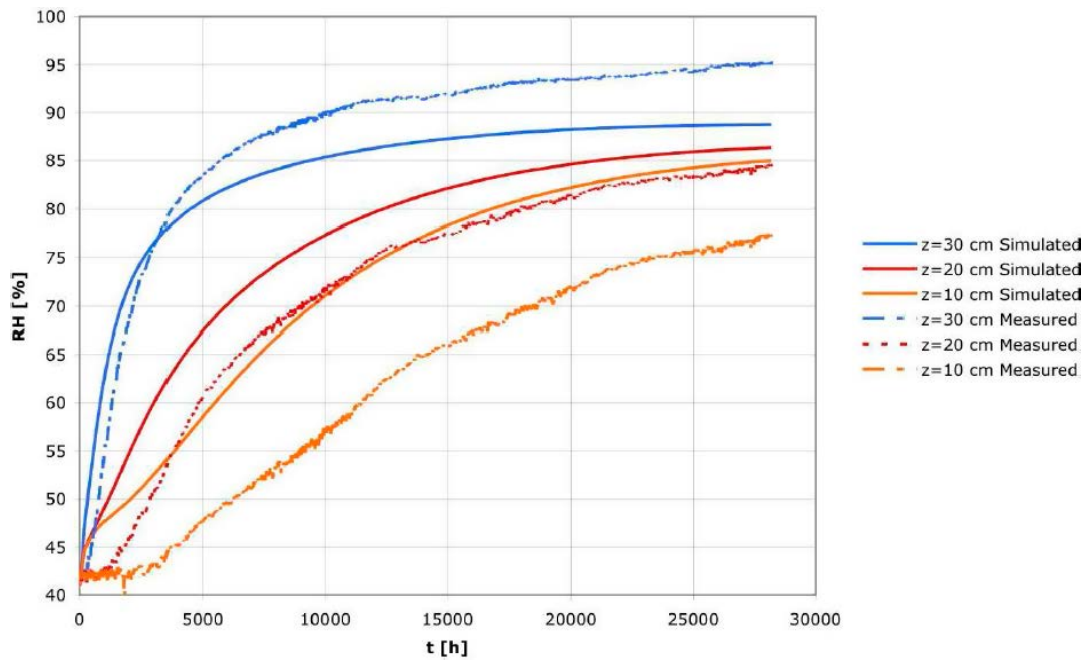


Figure 4-21b. Evolution of relative humidity with time. Isothermal test. Computed results and observations. MARINTEL.

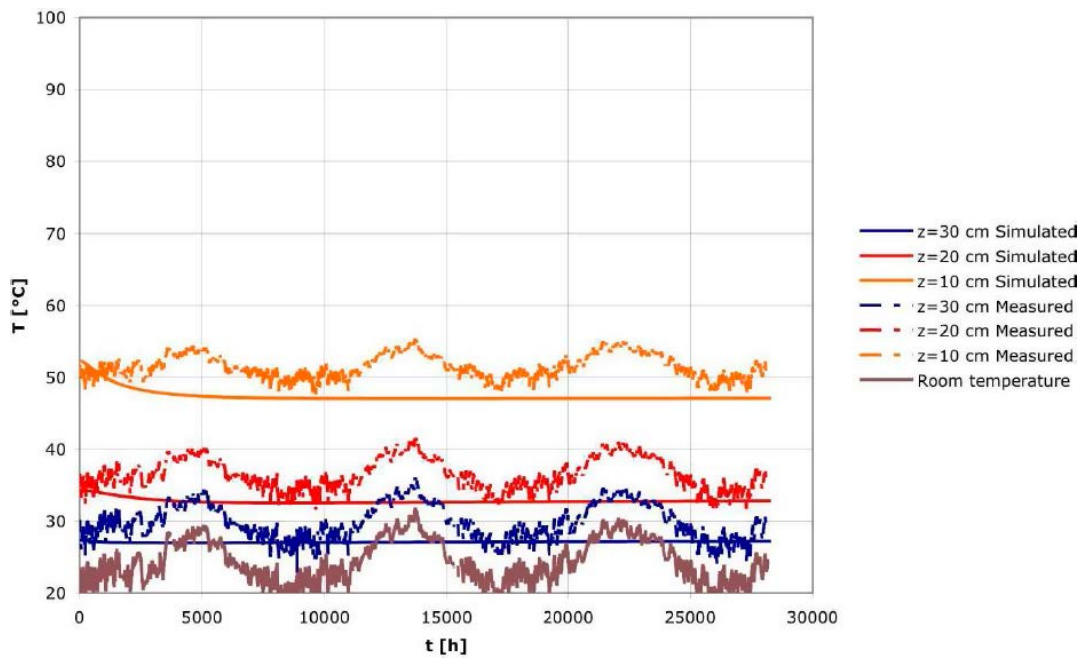


Figure 4-21c. Evolution of temperatures with time. Thermal Gradient Test. Computed results and observations. MARINTEL.

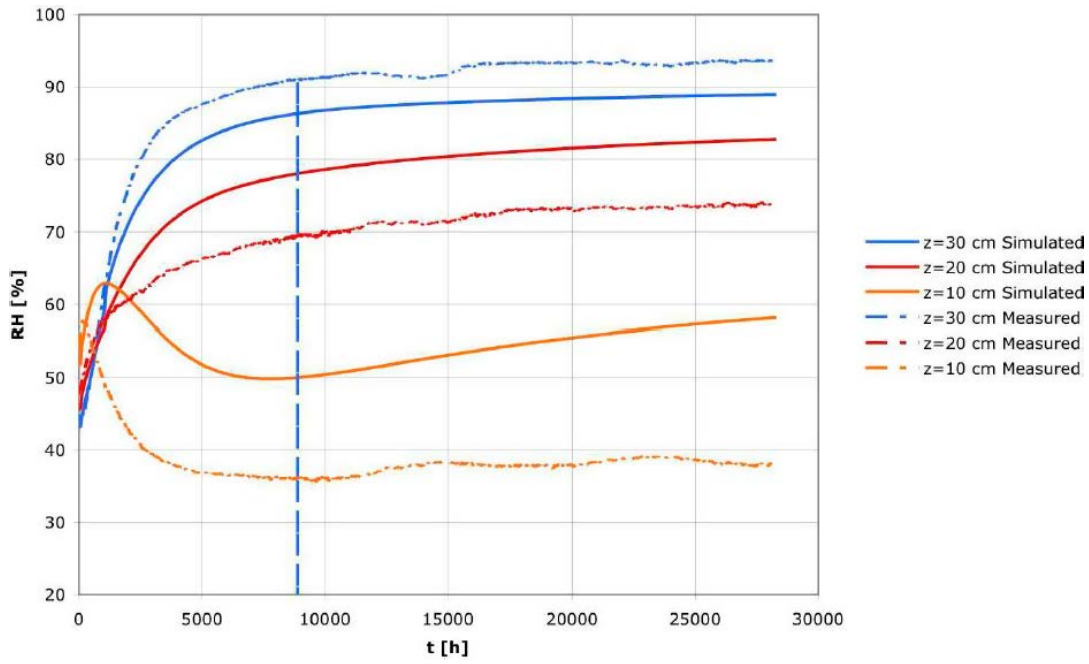


Figure 4-21d. Evolution of relative humidity with time. Thermal Gradient Test. Computed results and observations. MARINTEL.

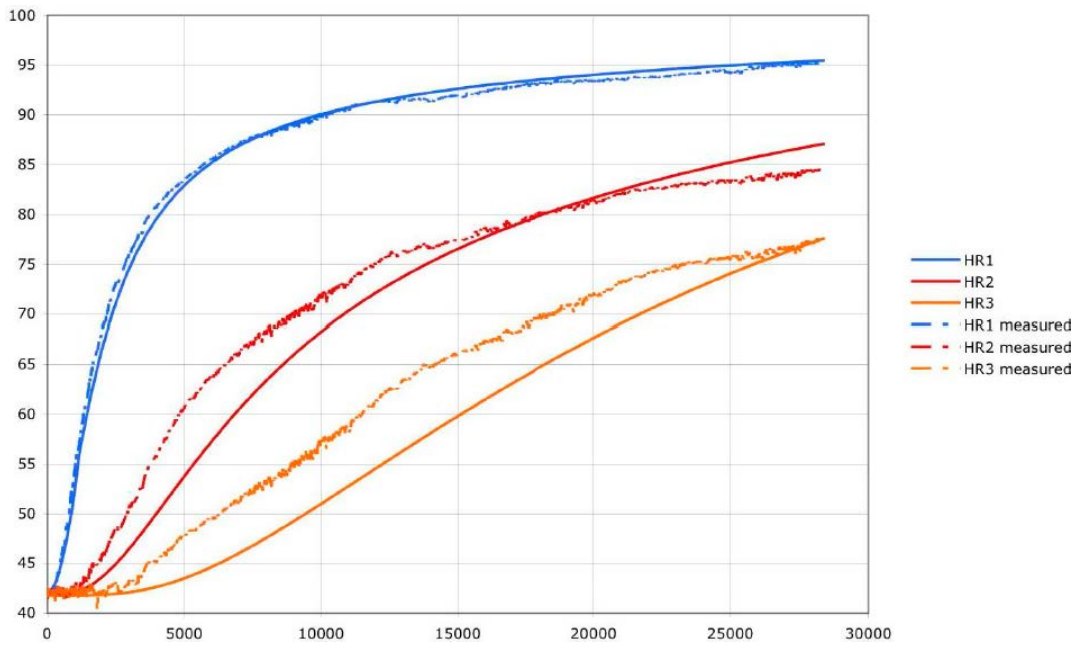


Figure 4-21e. Evolution of relative humidity with time. Isothermal test. Computed results using parameters derived from Subtask 1.3 and observations. MARINTEL.

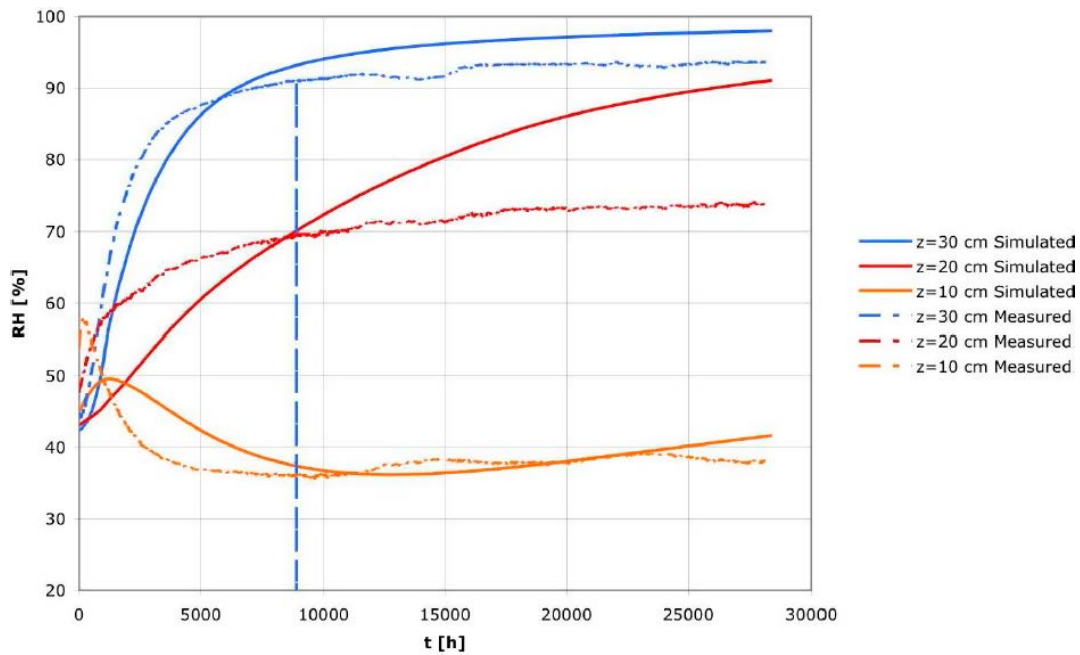


Figure 4-21f. Evolution of relative humidity with time. Thermal Gradient test. Computed results using parameters derived from Subtask 1.3 and observations. MARINTEL.

4.9.3 UPC heating test – Subtask 1.3 [14]

In Subtask 3 the mesh is made up of 444 triangular elements (Figure 4-22a). The results of the T-HM analysis are presented in Figures 4-22b to 4-22d.

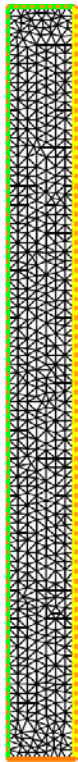


Figure 4-22a. Model mesh (76 mm long and 38 mm diameter). MARINTEL.

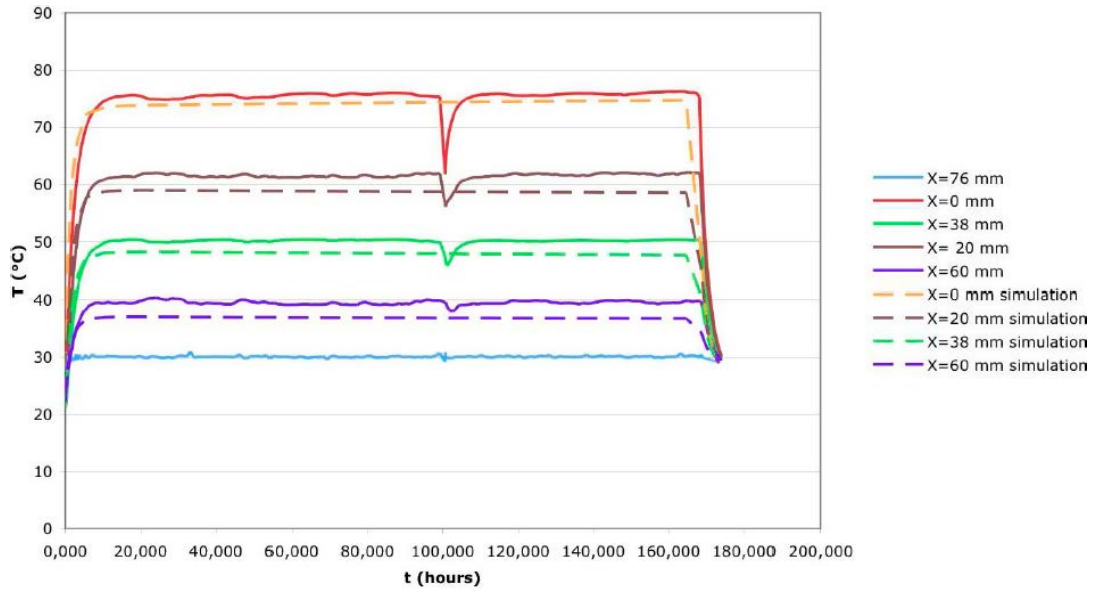


Figure 4-22b. Evolution of temperatures with time. Computed results and observations. MARINTEL.

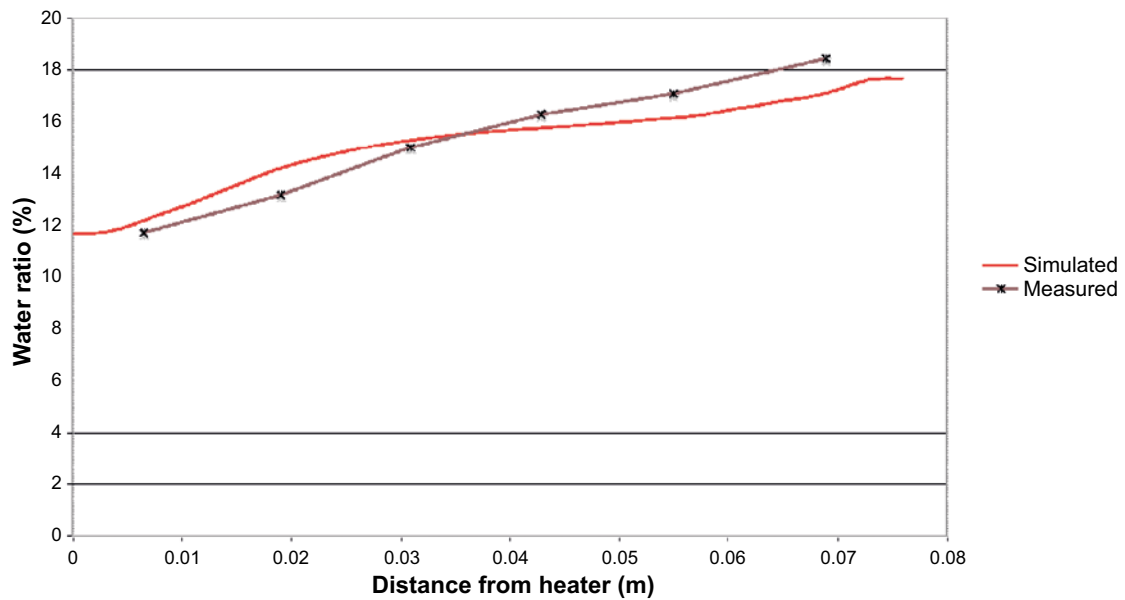


Figure 4-22c. Distribution of water content at the end of test. Computed results and observations. MARINTEL.

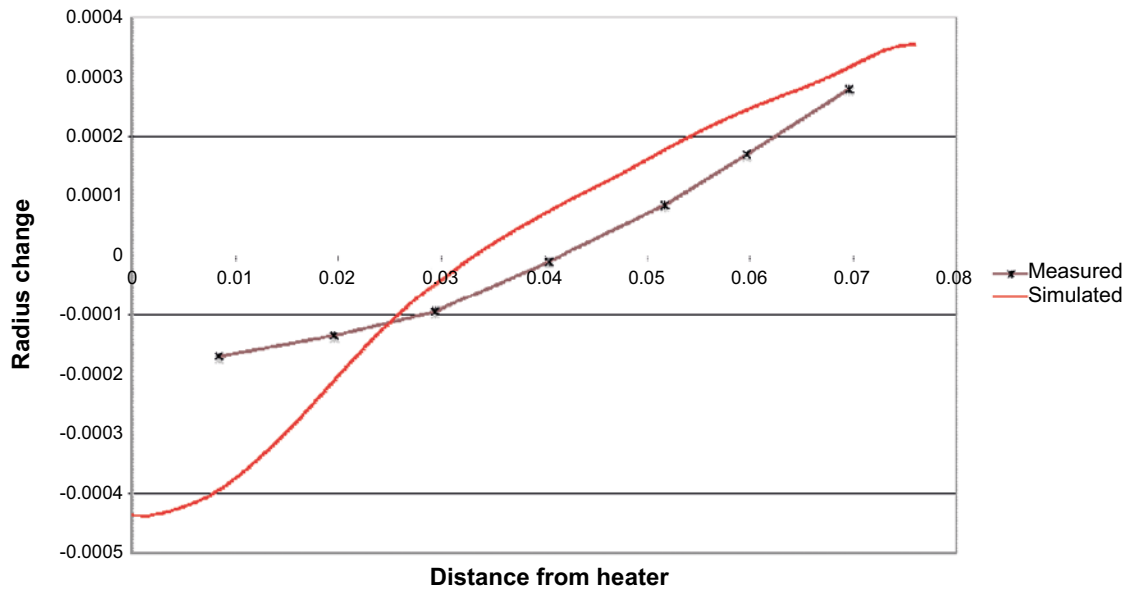


Figure 4-22d. Change of diameter along the specimens at the end of the test. Computed results and observations. MARINTEL.

4.9.4 Remarks

The distribution and evolution of temperatures are well reproduced throughout all cases. In Subtask 1.1, the evolution of relative humidity is not well reproduced in either of the two Cells. It should be pointed out that in the formulation used, the basic driving variable is water content and relative humidity has to be determined via the retention curve adding to the uncertainty of the results. The variation of axial stress is reasonably reproduced.

In Subtask 1.2, there are also significant departures of calculated relative humidity with respect to the observed evolution. Repeating the computations using the parameters derived from Subtask 1.3, the modelling for the Isothermal Test is satisfactory but the slow hydration of the Thermal Gradient Test is not captured. In Subtask 1.3, temperatures and water content at the end of the test are satisfactorily modelled. Sample diameter changes are correctly estimated in the swelling area but the shrinking is significantly overestimated.

4.10 TUL

4.10.1 CEA mock-up tests – Subtask 1.1 [15]

A three-dimensional model is used that is made equivalent to a 1-D analysis, via boundary conditions. Coupled HM formulation with water flow restricted to vapour diffusion. Exchange with absorbed water is also considered in the formulation. Figure 4-23a to 4-23e contain the results. Additional sensitivity analysis for Cell 1 have been performed to check the effects of diffusion coefficient, retention curve and exchange rate parameter.

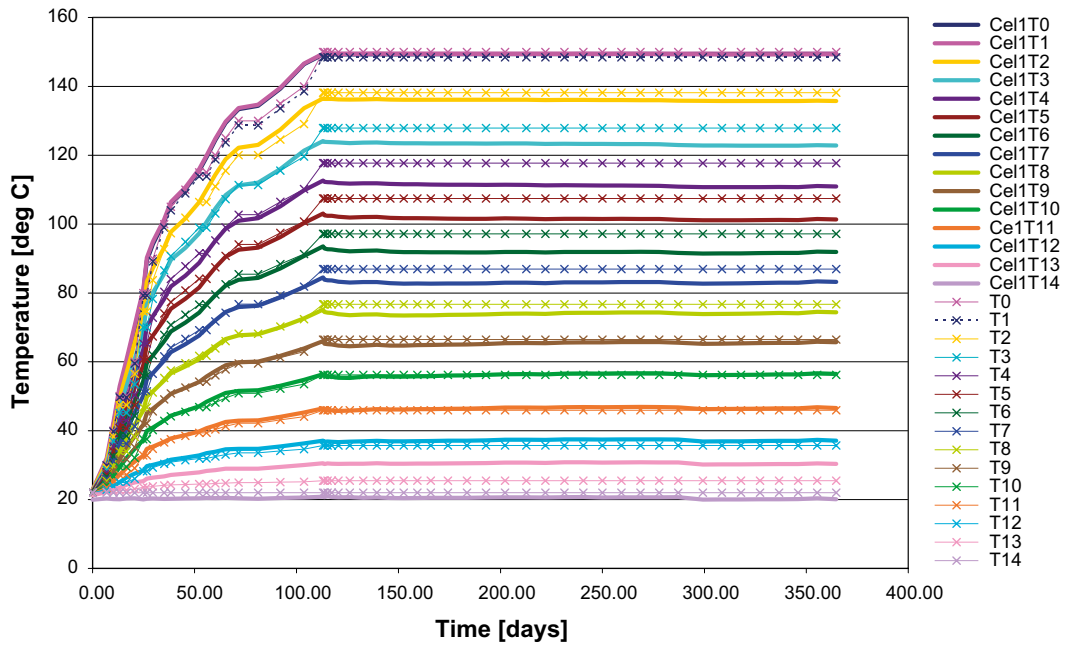


Figure 4-23a. Evolution of temperature with time, Cell 1. Computed results and observations. TUL.

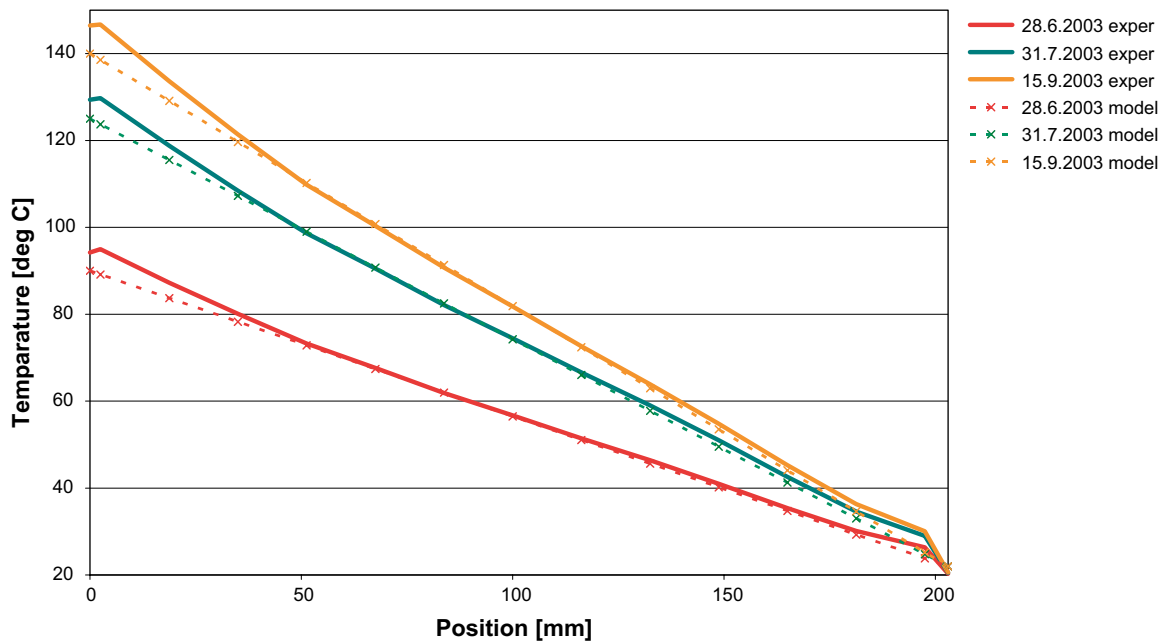


Figure 4-23b. Distributions of temperatures at different times. Cell 1. Computed results and observations. TUL.

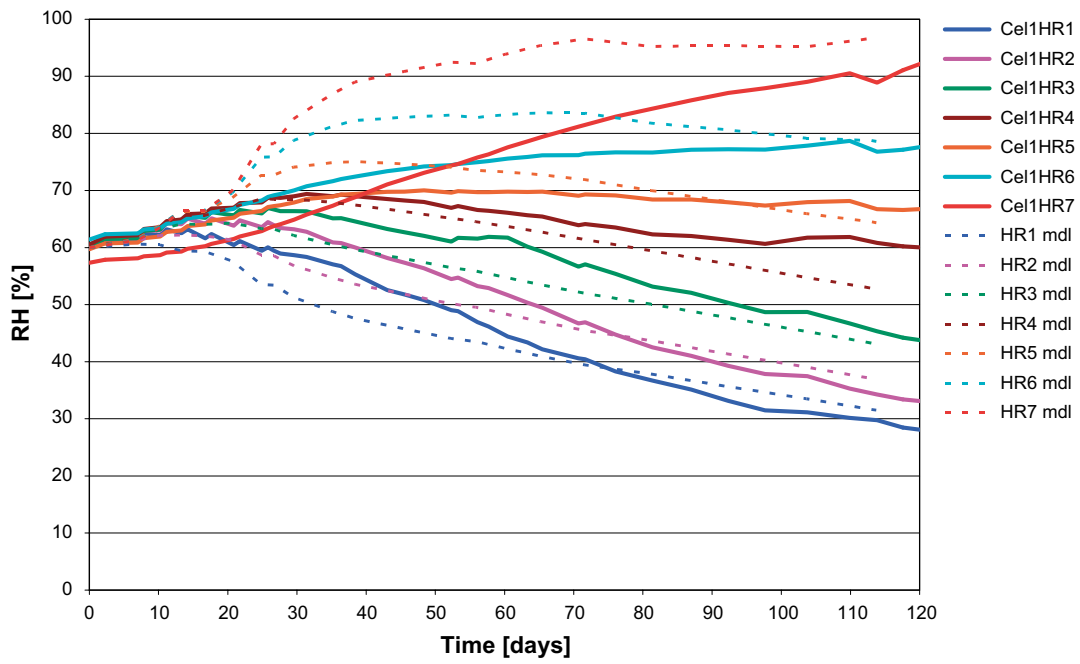


Figure 4-23c. Evolution of relative humidity with time, Cell 1. Computed results and observations. TUL.

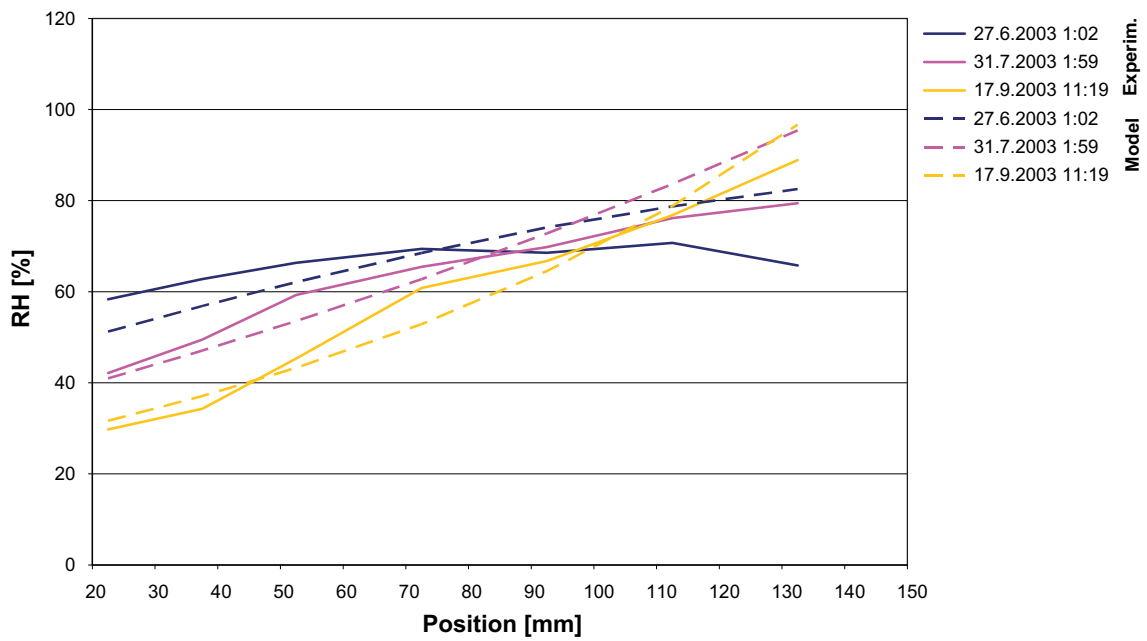


Figure 4-23d. Distributions of relative humidity with time, Cell 1. Computed results and observations. TUL.

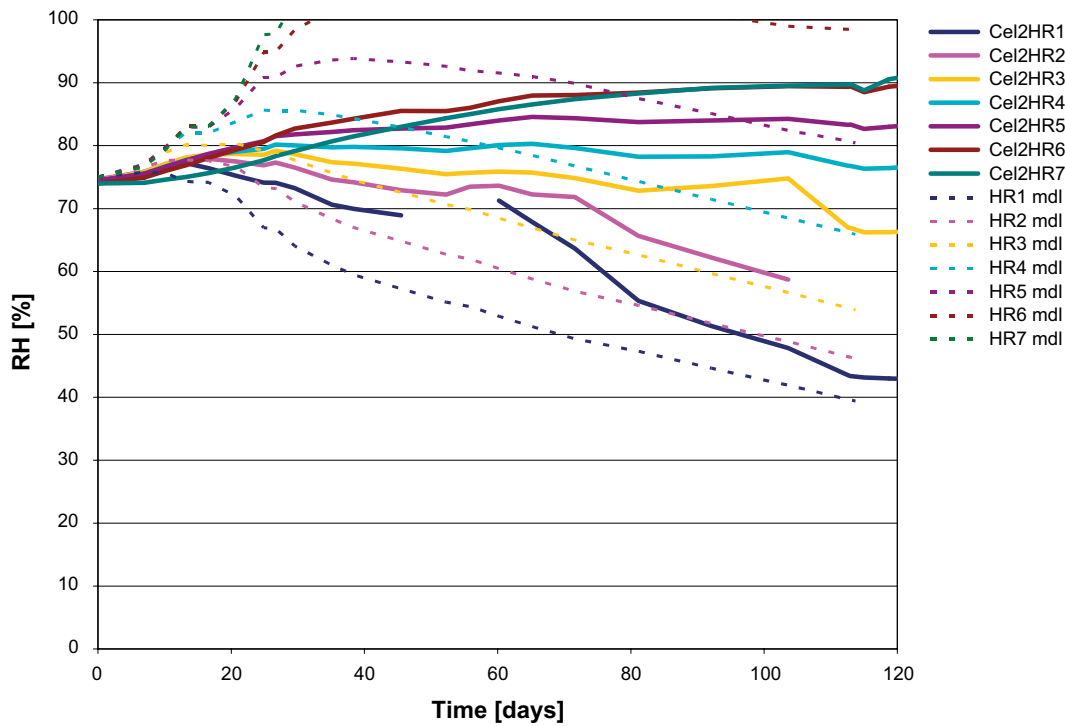


Figure 4-23e. Evolution of relative humidity with time, Cell 2. Computed results and observations. TUL.

4.10.2 UPC heating test – Subtask 1.3 [16]

A 2D geometry is used choosing a thickness that maintains the sample volume. The mesh is shown in Figure 4-24 a. A coupled TH analysis is performed with the same characteristics as outlined in the previous sections. The switching off period is ignored. The parameters have been obtained by an automated calibration procedure. The results are shown in Figure 4-24b to 4.24d.

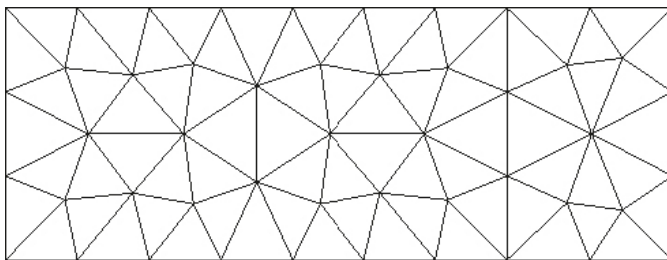


Figure 4-24a. Model mesh. TUL.

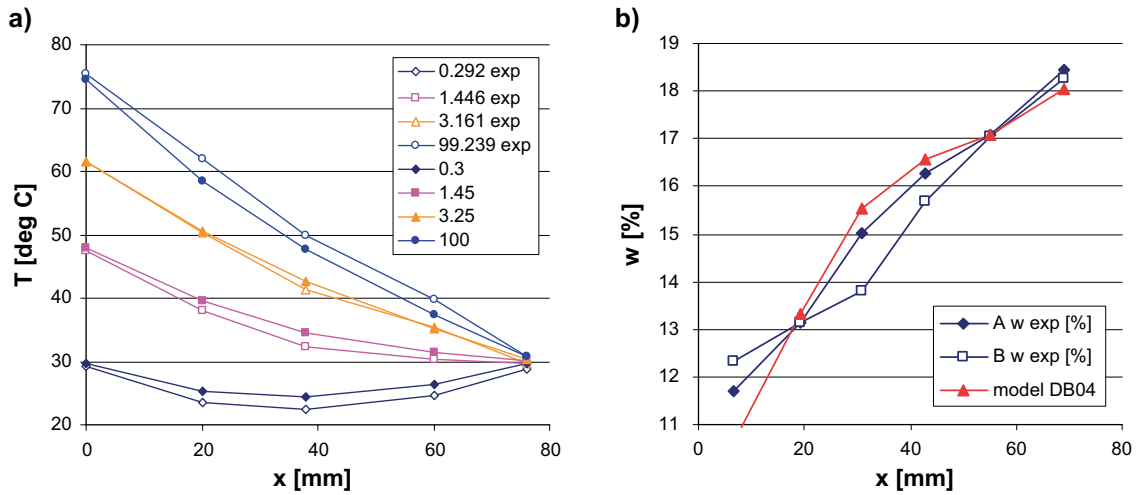


Figure 4-24b. Distributions of a) temperatures at different times and of b) water content at the end of the test. Computed results and observations. Initial reference parameters. TUL.

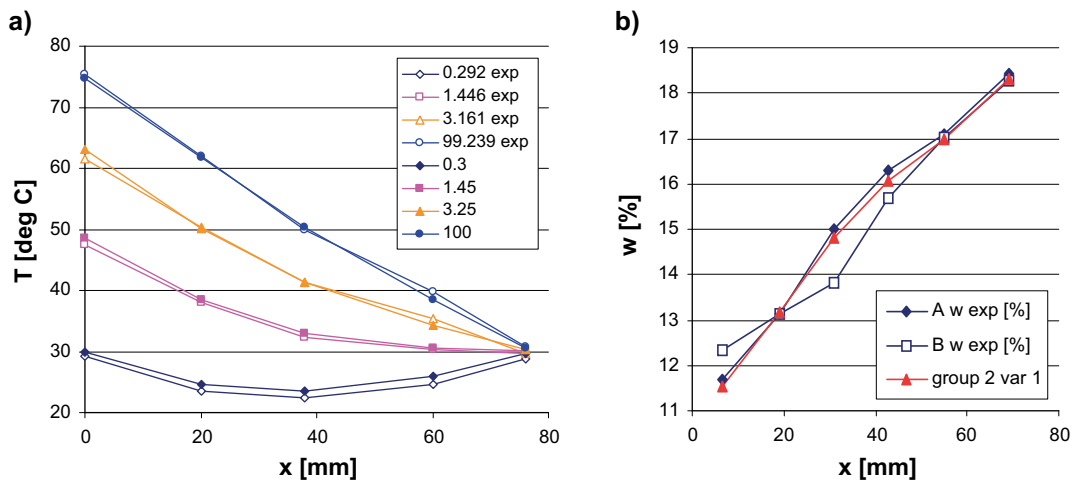


Figure 4-24c. Distributions of a) temperatures at different times and of b) water content at the end of the test. Computed results and observations. Best fit parameters allowing unrealistic values. TUL.

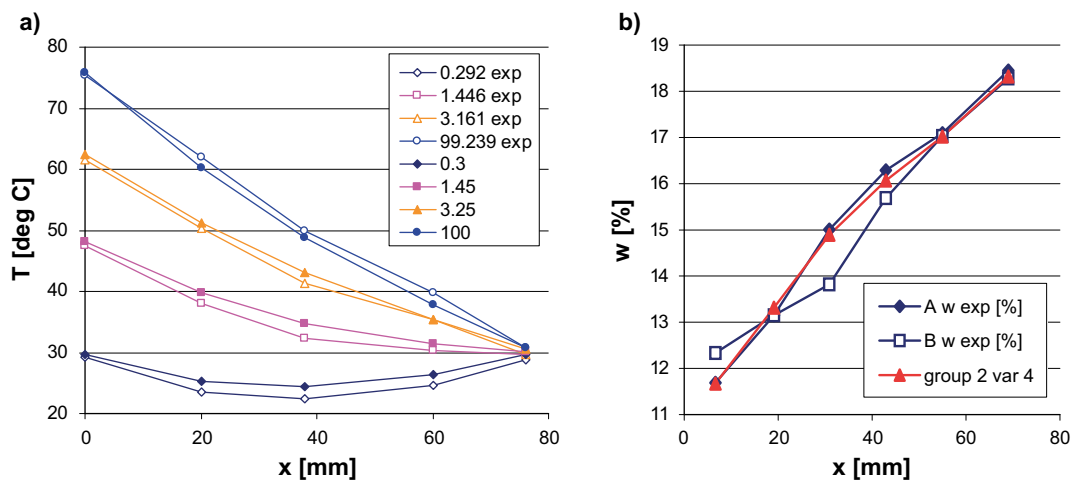


Figure 4-24d. Distributions of a) temperatures at different times and of b) water content at the end of the test. Computed results and observations. Best fit parameters but fixed heat conductivity values. TUL.

4.10.3 Remarks

This team uses a quite different formulation from most of the other modelling groups. Vapour transport is privileged and no mechanical effects are addressed. Coupled TH analyses are performed; storage terms are derived from exchanges with adsorbed water. Temperatures are correctly modelled in all cases. There are significant differences with observations concerning the evolutions of relative humidity in Subtask 1.1. Variations of parameters, allowed by the flexibility of the formulation, do not improve significantly the results. Because of the wide range of possible parameter values, this group has used an automatic optimisation procedure for parameter determination in Subtask 1.3. A good agreement with observations of temperatures and water content at the end of the test are achieved.

5 Concluding remarks

Formulations and codes

1. There is a variety of formulations and codes that have been used in this Task. Generally they can be classified in two groups: general formulations that attempt to cater for the full range of THM phenomena (AECL, BGR, CIMNE, Clay Technology-1, Clay Technology-2, CRIEPI and MARINTEL) and more restricted formulations that only consider water transport by vapour and do not incorporate mechanical aspects (GRS and TUL). The second group has a more limited scope of applicability and they have not been applied to the full set of Subtasks.
2. Except for MARINTEL, all general formulations are derived using a phenomenological approach. MARINTEL formulation is more directly based on thermodynamics considerations. However, such an approach leads to a quite similar set of equations. In MARINTEL formulation, liquid water flow is driven by gradients of water content which may create some difficulties from the physical and operational point of view.
3. The main difference between the general formulations is their capacity to incorporate or not the air balance equation. AECL, CIMNE and Clay Technology-1 (all using CODE_BRIGHT) have this possibility but not the other formulations. Without the gas equation, the usual assumption is that gas pressure is constant. This leads to non-physical situations when temperatures rise above 100 °C and the vapour pressure exceeds 1 atmosphere. It must be said, however, that when calculations with and without air balance equations have been compared in this Task, results were qualitatively similar and differences have not been very significant.
3. Thermal and hydraulic constitutive models are quite similar across all formulations. The main differences lie in the description of vapour diffusion. Two main families of constitutive laws are used: i) Fick's law, and ii) double diffusion coefficient, often related to Philip and de Vries (1957) formulation. No clear advantage of a particular approach has been identified from the examination of the pattern and quality of results.
4. The largest variety of constitutive models lies in the mechanical component. However, most of them are rather simple models (elastic, Drucker-Prager, poroelastic) with the addition of an ad-hoc swelling model. These additions do not constitute a full constitutive model, as they only address partial aspects of behaviour (generally, the development of volumetric strains). However, they have proved quite efficient in simulating the expansive nature of the bentonite during hydration.
5. AECL has used a fully defined constitutive model (BBM) but it has experienced severe convergence problems. Using the same model, CIMNE and Clay Technology-1 do not appear to have had similar difficulties. It is probable, however, that the plastic part of the model is seldom engaged in the cases solved in this Task. In any case, the elastic part of the original BBM had to be modified to account of the large swelling phenomena developed by the bentonite during hydration. Different modified versions of the elastic component were used by different Code Bright teams.
6. The thermomechanical aspects of the constitutive laws have not been addressed in detail by any of the teams. The only thermal effect on mechanical behaviour is the thermal expansion derived from a constant coefficient of thermal dilation.
7. In accordance with the criteria adopted to select the tests, the meshes used in all the analyses have been rather small in size. The computations performed, therefore, cannot be used as a suitable check on the efficiency and capabilities of the codes to tackle larger problems.

THM phenomena and modelling

8. In general, the temperature fields have been satisfactorily reproduced by all teams that solved the thermal problem. The successful modelling of the temperature fields and evolutions is helped by the fact that the tests are temperature-controlled. Clay Technology-2 (for Subtasks 1.1 and 1.2) and GRS have used the observed temperatures as direct input to the calculations.
9. The dominant heat transfer mechanism is conduction. A good modelling of the thermal problem requires the consideration of the changes of thermal conductivity with degree of saturation. This has been largely achieved by all groups solving the thermal problem.
10. To obtain adequate distributions of temperatures throughout the bentonite samples, it has proved essential to model the thermal effects of the whole experimental apparatus including all insulating layers.
11. The overall pattern of hydraulic behaviour has generally been reasonably well modelled by the teams. Variation in vapour diffusion formulations and parameters appear to underlie many of the differences between different teams. On several occasions, it has been found that vapour migration depends mainly on the ratio between tortuosity and intrinsic permeability (τ/k) rather than on the individual parameters.
12. The sensitivity of the hydraulic results to variations in retention curve has been noticed on several occasions but not examined in detail.
13. Two of the formulations (GRS and TUL) consider explicitly the presence of adsorbed water that is ignored by the other formulations. The potential effects of its inclusion in general formulations have not been investigated.
14. In general, hydraulic behaviour has been reproduced more closely in the isothermal test. Larger differences between computed and observed hydraulic results are apparent in the non-isothermal tests.
15. The main phenomenon not reproduced by the modelling teams is the slowing down of hydration at long times in non-isothermal tests, especially Cell 2 of CEA and the Thermal Gradient Test of CIEMAT. Varying the parameters has not been successful in bridging the differences. It is possible that this modelling shortcoming may indicate that some phenomena are not properly accounted although it is more likely that this slowing down of hydration is due, at least in good part, to vapour leaking out of the apparatuses.
16. Examining CIEMAT's Thermal Gradient Test, it is possible to observe that the final computed relative humidity obtained by the different teams differ widely. It appears that the main cause of the differences lies in the selection of the intrinsic permeability value for liquid flow.
17. Mass conservation of water has been checked using the results of the calculations of several codes with satisfactory results.
18. Mechanical results are scarce in the tests proposed in this Task: measurement of axial stresses in the CEA mock up tests and of the change of diameter in the UPC heating test. In general, they are quite adequately reproduced by quite a number of the teams that have incorporated the mechanical component of the formulation. However, the results available provide a too limited set of data and stress conditions to test meaningfully the capabilities of the mechanical constitutive models. There were no measurements of radial stresses available for comparison but very different results have been reported from different teams. This is not unexpected as this result depends strongly on quite specific details of the mechanical constitutive models.
19. The influence of the mechanical behaviour on thermal and hydraulic results is limited because porosity variations are small in the confined conditions of most tests. Thus, the lack of consideration of mechanical aspects does not affect significantly the capacity of modelling the thermo-hydraulic behaviour.
20. Generally, the modelling teams have adapted the parameters (and sometimes the formulations) to each particular Subtask being analysed in spite of the fact that Subtasks 1.2 and 1.3 involve the same material under very similar initial conditions. Only Clay Technology-2 maintained the same parameters for the two Subtasks.

General remarks

21. Considering the overall pattern of analyses, results and comparisons, it can be stated that the THM behaviour has been successfully modelled by most teams. This indicates that the formulations incorporate the most relevant THM phenomena and their mutual interactions and that the codes are capable to solve the relevant equations in a satisfactory manner.
22. The only exception concerns the failure to model adequately the observed slow hydration of non-isothermal tests. It has been indicated, however, that at least a substantial part of this failure may be due to vapour leakage from the call towards the exterior.
23. Although the analyses performed have not been predictive, from the examination of the various computational processes, it can be stated that it is likely that predictive capability of the thermal problem is quite high. However, and although hydraulic results have also been well reproduced a posteriori, it is however unlikely that the same predictive capability exists concerning the hydraulic problem. This problem has proved to be very sensitive to a large number of parameters making it doubtful that a stage of reliable true predictions in this area has been reached. The same remark is even more valid concerning the general mechanical problem although reasonable reliable predications can perhaps be achieved regarding partial aspects of mechanical behaviour such as swelling pressures in confined situations. Of course, swelling pressure is the main mechanical parameter related to the safety functions of an engineered barrier.

References

SKB's (Svensk Kärnbränslehantering AB) publications can be found at www.skb.com/publications. SKBdoc documents will be submitted upon request to document@skb.se.

Börgesson L, Hernelind J, 1999. Äspö Hard Rock Laboratory. Prototype Repository. Preliminary modeling of the water-saturation phase of the buffer and backfill materials. SKB IPR-00-11, Svensk Kärnbränslehantering AB.

Börgesson L, Johannesson L-E, Sandén T, Hernelind J, 1995. Modelling of the physical behaviour of water saturated clay barriers. Laboratory tests, material models and finite element application. SKB TR 95-20, Svensk Kärnbränslehantering AB.

Dang K D, Robinet J-C, 2004. Thermo-hydro-mechanical behaviour of MX80 bentonite for temperature ≥ 100 °C. Final report. Andra report C.RP.0EUG.02.008, Andra, France.

ENRESA, 1998. FEBEX. Bentonita: origen, propiedades y fabricación de bloques. Publicación Técnica ENRESA 04/98, ENRESA, Spain.

ENRESA, 2000. FEBEX Project. Full-scale engineered barriers experiment for a deep geological repository for high level radioactive waste in crystalline host rock. Final Report. Publicación Técnica ENRESA 1/2000, ENRESA, Spain.

Fernández A M, 2003. Caracterización y modelización del agua intersticial en materiales arcillosos: estudio de la bentonita de Cortijo de Archidona. PhD thesis. Universidad Autónoma de Madrid. (In Spanish.)

Gatabin C, Billaud P, 2005. Bentonite THM mock up experiments. Sensors data report. Rapport NT-DPC/SCCME 05-300-A, CEA, France.

Hokr M, Frydrych D, 2012. Fully coupled algorithm for heat and water transport – Estimation of non-linear parameters based on the experimental data. Mathematics and Computers in Simulation 82, 1908–1918.

Hökmark H, Fälth B, 2003. Temperature Buffer Test. Predictive Modelling Programme. SKBdoc 1012125 ver 1.0, Svensk Kärnbränslehantering AB.

Imbert C, Billaud P, Touze G, Dang K D, 2004. Comportement thermo-hydro-mécanique d'une argile gonflante méthodologique en situation de stockage. Rapport RT-DPC/SCCME 04-677-A, CEA, France. (In French.)

Komine H, Ogata N, 1996. Prediction for swelling characteristics of compacted bentonite. Canadian Geotechnical Journal 33, 11–22.

Komine H, Ogata N, 2003. New equations for swelling characteristics of bentonite-based buffer materials. Canadian Geotechnical Journal, 40, 460–475.

Lajudie A, Raynal J, Petit J-C, Toulhoat P, 1994. Clay based materials for engineered barriers: a review. Materials Research Society Symposium Proceedings 353, 221–230.

Lloret A, Villar M V, Pintado X, 2002. Ensayos THM: Informe de síntesis. Internal report CIEMAT/DIAE/54520/1/02. FEBEX Report 70-UPC-M-0-04, CIEMAT, Spain. (In Spanish).

Lloret A, Romero E, Villar M V, 2004. FEBEX II Project Final report on thermo-hydro-mechanical laboratory tests. Publicación Técnica ENRESA 10/04, ENRESA, Spain.

Olivella S, Carrera J, Gens A, Alonso E E, 1994. Non-isothermal multiphase flow of brine and gas through saline media. Transport in Porous Media 15, 271–293.

Olivella S, Gens A, Carrera J, Alonso E E, 1996. Numerical formulation for a simulator (CODE_BRIGHT) for the coupled analysis of saline media. Engineering Computations 13, 87–112.

Philip J R, de Vries D A, 1957. Moisture movement in porous materials under temperature gradients. Eos, Transactions American Geophysics Union 38, 222–232.

Pintado X, Ledesma A, Lloret A, 2002. Backanalysis of thermohydraulic bentonite properties from laboratory tests. Engineering Geology 64, 91–115.

Sánchez M, 2004. Thermo-hydro-mechanical coupled analysis in low permeability media. PhD thesis. Universitat Politècnica de Catalunya, Spain.

Tanaka Y, Nakamura K, 2004. Effect of seawater and high-temperature history on swelling characteristics of bentonite as an engineering barrier for disposal facilities of radioactive waste. CRIEPI report N04007, Central Research Institute of Electric Power Industry, Japan. (In Japanese.)

Villar M-V, 2002a. AESPOE Hard Rock Laboratory. CIEMAT contribution to 2002 Annual scientific report. CIEMAT/DIAE/54540/1/02, CIEMAT, Spain.

Villar M V, 2002b. Thermo-hydro-mechanical characterisation of a bentonite from Cabo de Gata. A study applied to the use of bentonite as sealing material in high level radioactive waste repositories. Publicación Técnica ENRESA 01/2002, ENRESA, Spain.

Villar M-V, 2003. AESPOE Hard rock laboratory“. CIEMAT contribution to 2001 Annual scientific report. CIEMAT internal report CIEMAT/DIAE/54540/2/03, CIEMAT, Spain.

Villar M V, Lloret A, 2004. Influence of temperature on the hydro-mechanical behaviour of a compacted bentonite. Applied Clay Science 26, 337–350.

Villar M V, Martín P L, Barcala J M, 2005. Infiltration tests at isothermal conditions and under thermal gradient. Technical Report CIEMAT/DMA /M2140/1/05, CIEMAT, Spain.

Reports annex

Listed below are unpublished working reports. Contact responsible organisation for possible requests of material.

- [1] **Guo, R.,** Dixon, D. Thermo-hydro-mechanical-gas modelling of the bentonite THM mock-up experiments, 2005. File: AECL Task 1.1.pdf
- [2] **Guo, R.,** Dixon, D. Thermo-hydro-mechanical modelling of infiltration tests of FEBEX bentonite at isothermal conditions and under thermal gradient, 2005. File: AECL Task 1.2.pdf
- [3] **Guo, R.,** Dixon, D. Thermo-hydro-mechanical numerical modeling of a laboratory heating test and comparison with measurements, 2006. File: AECL Task 1.3.pdf
- [4] **Nowak, T.** Task Force on Engineered Barrier Systems: Modeling of the Benchmarks 1.1.1 and 1.1.2, 2005. File: BGR Task 1.1-1.2.pdf
- [5] **Nowak, T.** Task Force on Engineered Barrier Systems: Modeling of Benchmark 1.1.3, 2007. File: BGR Task 1.3.pdf
- [6] **Chen, G.,** Ledesma, A. Modelling experiments regarding THM behaviour of bentonite within the framework of the EBD Task Force, 2006. File: CIMNE Task 1.pdf
- [7] **Birgersson, M.,** Akesson, M., Hökmark, H., Lönnqvist, M. EBS Task Force: Calculation of benchmark 1.1.1, 2007. File: Clay Technology-1 Task 1.1.pdf
- [8] **Birgersson, M.,** Akesson, M., Hökmark, H. EBS Task Force: Calculation of benchmark 1.1.2, 2007. File: Clay Technology-1 Task 1.2.pdf
- [9] **Birgersson, M.,** Akesson, M., Hökmark, H. EBS Task Force: Calculation of benchmark 1.1.3, 2007. File: Clay Technology-1 Task 1.3.pdf
- [10] **Börgesson, L.,** Deeck, A., Hernelind, J. EBS Task Force Benchmark 1.1. Modelling of laboratory tests, 2007. File: Clay Technology-2 Task 1.pdf
- [11] **Sawada, M.,** Okada, T., Hasegawa, T. THM coupled analyses of three different laboratory tests, 2007. File: CRIEPI Task 1.pdf
- [12] **Kröhn, K.-P.** Contribution to the test case 1.1.2 of the Task Force EBS, 2007. File: GRS Task 1.pdf
- [13] **Lempinen, A.** Simulations for EBS Task Force BMT 1, 2005. File: MARINTEL Task 1.1-1.2.pdf
- [14] **Lempinen, A.** Simulations for EBS Task Force BMT 1.3, 2007. File: MARINTEL Task 1.3.pdf
- [15] **Hokr, M.,** Frydrych, D. Simulation of BM1.1 problem with mobile moisture transport model with adsorbed water, 2007. File: TUL Task 1.1.pdf
- [16] **Hokr, M.,** Frydrych, D., Cizková, L. Simulation of BM1.3 problem with mobile moisture transport model ISERIT, 2007. File: TUL Task 1.3.pdf

Specifications of Subtask 1.1

Bentonite thm mock-up experiments performed by CEA

A1 Introduction

The Äspö HRL International Joint Committee, IJC, has set up a Task Force on Engineered Barrier System (EBS) incorporating also organisations not participating in the Äspö HRL programme. The long term objective is the development of general and effective tools for the advanced coupled THMC analysis of buffer and backfill behaviour. The tools developed should

- account for all relevant phenomena and their interactions (including interaction with host rock),
- deal with both short term and long term phenomena and behaviour,
- be computationally efficient in order to be applied to real engineering problems.

The Äspö HRL International Joint Committee decided, on May 19th 2004, that in the first phase of this Task Force (period 2004–2008), work should concentrate on:

- THM modelling of processes during water transfer in buffer, backfill and near-field rock (Task 1).
- Gas transport in saturated buffer (Task 2)

The work in Task 1 takes into account the interaction between the buffer and backfill barriers and the host rock. Only crystalline rock is considered initially, although other rock types could be incorporated later.

The activities planned for the first year of the development of the Task Force include the analysis of a number of benchmark tests in order to assess the capabilities of the codes and to identify the areas of required improvement. It is envisaged that this first set of benchmarks should involve a relatively large number of relevant phenomena but should not be too demanding in terms of computer resources. This first activity should focus in the conceptual capabilities of the codes in relation with THM and gas transport phenomena.

The Task Force is not set up as a competition between codes to determine, from a blind prediction, the best fit to a particular set of experimental results. The basic idea is to allow freedom to the participants to use and develop formulations and codes to try to reproduce in the best way possible the tests results provided in the Benchmark. This will provide the bases to assess the capabilities of the code and to identify areas of required improvement.

This document describes the proposal of Benchmark THM 1.1, based on the performance of THM mock-up experiments on MX-80 bentonite by CEA. The information provided by Claude Gatabin (CEA) on this experimental programme is very gratefully acknowledged.

A2 Description of the thm mock up tests

A2.1 General

Two THM mock up tests have been performed on vertical cylindrical columns of compacted MX-80 bentonite. Two different initial water contents have been used to form the samples.

Each test is composed of two phases. In Phase 1 heat is applied to one end of the column while the temperature at the other end is kept constant and equal to 20 °C. A maximum temperature of 150 °C is applied. Phase 2 starts after thermal equilibrium has been achieved and involves the gradual hydration of the sample. A constant water pressure is applied to the end opposite to the one where the temperature variation was prescribed. Constant volume conditions are ensured in the two phases of the test.

The following parameters are measured during the tests:

- Temperatures
- Relative humidity
- Pore pressure
- Total axial stress
- Total radial stress

It is advised to read carefully the CEA report: “Bentonite THM mock up experiments. Sensor data report (DPC/SCCME 05-300-A)” by C. Gatabin & P. Billaud that contains a detailed description of equipment and experiments. Only the most immediately relevant information is given in this document.

A2.2 Apparatus and monitoring system

The samples have both a diameter and a height of 203mm. The specimens are tested in an apparatus the diagram of which is shown in Figure A-1. The samples are tightly enclosed in a PTFE sleeve. To minimize heat losses, the cells were insulated with a heatproof envelope. Experiments are not gas tight. Heat is applied at the bottom plate whereas hydration proceeds from the top of the sample.

The monitoring sensors are installed normal to the vertical axis. Measurements of temperature, relative humidity and pore pressures are performed close to the axis of the column whereas radial stress sensors are placed in contact with the outside surface of the sample. The vertical location of the various sensors is given in Appendix A. In addition each cell is equipped with a force sensor to measure the axial load. This sensor is located at the top of the sample.

A2.3 Material

Compacted MX-80 bentonite has been used to manufacture the specimens tested. For the specimen of Cell 1, the bentonite was stabilised in an atmosphere with a relative humidity of 60 % whereas for the specimen of Cell 2, the bentonite was stabilised in an atmosphere with a relative humidity of 90 %. A target dry density of 1.7 g/cm³ was adopted for compaction. The characteristics of the material at the time of emplacement in the apparatus are given in Table A-1.

A review of the reported THM properties of MX-80 bentonite has yielded the information presented in Appendix B.

Table A-1. Characteristics of the MX-80 samples after compaction.

	Cell 1: 1858iA	Cell 2: 1857iA
Powder conditioning, HR (%)	60	90
Compaction pressure (MPa)	33	33
Sample mass (g)	13 332	13 395
Water content (%)	13.66	17.86
Diameter (mm)	202.7	202.7
Height (mm)	203.0	203.0
Bulk density (g/cm ³)	2.035	2.045
Dry density (g/cm ³)	1.791	1.735
Porosity	0.3242	0.3453
Void ratio	0.48	0.527
Degree of saturation	0.755	0.897
Swelling pressure at saturation (MPa)	24.5	18.2

Note: The selected density of MX80 grains used for calculation purposes is equal to 2.65 g/cm³.

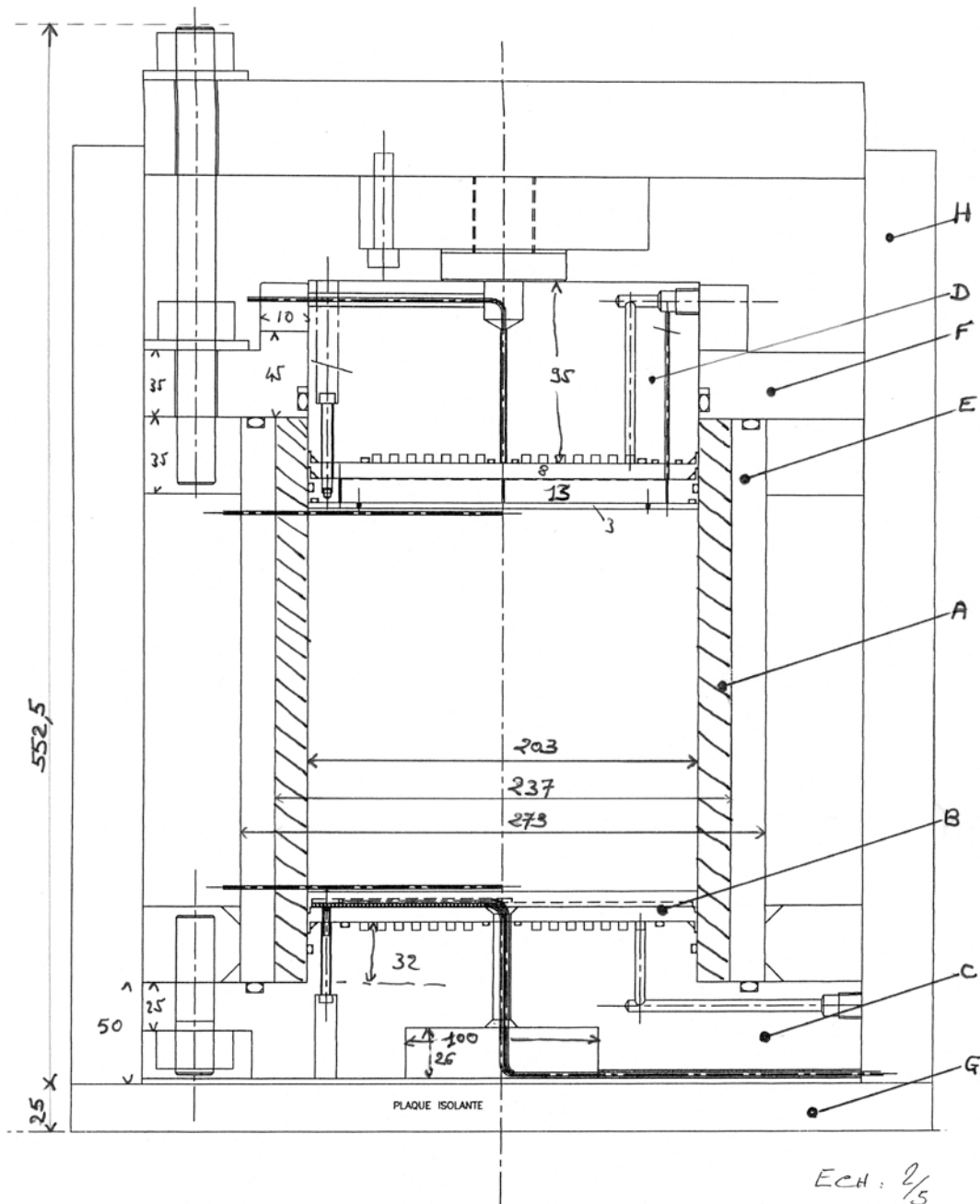


Figure A-1. Layout of the experimental cell.

A2.4 Protocol of the experiments

In Phase 1 of the experiments, the temperature at the bottom end of the specimen was raised in steps until reaching 150 °C. Table A-2 contains the temperature increase schedule. The temperature at the top end of the specimen was kept constant at 20 °C. For the two experiments Phase 1 started at 15:27 on May 26 2003 and it was considered finished, after 2706 hours, at 9:00 on September 16 2003.

Phase 2 involved the application of a 1 MPa water pressure at the top of the sample whereas at the bottom, the temperature was maintained at 150 °C. Some water leaks developed in Cell 1 but no leaks were apparently observed in Cell 2. Phase 2 for Cell 1 started at 14:23 on September 16 2003 and ended on May 25 2004 and for Cell 2, it started at 14:26 on September 18th 2003 and ended at 9:00 on March 12 2004.

It should be noted that the transition from Phase 1 to Phase 2 involved some manipulation of the apparatus resulting in a variation of the recorded stresses, notably the value of the axial stresses (Gatabin and Billaud 2005).

Table A-2. Protocol for temperature increase in Phase 1 of the experiments.

Start-up date	Initial temperature (°C)	Ending date	Final temperature (°C)	Heat velocity (°C/h)	Stable stage (h)	Gradient (°C/cm)
26/05/03 15:27	21.6	02/06/03 11:27	30	0.4	21	0.5
02/06/03 11:27	30	05/06/03 16:05	40	0.4	25	1.0
05/06/03 16:05	40	08/06/03 16:09	50	0.4	25	1.5
08/06/03 16:09	50	12/06/03 09:19	60	0.4	25	2.0
12/06/03 09:19	60	16/06/03 11:46	70	0.4	25	2.5
16/06/03 11:46	70	20/06/03 10:11	80	0.4	25	3.0
20/06/03 10:11	80	24/06/03 16:07	90	0.4	25	3.5
24/06/03 16:07	90	30/06/03 11:08	100	0.4	25	4.0
30/06/03 11:08	100	03/07/03 17:30	105	0.2	25	4.25
03/07/03 17:30	105	10/07/03 14:46	110	0.2	25	4.50
10/07/03 14:46	110	17/07/03 16:19	115	0.2	25	4.75
17/07/03 16:19	115	22/07/03 15:04	120	0.2	25	5.0
22/07/03 15:04	120	28/07/03 10:31	125	0.2	25	5.25
28/07/03 10:31	125	05/08/03 09:38	130	0.2	25	5.50
05/08/03 09:38	130	18/08/03 09:55	135	0.2	25	5.75
18/08/03 09:55	135	05/09/03 18:01	140	0.2	25	6.0
05/09/03 18:01	140	16/09/03 09:00	150	0.2	50	6.50

A2.5 Test results

A number of selected results can be seen in the report by Gatabin and Billaud (2005). The full data sets are included in the associated Excel files, as described below.

A2.5.1 Phase 1

Temperature: File “THM BM1.1 Phase 1 Temperature.xls”

- Cell 1: Sheet: *Cell 1*. Relevant columns: “Date/time” and “Cell1T0, Cell1T1, Cell1T2, Cell1T3, Cell1T4, Cell1T5, Cell1T6, Cell1T7, Cell1T8, Cell1T9, Cell1T10, Cell1T11, Cell1T12, Cell1T13, Cell1T14”.
- Cell 2: Sheet: *Cell 2*. Relevant columns: “Date/time” and “Cell2T0, Cell2T1, Cell2T2, Cell2T3, Cell2T4, Cell2T5, Cell2T6, Cell2T7, Cell2T8, Cell2T9, Cell2T10, Cell2T11, Cell2T12, Cell2T13, Cell2T14”.

Relative humidity: File “THM BM1.1 Phase 1 RH.xls”

- Cell 1: Sheet: *Cell 1*. Relevant columns: “Date/time” and “Cell1HR1, Cell1HR2, Cell1HR3, Cell1HR4, Cell1HR5, Cell1HR6, Cell1HR7”. The columns “Cell1HRT1, Cell1HRT2, Cell1HRT3, Cell1HRT4, Cell1HRT5, Cell1HRT6, Cell1HRT7” contain the associated temperatures data.
- Cell 2: Sheet: *Cell 2*. Relevant columns: “Date/time” and “Cell2HR1, Cell2HR2, Cell2HR3, Cell2HR4, Cell2HR5, Cell2HR6, Cell2HR7”. The columns “Cell2HRT1, Cell2HRT2, Cell2HRT3, Cell2HRT4, Cell2HRT5, Cell2HRT6, Cell2HRT7” contain the associated temperatures data.

Pore Pressures: File “THM BM1.1 Phase 1 Pore P.xls”

- Cell 1: Sheet: *Cell 1*. Relevant columns: “Date/time” and “PI1, PI2, PI3, PI4”.
- Cell 2: Sheet: *Cell 2*. Relevant columns: “Date/time” and “PI1, PI2, PI3, PI4”.

Radial stress: File “THM BM1.1 Phase 1 Radial P.xls”

- Cell 1: Sheet: *Cell 1*. Relevant columns: “Date/time” and “1PTK1, 1PTE2, 1PTK3, 1PTE4, 1PTK5, 1PTE6, 1PTK7, 1PTK8”
- Cell 2: Sheet: *Cell 2*. Relevant columns: “Date/time” and “2PTK1, 2PTE2, 2PTK3, 2PTE4, 2PTK5, 2PTE6, 2PTK7, 2PTE8”

Axial stress: File “THM BM1.1 Phase 1 Axial P.xls”

- Cell 1: Sheet: *Cell 1*. Relevant columns: “Date/time” and “Confining pressure”.
- Cell 2: Sheet: *Cell 2*. Relevant columns: “Date/time” and “Confining pressure”.

A2.5.2 Phase 2

Temperature: File “THM BM1.1 Phase 2 Temperature.xls”

- Cell 1: Sheet: *Cell 1*. Relevant columns: “Date/time” and “Cell1T0, Cell1T1, Cell1T2, Cell1T3, Cell1T4, Cell1T5, Cell1T6, Cell1T7, Cell1T8, Cell1T9, Cell1T10, Cell1T11, Cell1T12, Cell1T13, Cell1T14”.
- Cell 2: Sheet: *Cell 2*. Relevant columns: “Date/time” and “Cell2T0, Cell2T1, Cell2T2, Cell2T3, Cell2T4, Cell2T5, Cell2T6, Cell2T7, Cell2T8, Cell2T9, Cell2T10, Cell2T11, Cell2T12, Cell2T13, Cell2T14”.

Relative humidity: File “THM BM1.1 Phase 2 RH.xls”

- Cell 1: Sheet: *Cell 1*. Relevant columns: “Date/time” and “Cell1HR1, Cell1HR2, Cell1HR3, Cell1HR4, Cell1HR5, Cell1HR6, Cell1HR7”. The columns “Cell1HRT1, Cell1HRT2, Cell1HRT3, Cell1HRT4, Cell1HRT5, Cell1HRT6, Cell1HRT7” contain the associated temperatures data.
- Cell 2: Sheet: *Cell 2*. Relevant columns: “Date/time” and “Cell2HR1, Cell2HR2, Cell2HR3, Cell2HR4, Cell2HR5, Cell2HR6, Cell2HR7”. The columns “Cell2HRT1, Cell2HRT2, Cell2HRT3, Cell2HRT4, Cell2HRT5, Cell2HRT6, Cell2HRT7” contain the associated temperatures data.

Pore Pressures: File “THM BM1.1 Phase 2 Pore P.xls”

- Cell 1: Sheet: *Cell 1*. Relevant columns: “Date/time” and “PI1, PI2, PI3, PI4”.
- Cell 2: Sheet: *Cell 2*. Relevant columns: “Date/time” and “PI1, PI2, PI3, PI4”.

Radial stress: File “THM BM1.1 Phase 2 Radial P.xls”

- Cell 1: Sheet: *Cellule 1*. Relevant columns: “Date/time” and “1PTK1, 1PTE2, 1PTK3, 1PTE4, 1PTK5, 1PTE6, 1PTK7, 1PTK8”.
- Cell 2: Sheet: *Cellule 2*. Relevant columns: “Date/time” and “2PTK1, 2PTE2, 2PTK3, 2PTE4, 2PTK5, 2PTE6, 2PTK7, 2PTE8”.

Axial stress: File “THM BM1.1 Phase 2 Axial P.xls”

- Cell 1: Sheet: *Cellule 1*. Relevant columns: “Date/time” and “Confining pressure”.
- Cell 2: Sheet: *Cellule 2*. Relevant columns: “Date/time” and “Confining pressure”.

A3 Requested results

The following information is requested:

- a) Main features of the analyses performed.
- b) Results of the analyses and comparison with experimental results.

A3.1 Main features of the analyses performed

This basic description should contain summarised information on:

- Geometry adopted for the analysis.
- Type of analysis (e.g., 1-D, 2-D, axisymmetric...).
- Element types used.
- Constitutive laws adopted (thermal, hydraulic, mechanical).
- Constitutive parameters used and procedure used in their determination or estimation.

- Boundary conditions (thermal, hydraulic, mechanical).
- Initial conditions (thermal, hydraulic, mechanical).
- Hypothesis adopted for gas pressure and gas flow.
- Any other features that are deemed important in the analysis.

A3.2 Results of the analyses and comparison with experimental results

The following analysis results should be provided graphically together with comparison with observed data. The Excel files of the submitted graphs should also be made available. It should be noted that reliability of radial stress measurements is not high.

A3.2.1 Phase 1 (for both Cell 1 and Cell 2)

- Temperature vs. time for sensors T0, T1, T2, T3, T4, T5, T6, T7, T8, T9, T10, T11, T12, T13, T14.
- Relative humidity vs. time for sensors HR1, HR2, HR3, HR4, HR5, HR6, HR7.
- Radial stress vs. time for sensors PT1, PT2, PT3, PT4, PT5, PT6, PT7, PT8.
- Axial stress vs. time.
- Temperature vs. distance for days 28/06/03, 31/07/03 and 15/09/03.
- Relative humidity vs. distance days 28/06/03, 31/07/03 and 15/09/03.

A3.2.2 Phase 2 (for both Cell 1 and Cell 2)

- Temperature vs. time for sensors T0, T1, T2, T3, T4, T5, T6, T7, T8, T9, T10, T11, T12, T13, T14.
- Relative humidity vs. time for sensors HR1, HR2, HR3, HR4, HR5, HR6, HR7.
- Radial stress vs. time for sensors PT1, PT2, PT3, PT4, PT5, PT6, PT7, PT8.
- Axial stress vs. time.
- Temperature vs. distance for days 15/10/03, 14/01/04 and 4/03/04.
- Relative humidity vs. distance days 15/10/03, 14/01/04 and 4/03/04.

A3.3 Additional reporting

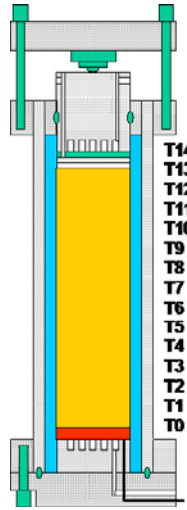
The reporting teams are encouraged to submit a brief introductory report outlining the aspects of the work and difficulties encountered that are considered to be especially relevant.

Location of the sensors

The vertical location of the various sensors is given in the following Tables.

Table AA1-1. Temperature sensors.

Sensor	Y (mm)
T 0	0
T 1	2.5
T 2	18.75
T 3	35.0
T 4	51.25
T 5	67.5
T 6	83.75
T 7	100
T 8	116.25
T 9	132.5
T 10	148.75
T 11	165
T 12	181.25
T 13	197.5
T 14	206*



T14	203.00 mm
T13	197.50 mm
T12	181.25 mm
T11	165.00 mm
T10	148.75 mm
T9	132.50 mm
T8	116.25 mm
T7	100.00 mm
T6	83.75 mm
T5	67.50 mm
T4	51.25 mm
T3	35.00 mm
T2	18.75 mm
T1	2.50 mm
T0	0.0 mm

* Taking into account a 3-mm stainless-steel plate.

Table AA1-2. Relative humidity sensors.

Relative-humidity sensor	Temperature sensor	Y (mm)
HR1	HRT1	22.5
HR2	HRT2	37.5
HR3	HRT3	52.5
HR4	HRT4	72.5
HR5	HRT5	92.5
HR6	HRT6	112.5
HR7	HRT7	132.5

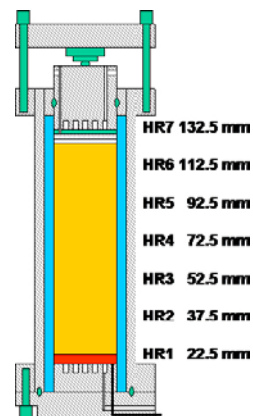
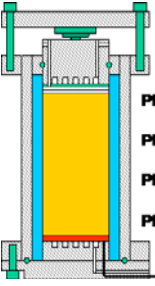


Table AA1-3. Pore pressure sensors.

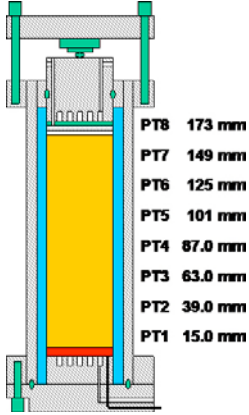
Sensor	Y (mm)
PI1	20.0
PI2	52.0
PI3	84.0
PI4	116.0



PI4	116.0 mm
PI3	84.0 mm
PI2	52.0 mm
PI1	20.0 mm

Table AA1-4. Radial stress sensors.

Sensor	Y (mm)
PT1	15.0
PT2	39.0
PT3	63.0
PT4	87.0
PT5	101.0
PT6	125.0
PT7	149.0
PT8	173.0



Properties of mx-80 bentonite

In this Appendix, information on THM properties of MX-80 bentonite obtained in previous investigations is collected. The sources of the various results presented are indicated in each case. More detailed information can be found in the references of this report.

AA2.1 Physical properties

MX-80 has a solid grain density equal to 2.82 g/cm³ (Villar 2002a). Note that this value is different from the 2.65 g/cm³ used in the reporting of the experiments (Gatabin and Billaud 2005).

AA2.2 Retention curve

Figure AA2-1 shows experimental results obtained for the retention curve of pure MX-80 bentonite at several dry densities. Data provided by CLAY TECHNOLOGY were found in Hökmark and Fälth (2003), by EUROGEOMAT in Dang and Robinet (2004) and by CIEMAT in Villar (2003).

Villar (2002a) presents data obtained on MX-80 compacted at 1 600 kg/m³ using water with 3 salt concentrations: 0, 0.5 and 1.2 %. Results are shown in Figure AA2-2. Water salinity appears to have little influence on the retention curve for suctions above 20 MPa. No data are available for lower suctions.

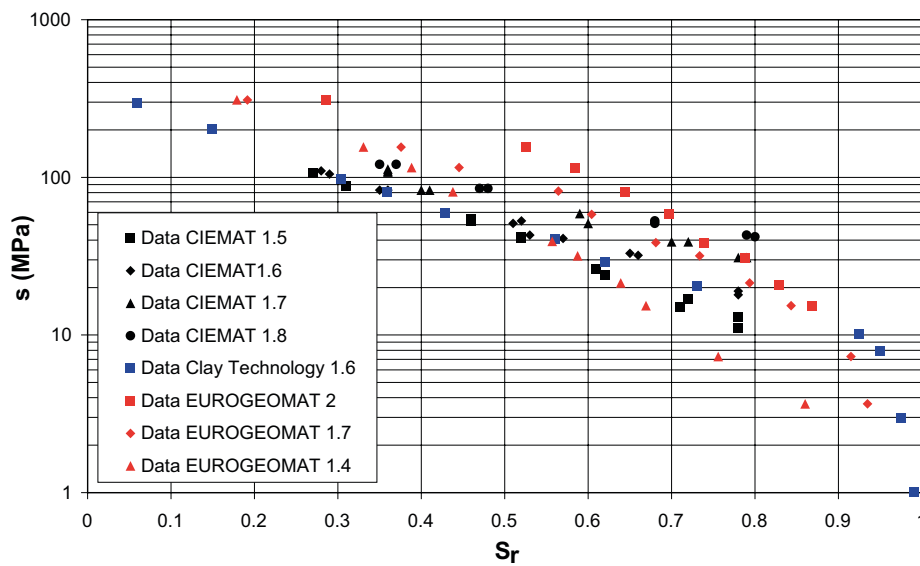


Figure AA2-1. Retention of MX-80 at constant volume and several dry densities.

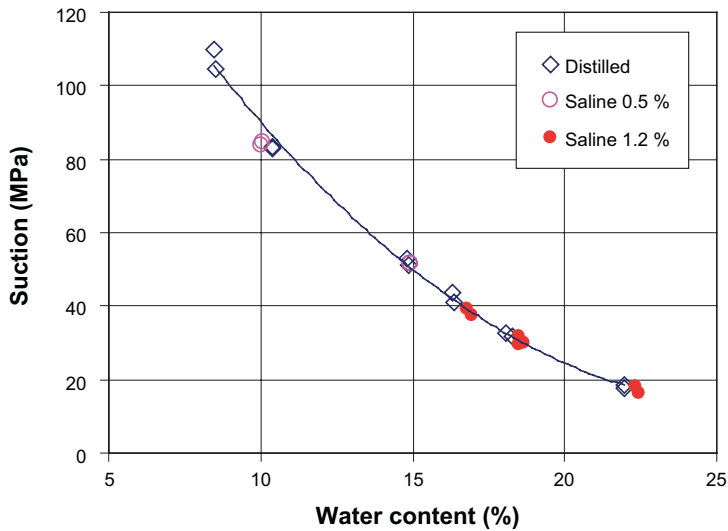


Figure AA2-2. Suction/water content relation for MX-80 clay compacted at dry density 1600 kg/m^3 and in presence of 3 water salinities (Villar 2002a).

AA2.3 Permeability

Figure AA2-3 shows the variation of the intrinsic permeability with porosity as obtained by several laboratories on water saturated MX-80 samples. Intrinsic permeability obtained in compacted samples is systematically one order of magnitude higher than intrinsic permeability obtained in bentonitic slurries.

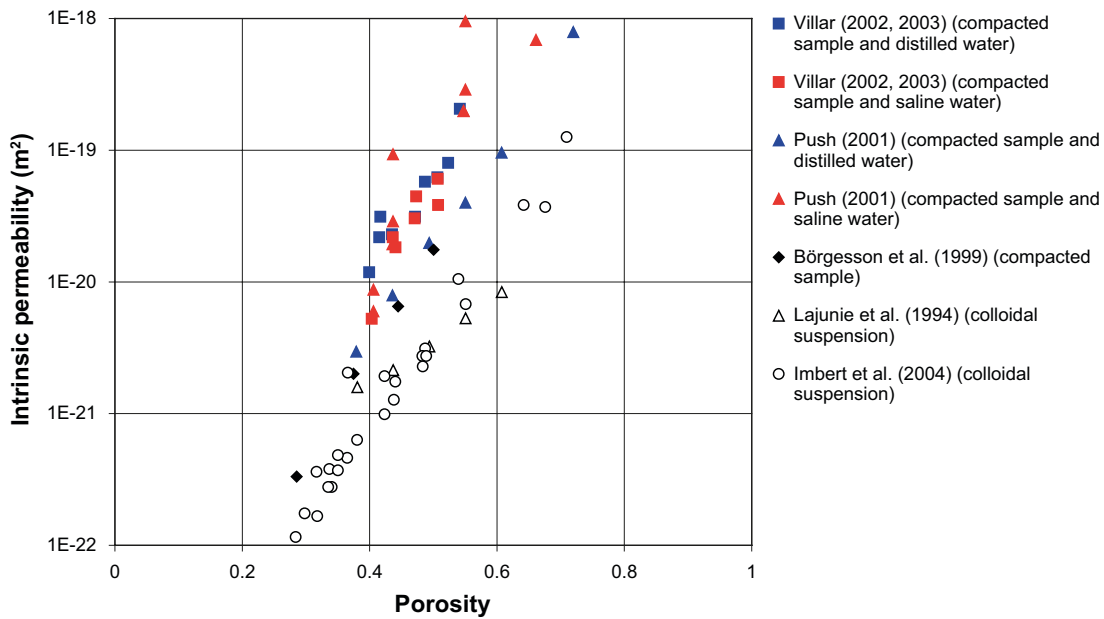


Figure AA2-3. Variation of intrinsic permeability with porosity as obtained by several laboratories in water-saturated samples.

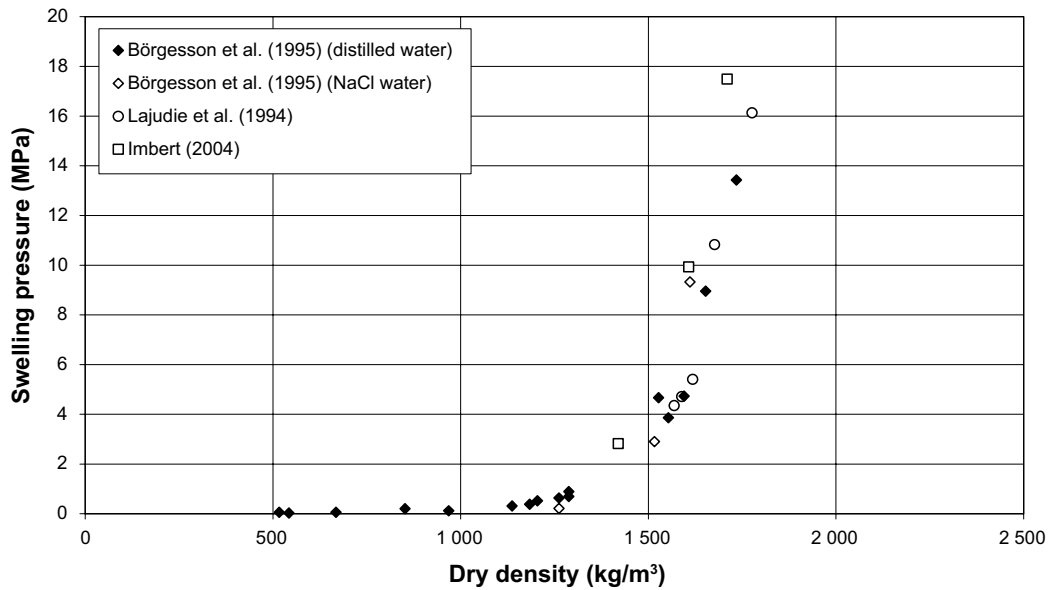


Figure AA2-4. Swelling pressure vs dry density as obtained by different laboratories.

AA2.4 Swelling properties

AA2.4.1 Swelling pressure

Data on swelling pressure reported by Börgesson et al. (1995), Lajudie et al. (1994) and Imbert et al. (2004) are compiled in Figure AA2-4.

Especially relevant are the results reported by Imbert et al. (2004) from tests performed in the CEA laboratory on samples compacted uniaxially:

Table AA2-1. Swelling pressure of uniaxially compacted MX-80 samples.

Specimen	Water content (%)	Compaction pressure (MPa)	Initial dry density (g/cm³)	Final dry density (g/cm³)	Swelling pressure (MPa)
1741u	14.25	10	1.490	1.485	4.20
1726u	14.25	20	1.639	1.632	9.93
1727u	14.25	40	1.770	1.749	19.98
1729u	14.25	60	1.823	1.798	26.06
1730u	14.25	100	1.858	1.836	29.73
1740u	14.25	181.5	1.888	1.863	36.49

AA2.4.2 Swelling strains

Villar (2002a, 2003) performed 4 swelling tests (EDN_4_9, EDN_4_10, EDN_2_13 and EDN_2_14) under constant load (0.1 MPa) in the oedometer cell. Tests EDN_4_9 and EDN_4_10 have an initial density equal to 1 666 kg/m³ and tests EDN_2_13 and EDN_2_14 to 1 790 kg/m³. Hydration was achieved by applying 6 suction reduction steps (to 14 MPa, 8 MPa, 5 MPa, 1.5 MPa, 0.5 MPa and 0.1 MPa). Equilibration time after each step lasted more than 40 days. Tests EDN_4_10 and EDN_2_14 were performed controlling suction by nitrogen pressure (labelled *nit* in Figure AA2-5) and tests EDN_4_9 and EDN_2_13 by a solution of sulphuric acid (labelled *sulf* in Figure AA2-5).

Void ratios at the end of the equilibration stage of each suction step are shown in Figure AA2-5 for all tests. Transient evolution of vertical strain during equilibration phases of test EDN_4_10 is presented in Figure AA2-6.

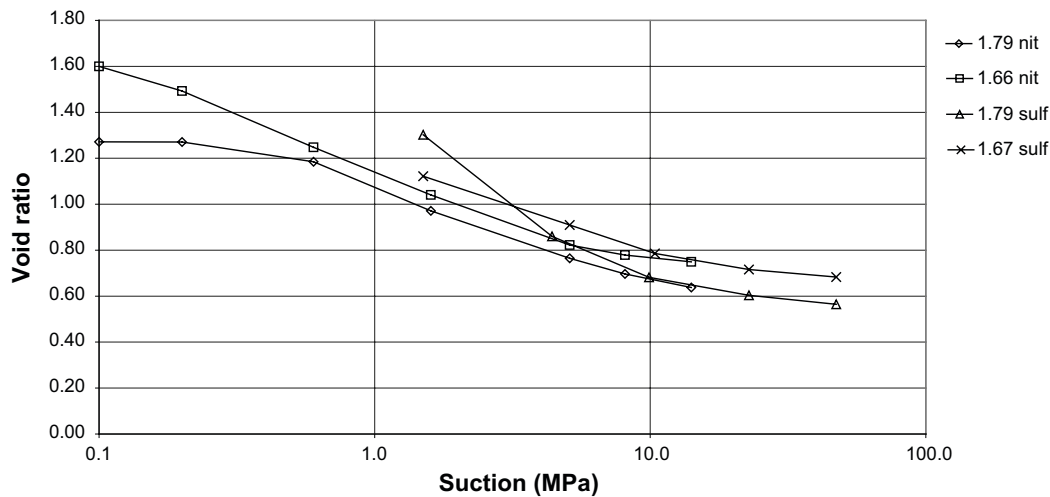


Figure AA2-5. Evolution of void ratio with applied suction during a wetting path performed in an oedometer cell under a constant load of 0.1 MPa (Villar 2003).

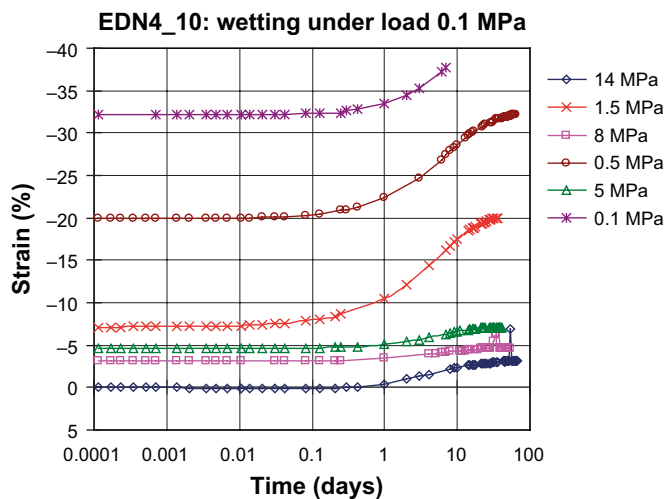


Figure AA2-6. Evolution of vertical strain with time during test EDN_4_10 (Villar 2002a).

AA2.5 Mechanical response of saturated MX-80

Once brought to saturation, samples in tests EDN_4_9, EDN_4_10, EDN_2_13 and EDN_2_14 were further loaded in oedometer conditions. Figure AA2-7 shows the compression lines obtained for each test.

AA2.6 Thermal conductivity

The variation of thermal conductivity with degree of saturation was determined by Börgesson and Hernelind (1999). The results are shown in Figure AA2-8.

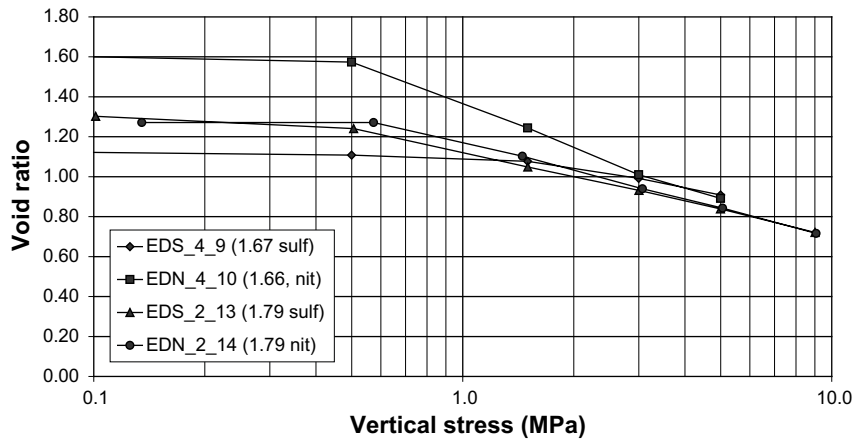


Figure AA2-7. Compression lines obtained during the drained loading following the saturation stage for samples EDN_4_9, EDN_4_10, EDN_2_13 and EDN_2_14 (Villar 2003).

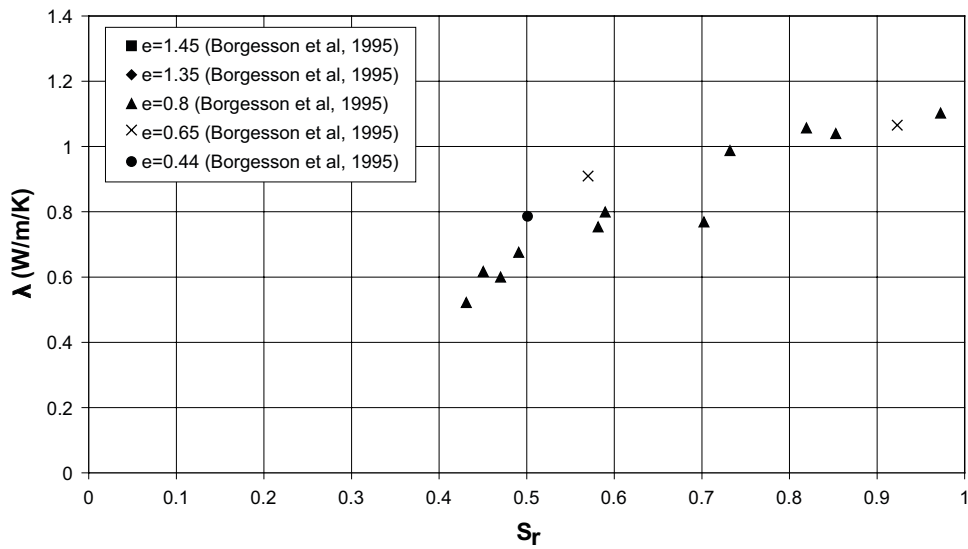


Figure AA2-8. Variation of thermal conductivity with degree of saturation.

Specifications of Subtask 1.2

Infiltration tests under isothermal conditions and under thermal gradient performed by CIEMAT

B1 Introduction

This document contains the specifications of Benchmark 1.2 of the Task Force on Engineered Barrier System (EBS) established by the Äspö HRL International Joint Committee. Benchmark 1.2 is based on the large-cell experiments currently being performed by CIEMAT in their laboratory in Madrid. One of the tests is kept under isothermal conditions whereas the second test is performed under a thermal gradient. Benchmark 1.1, based on THM mock-up experiments on MX-80 bentonite by CEA, was the subject of a previous document.

As stated there, the Task Force is not set up as a competition between codes to determine, from a blind prediction, the best fit to a particular set of experimental results. The basic idea is to allow freedom to the participants to use and develop formulations and codes to try to reproduce in the best way possible the tests results provided in the Benchmark.

The large cell infiltration tests and the results are described in detail in the Technical Report CIEMAT/DMA/M2140/1/05 by Villar et al. (2005) issued in April 2005 and made available to the participants. The information most relevant to the Benchmark is reproduced (often *verbatim*) in the present document but contributors are advised to study in detail the CIEMAT document.

B2 Description of the infiltration tests

B2.1 General

Two infiltration experiments being performed in CIEMAT's large cells (Figure B-1) have been selected; the first one is an isothermal test whereas the second one is a test with a thermal gradient applied. The material tested is FEBEX bentonite.

The following parameters are measured during the tests:

- Temperatures.
- Relative humidity.
- Water intake.

No mechanical parameters are measured during the test. As the experiments are still unfinished, no "post mortem" observations are available.

B2.2 Apparatus and monitoring system

The infiltration tests are being performed in cylindrical cells enclosing a specimen 7 cm diameter and 40 cm long (Figure B-2). The 15 mm thick cell wall is made of Teflon PTFE with a thermal conductivity of 0.25 W/mK. A 4 mm thick stainless steel shell provides mechanical reinforcement to resist the swelling pressures developed during the tests. The cell containing the thermal gradient test is additionally surrounded by a 15-mm thick foam layer with a thermal conductivity of 0.04 W/mK. Heat is applied to the bottom of the specimen. Hydration is performed from the top end of the specimen where a cooling system maintains the temperature constant.

Temperatures and relative humidity are measured inside the samples by means of sensors located at 30 cm (sensors RH1 and T1), 20 cm (sensors RH2 and T2) and 10 cm (sensors RH3 and T3) from the bottom end. The water intake into each of the experiments is also independently monitored. Further details of the equipment and monitoring system are presented in Villar et al. (2005).



Figure B-1. Large infiltration cells: isothermal test (left) and thermal gradient test (right).

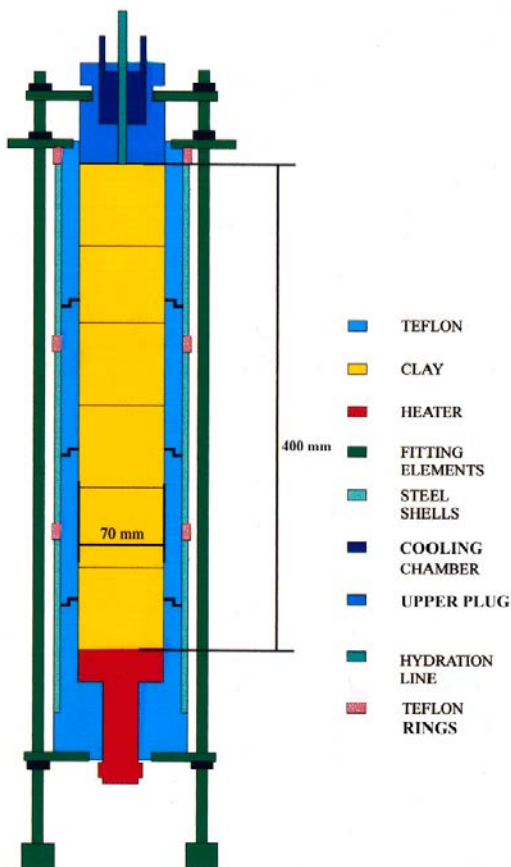


Figure B-2. Scheme of the large cells used in CIEMAT's infiltration tests.

B2.3 Material

The Febex bentonite has been used in the experiments. It is not a homoionic clay but it contains Na⁺, Ca²⁺ and Mg²⁺ in significant and similar amounts. The material has been extensively tested in the framework of the Febex project and the main results are collected in ENRESA (1998, 2000), Villar (2002b), Fernández (2003) and Lloret et al. (2004). A good summary is presented in Villar et al. (2005) and the main THM properties are summarised in Appendix A. Although a number of empirical laws are suggested in the Appendix, contributors may use alternative expressions, duly justified.

The clay was statically compacted (average compaction pressure of 30 MPa) at hygroscopic water content (around 13 %–14 % gravimetric water content) to a nominal dry density of 1.65 g/cm³. The specimens were made up of five blocks; the three inner ones were 10 cm long whereas the two placed at the ends were 5 cm long. Table B-1 provides an indication of the possible heterogeneity by listing the measurements of dry density and water content made in a 10 cm long spare block.

Table B-1: Results of the measurements performed in a 10-cm length spare block.

Position*	Dry density (g/cm ³)	Water content (%)
1.25	1.72	12.7
3.75	1.69	13.1
6.25	1.65	13.4
8.75	1.63	13.5

*Distance to the top of the block.

B2.4 Protocol of the experiments

Once the cell was assembled and the instrumentation installed in the *isothermal test (test I40)*, the cooling system was set up and data acquisition was started. After 18 hours the hydration system was connected. The test was started on 15/01/2002 and the hydration stage on 16/01/2002.

In the *thermal gradient test (test GT40)*, the cooling system and the heater were started simultaneously after cell assembly and instrument installation (initial phase). A temperature of 100 °C was applied at the bottom of the sample. After 65 hours of heating, hydration was started (second phase). The test began on 15/01/2002 and the hydration stage on 18/01/2002,

In both cases hydration was performed using low salinity water at a pressure of 1.2 MPa. The temperature applied by the cooling system corresponds to the ambient temperature of the laboratory and it undergoes some moderate variations. The temperatures recorded in the isothermal test can be used as reference values.

B2.5 Test results

The raw data obtained during the tests are collected in two Excel files: *i40v.xls* (isothermal test **I40**) and *gt40v.xls* (thermal gradient test **GT40**). The raw results have been reviewed and selected by Villar et al. (2005) to give a series of Tables of observed values that can be used directly for comparison with numerical analysis results.

Table B-2 contains the observations of relative humidity, temperature and water intake of the isothermal test (test **I40**) from the time of start of hydration. The results of the thermal gradient test are presented in Tables B-3 and B-4. Table B-3 refers to the observations during the initial phase of the test, from the start of heating to the time of connecting the hydration system. Table B-4 contains the results of the second stage of the experiment, from the time of the start of hydration. According to Villar et al. (2005), the water intake data is not totally reliable and should be taken as indicative only. The actual water intake will be determined at the end of the test from the difference between final and initial weights.

Table B-2. Isothermal test (test I40). Relative humidity (RH) and temperature (T) recorded by sensors after the initiation of hydration (sensor 1 placed at 30 cm from the bottom, sensor 2 at 20 cm and sensor 3 at 10 cm).

Time (h)	RH1 (%)	T1 (°C)	RH2 (%)	T2 (°C)	RH3 (%)	T3 (°C)	Water intake (cm ³)
0	42	20.6	41	20.7	42	20.5	0
1	42	20.9	42	20.9	42	20.7	
5	42	22.5	42	22.4	42	22.1	10
30	42	22.8	42	22.8	42	22.6	15
61	42	22.9	42	23.0	42	22.8	18
101	42	20.1	42	20.2	42	20.1	20
201	43	23.7	43	23.7	43	23.5	30
300	43	21.3	42	21.3	42	21.1	35
399	44	22.9	43	23.0	42	22.8	40
501	45	21.6	42	21.7	42	21.5	44
600	46	19.2	42	19.3	42	19.1	56
701	49	22.5	42	22.6	42	22.5	66
803	51	22.1	42	22.2	42	22.0	77
899	53	24.5	43	24.6	43	24.5	87
1 001	55	23.3	43	23.4	42	23.2	97
1 999	69	23.5	46	23.7	42	23.6	129
3 001	76	24.0	51	24.3	43	24.2	147
4 000	81	26.5	56	26.6	45	26.4	162
5 001	84	28.7	61	28.7	48	28.6	172
10 002	90	22.8	72	22.8	57	22.7	254
14 997	92	24.9	77	25.0	66	24.9	317
19 999	94	26.5	82	26.7	72	26.9	382
24 998	94	22.7	83	22.9	76	22.9	443
28 219	95	23.7	85	23.9	77	23.9	469

Table B-3. Thermal gradient test (test GT40): Initial Phase. Relative humidity (RH) and temperature (T) recorded by sensors (sensor 1 placed at 30 cm from the bottom, sensor 2 at 20 cm and sensor 3 at 10 cm).

Time ¹ (h)	RH1 (%)	T1 (°C)	RH2 (%)	T2 (°C)	RH3 (%)	T3 (°C)
0	42	21.9	42	21.7	42	21.4
1	42	22.5	42	22.3	43	23.3
2	42	22.6	43	22.5	44	27.5
3	42	22.7	43	23.0	45	30.9
4	43	22.9	43	24.4	47	36.6
5	43	23.1	44	26.1	48	40.5
6	43	23.5	44	27.6	49	43.2
7	43	24.0	45	28.9	50	45.1
8	43	24.5	45	30.0	50	46.4
9	43	24.9	45	30.8	50	47.3
10	43	25.3	45	31.4	51	47.9
20	44	27.1	46	33.5	52	49.1
30	45	29.2	47	35.6	52	50.9
40	44	28.2	47	34.9	53	50.1
49	44	29.2	47	35.7	53	51.1
60	45	29.1	48	35.5	54	50.8
65	45	28.6	48	35.1	54	50.5

¹Time since start of heating.

Table B-4. Thermal gradient test (test GT40): Second Phase. Relative humidity (RH) and temperature (T) recorded by sensors (sensor 1 placed at 30 cm from the bottom, sensor 2 at 20 cm and sensor 3 at 10 cm).

Time ¹ (h)	RH1 (%)	T1 (°C)	RH2 (%)	T2 (°C)	RH3 (%)	T3 (°C)	Water intake (cm ³)
0	44	28.9	48	35.5	54	50.9	0.0
1	44	29.0	48	35.6	54	51.1	0.0
5	45	30.2	48	36.6	54	51.8	0.8
10	45	30.0	48	36.4	55	51.5	0.9
21	45	28.8	48	35.3	55	50.6	1.0
30	45	28.3	48	34.9	55	50.4	1.1
40	44	27.7	48	34.4	56	49.9	1.3
50	44	27.1	48	34.0	56	49.7	1.4
61	44	26.5	49	33.6	56	49.4	1.5
69	44	26.1	49	33.2	56	49.1	7
81	45	27.7	49	34.6	57	50.2	8
87	44	27.5	49	34.4	57	50.1	9
101	45	28.5	49	35.3	57	50.9	10
200	45	26.8	51	33.8	58	49.5	17
299	47	29.6	52	36.3	57	51.3	23
401	48	26.9	53	33.9	56	49.6	28
500	50	27.5	54	34.5	55	49.9	32
599	52	26.9	55	34.0	54	49.6	59
701	55	28.0	56	34.7	53	50	63
803	57	30.2	57	36.6	52	51.5	66
899	59	28.8	57	35.5	51	50.7	70
1001	62	30.5	58	37.0	50	51.7	73
1998	76	29.7	61	36.2	43	51.1	101
3003	83	29.7	63	36.2	39	51.1	128
3999	86	31.6	65	38.2	38	52.8	145
5000	88	33.8	66	39.7	37	53.7	160
10001	92	28.6	70	35.3	36	50.3	220
14948	92	30.3	71	36.6	38	51.3	275
20004	93	30.6	73	37.2	38	52.1	330
25004	93	28.8	74	35.6	39	50.8	388
28170	94	29.4	74	36.1	38	51.2	417

¹Time since start of hydration.

B3 Requested results

The following information is requested:

- c) Main features of the analyses performed.
- d) Results of the analyses and comparison with experimental results.

B3.1 Main features of the analyses performed

This basic description should contain summarised information on:

- Geometry adopted for the analysis.
- Type of analysis (e.g., 1-D, 2-D, axisymmetric...).
- Element types used.
- Constitutive laws adopted (thermal, hydraulic, mechanical).
- Constitutive parameters used and procedure used in their determination or estimation.

- Boundary conditions (thermal, hydraulic, mechanical).
- Initial conditions (thermal, hydraulic, mechanical).
- Hypothesis adopted for gas pressure and gas flow.
- Any other features that are deemed important in the analysis.

B3.2 Results of the analyses and comparison with experimental results

The following analysis results should be provided graphically together with comparison with observed data. The Excel files of the submitted graphs should also be made available. The date and hour taken as time origin should be indicated.

B3.2.1 Isothermal test (test I40)

- Relative humidity vs. time for sensors HR1, HR2 and HR3.
- Water intake vs. time.

B3.2.2 Thermal gradient test (test GT40). Initial phase

- Temperature vs. time for sensors T1, T2, T3.
- Relative humidity vs. time for sensors HR1, HR2, HR3.

B3.2.3 Thermal gradient test (test GT40). Second phase

- Temperature vs. time for sensors T1, T2, T3.
- Relative humidity vs. time for sensors HR1, HR2, HR3.
- Water intake vs. time.

Although only TH parameters are provided for comparison, it is advised to adopt a full THM analysis whenever possible.

B3.3 Additional reporting

The reporting teams are encouraged to submit a brief introductory report outlining the aspects of the work and difficulties encountered that are considered to be especially relevant.

Properties of febex bentonite

In this Appendix, selected information on THM properties of FEBEX bentonite as reported in Villar et al. (2005) is highlighted. More detailed information can be found in the references of this report.

BA1.1 General properties

The liquid limit of the bentonite is 102 ± 4 , the specific gravity 2.70 ± 0.04 , and 67 ± 3 percent of particles are smaller than $2 \mu\text{m}$. The hygroscopic water content in equilibrium with the laboratory atmosphere (relative humidity 50 ± 10 %, temperature 21 ± 3 °C, total suction about 100 MPa) is 13.7 ± 1.3 percent. Table BA-1 shows the average content values of the exchangeable cations along with the cation exchange capacity (CEC), as determined by different methods and laboratories.

Table BA-1. Average values of exchangeable cations and cation exchange capacity (CEC) as determined by different methods (meq/100g).

	CSIC-Zaidín ¹	CIEMAT ¹	CIEMAT ²
Ca²⁺	43±5	42±3	35±2
Mg²⁺	32±3	32±2	31±3
Na⁺	24±4	25±2	27±0
K⁺	2.1±0.2	2.5±0.3	2.6±0.4
Sum of exchangeable cations	101±4		96±0
CEC³		102±4	

¹ Determined by displacement by 1M NH₄AcO at pH 7 after washing of soluble salts (ENRESA 2000), the values are recalculated to give a sum of cations equal to CEC.

² Determined by displacement by 0.5M CsNO₃ at pH 7 (Fernández 2003).

³ Determined by NaAcO/NH₄AcO pH=8.2 (ENRESA 2000).

BA1.2 Retention curve

The retention curve of the bentonite was determined in samples compacted to different dry densities under different temperatures (Lloret et al. 2004, Villar and Lloret 2004). The volume of the samples remained constant during the determinations, since they were confined in constant volume cells. To impose the different relative humidities (*i.e.* suctions) the cells were placed in desiccators with sulphuric acid solutions of various concentrations. Some data from these laboratory determinations are shown in Figure BA-1

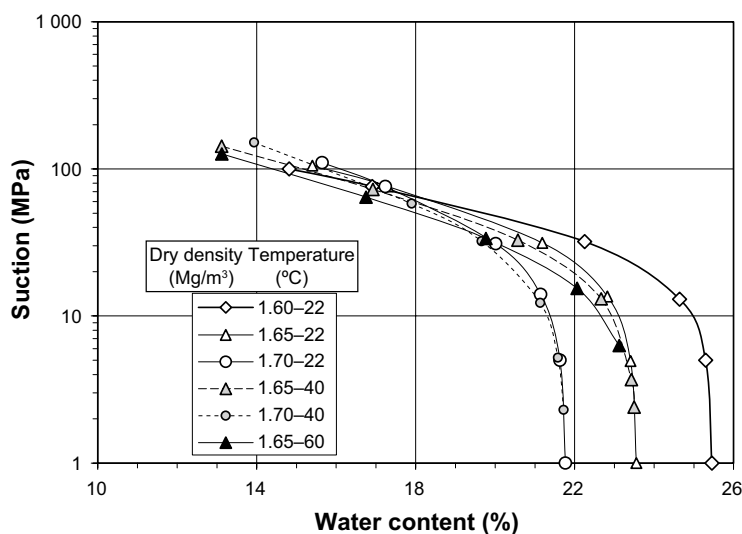


Figure BA-1. Water retention curves at different temperatures and for different bentonite densities (Lloret et al. 2004)

Following an approach similar to that presented by Sánchez (2004) to fit the data from these laboratory determinations, the following empirical equation can be obtained:

$$w = (a + b n) \left[1 + \left(\frac{s}{P_0 e^{-\eta(n-n_0)} e^{-\alpha(T-T_0)}} \right)^{\frac{1}{1-\lambda}} \right]^{-\lambda} \quad (\text{BA-1})$$

where w is the water content in percentage, n the porosity, s the suction in MPa, and T the temperature in °C. The values of parameters a , b , P_0 , η , n_0 , α , T_0 and λ are indicated in Table BA-2. The differences between measured values and the estimated values using Equation BA-1 are smaller than 2 percent in terms of water content.

Table BA-2. Values of parameters in Equation 4

a	b	P_0 (MPa)	η	n_0	α (1/°C)	T_0 (°C)
10.96	41.89	12.68	0.211	7.97	0.00647	20

In unconfined conditions, the relationship between suction (s , MPa) and water content (w , %) changes, taking into account the initial dry density of the bentonite (ρ_{d0} , g/cm³), it may be fitted to the following equation:

$$w = (45.1 \rho_{d0} - 39.2) - (18.8 \rho_{d0} - 20.34) \log s \quad (\text{BA-2})$$

BA1.3 Hydraulic properties

The saturated permeability to deionised water (k_w , m/s) of samples of untreated FEBEX bentonite compacted at different dry densities is exponentially related to dry density (ρ_d , g/cm³). A distinction may be made between two different empirical fittings depending on the density interval (Villar 2002b):

for dry densities of less than 1.47 g/cm³:

$$\log k_w = -6.00 \rho_d - 4.09 \quad (r^2 = 0.97, 8 \text{ points}) \quad (\text{BA-3})$$

for dry densities in excess of 1.47 g/cm³:

$$\log k_w = -2.96 \rho_d - 8.57 \quad (r^2 = 0.70, 26 \text{ points}) \quad (\text{BA-4})$$

The determinations were done at room temperature. The variation in the experimental values with respect to these fittings is smaller for low densities than it is for higher values, with an average –in absolute values– of 30 percent.

Some isothermal infiltration tests and heat flow tests at constant overall water content were performed during FEBEX I project and they were backanalysed using CODE_BRIGHT (Lloret et al. 2002, Pintado et al. 2002). It is possible to fit the experimental data using a cubic law for the relative permeability ($k_r = S_r^3$) and a value of 0.8 for the vapour tortuosity factor (τ).

BA1.4 Thermal properties

The thermal conductivity (λ , W/m·K) of the compacted bentonite at laboratory temperature is related to the degree of saturation (S_r) through the following expression:

$$\lambda = \frac{A_1 - A_2}{1 + e^{\frac{S_r - x_0}{dx}}} + A_2 \quad (\text{BA-5})$$

where A_1 represents the value of λ for $S_r=0$, A_2 the value of λ for $S_r=1$, x_0 the degree of saturation for which thermal conductivity is the average of the two extreme values and dx is a parameter. This equation was chosen because it accurately represents the behaviour of thermal conductivity versus water content (degree of saturation), which are directly related but not in a linear fashion (Villar 2002b). The fitting obtained, with an r^2 of 0.923, gives the following values for each parameter:

$$A_1 = 0.57 \pm 0.02$$

$$A_2 = 1.28 \pm 0.03$$

$$x_0 = 0.65 \pm 0.01$$

$$dx = 0.100 \pm 0.016$$

Alternatively, an approximate representation of the variation of thermal conductivity with degree of saturation (Figure BA-2) can be obtained using the expression

$$\lambda = \lambda_{sat}^{S_r} \lambda_{dry}^{(1-S_r)} \quad (\text{BA-6})$$

with the values of $\lambda_{sat} = 1.15$ W/mK and $\lambda_{dry} = 0.47$ W/mK (ENRESA 2000).

BA1.5 Swelling pressure

The swelling pressure (P_s , MPa) of FEBEX samples compacted with their hygroscopic water content and flooded with deionised water up to saturation at room temperature can be related to dry density (ρ_d , g/cm³) through the following equation (Villar 2002b):

$$\ln P_s = 6.77 \rho_d - 9.07 \quad (r^2 = 0.88, 52 \text{ measurements}) \quad (\text{BA-7})$$

In this case, the difference between experimental values and this fitting is, on average, 25 percent. This dispersion, which is wider for higher dry densities, is due both to the natural variability of bentonite and to the measurement method used, which does not allow high degrees of accuracy.

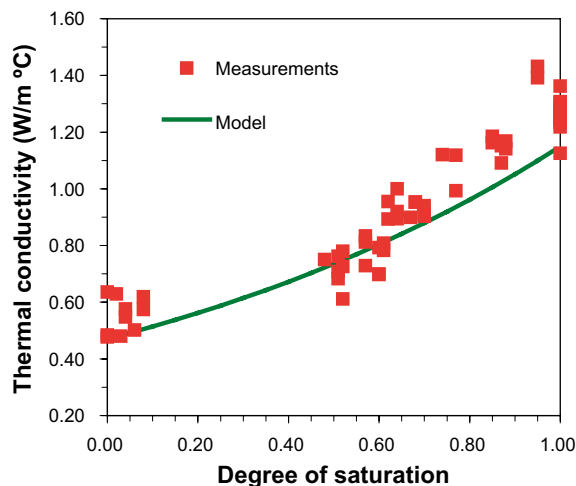


Figure BA-2. Thermal conductivity results and Equation (BA-6).

Specifications of Subtask 1.3

Heating test with no water infiltration performed by UPC

C1 Introduction

This document contains the specifications of Benchmark 1.3 of the Task Force on Engineered Barrier System (EBS) established by the Äspö HRL International Joint Committee. Benchmark 1.3 is based on a heating test with no water infiltration performed in the UPC laboratory. The material tested was compacted Febex bentonite.

C2 Description of the UPC heating test

C2.1 General

Conceptually, the test is depicted in Figure C-1. Two cylindrical samples of compacted Febex bentonite are subjected to a prescribed heat flow from one end. The temperature is kept constant at the other end. The two specimens are symmetrically placed with respect to the heater.

The following parameters are measured:

- Temperatures at various points throughout the test.
- Water content at the end of the test.
- Specimen diameter at the end of the test.

C2.2 Apparatus and monitoring system

The apparatus used for performing the test is depicted in Figure C-2. The two cylindrical specimens (38 mm diameter, 76 mm height) are placed vertically in the apparatus, with the heater located between them. A latex membrane that allows deformation and keeps constant the overall water content and a layer (5.5 cm thick) of heat insulating material (composed of deformable foam, expanded polystyrene and glass fibre) surround the specimen. The ensemble is contained in a perspex tube. It has been determined that the diffusion water loss from the specimens during the test was less than 0.1g/day. From the backanalysis of experiments, a value of thermal conductivity of the insulating layer of 0.039 W/mK has been estimated, although the teams are free to make their own estimates.

The heater is a copper cylinder (38 mm diameter, 50 mm height) with five small electrical resistances inside. The resistances are connected to an adjustable source of direct current that allows the control of input power from 0 to 5 W. At the cool ends, a constant temperature is maintained by flowing water through a stainless steel cap in contact with the soil. A temperature regulation system keeps the temperature of the contact between the cap and the soil practically constant, with variations smaller than 0.5 °C. In order to ensure a good contact between the caps and the samples, a light stress (about 0.05 MPa) was applied on top of the test ensemble.

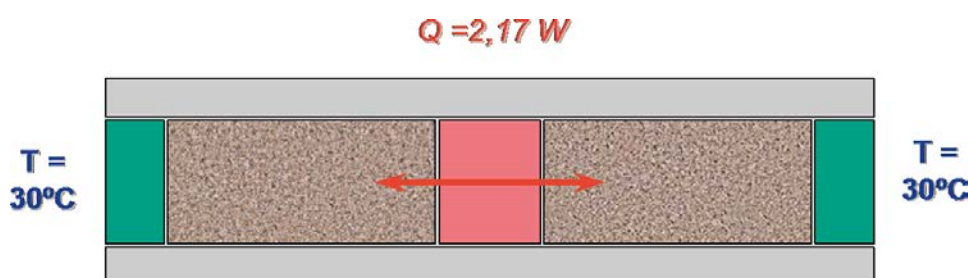


Figure C-1. Conceptual scheme of the UPC heating test.

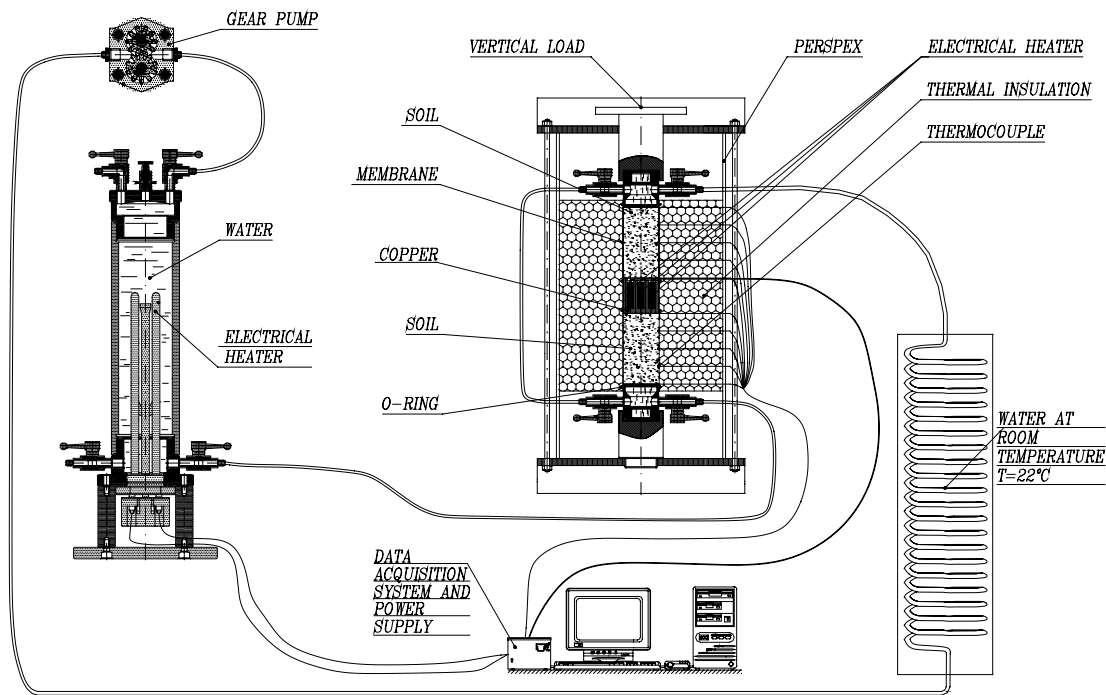


Figure C-2. Scheme of the UPC experimental device.

Only temperatures were measured during the test. Temperatures measurements were concentrated in one of the specimens; three measurements were made in the inside of the sample and two more on the hot and cool ends of the specimen. In the second sample, only one inside temperature measurement was made in the centre of the specimen that confirmed the symmetry of the temperature distribution.

C2.3 Material

The Febex bentonite has been used in the experiments. Information on the characteristics and properties of this bentonite has already been given in the specifications of benchmark THM 1.2. The bentonite has been compacted at a dry density of 1.63 g/cm^3 and with a water content of 15.33 % (degree of saturation of 0.63).

C2.4 Protocol of the experiments

A constant power of 2.17 W has been supplied by the heater during 7 days whereas at the opposite ends of the specimens a temperature of $30 \text{ }^\circ\text{C}$ was maintained. Initial temperature of the bentonite was $22 \text{ }^\circ\text{C}$.

At the end of the 7 days, the heaters were switched off, the apparatus dismantled and the diameter and water content at different points of the specimens determined. The diameter of the specimen was measured at 7 sections in each specimen with an accuracy of 0.01mm. To obtain the distribution of water content, each specimen was cut into six small cylinders, and the water content of each cylinder was determined.

C2.5 Test results

The data obtained during the tests are collected in the file: *UPC heating test.xls*

The Excel file contains the temperatures measured during the test and the water content and diameter determinations performed after the test. It also presents graphs of temperature evolution with time at various points and of distribution of water content and diameter changes at the end of the test.

In the water content case, the distance to the heater data corresponds to the distance to the centre of the small cylinders used in water content determination. Concerning the diameter increment data, a positive value indicates expansion and a negative value indicates contraction.

C3 Requested results

The following information is requested:

- e) Main features of the analyses performed.
- f) Results of the analyses and comparison with experimental results.

C3.1 Main features of the analyses performed

This basic description should contain summarised information on:

- Geometry adopted for the analysis.
- Type of analysis (e.g., 1-D, 2-D, axisymmetric...).
- Element types used.
- Constitutive laws adopted (thermal, hydraulic, mechanical).
- Constitutive parameters used and procedure used in their determination or estimation.
- Boundary conditions (thermal, hydraulic, mechanical).
- Initial conditions (thermal, hydraulic, mechanical).
- Hypothesis adopted for gas pressure and gas flow.
- Any other features that are deemed important in the analysis.

Special attention should be given to the information involved in water transfer (vapour diffusion, including tortuosity if used, and permeability and hydraulic conductivity) and in thermal diffusion (thermal conductivity and specific heat).

C3.2 Results of the analyses and comparison with experimental results

The following analysis results should be provided graphically together with comparison with observed data. The Excel files of the submitted graphs should also be made available.

C3.2.1 Temperatures

- Evolution of temperatures vs. time at $x=0$ mm, 20 mm, 38 mm, 60 mm, 76 mm throughout the test (coordinate x is the distance to the heater).
- Distributions of temperatures at the following times: 0.292 hours, 1.446 hours, 3.161 hours, 100.609 hours.

C3.2.2 Water content

- Distribution of water content along the specimen at the end of the test.

C3.2.3 Sample diameter

- Distribution of diameter increment along the specimen at the end of the test.

C3.3 Additional reporting

The reporting teams are encouraged to submit a brief introductory report outlining the aspects of the work and difficulties encountered that are considered to be especially relevant.

The teams are also strongly encouraged to revisit Benchmark THM 1.2, applying the information and parameters obtained in this Benchmark.

